Development of ABPBI-based Membranes and their Investigations for Forward Osmosis (FO)

by

Thorat Nitin Madhukarrao
20EE17A26041

A thesis submitted to the
Academy of Scientific & Innovative Research
for the award of the degree of
DOCTOR OF PHILOSOPHY
In
ENGINEERING

Under the supervision of
Dr. Ashish K. Lele and Dr. Ulhas K. Kharul

CSIR-National Chemical Laboratory, Pune-411008

Academy of Scientific and Innovative Research
AcSIR Headquarters, CSIR-HRDC campus
Sector 19, Kamla Nehru Nagar,
Ghaziabad, U.P. – 201 002, India

February 2025

Certificate

This is to certify that the work incorporated in this Ph.D. thesis entitled, "***Development of ABPBI-based Membranes and their Investigations for Forward Osmosis (FO)***", submitted by *Mr. Thorat Nitin Madhukarrao* to the Academy of Scientific and Innovative Research (AcSIR) in fulfillment of the requirements for the award of the Degree of *DOCTOR OF PHILOSOPHY in ENGINEERING*, embodies original research work carried out by the student. We, further certify that this work has not been submitted to any other University or Institution in part or full for the award of any degree or diploma. Research material(s) obtained from other source(s) and used in this research work has/have been duly acknowledged in the thesis. Image(s), illustration(s), figure(s), table(s), etc., used in the thesis from other source(s) have also been duly cited and acknowledged.

(Signature of Student)	(Signature of Co-Supervisor)	(Signature of Supervisor)
Mr. Thorat Nitin Madhukarrao	Dr. Ulhas K. Kharul	Dr. Ashish K. Lele

STATEMENTS OF ACADEMIC INTEGRITY

I Thorat Nitin Madhukarrao, a Ph.D. student of the Academy of Scientific and Innovative Research (AcSIR) with Registration No. 20EE17A26041 hereby undertake that, the thesis entitled "*Development of ABPBI-based Membranes and their Investigations for Forward Osmosis (FO)*" has been prepared by me and that the document reports original work carried out by me and is free of any plagiarism in compliance with the UGC Regulations on *"Promotion of Academic Integrity and Prevention of Plagiarism in Higher Educational Institutions (2018)"* and the CSIR Guidelines for "*Ethics in Research and in Governance (2020)*".

Signature of the Student
Date: 12-02-2025
Place: Pune

It is hereby certified that the work done by the student, under my/our supervision, is plagiarism-free in accordance with the UGC Regulations on *"Promotion of Academic Integrity and Prevention of Plagiarism in Higher Educational Institutions (2018)"* and the CSIR Guidelines for "*Ethics in Research and in Governance (2020)*".

Signature of the Co-supervisor
Name: Dr. Ulhas K. Kharul
Date: 12-02-2025
Place: Pune

Signature of the Supervisor
Name: Dr. Ashish K. Lele
Date: 13-02-2025
Place: Pune

ACKNOWLEDGEMENTS

I would like to express my sincere gratitude to my supervisor Dr. Ashish K. Lele. I thank Dr. Ashish K. Lele for allowing me to pursue my career as a Ph.D. student and for all his help, support, and suggestions during the course of this study. I would like to express my sincere gratitude to my co-supervisor Dr. Ulhas K. Kharul. It was impossible for me to complete the expedition without your support. He taught me useful skills for research work and technical writing during the course of work. My heartfelt thanks go to him for introducing me to the wonders of scientific research and for his persistent guidance, encouragement, inspiration, and support during every stage of my doctoral research work. I am very much thankful to him for his pursuit of improving me as a person and my scientific skills. His enthusiasm for transforming science into technology to improve the quality of life greatly inspired me to pursue membrane research as a career. Again, I thank him for his precious advice, analysis, criticism, and discussions on my research work. I consider myself to be fortunate that I got an opportunity to work under his guidance. I would also like to sincerely thank my DAC committee members, Dr. T. Raja, Dr. Ashish Orpe, and Dr. Samir Chikkali, for their constructive, innovative suggestions and comments throughout my Ph.D. work at CSIR-NCL, Pune.

I sincerely thank the Director of CSIR-NCL, Dr. Ashish K. Lele, and former Director, Dr. Ashwini Kumar Nangia. I sincerely thank the Head of the Polymer Science and Engineering division, Dr. Suresh Bhat, and the former Head of the Polymer Science and Engineering division, Dr. Asha S. K., for their kind help and encouragement during the course of this work. I would like to thank Dr. K. V. Pandare, Dr. S. S. Joshi, Dr. Nilesh Mali, Dr. Rahul Bhanbure, Dr. Harshawardhan Pol, and Mrs. Sangita for their valuable suggestions and for allowing me to use the analytical facilities. I must earnestly acknowledge the valuable scientific discussions, suggestions, constant support, and encouragement that I received from Dr. Rahul Shevate and Dr. Devin Shaffer.

I am very grateful to CSIR, New Delhi, for the fellowship support I need to conduct my research. I want to thank the non-academic staff of CSIR-NCL, especially the SAC, AcSIR, Bills, F&A, C&P, and EII sections. Also, special thanks to Mr. Gati Nayak and the staff of the CSIR-NCL library for their timely help whenever I needed it. I thank my seniors, Dr. Jayshri Thote, Dr. Harshal Chaudhari, and Dr. Shebeeb K. H., for teaching experimental skills and guiding me in my Ph.D. stage. I wish to thank my friendly and cooperative lab mates Nishina A. S, Vipin Sherwal, Mukesh Valvi, Suresh Valvi, Keerthana, Harshala, Shreetam, Lavanya Alladi, Saroj Gawas, Nitin Somuvunkar, Kiran Bansode, Vikas Mahule, Santhosh, Rohit

Ghanta, Karan Kubadikar, Yatha Sharma, Prachiti Bendhadur, Supriya Gigam, Supriya Jadhav, Chinmay Behara, Sanjivani Pal, Rutesh Gaikwad, Karan Deshpande, Varsha Bansode, Atharv Bachute, Fredin Poulson, Nishant Choudhari, Robin Kumar Patel, Sameer Vinay, Sheethal, Jyoti, Diksha, Harshad Tilekar and Omkar Jadhav for creating a cheerful and enjoyable working atmosphere in the lab. They were highly supportive and helpful during my tenure. I would like to thank Mr. Swaraj Sing for his support and for keeping my lab clean and neat without any hesitation. My stay on this campus has been pleasant with the association of all the research scholars and friends at CSIR-NCL. I am thankful to Dhammaraj, Sagar, Prashant, Apparav, and Ranjit for their support, guidance, and advice. I would like to thank Sathe Ji for his support and love. I am grateful to all my teachers, and I expressed gratitude for their encouragement in a different part of my life. I thank all the members of my family for their constant care and wishes. Last but not least, I would like to pay high regard to my parents, my wife Anuja, and my lovely son Abhimanyu for their continuous encouragement and inspiration throughout my research work and for lifting me up during this phase of life. I owe everything to them. Dedicating this thesis to them is a minor recognition of their valuable support and encouragement.

Thorat Nitin Madhukarrao

Dedicated to My Beloved Parents,
My Lovely Wife Anuja and
My Little Champ Abhimanyu

Table of Contents

		Page No.
List of Figures		**x**
List of Schemes		**xi**
List of Tables		**xii**
List of Acronyms		**xiii**
Chapter 1	**Introduction and Literature Survey**	**1**
1	Introduction to FO and OSFO	**2**
1.1	Principle of FO/OSFO	**2**
1.2	Applications of FO	**3**
1.2.1	*Desalination*	**3**
1.2.2	*Wastewater treatment*	**4**
1.2.3	*Agricultural irrigation/fertigation*	**6**
1.2.4	*Food processing and dairy industries*	**6**
1.2.5	*Chemical industries*	**7**
1.2.6	*Emergency drinks*	**8**
1.2.7	*Pharmaceutical industries*	**9**
1.2.8	*Metal recovery*	**10**
1.3	Membrane materials for FO and their morphology	**11**
1.3.1	*Asymmetric membranes*	**11**
1.3.2	*Thin film composite (TFC) membranes*	**11**
1.3.3	*Symmetric membranes*	**13**
1.4	Draw solutions	**14**
1.4.1	*Inorganic draw solutions*	**15**
1.4.2	*Organic draw solutions*	**16**
1.4.3	*Ionic liquids (ILs)*	**17**
1.4.4	*Polymeric draw solutions*	**18**
1.5	Concentration polarization (CP)	**18**
1.6	Scope of the present work	**20**
1.7	Aims of the present work	**21**
1.8	Objectives of the present work	**21**
1.9	Outline of the thesis	**21**
1.10	References	**22**

Chapter 2	**ABPBI-based Hollow Fiber Membranes for Forward Osmosis (FO) Possessing Low Reverse Salt Flux**	**33**
2.1	Introduction	**34**
2.2	Experimental	**36**
2.2.1	*Materials, ABPBI synthesis, and characterizations*	**36**
2.2.2	*Preparations of flat sheet membranes (FSMs)*	**37**
2.2.3	*Physical characterizations of FSMs*	**37**
2.2.4	*Sorption analysis using FSMs*	**37**
2.2.5	*Spinning of hollow fiber membranes (HFMs) and characterizations*	**38**
2.2.6	*Characterizations of HFMs and module making*	**38**
2.2.7	*FO experiments using HFM modules*	**39**
2.3	Results and discussion	**39**
2.3.1	*ABPBI synthesis and characterizations*	**39**
2.3.2	*Sorption analysis of FSMs*	**40**
2.3.3	*Preparation of HFMs and their characterizations*	**41**
2.3.4	*FO performance*	**43**
2.3.5	*Comparison with the literature reports*	**46**
2.4	Conclusions	**47**
2.5	References	**48**
Chapter 3	**ABPBI-based Flat Sheet Membrane Preparation, Characterizations, their FO Performance, and Acid Enrichment by FO**	**53**
3.1	Introduction	**54**
3.2	Experimental	**55**
3.2.1	*Materials*	**55**
3.2.2	*Preparation of FSMs*	**56**
3.2.3	*Physical characterizations of FSMs*	**56**
3.2.3	*FO analysis*	**57**
3.2.4	*Acid enrichment by FO*	**58**
3.3	Results and discussion	**59**
3.3.1	*Characterization of FSMs*	**59**
3.3.2	*Effect of membrane heat treatment and different DS*	**62**
3.3.3	*Effect of DS concentration and duration analysis*	**63**
3.3.4	*Comparison with the literature*	**64**
3.4	Acid enrichment by FO	**65**

3.4.1	*Comparison of FO-based acid enrichment with the literature*	**67**
3.5	Conclusions	**67**
3.6	References	**68**
Chapter 4	**Thin, Flat Sheet, Solvent-Stable ABPBI-based Membranes for Organic Solvent Forward Osmosis (OSFO)**	**73**
4.1	Introduction	**74**
4.2	Experimental	**75**
4.2.1	*Materials*	**75**
4.2.2	*Preparation of triethylammonium benzoate (TB) and its draw solution (DS)*	**76**
4.2.3	*OSFO analysis*	**76**
4.2.4	*Analysis using model organic compounds (MOCs)*	**77**
4.3	Results and discussion	**77**
4.3.1	*Effects of membrane heat treatment, DS concentration, and duration of analysis*	**77**
4.3.2	*OSFO using few industrially significant solvents*	**78**
4.3.3	*Long-duration analysis in the presence of MOCs*	**80**
4.3.4	*Comparison with the literature*	**82**
4.4	Conclusions	**84**
4.5	References	**85**
Chapter 5	**Conclusions and Future Directives**	**88**
5.1	Conclusions	**89**
5.2	Future directives	**89**

List of Figures

Fig.		Page No.
1.1.	Schematic of FO process.	**2**
1.2.	FO system coupled with a draw solutes regeneration unit.	**3**
1.3.	An integrated FO and RO desalination process.	**4**
1.4.	Schematic diagram of the FO–MD bench-scale test unit.	**4**
1.5.	FO–MD setup FGD wastewater.	**5**
1.6.	Operational configurations of FO-RO hybrid system (a) open-loop, (b) closed-loop.	**5**
1.7.	FDFO desalination process using DS containing mixtures of blended.	**6**
1.8.	Schematic of FO application in food industries.	**7**
1.9.	Carboxylic acid concentration by FO.	**8**
1.10.	(a) Water bag design (1 = the lid on the front of the bag, 2 = the lid on the back of the bag, 3 = polypropylene plastic, 4 = chitosan-starch membrane, 5 = draw solution), with the photographs of (b) the front side and (c) backside of the bag.	**8**
1.11.	Schematic diagram of a FO process for organic solvent recovery.	**9**
1.12.	Conceptual diagram of a FO-based system for precious metal (Pd) recovery.	**10**
1.13.	Illustration of the structure disparity of (a) skinned asymmetric membrane and (b) TFC membrane.	**11**
1.14.	The preparation procedures of GO-incorporated TFC membranes.	**13**
1.15.	Support free self-standing FO membrane.	**14**
1.16.	Schematic diagram of FO draw solutions with different handling approaches, including regeneration, direct use, and disposal.	**15**
1.17.	Schematic representation of a phase diagram showing the UCST (red) and LCST (blue) for thermos-responsive ionic liquid materials.	**17**
1.18.	Schematic illustration of ECP in the symmetrical dense FO membrane.	**19**
1.19.	Schematic representation of dilutive ICP (left) and concentrative ICP (right).	**20**
2.1.	a) Scheme of ABPBI synthesis, b) FT-IR and c) TGA spectra, d) WAXD pattern.	**40**
2.2.	Sorption of a) water, b) aq. 2 mol L^{-1} NaCl, and c) aq. 2 mol L^{-1} $MgCl_2$ in ABPBI FSMs.	**41**
2.3.	Characterization of ABPBI HFMs: a) FT-IR spectra, b) WAXD pattern, c) TGA curves, and d) microscopic images.	**42**
2.4.	SEM images of HFMs.	**43**

2.5.	The performance of ABPBI and ABPBI-MS treated at 80 °C: Variation in (a) J_W with an osmotic pressure of DS and (b) J_S with the concentration of DS.	**44**
2.6.	The performance of ABPBI and ABPBI-MS treated at 350 °C: Variation in (a) J_W with the osmotic pressure of DS and (b) J_S with the concentration of DS.	**44**
2.7.	The long-term analysis of ABPBI-MS_{350} using 2 mol L^{-1} NaCl (filled symbols) and $MgCl_2$ (unfilled symbols) as a DS: Variation of (a) J_W and (b) J_S with time.	**45**
3.1.	Schematic representation of flat sheet membrane preparation.	**56**
3.2	Photographs of the experimental setup of FO with FSM module.	**57**
3.3.	Characterizations of FSMs: a) FT-IR spectra, b) TGA of ABPBI-3, c) WARD pattern, d) contact angle of membrane surfaces, e) zeta potential curves, and f) stress-strain curves.	**60**
3.4.	Digital and FESEM images of present membranes.	**61**
3.5.	Top and bottom surface topography and 3D AFM images of present membranes.	**61**
3.6.	Variation in J_W and RSF (a) with membrane treatment condition (FS: DI water, DS: 1.5 mol L^{-1} aq. Na_2SO_4) and (b) for ABPBI-2 using different DS (conc. 1.5 mol L^{-1}).	**63**
3.7.	FO performance of ABPBI-2 using $MgCl_2$ as a DS and DI water as FS; (a) variation in DS concentration and (b) long duration stability (DS: 2 mol L^{-1}).	**64**
3.8.	Variation of acid concentration in FS with time.	**66**
4.1.	Variation in flux and RSF with (FS: MeOH) (a) membrane treatment condition (DS: 1 mol L^{-1} LiCl in MeOH), (b) DS concentration (DS: 0.5-2 mol L^{-1} LiCl in MeOH) using ABPBI-3, and (c) long duration stability of ABPBI-3 (DS: 0.5 mol L^{-1} LiCl in MeOH).	**78**
4.2.	OSFO performance using 1 mol L^{-1} TB as DS: (a) variation in the membrane using MeOH as FS (b) use of different solvents with ABPBI-3 as a membrane.	**79**
4.3.	Chemical structure of MOCs.	**80**
4.4.	OSFO experimental setup using MOCs in FS.	**81**
4.5.	UV-Vis spectra of (a) individual MOCs in MeOH, (b) FS and DS (1 mol L^{-1} LiCl) in MeOH after 10 h, (c) FS and DS (1 mol L^{-1} TB) in MeOH after 10 h.	**82**
4.6.	UV-Vis spectra of (a) individual MOCs in ACN, (b) FS and DS in ACN after 10 h.	**82**

List of Schemes

Scheme		**Page No.**
2.1.	a) Scheme of ABPBI synthesis.	**40**
4.1.	Preparation of triethylammonium benzoate (TB).	**76**

List of Tables

Table		Page No.
1.1	Symmetric FO membrane and their method of preparation	**14**
1.2	Physicochemical characteristics of inorganic compound-based draw solutions	**16**
1.3	Physicochemical characteristics of organic compound-based draw solutions	**17**
1.4	Physicochemical characteristics of ionic liquid-based draw solutions	**18**
1.5	Physicochemical characteristics of polymeric draw solutions utilized in FO applications	**18**
2.1	Spinning parameters used for making HFMs	**38**
2.2	Nomenclature of membranes	**38**
2.3	Physical size and helium permeation characteristics of HFMs	**43**
2.4	FO performance at 2 mol L^{-1} concentration of DS	**45**
2.5	Comparison of FO performances of fabricated ABPBI-based HFM with those of HFMs reported in the literature	**46**
3.1	Nomenclature of membranes	**56**
3.2	The roughness of the membrane surface	**62**
3.3	Comparison of present FO data with the relevant literature	**64**
3.4	FO performance of membrane prior to acid concentration	**65**
3.5	Acid and their concentration used for acid enrichment using $MgCl_2$ (4 mol L^{-1}) as DS and ABPBI-2 as a membrane	**66**
3.6	Acid concentration factor (*CF*), concentration in FS, acid rejection (R_{FO}), and acid flux (J_{fs}) of AA and MAA	**67**
3.7	Comparison of present FO-based acid enrichment with the literature reports	**67**
4.1.	DS conductivity	**79**
4.2.	OSFO performances of ABPBI-3 in the presence of MOCs	**82**
4.3.	Comparison of present data with those reported in the literature	**83**

List of Acronyms

Acronyms	Explanation
AA	Acetic Acid
AB	Aniline Blue
ABPBI	Poly(2,5-benzimidazole)
CAN	Acetonitrile
AFM	Atomic Force Microscopy
AKG	Alpha-Ketoglutaric Acid
APIs	Active Pharmaceutical Ingredients
ATR	Attenuated Total Reflectance
CA	Cellulose Acetate
$CaCl_2$	Calcium Chloride
CAP	Cellulose Acetate Propionate
$CdCl_2$	Cadmium Chloride
CF	Concentration Factor
CNTs	Carbon Nanotubes
CO_2	Carbon Dioxide
COF	Covalent Organic Framework
COOH	Carboxyl Group
CP	Concentration Polarization
CTA	Cellulose Triacetate
$CuSO_4$	Copper(II) Sulfate
DABA	3,4-Diaminobenzoic Acid
DAP	Diammonium Phosphate
DC	Draw Compartment
DI Water	Deionized Water
DMAc	*N,N*–Dimethylacetamide
DMF	Dimethylformamide
DMSO	Dimethyl Sulfoxide
DR	Direct Red 81
DS	Draw Solution
ECP	External Concentration Polarization
EtOH	Ethanol
FDFO	Fertilizer-Drawn Forward Osmosis
FE-SEM	Field Emission Scanning Electron Microscope
FGD	Flue Gas Desulfurization
FO	Forward Osmosis
FS	Feed Solution
FSM	Flat Sheet
FT-IR	Fourier Transform Infrared
GO	Graphene Oxide
H_2SO_4	Sulfuric Acid
HCl	Hydrochloric Acid
HFM	Hollow Fiber Membrane
HLGO	Highly Laminated GO
ICP	Internal Concentration Polarization
IL	Ionic Liquids
IP	Interfacial Polymerization

CHAPTER 1

Introduction and Literature Survey

Abstract

Forward osmosis (FO) is a promising upcoming separation technology that can overcome the challenges of pressure-driven membrane processes. Despite intense research efforts over the past 15 years, industrial and commercial applications of FO technology face some challenges. In this chapter, the recent developments in FO technology are reviewed. Initially, the FO process is briefly introduced, with a subsequent critical focus on FO applications, hybrid processes incorporating combined benefits from concentration–dilution (e.g., fertilizer-based solutions for agricultural irrigation), advances in the development of FO membrane materials, membrane fabrication techniques, and tailoring and improvements in draw solutions (e.g., thermo-responsive polymers) for targeted applications with minimized reverse solute flux and draw solution regeneration methods. The limiting factors (such as concentration polarization, membrane stability, etc.) that compromise the application of the FO process to real applications are discussed.

1 Introduction to FO and OSFO

1.1 Principle of FO/OSFO

The osmosis occurs when a selectively permeable membrane separates two solutions containing solutes of different concentrations. Driven by the osmotic pressure difference, small-sized solvent molecules pass through the membrane from the low-concentration side to the high-concentration side. The forward osmosis (FO) process exploits the natural phenomenon of osmosis. It utilizes the osmotic pressure gradient across a semi-permeable membrane to drive water (or solvent) transport from a feed possessing low osmotic pressure to the draw solution with high osmotic pressure [1]. FO process continues until an equilibrium is attained, as illustrated in Fig. 1.1.

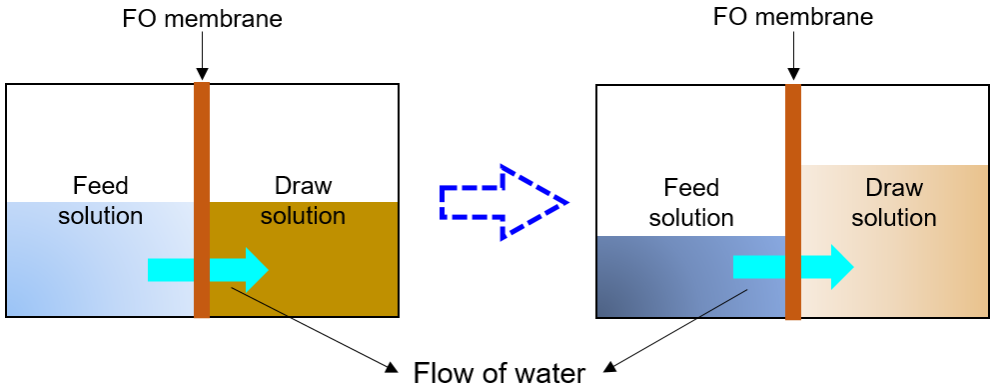

Fig. 1.1. Schematic of FO process.

Utilizing the same principle, OSFO, proposed and described in detail by Lively and Sholl [2], can concurrently concentrate the pharmaceutical products in the feed side while transporting the organic solvent to the draw solution. Although the basic principles of FO and OSFO are similar, there are differences between their applications in water and organic solvents, respectively [3].

The process in a practical FO application includes a high-efficiency membrane separation unit and a draw solution recovery system, as illustrated in Fig. 1.2 below. The draw solute must be regenerated unless the diluted draw solution is the final product. Although a low or no hydraulic pressure is required for the FO separation unit, the regeneration of draw solutes may consume a considerable amount of energy, and a careful design and selection of a draw solute is needed for an efficient FO process [1].

1.2 Applications of FO

Applications of the FO technology cover a wide range, from bench-scale laboratory experiments to pilot-scale demonstrations in industries. FO is used in the food and beverage

industry, pharmaceutical and juice concentration, wastewater reclamation, brackish water/seawater desalination, fertigation in agriculture, zero liquid discharge (ZLD), and many other industrial processes [4]. Applications in newer areas, such as hydrogen production, are also being invented [5,6].

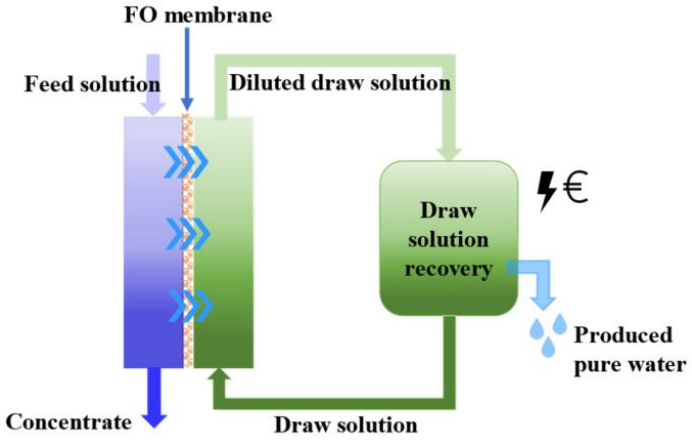

Fig. 1.2. FO system coupled with a draw solutes regeneration unit [1] "Reprinted from Membranes, 12, Tian, et al., Forward osmosis membranes: The significant roles of selective layer, 1-8, Copyright (2022), Licensee MDPI, Basel, Switzerland".

1.2.1 Desalination

In recent years, several hybrid FO systems have been incorporated into existing or combined processes, e.g., seawater/brackish water desalination. It replaces conventional pretreatment or post-treatment technologies to reduce the extra volume of industrial waste. The combination of FO and RO in a hybrid process, where FO uses a wastewater stream to dilute seawater before an RO step, is proven to be feasible (Fig. 1.3) [4,7,8].

Another promising approach to desalination is the hybrid process combining FO and membrane distillation (MD), leveraging the advantages of both technologies. FO uses a concentration gradient across a semi-permeable membrane, effectively separating impurities while operating at low hydraulic pressures [10,11]. This reduces energy consumption and fouling risks. The diluted draw solution from FO can then be treated by MD, which employs thermal energy to evaporate and condense water through a hydrophobic membrane, ensuring high salt rejection and water recovery (Fig. 1.4).

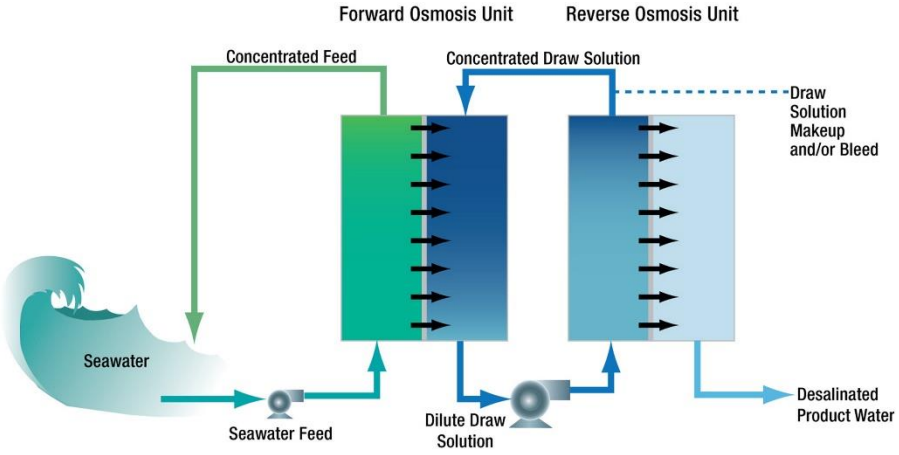

Fig. 1.3. An integrated FO and RO desalination process [9] "Reprinted from J. Membr. Sci., 415-416, Shaffer, et al., Seawater desalination for agriculture by integrated forward and reverse osmosis: Improved product water quality for potentially less energy, 1-8, Copyright (2012), with permission from Elsevier".

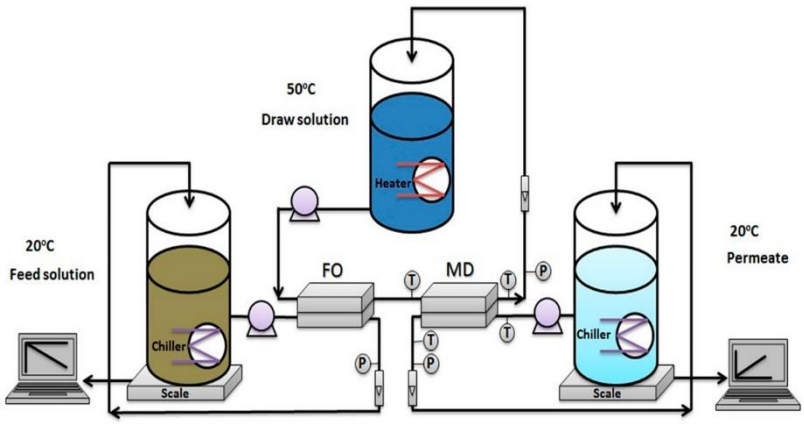

Fig. 1.4. Schematic diagram of the FO–MD bench-scale test unit [10] "Reprinted from Ind. Eng. Chem. Res., 58, Al-Furaiji, et al., Use of a forward osmosis−membrane distillation integrated process in the treatment of high-salinity oily wastewater, 956−962. Copyright © 2019 with permission from American Chemical Society."

1.2.2 Wastewater treatment

The municipal wastewater was treated by FO using seawater concentrate as DS [12]. This simultaneously achieved the sewage concentration and brine dilution. The RO concentrate is a potential DS candidate in the FO process since i) the high salt concentration (i.e., high osmotic pressure) offers enhanced permeation flux, thus high-water recovery in a shorter running time, and ii) the dilution by FO would reduce the environmental impact of discharging.

Coupling FO and MD was reported for its applicability to treat flue gas desulfurization (FGD) wastewater under conditions expected at coal-fired power plants (Fig. 1.5) [13]. The growing demand for freshwater, increasing frequency of water shortages, strict environmental regulations, and a need for sustainable development make the ZLD technology a valuable wastewater treatment option. Owing to these reasons, there has been a substantial investment in ZLD technology. FO is becoming an attractive salt-concentrating technique [4]. Thus, it is

becoming an inherent part of ZLD technology for further concentrating the wastewater after the RO stage. The produced brine is sent to a brine crystallizer or an evaporation pond, whereas the draw solutes are separated from the desalinated water to regenerate the concentrated draw solution. Since the driving force in FO is osmotic pressure, it can treat water with much higher salinity than RO. By using FO to concentrate feedwater beyond the salinity limit of RO, the osmotic pressure of the diluted draw solution surpasses the bearable pressure limit of RO (Fig. 1.6) [14].

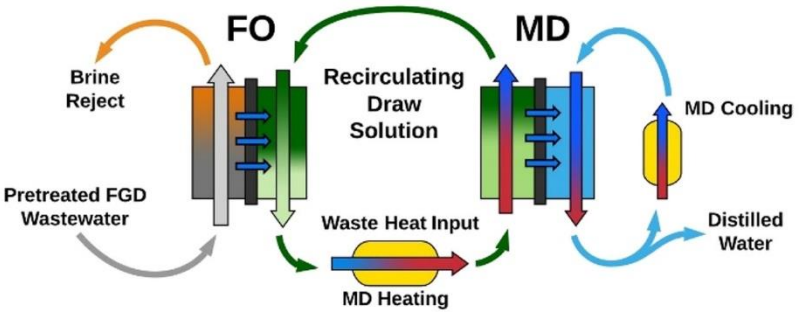

Fig. 1.5. FO–MD setup FGD wastewater [13] "Reprinted from Energy Fuels, 35, Anderson, et al., Forward osmosis-membrane distillation process for zero liquid discharge of flue gas desulfurization wastewater, 5130-5140. Copyright © 2021 with permission from American Chemical Society".

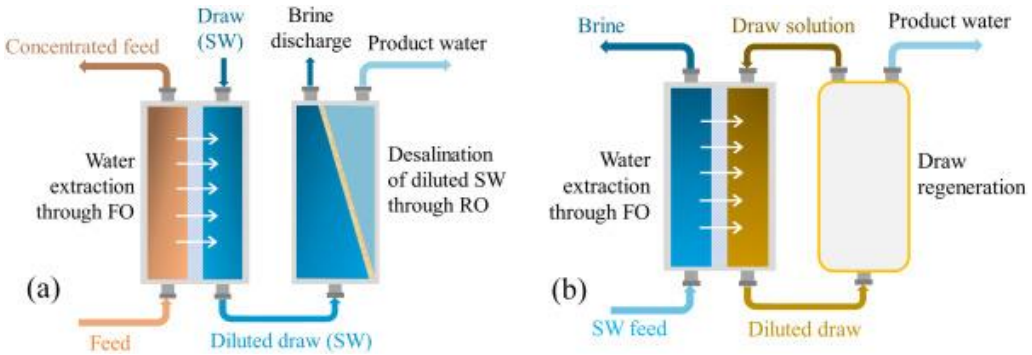

Fig. 1.6. Operational configurations of FO-RO hybrid system (a) open-loop, (b) closed-loop [15] "Reprinted from Desal., 585, Yalamanchili, et al., Can a forward osmosis-reverse osmosis hybrid system achieve 90 % wastewater recovery and desalination energy below 1 kWh/m3? A design and simulation study, 1-8, Copyright (2024), with permission from Elsevier".

The world's first FO-based ZLD system was successfully constructed at the Changxing power plant in Zhejiang Province, China [14]. The system treats a mixture of FGD wastewater and cooling tower blowdown at 650 m^3/day. The RO initially concentrates feedwater to ~60000 mg L^{-1}. The NH_3/CO_2 FO process is then used as a brine concentrator to further concentrate the RO brine above 220000 mg L^{-1} of TDS. As the last step, the FO brine is fed to a crystallizer for further concentration. At the same time, a high-quality product water (TDS < 100 mg L^{-1} after polishing by a secondary RO) is produced for reuse as boiler makeup water.

1.2.3 Agricultural irrigation/fertigation

The fertigation is an agricultural irrigation process employed on a wide scale where water-soluble fertilizers are added to the irrigation water to improve and enhance crop yield. In the concept of fertilizer-drawn FO (FDFO), fertilizers are used as draw solutions (DS). FDFO is a potential alternative to recover and reuse water and nutrients from agricultural wastewater, such as palm oil mill effluent, which consists of 95% water and is rich in nutrients [16].

The diluted draw solution after FO can be directly used for fertigation without the need for recovery and regeneration of DS as it contains essential plant nutrients (Fig. 1.7) [17][. In FDFO, the final nutrient concentration (nitrogen, phosphorus, potassium, NPK) in the product water is essential for direct fertigation to avoid over-fertilization [18]. Various fertilizers, e.g., ammonium sulfate ($(NH_4)_2SO_4$), ammonium nitrate (NH_4NO_3), monoammonium phosphate (MAP), diammonium phosphate (DAP), potassium chloride (KCl), and potassium nitrate (KNO_3) were demonstrated as DS [16].

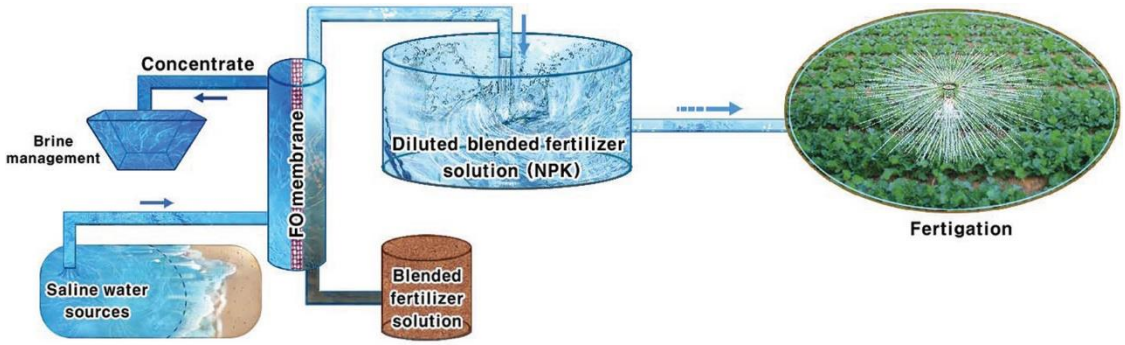

Fig. 1.7. FDFO desalination process using DS containing mixtures of blended [19] "Reprinted from Environ. Sci. Technol., 46, Phuntsho, et al., Blended fertilizers as draw solutions for fertilizer-drawn forward osmosis desalination, 4567−4575. Copyright © 2012 with permission from American Chemical Society".

1.2.4 Food processing and dairy industries

The food processing/preservation processes need to maintain the fresh-like properties of food. They also need to have an appropriate shelf life to maintain nutritional value. Since consumers demand quality food with natural flavor and taste, the use of additives or preservatives needs to be avoided. These aspects necessitated the use of membrane-based approaches (non-thermal), to concentrate liquid foods. Among them, FO has proven to be the most valuable one. Its novel features, such as liquid food concentration at room temperature without membrane fouling, made the FO technology attractive [20]. A potential is to concentrate streams >20 fold with a high rejection and preservation of added-value products [21].

In producing fruit juices, milk/concentrated skim milk using FO, the feed stream is demonstrated to concentrate [4]. In this process, the water goes into the draw side since it is not important as a product. This makes the draw solution regeneration in dairy processing more practical and feasible than in the desalination processes (Fig. 1.8).

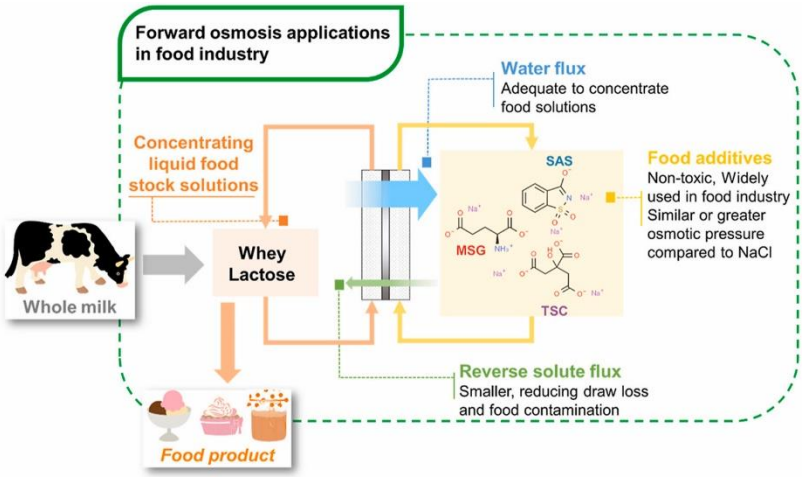

Fig. 1.8. Schematic of FO application in food industries [22] "Reprinted from J. Membr. Sci., 638, Yang, et al., Enhancing the applicability of forward osmosis membrane process utilizing food additives as draw solutes, 119705-119713, Copyright (2021), with permission from Elsevier".

1.2.5 Chemical industries

The FO has great potential in the chemical industry. Treatment of wastewater from esterification is reported [23]. Total organic carbon (TOC) rejection was shown to be high (> 96%), and water recovery was shown as 57.1%. In another FO study, wastewater from ammonia absorption processes was used as DS [24]. This wastewater contained high sulfate and ammonia conc., thus exhibiting high osmotic pressure. It is widely reported that organic acids (acetic acid, succinic acid, alpha-ketoglutaric acid, lactic acid, butyric acid, and valeric acid) produced by fermentation could be concentrated by FO treatment [25-28]. Alpha-ketoglutaric acid (AKG) is a biological compound, It is found in the human body. Its vital role in the tricarboxylic acid cycle by releasing stored energy into the body is known [28]. AKG can only be synthesized from inessential amino acids from the body. It is generally used as a supplement, in the form of tablets [28]. Carboxylic acids are extensively used as the basic building block chemicals in various types of industries, viz., pharmaceuticals and chemical, beverages, etc. Acetic acid is essential in synthesizing cellulose acetate, printing, textile, dyeing, and food industries [25]. Acetic acid-containing wastewater is usually discharged from various manufacturing processes, e.g., cellulose acetate, acetic anhydride, terephthalic acid (as solvent), dimethyl phthalate, isophthalic acid, etc. [29]. The concentration of acetic acid in the wastewater discharged is usually < 5 wt.%, and such streams can be treated using FO.

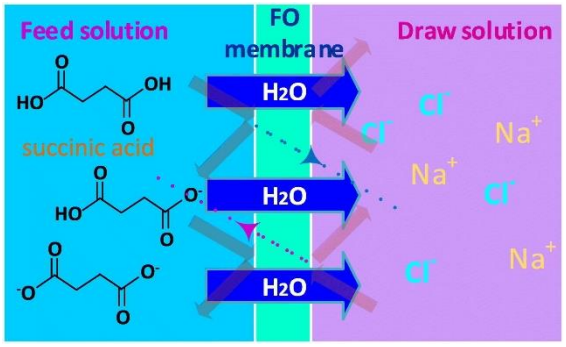

Fig. 1.9. Carboxylic acid concentration by FO [27] "Reprinted from Chin. J. Chem. Eng., 26, Law, et al., Osmotic concentration of succinic acid by forward osmosis: Influence of feed solution pH and evaluation of seawater as draw solution, 976-983, Copyright (2019), with permission from Elsevier".

1.2.6 Emergency drinks

The demand for clean and fresh water during emergencies/calamities is usually elevated in comparison to normal conditions due to the anticipated/unanticipated interruptions of public utilities. Still, the water quality needs to be maintained in order to meet the standards. Alternative methods to provide clean drinking water during such insurgencies are needed (disaster areas, conflict zones, water crises, and other emergencies). An FO-based filter was assembled in a water filter bag made up of polypropylene and aluminum foil (Fig. 1.10) [30]. The brackish water was used as feed, while the draw solution (DS) was made up of fructose, sucrose, or their mixture. The DS concentration used was 3 mol L^{-1}.

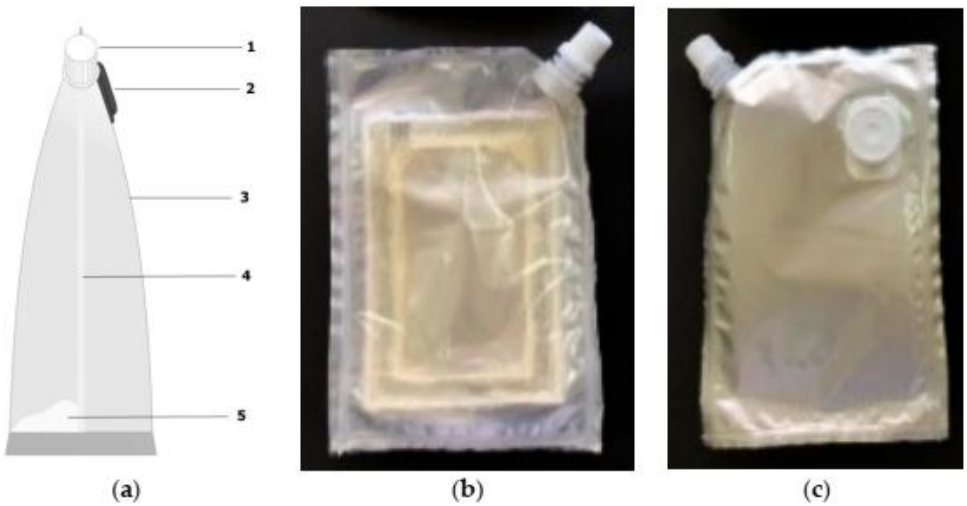

Fig. 1.10. (a) Water bag design (1 = the lid on the front of the bag, 2 = the lid on the back of the bag, 3 = polypropylene plastic, 4 = chitosan-starch membrane, 5 = draw solution), with the photographs of (b) the front side and (c) backside of the bag [30] "Reprinted from Membranes, 10, Saiful, et al., Development of chitosan/starch-based forward osmosis water filtration bags for emergency water supply, 414-426, Copyright (2020), Licensee MDPI, Basel, Switzerland".

Another technology, named as 'point-of-use water treatment' (PoUWT technology) is Hydration Technology Innovations'™ (HTI's) demonstrated for osmotic water purification

[31]. It produces a clean sugar–electrolyte drink from almost any water source. This drink not only hydrates users but also relieves malnutrition and diarrheal illness, two of the most prolific killers in refugee camps and disaster relief scenarios.

1.2.7 Pharmaceutical industries

The synthesis of APIs involves multi-step molecular constructions while synthesizing target compounds. Different organic solvents are used in various steps. Thus, purification is required for pharmaceuticals and their intermediates, which usually contain multi-stage systems. This makes the removal of organic solvents necessary, which is considered to be an essential step in pharmaceutical industries. Usually, most of the waste solvents are sent to incineration, as solvent recovery by conventional methods such as distillation is a costly affair. Owing to stricter environmental legislations and increasing prices of organic solvents, their recovery is becoming highly important. Furthermore, most pharmaceutical compounds are temperature-sensitive. At high temperatures, they may decompose or de-nature. Thus, the simultaneous concentration of the pharmaceutical products and recovery of solvent are becoming highly necessary [3]. As shown in Fig. 1.11, the OSFO process has a high potential to concentrate the active pharmaceutical ingredients (APIs) and also recover the organic solvents. Various draw solutes, viz., lithium chloride, citric acid, polyethylene glycol-400/-1000, methyl palmitate, and diethanolamine are proposed for OSFO [32]. Recovery of various solvents, e.g., methanol, ethanol, isopropanol, acetone, *N*,*N*-dimethylformamide, and hexane, is demonstrated using OSFO [3,33-38,32].

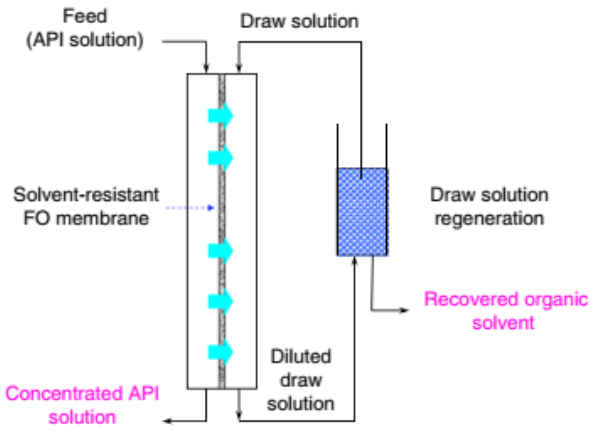

Fig. 1.11. Schematic diagram of a FO process for organic solvent recovery [3].

1.2.8 Metal recovery

The electronics industry generates wastewater containing valuable heavy metals. They may be toxic and pose significant risks. Moreover, the presence of heavy metals in water is becoming a severe environmental issue as their use in various industrial processes is increasing

exponentially. The FO-based concentration is emerging as a promising application for this industrial sector. The precious metal recovery from printed circuit board (PCB) wastewater is reported [39]. This process uses a dilution-needed waste solution as a DS (draw solution). Thus, an external supply of DS and a re-concentration process for the diluted draw solution are eliminated. FO experiments were demonstrated using a Pd-catalyst solution needing concentration [39]. This work demonstrates a major success in the effective Pd-solution concentration. An electroless (E'less) nickel plating solution was evaluated as a dilution-needed waste stream-based draw solution, and the test results confirmed that the selected Ni solution could produce an acceptable FO performance. Since heavy metals cannot be metabolized by the body or decomposed naturally, they tend to accumulate inside the body, causing severe body dysfunction [40]. This article successfully demonstrated the removal of six heavy metal solutions ($Na_2Cr_2O_7$, $Pb(NO_3)_2$, $CdCl_2$, Na_2HAsO_4, $CuSO_4$, and $Hg(NO_3)_2$) using the FO process.

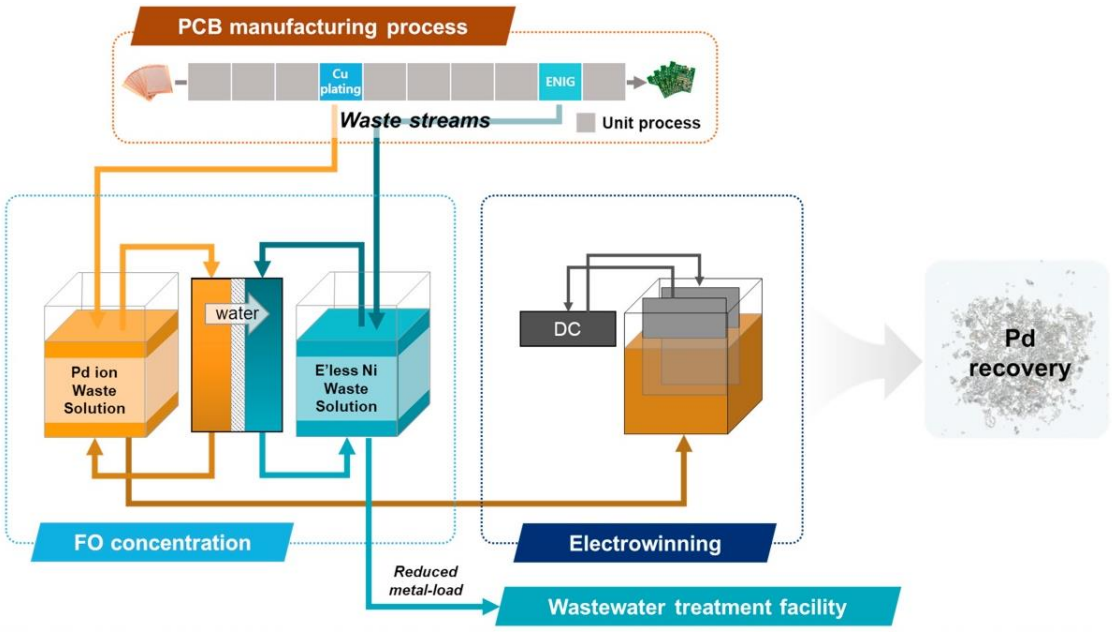

Fig. 1.12. Conceptual diagram of a FO-based system for precious metal (Pd) recovery [39]
"Reprinted from J. Membr. Sci., 552, Gwak, et al., New industrial application of forward osmosis (FO): Precious metal recovery from printed circuit board (PCB) plant wastewater, 234-242, Copyright (2018), with permission from Elsevier".

1.3 Membrane materials for FO and their morphology

The flat sheet as well as hollow fiber membrane forms are demonstrated for FO. They can be classified into single-layer, dual-layer, double-skinned, impregnated, and the biomimetic membranes. The membrane fabrication process is highly important for attaining high performance [41]. An efficient FO membrane needs to be mechanically stable, chemical

resistant, and resistant to fouling [4]. There are two types of FO membranes based on the structural difference: integrally skinned asymmetric membranes and thin-film composite (TFC) membranes, as shown in Fig. 1.13.

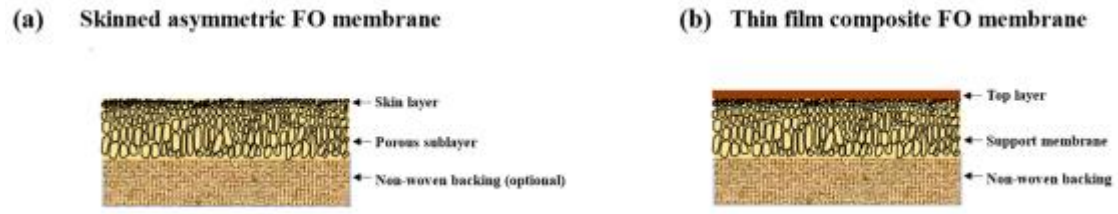

Fig. 1.13. Illustration of the structure disparity of (a) skinned asymmetric membrane and (b) TFC membrane [1] "Reprinted from Membranes, 12, Tian, et al., Forward osmosis membranes: the significant roles of selective layer, 955-976, Copyright (2022), Licensee MDPI, Basel, Switzerland".

1.3.1 Asymmetric membranes

An asymmetric membrane combines a thin separation layer (skin) with a high permeable support layer, made up of a single polymer material. The dense skin layer is thin (0.1 to 1 µm) and is present on the top of a thicker (100 to 200 µm) porous support [42]. Most FO process investigations were performed using CA (cellulose acetate)-based RO membranes and CTA (cellulose triacetate))-based FO membranes. Francis et al. [4] found that water flux was much lower than anticipated values due to various reasons, e.g., internal and external concentration polarization [43]. The most common method used to fabricate asymmetric FO membrane is the non-solvent-induced wet phase inversion (NIPS), demonstrated by Loeb and Sourirajan [44,45]. The early study of FO membranes employed RO membranes of hydrophilic cellulose acetate (CA) and/or cellulose triacetate (CTA) polymers as low-cost and readily available materials [46-50]. In addition to CA or CTA, other commonly explored FO asymmetric materials include polyethersulfone (PES) and polybenzimidazole (PBI) [51-54]. All these membranes are asymmetric in nature (Fig. 1.13a).

1.3.2 Thin film composite (TFC) membranes

Cadotte et al. introduced the TFC membrane preparation on porous support via interfacial polymerization (IP) [55]. In the TFC membrane type, thin film is developed on the porous substrate by an in-situ IP reaction between two monomer solutions, viz., aqueous di/trifunctional amines and acid chloride [56] (Fig. 1.13b). The TFC structure is characterized by a thin, smooth, and hydrophilic selective layer atop a microporous substrate. The selective layer is crucial for (1) preventing the forward diffusion of feed solutes, (2) preventing fouling, and (3) inhibiting a reverse diffusion of the draw solutes [57]. The FO membranes were fabricated using polyamide TFC membrane via interfacial polymerization (IP) on various

substrates (cellulose acetate propionate (CAP), polysulfone (Psf), and non-woven electrospun nanofibrous) [58-61,41]. The asymmetric type is studied less in the literature than the counterpart TFC type. TFC membranes show better FO process performance than that of cellulose-based membranes.

The FO performance is usually characterized by various parameters, including water permeance (A), solute permeability coefficient (B), structural parameter (S values) of the membrane, etc. These depend on the membrane structure and the type of solute [4]. Conversely, the substrate should possess a minimal 'S' value to facilitate the diffusion of draw solutes within its inner pores. It leads to the reduction in the transport resistance of water and draw solutes. The hydrophilicity of the substrate needs to be taken into account during the FO membrane design/fabrication for diffusing draw solute from the porous layer. This is more important when the draw solute used is of large molecular weight, such as polymer or ionic liquids [57]. The major focus is to minimize the support S-values via the in tortuosity, thickness, and increase in the porosity. Reducing the thickness beyond a certain level could compromise the mechanical integrity of the membrane [62]. The TFC membrane has a smaller 'S' value and higher 'A' value than that of asymmetric membranes. This is due to the two-step preparation of the substrate and rejection layer, which enables the optimization of the two layers individually [1]. In order to enhance the FO performance by tuning the membrane structural parameters, researchers introduced various advancements via chemical/physical membrane modifications and by employing novel membrane materials and draw solutions [4]. To enhance membrane performance, nanomaterials are also demonstrated, including silica nanoparticles [63], carbon nanotubes (CNTs) [64], graphene oxide (GO) [65], metal-organic framework (MOF) [66,67], covalent organic framework (COF) [68]. These material are incorporated into the selective layer of the TFC membrane to form thin film nanocomposite (TFN) membranes (Fig. 1.14).

A support layer of the asymmetric TFC membrane poses structural resistance (concentration polarization) [70]. It significantly undermines the engineered osmosis. Increasing porosity, reducing thickness as well as tortuosity of the support layer reduces structural resistance. However, internal concentration polarization (ICP) still impacts the membrane performance. The impact of internal concentration polarization on the FO water flux can be very severe, sometimes leading to a decrease in water flux over 80% [4]. To address this issue, using support layer-free thin films with a symmetric and homogeneous structure merits attention (Fig. 1.15) [71].

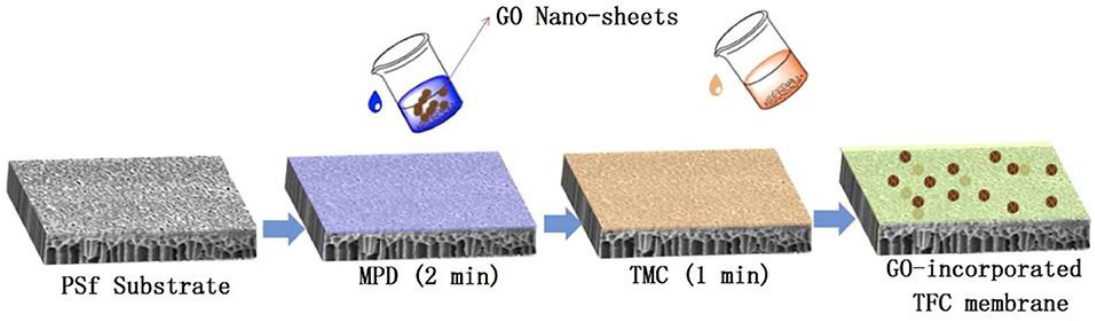

Fig. 1.14. The preparation procedures of GO-incorporated TFC membranes [69] "Reprinted from Front. Chem., 7, Li, et al., Forward osmosis membranes with enhanced desalination performance and chlorine resistance, 877-888, Copyright (2020), Licensee Frontiers in Chemistry".

1.3.3 Symmetric membranes

Freely suspended ultrathin membranes remained a theoretical and experimental curiosity for several decades [72,73]. With macroscopic size and infinitesimal thickness, they are capable of combining properties of macroscopic materials and individual molecules. Moreover, interference from the support layer is now absent, a free-standing structure could make the thin membrane highly important for practical applications [74,73]. By removing the support layer, a self-standing nanofilm becomes attractive as a FO membrane [75]. It is looked at as a promising water treatment process, which would have much lower energy consumption and much less membrane fouling than the pressure-driven membrane processes.

The concept of an FO membrane wherein internal concentration polarization can be absent was proposed in nanoporous graphene. The FO membrane of monolayer graphene was studied using molecular dynamic (MD) simulations [76]. There are many reports wherein the support-free, symmetric nonporous membranes are explored for FO [77,78,75,71,79,80,70] and PRO applications [81]. The membrane materials for support-free membranes and their preparation methods are summarized in Table 1.1.

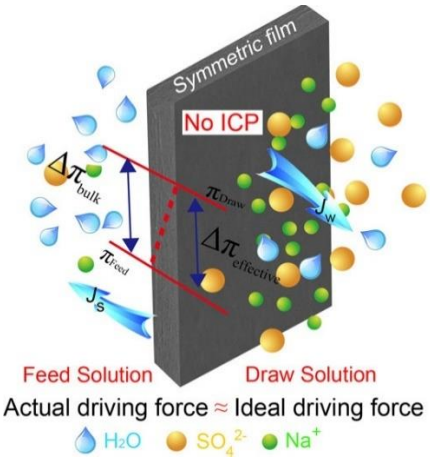

Fig. 1.15. Support free self-standing FO membrane [71] "Reprinted from Environ. Sci. Technol. Lett., 5, Li, et al., A self-standing, support-free membrane for forward osmosis with no internal concentration polarization, 266-271. Copyright © 2018 with permission from American Chemical Society".

Table 1.1. Symmetric FO membrane and their method of preparation

Membrane material	**Preparation method**	**Ref.**
Sulfonated polyether ketone (SPEK)	Solvent evaporation	[70]
Polytriazole-co-oxadiazole-cohydrazide (PTAODH)	Solvent evaporation	[71]
Psf doped with sPsf	Solvent evaporation	[75]
Reduced GO (rGO)	Vacuum filtration	[77]
Polyamide	IP	[78]
Sulfonated PBI	Solvent evaporation	[79]
PA	IP	[80]
Polyacrylamide hydrogels	Track-Etching	[81]

1.4 Draw solutions

The osmotic agent, also termed as the draw solution (DS), provides the driving force to the FO process. It plays an important role in obtaining the high efficiency of a FO process. It is responsible for water transport from the feed solution (FS) through a semi-permeable membrane [82]**.** The product of an FO process is not pure water, but it is a diluted draw solution. Therefore, another process is needed to regenerate the draw solution and simultaneously produce pure water. There are some exceptions where the second process of draw solution regeneration becomes unnecessary [4]. The diluted draw solution can be directly used or discharged if the FO process is employed to concentrate the feed solutions rather than to produce pure water (Fig. 1.16).

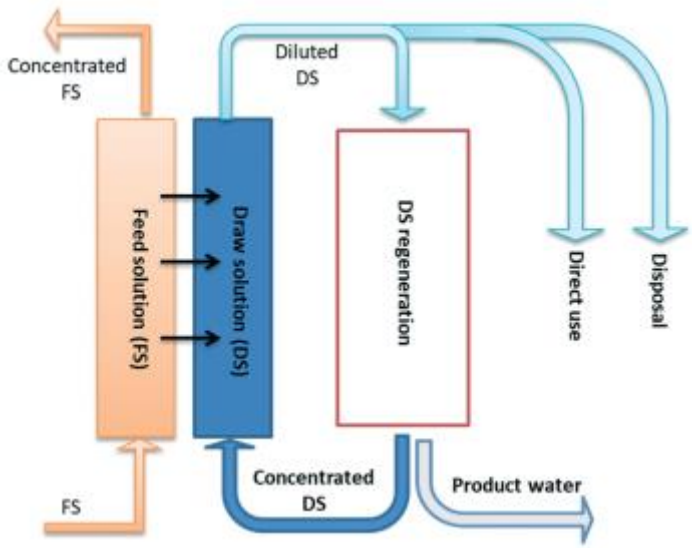

Fig. 1.16. Schematic diagram of FO draw solutions with different handling approaches, including regeneration, direct use, and disposal [4] "Reprinted from Environ. Sci.: Water Res. Technol., 6, Francis, et al., A comprehensive review of forward osmosis and niche applications, 266-271. Copyright © 2020 with permission from Royal Society of Chemistry".

An ideal DS must meet various criteria to drive the FO process, as listed below [83].

(i) Ability to generate high enough osmotic pressure. It should possess high solubility in solvent (water or organic solvent) so that the osmotic pressure can be regulated.

(ii) Its solution should have low viscosity to facilitate easy pumping throughout the system (and improve water flux).

(iii) It should exhibit a low reverse solute flux. The molecular size and shape become important for this factor.

(iv) No toxicity: Any such issue of the draw solute will be a great concern. It is highly risky if the finished product water gets contaminated.

(v) Availability in large quantities.

(vi) It should be available at a low price.

Different draw solutions are demonstrated for the FO process. They can be classified into four categories: inorganic, organic, ionic liquids, and polymeric draw solutions, as elaborated briefly in the following sections.

1.4.1 Inorganic draw solutions

Among inorganic salts, sodium chloride (NaCl) is a widely used draw solute. It has high solubility in water. They usually possess high osmotic pressure, lower cost, and negligible toxicity. However, the low molecular weight of sodium chloride leads to high reverse solute flux. This results in the leakage of the draw solute in the feed solution, reduces osmotic pressure gradient, FS pollution, and other passive effects on FO process. The solute recovery methods of NaCl include distillation, RO, electrodialysis, etc. The recovery methods consume high amounts of energy [84]. Other than NaCl solution, KCl, KNO_3, NH_4Cl, KBr, Na_2SO_4, $MgCl_2$, $CaCl_2$, $MgSO_4$, $NaNO_3$, NH_4NO_3, and $Ca(NO_3)_2$ solutions are commonly demonstrated draw solutions [85-87]. Some of the characteristics of the inorganic draw solutions reported in the literature are given in Table 1.2.

Table 1.2. Physicochemical characteristics of inorganic compound-based draw solutions

Draw solute	Concentration	Osmotic pressure	Regeneration method	Ref.
$(NH_4)_2SO_4$	2 mol L^{-1}	92.1 atm	Direct fertigation	[17]
$NH_4H_2PO_4$	2 mol L^{-1}	86.3 atm	Direct fertigation	
$(NH_4)_2HPO_4$	2 mol L^{-1}	95 atm	Direct fertigation	
NaCl	0.5 mol L^{-1}	0.50 bar	-	[85]
$MgCl_2$	1 mol L^{-1}	73.5 bar	-	
Na_2SO_4	1 mol L^{-1}	73.5 bar	-	
KCl	2 mol L^{-1}	98.1 bar	Direct fertigation	
$Mg(NO_3)_2$	1 mol L^{-1}	84 bar	Direct fertigation	[86]
$MgSO_4$	2 mol L^{-1}	54.8 bar	Direct fertigation	
NH_4Cl	0.5 mol L^{-1}	21.881 atm	-	[87]
$NaNO_3$	0.5 mol L^{-1}	21.3 atm	-	
KNO_3	0.5 mol L^{-1}	20.125 atm	-	
NH_4NO_3	0.5 mol L^{-1}	17.764 atm	-	
$Ca(NO_3)_2$	0.5 mol L^{-1}	26.491 atm	-	
$CaCl_2$	0.5 mol L^{-1}	34.983 atm	-	
NH_4HCO_3	3.6 mol L^{-1}	100 atm	Moderate heating	[88]
$KHCO_3$	1.4 mol L^{-1}	2.8 MPa	RO	[89]
KBr	0.6 mol L^{-1}	2.8 MPa	RO	
$NaHCO_3$	0.72 mol L^{-1}	26.91 bar	-	[90]
NaH_2PO_4	22 g L^{-1}	23.73 bar	Direct fertigation	[91]

1.4.2 Organic draw solutions

Organic compounds, mostly glucose and fructose solutions, are demonstrated as draw solutions for seawater desalination by FO [92-94] and food production [95,96] applications. FO water filtration bags, demonstrated for emergency water supply, use fructose, sucrose, and fructose/sucrose mixture as draw solution [30]. Although organic draw solutes are usually nonelectrolyte in nature, they possess the potential to generate high osmotic pressure since they exhibit high solubility [83] (Table 1.3). The metal complexes of organic ligands are also demonstrated by Ge et al. and Cui et al. [97,40]. A series of Cu^{+2} and Fe^{+3} complexes using hydroxyl acids (malic acid, citric acid, and tartaric acid) as ligands were demonstrated. They possess a low reverse flux and easy solute regeneration in post-treatment. They can be designed freely according to the required functions by varying metals or ligands. Such characteristics make complexes appropriate candidates to be draw solutes.

Table 1.3. Physicochemical characteristics of organic compound-based draw solutions

Draw solute	Concentration	Osmotic pressure (atm)	Regeneration method	Ref.
Cobaltic complex (Na-Co-CA)	1 mol L^{-1}	45	MD or NF	[40]
Glucose	2 mol L^{-1}	55.03	Direct use	[83]
Fructose		55.02		
Sucrose	2 mol L^{-1}	56.81		[98]
Cu complex (Cu-CA)	2 mol L^{-1}	62	-	[97]
Fe complex (Fe-CA)	2 mol L^{-1}	105	-	

1.4.3 Ionic liquids (IL)

The ILs are molten salts that are archetypally liquid at <100°C, in atmospheric pressure. They have unique properties, including high negligible vapor pressure, chemical and thermal stability, ionic conductivity, and solubility, and are non-flammable in nature[99,100]. Thermo-responsive ILs seem to be prominent candidates as they usually possess high osmotic pressure [101]. Thermo-responsive ILs can be used as draw solutes that consist of lower critical solution temperature (LCST) and upper critical solution temperature (UCST) [102,103]. The critical solution temperature is where the ionic liquid and water separate into two phases. The LCST-type ionic liquid reaches its critical solution temperature with the increase in temperature. These ILs are in a two-phase state above this temperature (a min. temperature at which they are separated into two phases) (Fig. 1.17). The UCST-type ILs reach their transition temperature by increasing the temperature of these materials. Such ILs are in soluble state above this temperature (the min. temperature at which they begin to merge into one phase) (Fig. 1.17) [104].

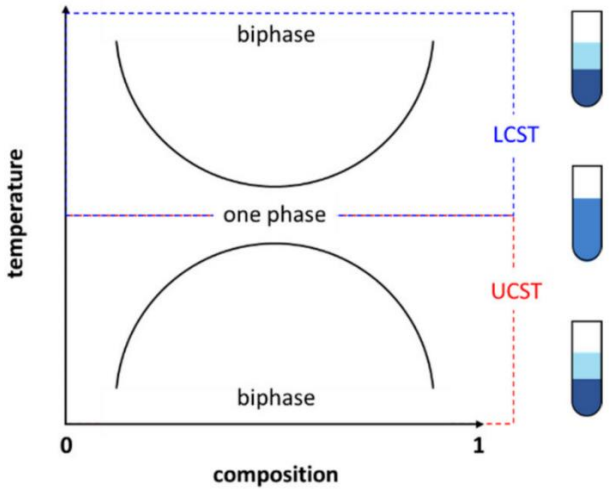

Fig. 1.17. Schematic representation of a phase diagram showing the UCST (red) and LCST (blue) for thermos-responsive ionic liquid materials [104]. "Reprinted from Molecules, 28(19), Li et al., Expeditious discovery of small-molecule thermos-responsive ionic liquid materials: a review, 6817-6839, Copyright (2023), Licensee MDPI, Basel, Switzerland".

Table 1.4. Physicochemical characteristics of ionic liquid-based draw solutions

Draw solute	Concentration	Osmotic pressure	Regeneration method	Ref.
[Hbet][Tf_2 N]	3.2 mol L^{-1}	-	Cooling at 23 °C	[102]
[P_{4444}][DMBS]	0.96 mol L^{-1}	511.4 osmol kg^{-1}	Heating (30 °C)	[105]
[P_{4444}][TMBS]	1.35 mol L^{-1}	508.6 osmol kg^{-1}	Heating (30 °C)	
[N_{4444}][TMBS]	0.75 mol L^{-1}	516.6 osmol kg^{-1}	Heating (50 °C)	
[N_{4444}][DMBS]	0.42 mol L^{-1}	503.8 osmol kg^{-1}	-	
[N_{4444}][CF_3COO]	0.24 mol L^{-1}	511.0 osmol kg^{-1}	Heating at 70 °C	
[BMIM][BF_4]	0.087 mol L^{-1}	-	Cooling 4-6 °C	[106]

1.4.4 Polymeric draw solutions

The polymeric draw solutes were also employed as a draw solution because of their high molecular weight and easy recovery possible in an ultrafiltration (UF) process. The polyelectrolytes of different molecular weights, (poly(sodium-*4*-styrene sulfonate), PSS)) were demonstrated as DS at varying concentrations. They could be easily recycled by a a simple ultrafiltration (UF) membrane system using 2 bars of pressure [107]. Polymeric hydrogels have attracted attention as a draw solution due to their high capacity to absorb water and low reverse solute flux [108].

Table 1.5. Physicochemical characteristics of polymeric draw solutions utilized in FO applications

Draw solute	Concentration	Osmotic pressure	Regeneration method	Ref.
Poly(aspartic acid sodium salt) (PAsp-Na)	0.3 g ml^{-1}	51.5 atm	MD and NF	[39]
Poly(sodium4-styrene sulfonate) (PSS (Mw = 1200))	0.24 g ml^{-1}	-	UF	[107]
Sodium salt of polyacrylic acid (PAA-Na (Mw= 1200))	0.72 g L^{-1}	44 atm	UF	[109]
Polyamidoamine with terminal carboxyl groups (PAMAM-COONa (2.5 G))	0.5 g ml^{-1}	3603 mOsm Kg^{-1}	MD	[110]
Poly(isobutylene-altmaleic acid) sodium salt (PIMA-Na)	0.375 g ml^{-1}	-	MD	[111]
Poly(maleic acid) sodium (PMAS)	0.5 mol Kg^{-1}	143 bar	NF	[112]
Thermo-responsive (PNIPAM /γ-PGA/PEG)hydrogel	-	-	Heating at 40 °C	[113]

1.5 Concentration polarization (CP)

Although FO processes have advantages, they face significant challenges. The CP and reverse diffusion of the draw solute are the major ones. During FO operation, the draw solute near the membrane surface gets diluted (because water passes through the membrane). These solutes can also be trapped in the porous structure of the membrane support layer during their diffusion. This movement of solute is related to a primary transport phenomenon, the CP effect, which can cause the reduction in osmotic pressure difference and consequently reduce the water flux. The CP can be categorized into external concentration polarization (ECP, which happens at the membrane surface) and internal concentration polarization (ICP, which is within the membrane support layer) [85].

An external concentration polarization, ECP, occurs using a symmetric dense membrane (Fig. 1.18). When the water from FS (feed solution) passes through the permeable membrane to the DS (draw solution) side, the solute accumulates on the feed side surface of the dense membrane, thereby inducing 'concentrative' ECP. Conversely, as the DS side absorbs water from the FS, the solution in the vicinity of the membrane on the draw side is diluted significantly, thereby inducing 'dilutive' ECP. Experimental studies showed that increasing flow rate disturbs the membrane's vicinity, leading to a reduction in the ECP [114].

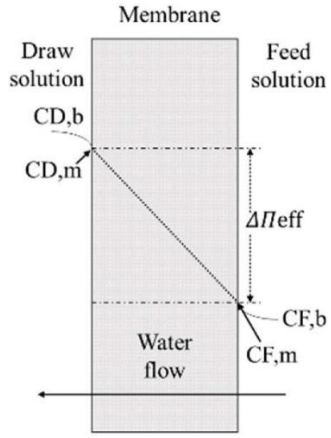

Fig. 1.18. Schematic illustration of ECP in the symmetrical dense FO membrane [114] "Reprinted from Int. J. Environ. Res. Public Health, 19, Xu, et al., A comprehensive review on forward osmosis water treatment: recent advances and prospects of membranes and draw solutes, 8215-8252, Copyright (2022), Licensee MDPI, Basel, Switzerland".

The ICP is characterized by differing solute concentrations at the transverse boundaries of that layer. As a result, the osmotic pressure gradient across the active layer of the membrane is reduced, leading to a decrease in water flux [115]. When the feed solution faces the active layer, and the draw solution faces the support layer, the ICP occurs on the permeate side (draw side). This is called 'dilutive' ICP, as the draw solution gets diluted by the permeated water within the porous support layer of the membrane [116]. The 'dilutive' ICP is illustrated in Fig.

1.19. When the feed solution faces the porous support layer of an asymmetric membrane, the solute in the feed gets concentrated in the porous support layer (than its bulk concentration) as water diffuses across the active layer into the draw solution. This is termed as concentrative ICP [116]. It is further illustrated in Fig. 1.19 (right side).

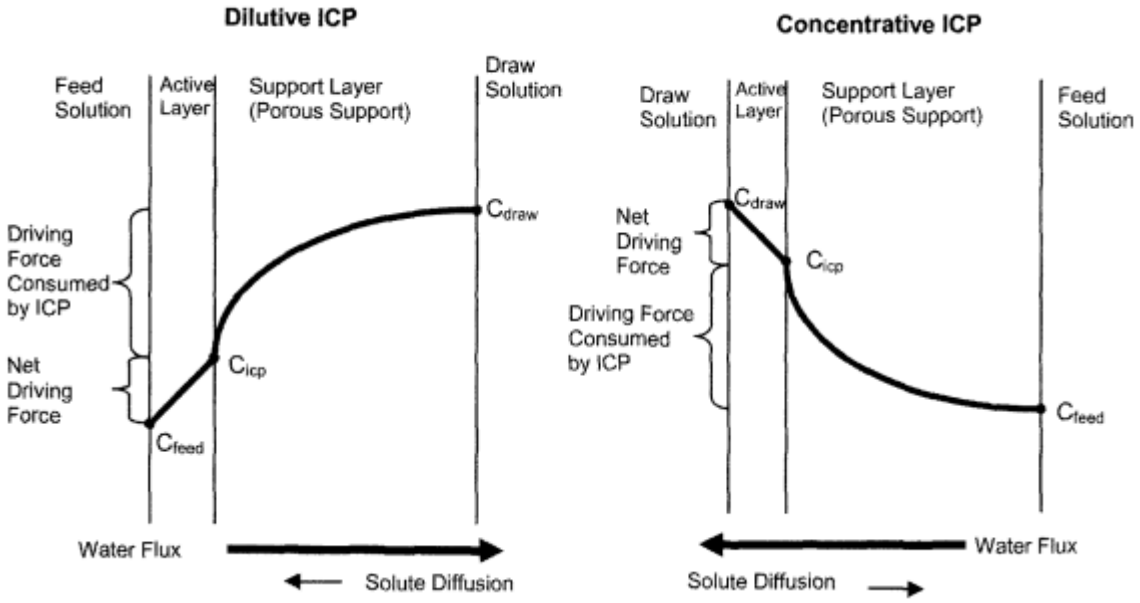

Fig. 1.19. Schematic representation of dilutive ICP (left) and concentrative ICP (right) [115]
"Reprinted from Desal., 197, Gray, et al., Internal concentration polarization in forward osmosis: Role of membrane orientation, 1-3, Copyright (2006), with permission from Elsevier".

A membrane substrate structure parameter (S = thickness x tortuosity/porosity) is reported to benefit the reduction in ICP [77]. The substrate should be thin and highly porous. It should possess well-interconnected pores to facilitate the solute diffusion from the DS to the selective layer and yet have adequate chemical, mechanical, and thermal stability to withstand industrial operations. Increased hydrophilicity/wettability of the substrate is used to mitigate ICP.

1.6 Scope of the present work

The present work focuses on investigating new membrane materials for FO, a crucial membrane application that is picking up quickly. One important arm, OSFO, would find a niche role in pharmaceutical and chemical industries if solvent-stable membranes are demonstrated. The membrane material requirements include thermo-mechanical and solvent stability, appropriate flux and rejection properties, etc. Polybenzimidazoles (PBI) as a family of materials look attractive, wherein the initial two properties are well fulfilled in a stringent application of proton exchange membrane bases fuel cells (PEMFC). Although the common PBI (based on isophthalic acid and *3,3'*-diaminobenzidine) is demonstrated for FO, other structural variants of this family of polymers need attention. One of the polymers of this family

is poly(2,5-benzimidazole), commonly known as ABPBI. Its better thermomechanical stability than common PBI and applicability as a promising membrane material for separation applications are documented by our group. Its peculiar properties, viz. high N-H group density, higher chain packing density, and insolubility in a wide range of solvents, deserve its investigation for FO and OSFO applications. It may be noted that the monomer used for polymerizing ABPBI, viz., *3,4*-diaminobenzoic acid, is cheaper, easier to polymerize, and non-carcinogenic than the monomer used for common PBI (*3,3'*-diaminobenzidine).

1.7 Aims of the present work

1) Investigate ABPBI as a membrane material for forward osmosis in two forms: hollow fiber and flat sheet.
2) Evaluate the practical applicability of these membranes for FO/OSFO while investigating necessary physical/transport properties.

These broader aims set the following objectives.

Objectives

1) Synthesize ABPBI polymer with high enough molecular weight.
2) Optimization of membrane preparation in hollow fiber and flat sheet form.
3) Investigating the FO performance of these membranes in (a) neutral and (b) acid-doped forms
4) Investigating the capability of ABPBI as a membrane material for OSFO: In addition to the reported DS, design a new draw solute that would widen the applicability of OSFO in various solvents, thereby addressing the needs of the pharma/chemical industries.
5) Investigating FO/OSFO for select model compounds to evaluate practical applicability.

1.9 Outline of the thesis

The thesis begins with an introduction covering a literature survey, followed by three working chapters and conclusions.

Chapter 1: This chapter briefly introduces the FO process and its various applications reported in the literature. This is followed by commonly used FO membranes and draw solutes. Current practices used for FO membrane preparation are briefly discussed. This chapter ends with the scope of the present work, aims, objectives, and the organization of the thesis.

Chapter 2: This chapter begins with preparing the hollow fiber membrane (HFM) by phase-inversion method using an MSA-based dope solution. The membranes in MSA-doped and neutral form treated at chosen temperatures were evaluated for FO. The performance was

determined in terms of water flux and reverse salt flux. In the end, the long-term performance of the HFM was assessed. Given the lower fluxes obtained for HFMs owing to their higher membrane thickness, it was decided to fabricate thin, mechanically stable membranes, as covered in the following Chapter.

Chapter 3: ABPBI-based flat sheet membranes (FSMs) were prepared using the phase inversion method and MSA-based dope solution. The membrane casting parameters were set to obtain a thinner membrane. The effect of membrane heat treatment on FO performance in terms of water and reverse solute flux was determined. A long-term FO experiment analyzed the integrity of the membrane. A systematic study on the applicability of these FO membranes for the concentration of industrially relevant acetic acid and methacrylic acid was carried out at the end.

Chapter 4: This chapter evaluates the applicability of the flat sheet ABPBI-based membranes treated at different temperatures for OSFO. Solvents of industrial significance (methanol, ethanol, acetonitrile, *N*,*N*-dimethylformamide, and dimethyl sulphoxide) were used. Although LiCl could be employed as a draw solute with methanol as a solvent, its limited solubility in organic solvents led to the use of a new, simple-to-synthesize and scalable acid-base salt, viz., triethylammonium benzoate (TB). A study on the effects of membrane treatment temperature on solvent flux, reverse salt flux, ability to use TB as draw solute with other solvents, long-duration analysis, and use of model organic compounds in the feed side provided promises of the applicability of present thin, scalable ABPBI membranes for OSFO.

Chapter 5: This Chapter summarizes the major conclusions of the present work. In the end, a thought on future directives for ABPBI-based membranes for FO applications is given.

1.10 References

[1] M. Tian, T. Ma, K. Goh, Z. Pei, J. Y. Chong, Y. Wang, Forward osmosis membranes: the significant roles of selective layer, Membranes 12 (2022) 955-976. https://doi.org/10.3390/membranes12100955.

[2] R. P. Lively, D. S. Sholl, From water to organics in membrane separations, Nat. Mater. 16 (2007) 276-281. https://doi.org/10.1038/nmat4860.

[3] Y. Cui, T. Chung, Pharmaceutical concentration using organic solvent forward osmosis for solvent recovery, Nat. Commun. 9 (2018) 1426-1434. https://doi.org/10.1038/s41467-018-03612-2.

[4] L. Francis, O. Ogunbiyi, J. Saththasivam, J. Lawler, Z. Liu, A comprehensive review of forward osmosis and niche applications, Environ. Sci.: Water Res. Technol. 6 (2020) 1986-2015. https://doi.org/10.1039/d0ew00181c.

[5] S. S. Veroneau, A. C. Hartnett, A. E. Thorarinsdottir, D. G. Nocera, Direct seawater splitting by forward osmosis coupled to water electrolysis, ACS Appl. Energy Mater. 5 (2022) 1403–1408. https://doi.org/10.1021/acsaem.1c03998.

[6] G.S. Cassol, C. Shang, A.K. An, N.K. Khanzada, F. Ciucci, A. Manzotti, P. Westerhoff, Y. Song, L. Ling, Ultra-fast green hydrogen production from municipal wastewater by an integrated forward osmosis-alkaline water electrolysis system, Nat. Commun. 15 (2024) 2617-2626. https://doi.org/10.1038/s41467-024-46964-8.

[7] S.-J. Im, S. Jeong, A. Jang, Forward osmosis (FO)-reverse osmosis (RO) hybrid process incorporated with hollow fiber FO, Npj Clean Water 4 (2021) 51-60. https://doi.org/10.1038/s41545-021-00143-0.

[8] G. Blandin, A.R.D. Verliefde, J. Comas, I. Rodriguez-Roda, P. Le-Clech, Efficiently combining water reuse and desalination through forward osmosis-reverse osmosis (FO-RO) hybrids: A critical review, Membranes (Basel) 6 (2016) 37-60. https://doi.org/10.3390/membranes6030037.

[9] D.L. Shaffer, N.Y. Yip, J. Gilron, M. Elimelech, Seawater desalination for agriculture by integrated forward and reverse osmosis: Improved product water quality for potentially less energy, J. Memb. Sci. 415–416 (2012) 1–8. https://doi.org/10.1016/j.memsci.2012.05.016.

[10] M. Al-Furaiji, N. Benes, A. Nijmeijer, J.R. McCutcheon, Use of a forward osmosis–membrane distillation integrated process in treating high-salinity oily wastewater, Ind. Eng. Chem. Res. 58 (2019) 956–962. https://doi.org/10.1021/acs.iecr.8b04875.

[11] N.C. Nguyen, H.C. Duong, H.T. Nguyen, S.-S. Chen, H.Q. Le, H.H. Ngo, W. Guo, C.C. Duong, N.C. Le, X.T. Bui, Forward osmosis–membrane distillation hybrid system for desalination using mixed trivalent draw solution, J. Memb. Sci. 603 (2020) 118029-118035. https://doi.org/10.1016/j.memsci.2020.118029.

[12] S. Yang, B. Gao, A. Jang, H.K. Shon, Q. Yue, Municipal wastewater treatment by forward osmosis using seawater concentrate as draw solution, Chemosphere 237 (2019) 124485-124505. https://doi.org/10.1016/j.chemosphere.2019.124485.

[13] W.V. Anderson, C.-M. Cheng, T.S. Butalia, L.K. Weavers, Forward osmosis–membrane distillation process for zero liquid discharge of flue gas desulfurization wastewater, Energy Fuels 35 (2021) 5130–5140. https://doi.org/10.1021/acs.energyfuels.0c03415.

[14] T. Tong, M. Elimelech, The global rise of zero liquid discharge for wastewater management: Drivers, technologies, and future directions, Environ. Sci. Technol. 50 (2016) 6846–6855. https://doi.org/10.1021/acs.est.6b01000.

[15] R. Yalamanchili, I. Rodriguez-Roda, A. Galizia, G. Blandin, Can a forward osmosis-reverse osmosis hybrid system achieve 90 % wastewater recovery and desalination energy below 1 kWh/m3? A design and simulation study, Desalination 585 (2024) 117767-117777. https://doi.org/10.1016/j.desal.2024.117767.

[16] R.A. Wahid, W. Ang, A. Mohammad, D.J. Johnson, N. Hilal, Evaluating fertilizer-drawn forward osmosis performance in treating anaerobic palm oil mill effluent, Membranes (Basel) 11 (2021) 566-587. https://doi.org/10.3390/membranes11080566.

[17] S. Phuntsho, H.K. Shon, S. Hong, S. Lee, S. Vigneswaran, A novel low energy fertilizer driven forward osmosis desalination for direct fertigation: Evaluating the performance of fertilizer draw solutions, J. Memb. Sci. 375 (2011) 172–181. https://doi.org/10.1016/j.memsci.2011.03.038.

[18] S. Phuntsho, S. Vigneswaran, J. Kandasamy, S. Hong, S. Lee, H.K. Shon, Influence of temperature and temperature difference in the performance of forward osmosis desalination process, J. Memb. Sci. 415–416 (2012) 734–744. https://doi.org/10.1016/j.memsci.2012.05.065.

[19] S. Phuntsho, H.K. Shon, T. Majeed, I. El Saliby, S. Vigneswaran, J. Kandasamy, S. Hong, S. Lee, Blended fertilizers as draw solutions for fertilizer-drawn forward osmosis desalination, Environ. Sci. Technol. 46 (2012) 4567–4575. https://doi.org/10.1021/es300002w.

[20] N.K. Rastogi, Opportunities and challenges in application of forward osmosis in food processing, Crit. Rev. Food Sci. Nutr. 56 (2016) 266–291. https://doi.org/10.1080/10408398.2012.724734.

[21] G. Blandin, F. Ferrari, G. Lesage, P. Le-Clech, M. Héran, X. Martinez-Lladó, Forward osmosis as concentration process: Review of opportunities and challenges, Membranes (Basel) 10 (2020) 284-323. https://doi.org/10.3390/membranes10100284.

[22] S. Yang, S. Lee, S. Hong, Enhancing the applicability of forward osmosis membrane process utilizing food additives as draw solutes, J. Memb. Sci. 638 (2021) 119705-119713. https://doi.org/10.1016/j.memsci.2021.119705.

[23] Q. Ji, Z. Lv, Y. Yun, J. Li, C. Li, S. Zhu, Preparation of cellulose triacetate forward osmosis membranes for treating esterification wastewater, Desalination Water Treat. 61 (2017) 88–97. https://doi.org/10.5004/dwt.2016.0129.

[24] M.J. Luján-Facundo, J.L. Soler-Cabezas, J.A. Mendoza-Roca, M.C. Vincent-Vela, A. Bes-Piá, S. Doñate-Hernández, A study of the osmotic membrane bioreactor process using a sodium chloride solution and an industrial effluent as draw solutions, Chem. Eng. J. 322 (2017) 603–610. https://doi.org/10.1016/j.cej.2017.04.062.

[25] T. Ruprakobkit, L. Ruprakobkit, C. Ratanatamskul, Carboxylic acid concentration by forward osmosis processes: Dynamic modeling, experimental validation and simulation, Chem. Eng. J. 306 (2016) 538–549. https://doi.org/10.1016/j.cej.2016.07.091.

[26] G. Blandin, B. Rosselló, V.M. Monsalvo, P. Batlle-Vilanova, J.M. Viñas, F. Rogalla, J. Comas, Volatile fatty acids concentration in real wastewater by forward osmosis, J. Memb. Sci. 575 (2019) 60–70. https://doi.org/10.1016/j.memsci.2019.01.006.

[27] J.Y. Law, A.W. Mohammad, Z.K. Tee, N.K. Zaman, J.M. Jahim, J. Santanaraj, M.S. Sajab, Recovery of succinic acid from fermentation broth by forward osmosis-assisted

crystallization process, J. Memb. Sci. 583 (2019) 139–151. https://doi.org/10.1016/j.memsci.2019.04.036.

[28] M. Szczygiełda, M. Krajewska, L. Zheng, L.D. Nghiem, K. Prochaska, Implementation of forward osmosis to concentrate alpha-ketoglutaric acid from fermentation broth: Performance and fouling analysis, J. Memb. Sci. 637 (2021) 119593-119600. https://doi.org/10.1016/j.memsci.2021.119593.

[29] J.-W. Jung, H.-S. Lee, K.-J. Kim, Purification of acetic acid wastewater using layer melt crystallization, Sep. Sci. Technol. 43 (2008) 1021–1033. https://doi.org/10.1080/01496390701885257.

[30] S. Saiful, M. Ajrina, Y. Wibisono, M. Marlina, Development of chitosan/starch-based forward osmosis water filtration bags for emergency water supply, Membranes (Basel) 10 (2020) 414-426. https://doi.org/10.3390/membranes10120414.

[31] E. Butler, A. Silva, K. Horton, Z. Rom, M. Chwatko, A. Havasov, J.R. McCutcheon, Point of use water treatment with forward osmosis for emergency relief, Desalination 312 (2013) 23–30. https://doi.org/10.1016/j.desal.2012.12.013.

[32] R. Takada, R. Takagi, H. Matsuyama, High-degree concentration organic solvent forward osmosis for pharmaceutical pre-concentration, Membranes (Basel) 14 (2024) 14-26. https://doi.org/10.3390/membranes14010014.

[33] Z. Tong, H. Guo, X. Liu, B. Zhang, Organic solvent forward osmosis of graphene oxide-based membranes for enrichment of target products, Ind. Eng. Chem. Res. 59 (2020) 19012–19019. https://doi.org/10.1021/acs.iecr.0c03780.

[34] X. Wu, M. Ding, H. Xu, W. Yang, K. Zhang, H. Tian, H. Wang, Z. Xie, Scalable Ti3C2Tx MXene interlayered forward osmosis membranes for enhanced water purification and organic solvent recovery, ACS Nano 14 (2020) 9125–9135. https://doi.org/10.1021/acsnano.0c04471.

[35] Y. Wei, Y. Wang, L. Wang, H. Yang, H. Jin, P. Lu, Y. Li, Simultaneous phase-inversion and crosslinking in organic coagulation bath to prepare organic solvent forward osmosis membranes, J. Memb. Sci. 620 (2021) 118829-118839. https://doi.org/10.1016/j.memsci.2020.118829.

[36] K.S. Goh, Y. Chen, D.Y.F. Ng, J.W. Chew, R. Wang, Organic solvent forward osmosis membranes for pharmaceutical concentration, J. Memb. Sci. 642 (2022) 119965-119974. https://doi.org/10.1016/j.memsci.2021.119965.

[37] L. Ma, X. Han, S. Zhang, L. Wang, Sulfonated metal–organic framework nanostructure-based membranes with precise sieving for organic solvent forward osmosis, ACS Appl. Nano Mater. 5 (2022) 11324–11333. https://doi.org/10.1021/acsanm.2c02435.

[38] L. Chen, C. Zhou, T. Yang, W. Zhou, Y. Chen, L. Wang, C. Lu, L. Dong, Imparting outstanding dispersibility to nanoscaled 2D COFs for constructing organic solvent forward osmosis membranes, Small 19 (2023) 2300456-300463. https://doi.org/10.1002/smll.202300456.

[39] G. Gwak, D.I. Kim, S. Hong, New industrial application of forward osmosis (FO): Precious metal recovery from printed circuit board (PCB) plant wastewater, J. Memb. Sci. 552 (2018) 234–242. https://doi.org/10.1016/j.memsci.2018.02.022.

[40] Y. Cui, Q. Ge, X.-Y. Liu, T.-S. Chung, Novel forward osmosis process to effectively remove heavy metal ions, J. Memb. Sci. 467 (2014) 188–194. https://doi.org/10.1016/j.memsci.2014.05.034.

[41] S. Shokrollahzadeh, S. Tajik, Fabrication of thin film composite forward osmosis membrane using electrospun polysulfone/polyacrylonitrile blend nanofibers as porous substrate, Desalination 425 (2018) 68–76. https://doi.org/10.1016/j.desal.2017.10.017.

[42] T. Duolikun, N. Ghazali, B.F. Leo, H.V. Lee, C.W. Lai, M.R.B. Johan, Asymmetric cellulosic membranes: Current and future aspects, Symmetry (Basel) 12 (2020) 1160-1171. https://doi.org/10.3390/sym12071160.

[43] I. S. Al-Mutaz, A. Alalawi, N. B. Darwish, Explicit expression for water permeation fux in forward osmosis desalination process, Appl. Water Sci. 14 (2024) 149-156. https://doi.org/10.1007/s13201-024-02209-z.

[44] S. Loeb, S. Sourirajan, Sea water demineralization by means of an osmotic membrane, Advances in Chemistry 38 (1963) 117–132. https://doi.org/10.1021/ba-1963-0038.ch009.

[45] C. Kahrs, J. Schwellenbach, Membrane formation via non-solvent induced phase separation using sustainable solvents: A comparative study, Polymer (Guildf.) 186 (2020) 122071-122090. https://doi.org/10.1016/j.polymer.2019.122071.

[46] K. Vasarhelyi, J. Ronner, M. Mulder, C.A. Smolders, Development of wet-dry reversible reverse osmosis membrane with high performance from cellulose acetate and cellulose triactate blend, Desalination 61 (1987) 211–235. https://doi.org/10.1016/0011-9164(87)80020-6.

[47] A. Idris, A. Ismail, M. Noordin, S. Shilton, Optimization of cellulose acetate hollow fiber reverse osmosis membrane production using Taguchi method, Journal of Membrane Science 205 (2002) 223–237. https://doi.org/10.1016/S0376-7388(02)00116-3.

[48] K.Y. Wang, R.C. Ong, T.-S. Chung, Double-skinned forward osmosis membranes for reducing internal concentration polarization within the porous sublayer, Ind. Eng. Chem. Res. 49 (2010) 4824–4831. https://doi.org/10.1021/ie901592d.

[49] T.P.N. Nguyen, E.-T. Yun, I.-C. Kim, Y.-N. Kwon, Preparation of cellulose triacetate/cellulose acetate (CTA/CA)-based membranes for forward osmosis, J. Memb. Sci. 433 (2013) 49–59. https://doi.org/10.1016/j.memsci.2013.01.027.

[50] H.-M. Song, L.-J. Zhu, Z.-X. Zeng, Q.-J. Xue, High performance forward osmosis cellulose acetate (CA) membrane modified by polyvinyl alcohol and polydopamine, J. Polym. Res. 25 (2018) 159-166. https://doi.org/10.1007/s10965-018-1555-x.

[51] K.Y. Wang, T.-S. Chung, J.-J. Qin, Polybenzimidazole (PBI) nanofiltration hollow fiber membranes applied in forward osmosis process, J. Memb. Sci. 300 (2007) 6–12. https://doi.org/10.1016/j.memsci.2007.05.035.

[52] Q. Yang, K.Y. Wang, T.-S. Chung, Dual-layer hollow fibers with enhanced flux as novel forward osmosis membranes for water production, Environ. Sci. Technol. 43 (2009) 2800–2805. https://doi.org/10.1021/es803360t.

[53] Y. Yu, S. Seo, I.-C. Kim, S. Lee, Nanoporous polyethersulfone (PES) membrane with enhanced flux applied in forward osmosis process, J. Memb. Sci. 375 (2011) 63–68. https://doi.org/10.1016/j.memsci.2011.02.019.

[54] M.F. Flanagan, I.C. Escobar, Novel charged and hydrophilized polybenzimidazole (PBI) membranes for forward osmosis, J. Memb. Sci. 434 (2013) 85–92. https://doi.org/10.1016/j.memsci.2013.01.039.

[55] J. E. Cadotte, Interfacially synthesized reverse osmosis membranes, (1979) (U.S. Patent No. US4277344).

[56] P. Sukitpaneenit, T.-S. Chung, Fabrication and use of hollow fiber thin film composite membranes for ethanol dehydration, J. Memb. Sci. 450 (2014) 124–137. https://doi.org/10.1016/j.memsci.2013.08.047.

[57] Z.H. Chang, J.Y. Sum, W.J. Lau, W.L. Ang, Y.H. Teow, B.S. Ooi, S.P. Yeap, Current state-of-the-art of non-reverse osmosis-like forward osmosis technology, J. Memb. Sci. 711 (2024) 123209-123231. https://doi.org/10.1016/j.memsci.2024.123209.

[58] N.Y. Yip, A. Tiraferri, W.A. Phillip, J.D. Schiffman, M. Elimelech, High performance thin-film composite forward osmosis membrane, Environ. Sci. Technol. 44 (2010) 3812–3818. https://doi.org/10.1021/es1002555.

[59] X. Song, Z. Liu, D.D. Sun, Nano gives the answer: breaking the bottleneck of internal concentration polarization with a nanofiber composite forward osmosis membrane for a high water production rate, Adv. Mater. 23 (2011) 3256–3260. https://doi.org/10.1002/adma.201100510.

[60] K.Y. Wang, T.-S. Chung, G. Amy, Developing thin-film-composite forward osmosis membranes on the PES/SPSf substrate through interfacial polymerization, AIChE J. 58 (2012) 770–781. https://doi.org/10.1002/aic.12635.

[61] X. Li, K.Y. Wang, B. Helmer, T.-S. Chung, Thin-film composite membranes and formation mechanism of thin-film layers on hydrophilic cellulose acetate propionate substrates for forward osmosis processes, Ind. Eng. Chem. Res. 51 (2012) 10039–10050. https://doi.org/10.1021/ie2027052.

[62] K.S. Piash, O. Sanyal, Design strategies for forward osmosis membrane substrates with low structural parameters-A review, Membranes (Basel) 13 (2023) 73-102. https://doi.org/10.3390/membranes13010073.

[63] M.S. Islam, K. Touati, M.S. Rahaman, High flux and antifouling thin-film nanocomposite forward osmosis membrane with ingrained silica nanoparticles, ACS ES T Eng. 1 (2021) 467–477. https://doi.org/10.1021/acsestengg.0c00177.

[64] Y. Li, Y. Zhao, E. Tian, Y. Ren, Preparation and characterization of novel forward osmosis membrane incorporated with sulfonated carbon nanotubes, RSC Adv. 8 (2018) 41032–41039. https://doi.org/10.1039/c8ra08900k.

[65] S. Gupta, B. Evans, Interplay of graphene oxide and interfacial polymerized polyamide-crosslinked thin-film composite membranes for enhanced performance during reverse osmosis, Desalination Water Treat. 218 (2021) 177–192. https://doi.org/10.5004/dwt.2021.26967.

[66] Y. Wang, X. Li, S. Zhao, Z. Fang, D. Ng, C. Xie, H. Wang, Z. Xie, Thin-film composite membrane with interlayer decorated metal–organic framework UiO-66 toward enhanced forward osmosis performance, Ind. Eng. Chem. Res. 58 (2019) 195–206. https://doi.org/10.1021/acs.iecr.8b04968.

[67] M. He, L. Wang, Y. Lv, X. Wang, J. Zhu, Y. Zhang, T. Liu, Novel polydopamine/metal organic framework thin film nanocomposite forward osmosis membrane for salt rejection and heavy metal removal, Chem. Eng. J. 389 (2020) 124452-124465. https://doi.org/10.1016/j.cej.2020.124452.

[68] L. Xu, T. Yang, M. Li, J. Chang, J. Xu, Thin-film nanocomposite membrane doped with carboxylated covalent organic frameworks for efficient forward osmosis desalination, J. Memb. Sci. 610 (2020) 118111-118119. https://doi.org/10.1016/j.memsci.2020.118111.

[69] Z. Li, Y. Wang, M. Han, D. Wang, S. Han, Z. Liu, N. Zhou, R. Shang, C. Xie, Graphene oxide incorporated forward osmosis membranes with enhanced desalination performance and chlorine resistance, Front. Chem. 7 (2019) 877-888. https://doi.org/10.3389/fchem.2019.00877.

[70] S. Phuntsho, J.E. Kim, V.H. Tran, S. Tahara, N. Uehara, N. Maruko, H. Matsuno, S. Lim, H.K. Shon, Free-standing, thin-film, symmetric membranes: Next-generation membranes for engineered osmosis, J. Memb. Sci. 607 (2020) 118145-118154. https://doi.org/10.1016/j.memsci.2020.118145.

[71] M. Li, V. Karanikola, X. Zhang, L. Wang, M. Elimelech, A self-standing, support-free membrane for forward osmosis with no internal concentration polarization, Environ. Sci. Technol. Lett. 5 (2018) 266–271. https://doi.org/10.1021/acs.estlett.8b00117.

[72] R. Vendamme, S.-Y. Onoue, A. Nakao, T. Kunitake, Robust free-standing nanomembranes of organic/inorganic interpenetrating networks, Nat. Mater. 5 (2006) 494–501. https://doi.org/10.1038/nmat1655.

[73] H. Liu, H. Wang, X. Zhang, Facile fabrication of freestanding ultrathin reduced graphene oxide membranes for water purification, Adv. Mater. 27 (2015) 249–254. https://doi.org/10.1002/adma.201404054.

[74] E. Stratakis, G. Eda, H. Yamaguchi, E. Kymakis, C. Fotakis, M. Chhowalla, Free-standing graphene on microstructured silicon vertices for enhanced field emission properties, Nanoscale 4 (2012) 3069–3074. https://doi.org/10.1039/c2nr30622k.

[75] H.-G. Yuan, Y.-Y. Liu, T.-Y. Liu, X.-L. Wang, Self-standing nanofilms of polysulfone doped with sulfonated polysulfone via solvent evaporation for forward osmosis, J. Memb. Sci. 523 (2017) 567–575. https://doi.org/10.1016/j.memsci.2016.09.034.

[76] J.-G. Gai, X.-L. Gong, Zero internal concentration polarization FO membrane: functionalized graphene, J. Mater. Chem. A 2 (2014) 425-429. https://doi.org/10.1039/c3ta13562d.

[77] Q. Liu, J. Li, Z. Zhou, J. Xie, J.Y. Lee, Hydrophilic mineral coating of membrane substrate for reducing internal concentration polarization (ICP) in forward osmosis, Sci. Rep. 6 (2016) 19593-19602. https://doi.org/10.1038/srep19593.

[78] Y. Cui, X.-Y. Liu, T.-S. Chung, Ultrathin polyamide membranes fabricated from free-standing interfacial polymerization: Synthesis, modifications, and post-treatment, Ind. Eng. Chem. Res. 56 (2017) 513–523. https://doi.org/10.1021/acs.iecr.6b04283.

[79] W. Cheng, J. Ma, X. Zhang, M. Elimelech, Sub-1 μm free-standing symmetric membrane for osmotic separations, Environ. Sci. Technol. Lett. 6 (2019) 492–498. https://doi.org/10.1021/acs.estlett.9b00364.

[80] M. Zheng, X. Zhao, S. Xu, D. Lu, Ultrathin support-free membrane with high water flux for forward osmosis desalination, Water Air Soil Pollut. 230 (2019) 138-145. https://doi.org/10.1007/s11270-019-4192-z.

[81] T. Ma, E. Balanzat, J.-M. Janot, S. Balme, Nanopore functionalized by highly charged hydrogels for osmotic energy harvesting, ACS Appl. Mater. Interfaces 11 (2019) 12578–12585. https://doi.org/10.1021/acsami.9b01768.

[82] B.M. Ibraheem, S.A. Aani, A.A. Alsarayreh, Q.F. Alsalhy, I.K. Salih, Forward osmosis membrane: Review of fabrication, modification, challenges and potential, Membranes (Basel) 13 (2023) 379-432. https://doi.org/10.3390/membranes13040379.

[83] L. Chekli, S. Phuntsho, H.K. Shon, S. Vigneswaran, J. Kandasamy, A. Chanan, A review of draw solutes in forward osmosis process and their use in modern applications, Desalination Water Treat. 43 (2012) 167–184. https://doi.org/10.1080/19443994.2012.672168.

[84] L. Li, W. Shi, S. Yu, Research on forward osmosis membrane technology still needs improvement in water recovery and wastewater treatment, Water (Basel) 12 (2019) 107-133. https://doi.org/10.3390/w12010107.

[85] S. Ma, X. Wu, L. Fan, Q. Wang, Y. Hu, Z. Xie, Effect of different draw solutions on concentration polarization in a forward osmosis process: Theoretical modeling and experimental validation, Ind. Eng. Chem. Res. 62 (2023) 3672–3683. https://doi.org/10.1021/acs.iecr.2c03723.

[86] F. Volpin, L. Chekli, S. Phuntsho, J. Cho, N. Ghaffour, J.S. Vrouwenvelder, H. Kyong Shon, Simultaneous phosphorous and nitrogen recovery from source-separated urine: A novel application for fertiliser drawn forward osmosis, Chemosphere 203 (2018) 482–489. https://doi.org/10.1016/j.chemosphere.2018.03.193.

[87] P. Zhao, Q. Yue, B. Gao, J. Kong, H. Rong, P. Liu, H.K. Shon, Q. Li, Influence of different ion types and membrane orientations on the forward osmosis performance, Desalination 344 (2014) 123–128. https://doi.org/10.1016/j.desal.2014.03.018.

[88] J.R. Mc Cutcheon a, R.L. Mc Ginnis b, E. a. Menachem, A novel ammonia-carbon dioxide forward (direct) osmosis desalination process, Desalination 174 (2005) 1–11. https://doi.org/10.1016/j.desal.2004.11.002.

[89] A. Achilli, T.Y. Cath, A.E. Childress, Selection of inorganic-based draw solutions for forward osmosis applications, J. Memb. Sci. 364 (2010) 233–241. https://doi.org/10.1016/j.memsci.2010.08.010.

[90] M. Nematzadeh, A. Samimi, S. Shokrollahzadeh, Application of sodium bicarbonate as draw solution in forward osmosis desalination: influence of temperature and linear flow velocity, Desalination Water Treat. 57 (2016) 20784–20791. https://doi.org/10.1080/19443994.2015.1111816.

[91] M. Gulied, F. Al Momani, M. Khraisheh, R. Bhosale, A. AlNouss, Influence of draw solution type and properties on the performance of forward osmosis process: Energy consumption and sustainable water reuse, Chemosphere 233 (2019) 234–244. https://doi.org/10.1016/j.chemosphere.2019.05.241.

[92] R. E. Kravath, J. A. Davis, Desalination of sea water by direct osmosis, Desalination 16 (1975) 151-155. https://doi.org/10.1016/S0011-9164(00)82089-5.

[93] J. O. Kessler, C. D. Moody, Drinking water from sea water by forward osmosis, Desalination 18 (1976) 297–306. https://doi.org/10.1016/S0011-9164(00)84119-3.

[94] S.O. Alaswad, S.A. Aibi, E. Alpay, A.O. Sharif, Efficiency of organic draw solutions in a forward osmosis process using nano-filtration flat sheet membrane, J. Chem. Eng. Process Technol. 09 (2018) 1-9. https://doi.org/10.4172/2157-7048.1000370.

[95] R.E. Wrolstad, M.R. Mcdaniel, R.W. Durst, N. Micheals, K.A. Lampi, E.G. Beaudry, Composition and sensory characterization of red raspberry juice concentrated by direct-osmosis or evaporation, J. Food Sci. 58 (1993) 633–637. https://doi.org/10.1111/j.1365-2621.1993.tb04344.x.

[96] J. R. Herron, E. G. Beaudry, C. E. Jochums, L. E. Medina, Osmotic concentration apparatus and method for direct osmotic concentration of fruit juices, (1994) (U. S, Patent No. US005281430A).

[97] Q. Ge, T.-S. Chung, Hydroacid complexes: a new class of draw solutes to promote forward osmosis (FO) processes, Chem. Commun. (Camb.) 49 (2013) 8471–8473. https://doi.org/10.1039/c3cc43951h.

[98] J. Su, T.-S. Chung, B.J. Helmer, J.S. de Wit, Enhanced double-skinned FO membranes with inner dense layer for wastewater treatment and macromolecule recycle using Sucrose as draw solute, J. Memb. Sci. 396 (2012) 92–100. https://doi.org/10.1016/j.memsci.2012.01.001.

[99] X. Xiaohua, Z. Liang, L. Xia, J. Shengxiang, Ionic liquids as additives in high performance liquid chromatography, Anal. Chim. Acta 519 (2004) 207–211. https://doi.org/10.1016/j.aca.2004.06.038.

[100] E. Alvarez-Guerra, S.P.M. Ventura, J.A.P. Coutinho, A. Irabien, Ionic liquid-based three phase partitioning (ILTPP) systems: Ionic liquid recovery and recycling, Fluid Phase Equilib. 371 (2014) 67–74. https://doi.org/10.1016/j.fluid.2014.03.009.

[101] M.A.M. Abdullah, M.S. Man, S.B. Abdullah, S.M. Saufi, A glance on thermo-responsive ionic liquids as draw solution in forward osmosis system, Desalination Water Treat. 206 (2020) 165–176. https://doi.org/10.5004/dwt.2020.26317.

[102] Y. Zhong, X. Feng, W. Chen, X. Wang, K.-W. Huang, Y. Gnanou, Z. Lai, Using UCST ionic liquid as a draw solute in forward osmosis to treat high-salinity water, Environ. Sci. Technol. 50 (2016) 1039–1045. https://doi.org/10.1021/acs.est.5b03747.

[103] Y. Cai, W. Shen, J. Wei, T.H. Chong, R. Wang, W.B. Krantz, A.G. Fane, X. Hu, Energy-efficient desalination by forward osmosis using responsive ionic liquid draw solutes, Environ. Sci. (Camb.) 1 (2015) 341–347. https://doi.org/10.1039/c4ew00073k.

[104] H.-Y. Li, Y.-H. Chu, Expeditious discovery of small-molecule thermoresponsive ionic liquid materials: A review, Molecules 28 (2023) 6817-6839. https://doi.org/10.3390/molecules28196817.

[105] E. Kamio, A. Takenaka, T. Takahashi, H. Matsuyama, Fundamental investigation of osmolality, thermo-responsive phase diagram, and water-drawing ability of ionic-liquid-based draw solution for forward osmosis membrane process, J. Memb. Sci. 570–571 (2019) 93–102. https://doi.org/10.1016/j.memsci.2018.10.004.

[106] M. A. M. Abdullah, M. S. Man, P. S. Nyan, S. M. Saufi, S. B. Abdullah, Potential thermo-responsive ionic liquid as draw solution in forward osmosis application, J. Eng. Sci. Technol. 14 (2019) 1031-1042.

[107] E. Tian, C. Hu, Y. Qin, Y. Ren, X. Wang, X. Wang, P. Xiao, X. Yang, A study of poly (sodium *4*-styrenesulfonate) as draw solute in forward osmosis, Desalination 360 (2015) 130–137. https://doi.org/10.1016/j.desal.2015.01.001.

[108] A. Bardhan, S. Subbiah, K. Mohanty, I. Ibrar, A. Altaee, Feasibility of poly (vinyl alcohol)/poly (diallyldimethylammonium chloride) polymeric network hydrogel as draw solute for forward osmosis process, Membranes (Basel) 12 (2022) 1097-1112. https://doi.org/10.3390/membranes12111097.

[109] Q. Ge, J. Su, G.L. Amy, T.-S. Chung, Exploration of polyelectrolytes as draw solutes in forward osmosis processes, Water Res. 46 (2012) 1318–1326. https://doi.org/10.1016/j.watres.2011.12.043.

[110] D. Zhao, S. Chen, P. Wang, Q. Zhao, X. Lu, A dendrimer-based forward osmosis draw solute for seawater desalination, Ind. Eng. Chem. Res. 53 (2014) 16170–16175. https://doi.org/10.1021/ie5031997.

[111] R. Kumar, S. Al-Haddad, M. Al-Rughaib, M. Salman, Evaluation of hydrolyzed poly(isobutylene-alt-maleic anhydride) as a polyelectrolyte draw solution for forward

osmosis desalination, Desalination 394 (2016) 148–154. https://doi.org/10.1016/j.desal.2016.05.012.

[112] Q. Long, J. Huang, S. Xiong, L. Shen, Y. Wang, Exploration of oligomeric sodium carboxylates as novel draw solutes for forward osmosis, Chem. Eng. Res. Des. 138 (2018) 77–86. https://doi.org/10.1016/j.cherd.2018.08.020.

[113] K. Zhang, F. Li, Y. Wu, L. Feng, L. Zhang, Construction of ionic thermo-responsive PNIPAM/γ-PGA/PEG hydrogel as a draw agent for enhanced forward-osmosis desalination, Desalination 495 (2020) 114667-114677. https://doi.org/10.1016/j.desal.2020.114667.

[114] Y. Xu, Y. Zhu, Z. Chen, J. Zhu, G. Chen, A comprehensive review on forward osmosis water treatment: Recent advances and prospects of membranes and draw solutes, Int. J. Environ. Res. Public Health 19 (2022) 8215-8252. https://doi.org/10.3390/ijerph19138215.

[115] G.T. Gray, J.R. McCutcheon, M. Elimelech, Internal concentration polarization in forward osmosis: role of membrane orientation, Desalination 197 (2006) 1–8. https://doi.org/10.1016/j.desal.2006.02.003.

[116] J.R. McCutcheon, M. Elimelech, Influence of concentrative and dilutive internal concentration polarization on flux behavior in forward osmosis, J. Memb. Sci. 284 (2006) 237–247. https://doi.org/10.1016/j.memsci.2006.07.049.

CHAPTER 2

ABPBI-based Hollow Fiber Membranes for Forward Osmosis (FO) Possessing Low Reverse Salt Flux

Abstract

The poly(2,5-Benzimidazole), known for its excellent thermochemical stability, was evaluated as a membrane material for forward osmosis. The dope solution in methane sulfonic acid was used to make hollow fiber membranes by phase inversion in water. The FO performance of membranes with and without bound MSA in HFMs was compared. Aqueous solutions of two common salts reported for FO (NaCl and $MgCl_2$) were used as a draw solution at varying concentrations. The performance was determined in terms of water flux and reverse salt flux. The heat pretreatment of membranes was beneficial in offering low reverse salt flux, a crucial parameter in FO. The heat treatment at 350 °C exhibited excellent performance of low-RSF, irrespective of the draw solute used. The presence of MSA in the membrane matrix was found to be beneficial. The present HFMs exhibited reverse salt flux as low as 0.003 mol m^{-2} h^{-1} using 2 mol L^{-1} $MgCl_2$ as a draw solution. The water flux of present membranes was lower than that of reported FO-membranes, which is attributable to the larger thickness of the present membranes. The long-term performance of the membrane was assessed.

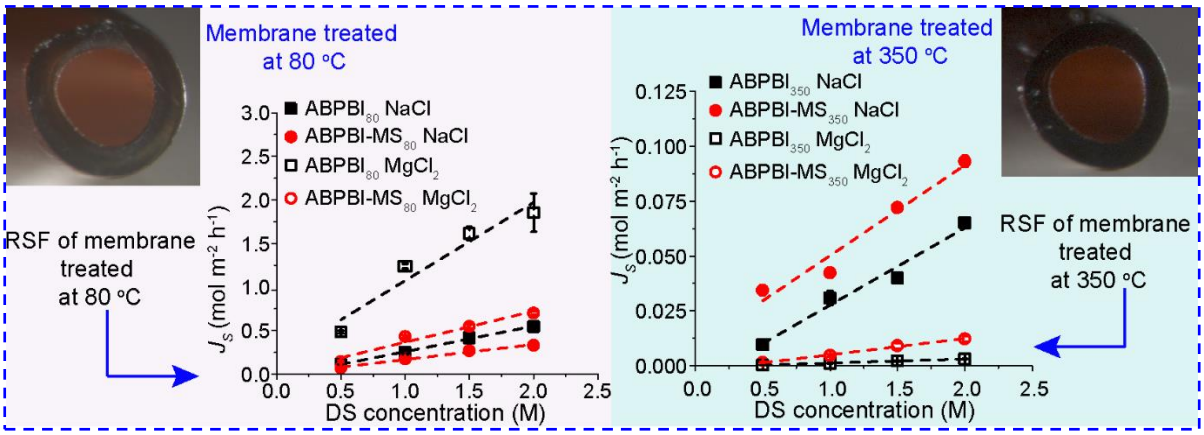

2.1 Introduction

FO is emerging as a crucial membrane separation technology for organic solvent recovery in pharmaceutical industries [1], seawater desalination [2], wastewater treatment [3], fertigation [4,5], fruit juice concentration [6,7], and emergency drinking water [8]. Its advantages over conventional methods include energy efficiency, lower Fouling, resource recovery, and better operational flexibility and scalability [1,2,9,10]. Unlike pressure-driven processes, FO is a concentration-driven membrane process for transporting water or organic solvent, utilizing osmotic pressure difference across a selectively permeable membrane as the driving force [11]. The main advantages of FO are that it operates at low or no hydraulic pressure, it can achieve high rejection of a wide range of contaminants, and it may have lower irreversible fouling than pressure-driven membrane processes [12]. Energy efficiency is brought by the usage of waste or low-quality energy (e.g., high saline brine or residual heat) instead of clean energy (electricity) [13]. The semipermeable membrane is a barrier between DS (possessing high osmotic pressure) and feed solution (FS, containing solute of interest). The FO membrane allows water or organic solvents to be transported while FS concentrates. The highly selective membranes enabling rapid water transport and maintaining low salt permeation are the core requirements of this emerging process [14].

The FO process faces challenges in achieving techno-economic feasibility in various industrial applications. The need for a draw solute includes its high solubility in water, high osmotic pressure, and ease of regeneration [15]. The membranes with high water/solvent permeability, high mechanical strength combined with low RSF (diffusion of draw solutes into the FS), fouling, and internal concentration polarization (ICP) [13,16,17] still need to be addressed to enlarge the application canvas of FO process. Some efforts are made to fabricate self-standing, thin film membranes with a symmetric homogeneous structure that reduces the ICP effect.

A polysulfone (PSf) based self-standing nanofilm was designed for FO by the solvent evaporation method and doping sulfonated polysulfone from 0 to 5 wt.% to tune the structure and surface properties of the nanofilm [18]. Li et al. [19] reported the synthesis of the COOH derived polyoxadiazole copolymer for the fabrication of a self-standing selective thin film without a support layer. Other polymers demonstrated for making FO membranes; including cellulose acetate (CA), cellulose triacetate (CTA), polysulfone (PS)/polyethersulfone (PES), polyamide TFC, polybenzimidazole (PBI) [16]. These membranes are either asymmetric or thin film composite (TFC), consisting of an active thin layer on the top of a porous substrate [20,21]. Since most membranes are asymmetric, ICP reduces effective driving force and thus

lowers fluxes [19,21]. The ICP occurs within the support layer of a membrane and is characterized by differing solute concentrations at the transverse boundaries of that layer. This results in reduction in the osmotic pressure gradient across the active layer of the membrane and a corresponding decrease in water flux [23]. FO also faces external concentration polarization (ECP) at the active surface of the membrane, leading to the lowering of the osmotic driving force [24]. Such results indicate the need for a support-free membrane to further the FO technology.

Membranes used for FO are either in flat sheet or hollow fiber form. Compared to flat sheets, most of the developed hollow fiber FO membranes demonstrated proven performance in terms of high water flux and lower RSF [25]. The HFMs possess desired properties such as high surface area and packing density relative to flat sheets [26]. Moreover, the HFM is easier to scale up and simpler in module fabrication than the flat sheet membranes [27].

One of the PBI family of polymers, poly(2,5-Benzimidazole), usually referred to as ABPBI, possesses higher water uptake than conventional PBI [28] and has high solvent and pH stability [29]. It has a high N-H group density [30], which can take part in H-bonding with water/polar solvent and could possess high flux if employed as an FO. Although it is well investigated as a membrane material for proton exchange membrane fuel cells (PEMFCs) [31,32], the applicability of its niche characteristics (especially solvent and pH stability) as a membrane material for separation are feebly addressed in the literature. Its investigation as a FO membrane material could open up new avenues.

The present work examines the intrinsic FO performance of ABPBI-based hollow fiber membranes (especially rejection, since higher membrane thickness in hollow fiber form could restrict the flux). ABPBI in neutral and in the presence of methane sulfonic acid in the membrane matrix was evaluated as a membrane material to generate an understanding of the effects of the absence/presence of acid in the membrane matrix. Aqueous solutions of two different draw solutes at varying concentrations were evaluated to determine water flux and RSF, the niche characteristics of an FO membrane. It is demonstrated that ABPBI could be a potential membrane material for FO, possessing low RSF.

2.2 Experimental

2.2.1 Materials, ABPBI synthesis and characterizations

A *3,4*-diaminobenzoic acid (DABA) was obtained from Gharada Chemicals. The polyphosphoric acid (PPA, ca. 84% P_2O_5) was procured from Avra Synthesis (India). The *ortho*-phosphoric acid (OPA), NaCl, and $MgCl_2$ were procured from Merck. Methanesulfonic

acid (MSA) and sulphuric acid (H_2SO_4) (98%) were supplied by Thomas Baker. A 2-component epoxy resin (Epocast 130 resin and hardener PX 01) was provided by Rand Polyproducts (India). These chemicals were used without further purification. All draw solutions (DSs) were prepared in deionized water.

The ABPBI was synthesized by self-condensation of DABA in PPA, which acts as a solvent and dehydrating agent [28,31]. The reactor with an overhead stirrer and heating assembly was charged with 2250 g of PPA, heated to 120 °C, and 75 g of DABA was added while stirring. After dissolution, the temperature was raised to 170 °C and maintained for 1 h. The temperature was increased to 210 °C while stirring. After 1 h, 600 g of OPA was added and stirred for an additional hour. The polymer was precipitated in water, crushed in a blender, and washed with water (to remove excess acid) until it was neutral to pH. The polymer was agitated with 0.1 mol L^{-1} aq. $NaHCO_3$ for 8 h to remove bound acid present in the polymer matrix. The polymer collected by filtration was washed with water until it was neutral to pH. After soaking in methanol for 15 h, the polymer was filtered, dried at 60 °C for 8 h, and kept in a vacuum oven at 100 °C for 7 days. The inherent (η_{inh}) and intrinsic ([η]) viscosity of the obtained polymer was determined using a Ubbelohde viscometer and 98% H_2SO_4 as a solvent at 35 °C. The FTIR spectra were recorded using Bruker Optics ALPHA-E spectrometer with a universal Zn-Se ATR accessory in a 600-4000 cm^{-1} frequency region. The wide-angle X-ray diffraction (WAXD) spectra were recorded with Rigaku SmartLab X-ray diffractometer in reflection mode using CuKα radiation (λ =1.5418 Å). The 2θ scan range was 5-40° at a scan rate of 3° min^{-1}. The thermogravimetric analysis (TGA) was performed on TGA-STA6000 (TA Instruments) in an N_2 atmosphere with a heating rate of 10 °C min^{-1}. FTIR analysis aimed to compare the characteristic IR bands with those reported earlier for ABPBI. Similarly, WAXD analysis and TGA were performed to compare the X-ray and degradation patterns (typical water loss usually observed for ABPBI, its degradation temperature, and the char yield) with that reported in the literature.

2.2.2 Preparation of flat sheet membranes (FSMs)

A 5% (wt/wt) dope solution was prepared by dissolving ABPBI in MSA at 80 °C while stirring for 24 h, filtered to remove undissolved particles, if any, and degassed for 30 min. The casting was done at ambient using a continuous casting machine with a speed of 0.75 m min^{-1} and water as a non-solvent. The membrane was peeled off from the surface while it was in the water. The delaminated membrane was cut into pieces. Some of them were washed with DI water until it was neutral pH. They were heated in a quartz tube furnace under an N_2 atmosphere

for 9 h at 80 and 350 °C and were designated as ABPBI-MS_{80FSM} and ABPBI-MS_{350FSM}, respectively. The remaining membranes were dipped in 0.1 N $NaHCO_3$ for 8 h, washed with DI water until neutral to pH, and thermally treated as above. These membranes were designated as $ABPBI_{80FSM}$ and $ABPBI_{350FSM}$. These FSMs were prepared for the sorption analysis.

2.2.3 Physical characterizations of FSMs

The FTIR spectra were recorded at ambient using Bruker Optics ALPHA-E spectrometer with a universal Zn-Se ATR (attenuated total reflection) accessory in a 600-4000 cm^{-1} region. The wide-angle X-ray diffraction (WAXD) spectra were recorded with Rigaku SmartLab X-ray diffractometer in reflection mode using CuKα radiation (λ =1.5418 Å). The 2θ scan range was 5-40 ° at a scan rate of 3° min^{-1}. The thermogravimetric analysis (TGA) was performed on TGA-STA6000 (TA Instruments, USA) in an N_2 atmosphere with a heating rate of 10 °C min^{-1}. The water contact angle of the membranes was obtained using Drop Shape Analyzer DSA25- KRÜSS GmbH. Water drops of constant size were placed on the membrane surface. The digital image from the camera was analyzed using a built-in drop-shape analysis tool. The reported contact angle for each membrane is an average of 6 samples.

2.2.4 Sorption analysis using FSMs

The sorption of water, 2 mol L^{-1} NaCl, and 2 mol L^{-1} $MgCl_2$ in FSMs was evaluated at 40 °C. The 2 mol L^{-1} solutions were chosen for sorption since they were the maximum concentration used in the FO experiments. The samples were taken out at regular time intervals, wiped out, and weighed. The sorption experiments were continued till the equilibrium was reached. Five samples were analyzed for each FSM type, and the data was averaged (deviation: $\pm$ 1.53%). The sorption was calculated using Eq. 2.1.

$$Sorption\ (\frac{wt}{wt}) = \frac{W_t - W_0}{W_0} \quad (2.1)$$

where, W_0 and W_t represent the weight of the membrane in the dry state and after sorption at the time, t, respectively.

2.2.5 Spinning of hollow fiber membranes (HFMs) and characterizations

The dope solution of 2.5% (wt/wt) ABPBI was prepared in MSA while heating at 80 °C for 24 h. The spinning was done using the dry-jet/wet phase inversion method using a tube-in-orifice spinneret. The spinning parameters are given in Table 2.1. The spun HFMs were post-treated as that of FSMs, as provided in Section 2.2.2. They were designated based on the treatment conditions, as shown in Table 2.2.

Table 2.1. Spinning parameters used for making HFMs

Parameters	**Specifications**
Dope pressure (psi)	40
Bore fluid	DI water
Bore fluid flow rate (ml min^{-1})	0.5
Air gap (cm)	1
Take-up speed (m min^{-1})	9.8
External Coagulant	Water at ambient temperature
Dimensions of spinneret (mm)	ID/OD = 0.7/2

Table 2.2. Nomenclature of membranes

FSM/HFM	**Form of ABPBI**	**Treatment temperature for 9 h duration**
$ABPBI_{80}$	Neutral	80 ºC
$ABPBI_{350}$		350 ºC
$ABPBI\text{-}MS_{80}$	As spun, MSA-bound	80 ºC
$ABPBI\text{-}MS_{350}$		350 ºC

2.2.6 Characterizations of HFMs and module making

The HFM cross-sectional images were recorded using gold-sputtered samples on an FEI Nova NanoSEM 650 Scanning Electron Microscope (SEM) with a field emitter as an electron source. The FTIR, WAXD spectra, and TGA were recorded using the same equipment as for FSMs. The membrane modules were prepared using 50 HFMs (active membrane area: 250 cm^2) in PVC shells. The potting was done using 2-component epoxy resin. The membrane integrity was assessed by analyzing the permeation of helium gas at 50 and 60 psi upstream pressure.

2.2.7 FO experiments using HFM modules

The performance of HFM modules was evaluated at 25 ℃ using the FO setup. All membranes shown in Table 2 were initially saturated with DI water for 1 h. Each FO experiment was performed for an 8 h duration. The DS and FS used were aq. 0.5-2 mol L^{-1} NaCl/$MgCl_2$ and DI water, respectively. The FS and DS were passed through the shell and lumen side at the flow rate of 10 ml min^{-1}, respectively. For each membrane type, 3 modules were evaluated, and results were averaged. The water flux, J_W (L m^{-2} h^{-1}), was calculated using Eq. 2.2.

$$J_W = \frac{\Delta V}{A_m \Delta t} \tag{2.2}$$

where, ΔV (L) is the change in the volume of FS over the defined experimental time Δt (h) and A_m (m^2) is the active membrane area. The conductivity meter, Metler Toledo MC226, was used to determine the salt concentration in a solution. The reverse salt flux (J_S, mol m^{-2} h^{-1}) from the DS to the FS side was determined from the increased conductivity of the FS (DI water) and was calculated using Eq. 2.3.

$$J_S = \frac{\Delta(CV)}{A_m \Delta t} \tag{2.3}$$

where, ΔC (mol L^{-1}) is the change in the salt concentration in FS, and ΔV (L) is the change in the volume of FS. The osmotic pressure, π of a DS, was calculated using Eq. 2.4 [34].

$$\pi = nMRT \tag{2.4}$$

where, n is a Van't Hoff factor (2 for NaCl and 3 for $MgCl_2$), M is the molar concentration of the solute, R (0.0831 L bar K^{-1} mol^{-1}) is a universal gas constant, and T is the temperature of the solution (298 K).

2.3 Results and discussion

2.3.1 ABPBI synthesis and characterizations

The ABPBI synthesized by polycondensation (Fig. 2.1a) exhibited an inherent viscosity of 4.4 dL g^{-1}. The FT-IR spectra (Fig. 2.1b) showed the characteristic bands at 1630, 1552, and 1419 cm^{-1}; attributable to the C=C and C=N stretching of the benzimidazole groups of ABPBI. The broad band at ~3165 cm^{-1} is attributable to the N-H stretching vibrations.

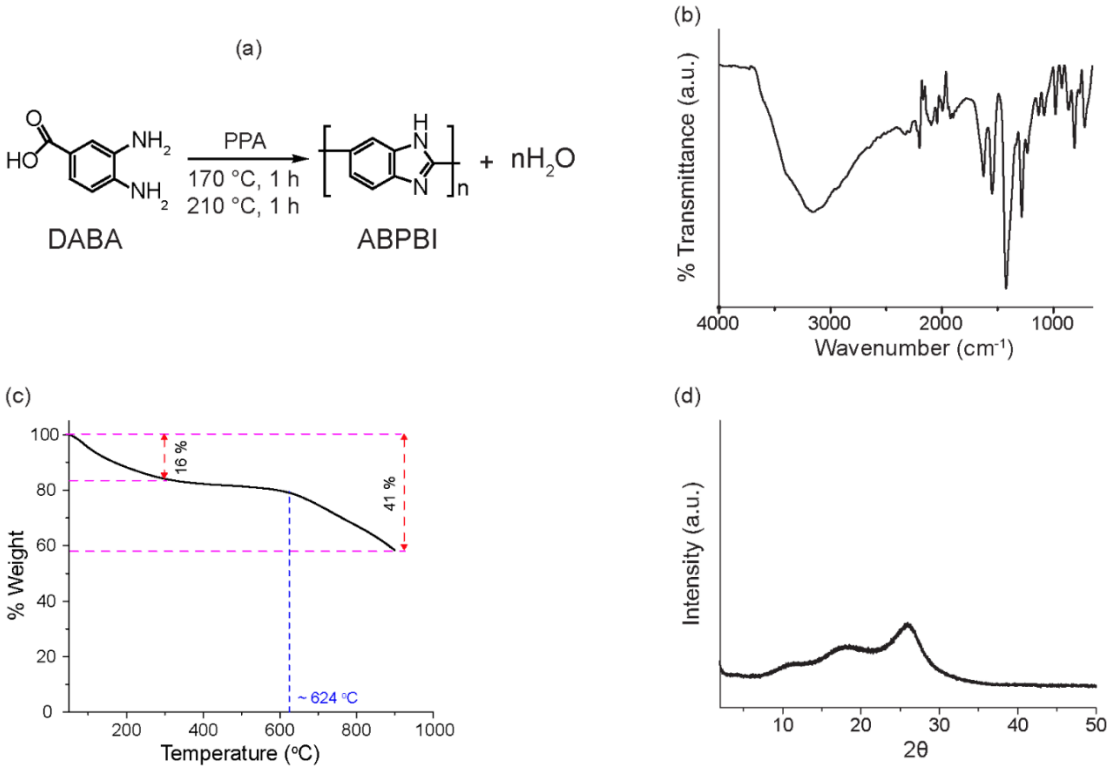

Fig. 2.1. a) Scheme of ABPBI synthesis, b) FT-IR and c) TGA spectra, d) WAXD pattern.

The TGA thermogram (Fig. 2.1c) showed an initial decomposition temperature of 295 °C, amounting to 16% water loss from the membrane matrix. The polymer decomposition started at 624 °C, conveying its excellent thermal stability. The char yield at 900 °C was 69.7 %. The FTIR bands, sluggish loss of water, and degradation temperature seen from the TGA and WAXD pattern of ABPBI (Fig. 2.1b, c, and d) matched well with those reported earlier [27]. The $ABPBI_{350}$ membrane showed the highest contact angle of 84.2°. All remaining types of membrane showed a contact angle of 76-78°.

2.3.2 Sorption analysis of FSMs

The sorption was studied with a 2 mol L^{-1} concentration of salt ($NaCl/MgCl_2$). As seen from Fig.2.2, FSMs, after dipping in DI water or salt solutions, the sorption increased rapidly within half an hour and equilibrated after ~ 50 h. After this time, sorption still seems to rise until the time of evaluation (400 h), but at a sluggish rate. This slow increase in sorption can be attributed to the sluggish swelling of the polymer matrix by a sorbent (water, salt solution). ABPBI is well known to be a rigid polymer with a high glass transition temperature of 485 °C [35]. The imidazole group in the ABPBI backbone is known to facilitate the sorption of water molecules by hydrogen bonding [36,37]. ABPBI, being wholly aromatic and rigid in nature, might take a long time to achieve a 'thermodynamically stable configuration' of polymer chains.

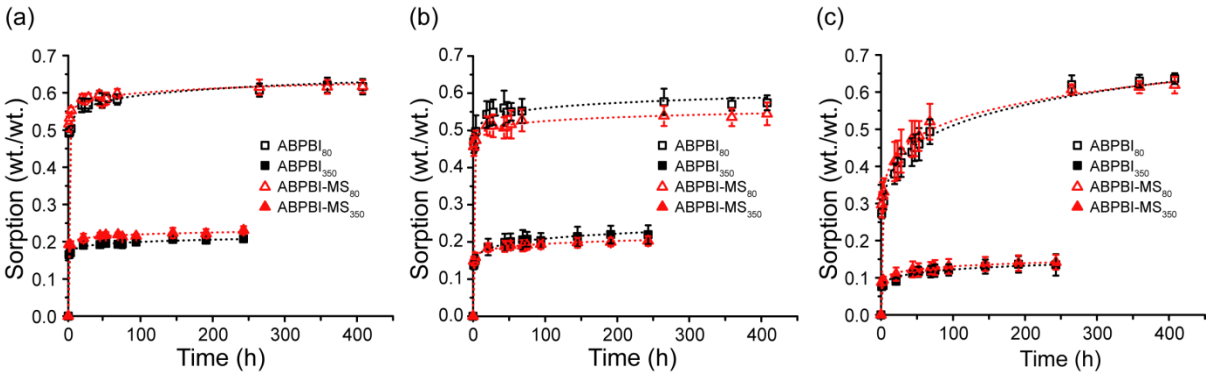

Fig. 2.2. Sorption of a) water, b) aq. 2 mol L^{-1} NaCl, and c) aq. 2 mol L^{-1} $MgCl_2$ in ABPBI FSMs.

The amount of sorption of either water or salt solutions mainly depended on the treatment temperature of FSM. The effect of chemical nature (ABPBI in neutral form or MS-based) is not quantitatively distinctive. Fig. 2.2a shows that after ~ 50 h, the amount of water sorbed by $ABPBI_{80}$ or $ABPBI\text{-}MS_{80}$ is ~ 3 times higher than that of $ABPBI_{350}$ or $ABPBI\text{-}MS_{350}$. Similar holds for the sorption of salt solutions (Fig 2b, c). FSMs treated at 350 °C are associated with water removal, as indicated by TGA (Fig 2.1c). Removing water from the polymer matrix increases H-bonding between polymer chains, leading to their better packing. When such

membranes undergo sorption, diffusion of sorbent (water/salt solution) through the membrane matrix could be sluggish as polymer chains are densely packed.

When the sorption of salt solutions for FSM heated at 80 °C is compared (Fig. 2.2b, c), it was seen that the sorption of the $MgCl_2$ solution is almost half of that of NaCl. For membranes treated at 350 °C, the sorption of the $MgCl_2$ solution is sluggish as compared to NaCl. This behaviour is prominently seen up to ~ 50 h duration. Beyond 200 h, sorption of aq. $MgCl_2$ is slightly higher than that of water or aq. NaCl. This could be due to the further swelling of the polymer matrix, which was assisted by the coordination of divalent $MgCl_2$ with the imidazole group of the PBI matrix, as it is a known phenomenon [38].

2.3.3 Preparation of HFMs and their characterizations

The dope ABPBI solution concentration of ABPBI was 2.5% (wt./wt.). At such a low concentration, the dope pressure needed was 40 psi, and the take-up was 9.8 m min^{-1} (Table 2.1), owing to the higher molecular weight of the polymer indicated by its high inherent viscosity of 4.4 dL g^{-1}. The obtained wet HFMs were rubbery in nature. The FTIR spectra (Fig. 2.3a) of $ABPBI_{80}$, especially in the fingerprint region, matched well with that of the ABPBI polymer (Fig. 2.1b). The MSA-bound membranes ($ABPBI\text{-}MS_{80}$ and $ABPBI\text{-}MS_{350}$) showed a new band at 1171 cm^{-1} due to O=S=O stretching, as reported earlier [39,40]. Although the main peak position in WAXD spectra of all HFMs (Fig. 2.3b) remains similar at ~ 26°, irrespective of their treatment temperature (80 or 350 °C), the pattern at lower 2θ values is different. Their smoothened pattern indicated that thermal treatment suppresses domains with larger d-spacing. It may be recalled from Section 2.3.2 that the sorption of FSMs treated at 350 °C is much lower than that of FSMs treated at 80 °C due to denser chain packing in the earlier cases. It could be due to the elimination of domains with larger d-spacing. The TGA curves (Fig. 2.3c) of ABPBI and ABPBI-MS HFMs show initial decomposition till ~ 300 °C, attributable to water loss, as observed for FSM (Fig. 2.1c). The degradation for ABPBI-based HFM started at ~ 624 °C, while for ABPBI-MS, the degradation started at ~ 456 °C attributable to sulfonate groups [38,39]. At 900 °C, the char yield was high, viz., 71.3 and 62.4 % for ABPBI and ABPBI-MS HFMs, respectively. Higher char yield is a peculiar property of ABPBI, as observed earlier [42].

The cross-sectional microscopic (Fig. 2.3d) and SEM images (Fig. 2.4) of HFMs based on ABPBI and ABPBI-MS treated at 80/350 °C did not reveal any porosity. The structure seems to be uniform throughout the membrane thickness. The HFM modules were prepared

using all four types of HFMs. The integrity of membranes and modules was evaluated by pressurizing helium from the shell side at different pressures.

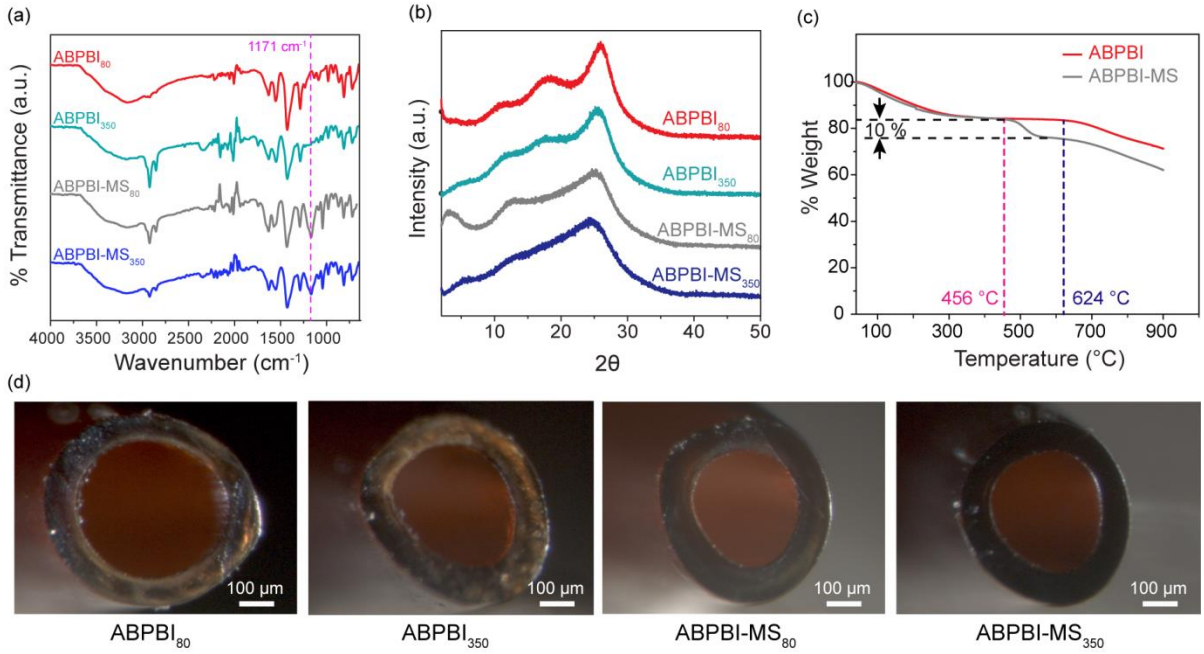

Fig. 2.3. Characterization of ABPBI HFMs: a) FT-IR spectra, b) WAXD pattern, c) TGA curves, and d) microscopic images.

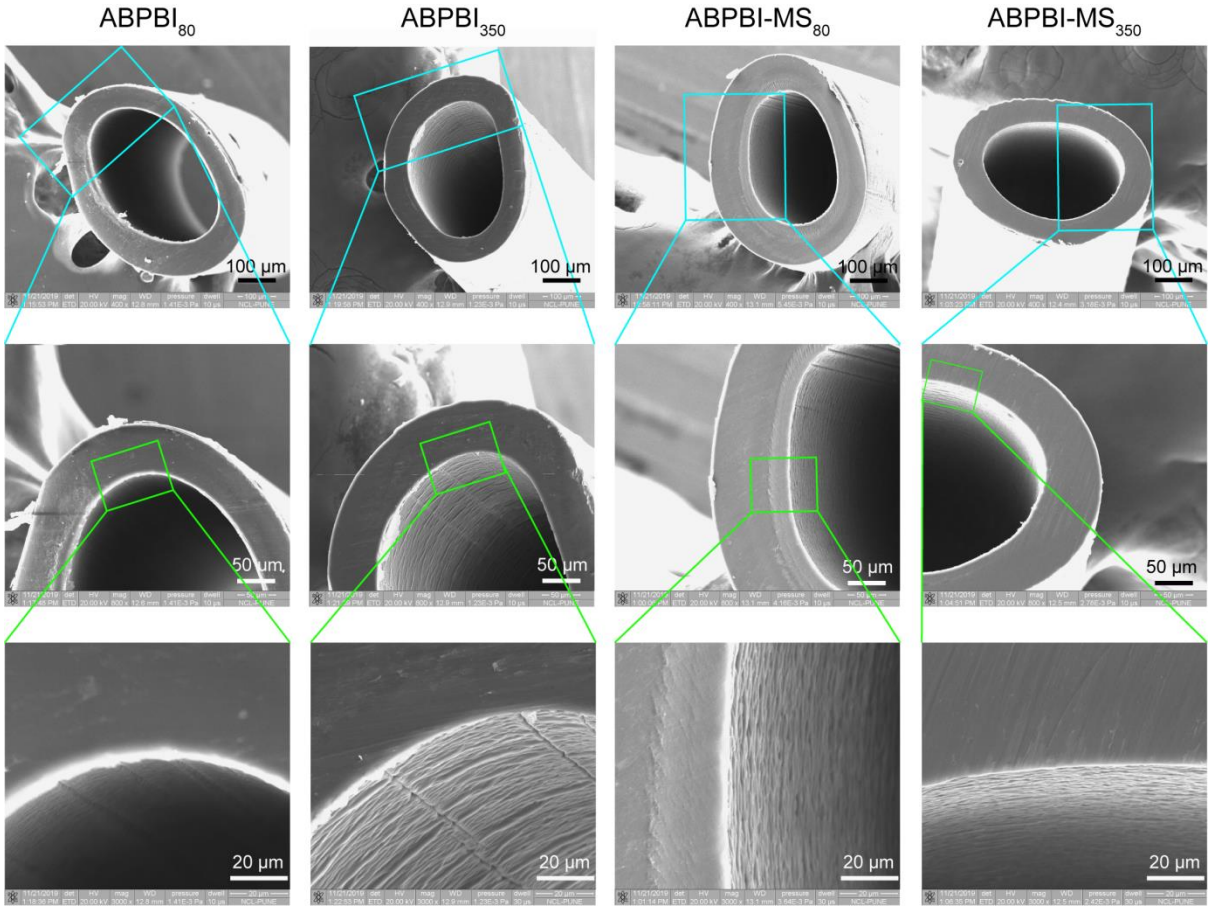

Fig. 2.4. SEM images of HFMs.

The obtained permeance is given in Table 2.3. For the $ABPBI_{350}$ module, no permeance was observed at either applied pressure. Other modules exhibited extremely low helium permeance, owing to the gas diffusion through the membrane matrix. It confirms the SEM observation that the membranes do not have any porosity and are dense in nature.

Table 2.3. Physical size and helium permeation characteristics of HFMs

Membrane identification	**Average membrane dimensions (μm)**			**Permeance of He (GPU*)**	
	Thickness	**Outer diameter**	**Inner diameter**	**At 50 psi**	**At 60 psi**
$ABPBI_{80}$	98.2 ±23	587.3±69	388.6±44	0.0065	0.007
$ABPBI_{350}$	99.7±8	514.4±45	315±41	Nil	
$ABPBI\text{-}MS_{80}$	107.7±26	573.1±65	370.5±50	0.087	0.1
$ABPBI\text{-}MS_{350}$	95.6±9	519±29	331.1±35	0.00089	0.00095

*1 GPU= 10^{-6} (cm^3(STP)/cm^2·cmHg·sec)

2.3.4 FO performance

Initially, membranes heated at 80 °C were analyzed with varying concentrations of NaCl and $MgCl_2$ (Fig. 2.5). The water flux (J_W) and reverse salt flux (J_S) increased linearly with increasing osmotic pressure/concentration of DS. The J_W in the case of $ABPBI_{80}$ with $MgCl_2$ as DS was higher than that of the other 3 cases (Fig 2.5a). A similar observation is noted for salt flux in this case (Fig 2.5b). For membranes treated at 350 °C, the J_W and J_S reduced considerably more than those treated at 80 °C. As elaborated above, it could be related to the tighter chain packing and lower sorption caused by this membrane type.

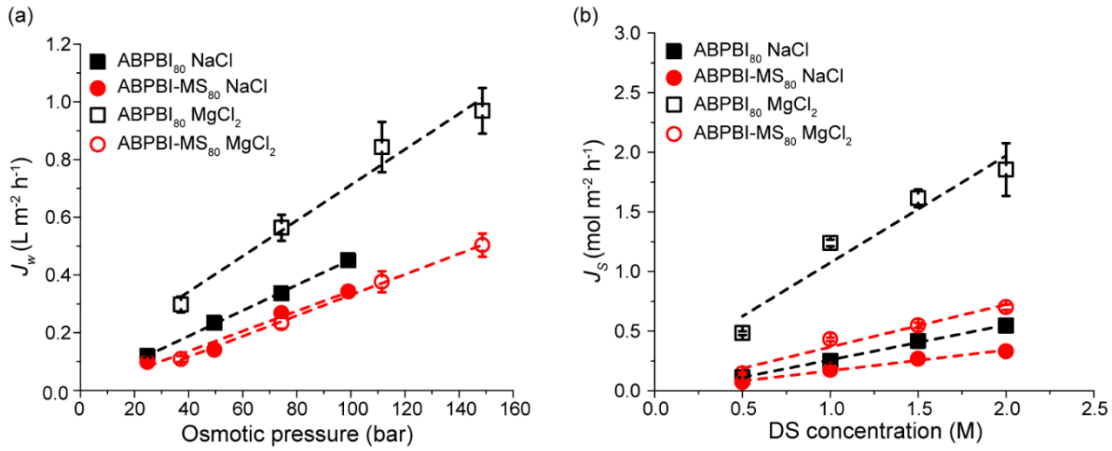

Fig. 2.5. The performance of ABPBI and ABPBI-MS treated at 80 °C: Variation in (a) J_W with an osmotic pressure of DS and (b) J_S with the concentration of DS.

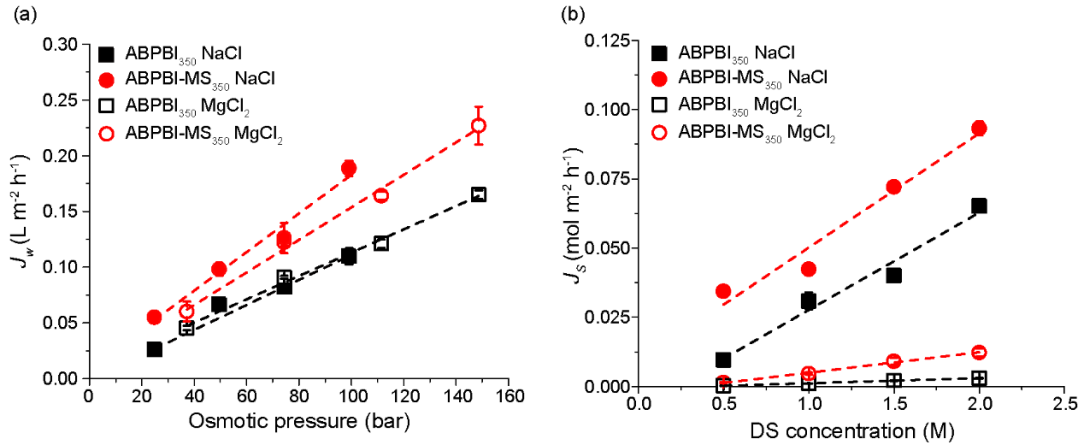

Fig. 2.6. The performance of ABPBI and ABPBI-MS treated at 350 °C: Variation in (a) J_W with the osmotic pressure of DS and (b) J_S with the concentration of DS.

The effect of membrane treatment temperature (80/350 °C), type (ABPBI/AMPBI-MS), and draw solute used (NaCl/$MgCl_2$) can be better visualized from Table 2.4, wherein results obtained using 2 mol L^{-1} DS are tabulated. When the performance of membranes treated at 80 °C is compared, the flux (J_W or J_S) is lower for ABPBI-MS_{80} than for $ABPBI_{80}$ for a particular DS. It could be due to multiple H-bonding possible between an MSA molecule with different imidazole groups that might bring chins closer. When membranes are treated at 350 °C, the chain compactness caused by heating offers an appreciable reduction in the salt flux compared to the decrease in water flux of membranes treated at 80 °C. For a particular DS, the J_W in the case of ABPBI-MS_{350} was higher than that exhibited by $ABPBI_{350}$ (Fig. 2.6). The difference in J_S (either for NaCl or $MgCl_2$) is insignificant. Here, the peculiarity of the presence of MSA in the membrane matrix is visualized. From Fig. 2.3b, it can be deduced that the d-spacing of ABPBI-MS_{350} in dry form is ~3.6 Å, while for $ABPBI_{350}$, it is 3.54 Å. Although the difference is small, it may be responsible for increased water flux. It may be noted that the present membranes are dense in nature, having a thickness of ~ 100 μm (Table 2.3). Although the water flux values appear much smaller, the significance of membrane drying and the presence of MSA in the membrane matrix leading to considerably lower J_S offers highly significant inputs in membrane material design.

Table 2.4. FO performance at 2 mol L^{-1} concentration of DS

Membrane identification	J_W (L m^{-2} h^{-1})		J_S (mol m^{-2} h^{-1})	
	DS: NaCl	DS: $MgCl_2$	DS: NaCl	DS: $MgCl_2$
$ABPBI_{80}$	0.45	0.97	0.55	1.85
ABPBI-MS_{80}	0.34	0.50	0.32	0.70
$ABPBI_{350}$	0.11	0.16	0.07	0.003
ABPBI-MS_{350}	0.19	0.23	0.09	0.012

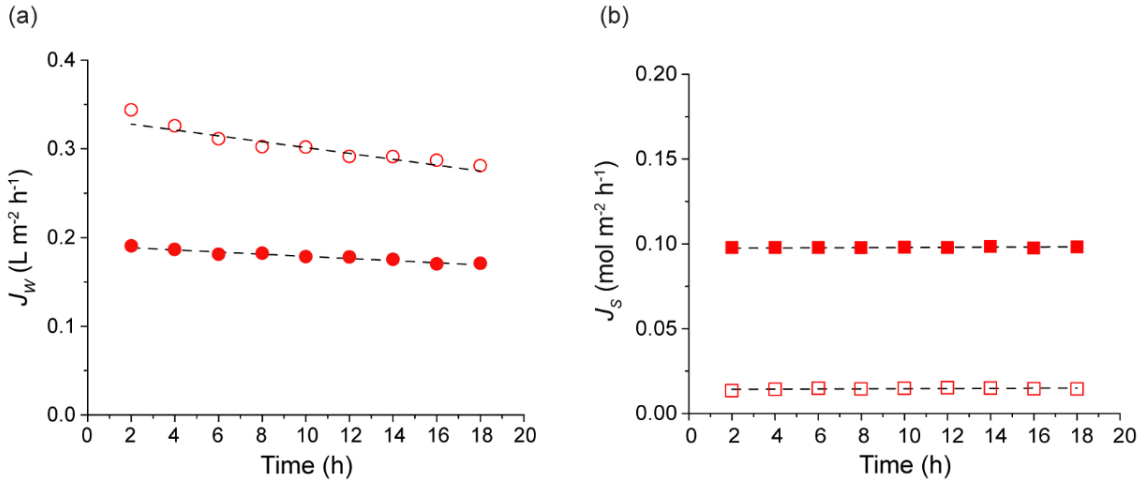

Fig. 2.7. The long-term analysis of ABPBI-MS$_{350}$ using 2 mol L^{-1} NaCl (filled symbols) and $MgCl_2$ (unfilled symbols) as a DS: Variation of (a) J_W and (b) J_S with time.

Based on the above study (especially Fig. 2.6b), ABPBI-MS$_{350}$ was chosen as a membrane for the long-term study, and the obtained results are plotted in Fig. 2.7. In a continuous experiment for 18 h, a slight decrease in J_W and a linear nature of J_S were observed. The observed decrease in J_W can be attributed to a slight reduction in DS concentration due to the passage of water from the DS side to the FS side, leading to a lowering of the DS concentration. This effect is more pronounced for $MgCl_2$, owing to its high osmotic pressure (Fig. 2.7a). The consistency in J_S (Fig. 2.7b) indicated excellent membrane stability over time.

2.3.5 Comparison with the literature reports

It would be worth comparing the FO performance of present ABPBI-based membranes with those reported in the literature. Table 2.5 lists the reverse salt flux (J_S)/rejection, water flux (J_W), and normalized flux (J_N) as FO performance of hollow fiber membranes. Normalized flux (J_N) is a common way of representing the performance of pervaporation membranes [43,44]. Present membranes are dense, with 95-100 µm thickness, while most of the reported membranes are asymmetric. The skin layer thickness (wherever available) is used to calculate J_N for reported membranes. It could be seen that the rejection of present membranes is similar to/better than that of reported PBI membranes [45]. The water flux, J_W, of present membranes is much lower than that of reported membranes. This is attributable to the dense nature and, thus, the large thickness of present membranes (66-83 times higher than reported membranes [46,47]). Thus, J_N could be a better term for comparing fluxes. The estimated values of J_N for present membranes are lower by 3.6 to 63% than those for reported data [46,47]. It indicates that the thickness reduction in present membranes could bring remarkable improvements in the water flux, assuming rejection performance remains the same. It may be recalled that ABPBI

is stable in harsh environments of pH and solvents (DMF, DMAc, chloroform, toluene, and hexane), as reported earlier [29]. The present work thus offers a new avenue for broader applications, especially in harsher environments of solvent and temperature, provided membrane thickness could be reduced. It becomes the next path of our future work.

Table 2.5. Comparison of FO performances of fabricated ABPBI-based HFM with those of HFMs reported in the literature

Membrane/ thickness (µm)	**DS**	J_S (mol m^{-2} h^{-1}) /**Rejection** (%)[b]	J_W (L m^{-2} h^{-1})	J_N[a] (L µm m^{-2} h^{-1})	**Reference**
ABPBI-MS_{350}/95	2 mol L^{-1} NaCl	0.09/99.1	0.19	18	This work
	2 mol L^{-1} $MgCl_2$	0.012/99.9	0.23	21.7	This work
$ABPBI_{350}$/100	2 mol L^{-1} NaCl	0.07/98.4	0.11	11.2	This work
	2 mol L^{-1} $MgCl_2$	0.003/99.9	0.16	16.4	This work
PBI/-	2 mol L^{-1} NaCl	97.31[c]	3.84	-	[45]
	2 mol L^{-1} $MgCl_2$	99.79[c]	9.02	-	
PBI-PES DL/1.5	2 mol L^{-1} $MgCl_2$	0.003	15	22.5	[46]
PBI-POSS/1.2	2 mol L^{-1} NaCl	0.8	25.4	30.38	[47]
PA-PVDF TFC/-	1 mol L^{-1} NaCl	0.14	18.9	-	[48]

[a]Normalized water flux (J_N, L µm m^{-2} h^{-1}) = J_W x Membrane thickness (active layer); [b]Rejection of draw solute (%) = [1-(Salt concentration in FS/Salt concentration in DS)]x100; [c]Salt selectivity.

2.4 Conclusions

This work presents the preparation of symmetric, dense, flat sheet (FSM) and hollow fiber (HFM) membranes based on ABPBI using methane sulfonic acid as a solvent for the dope. The prepared membranes were categorized based on chemical (neutral and containing MSA in the membrane matrix) and thermal treatment (80 and 350 °C). The membranes were characterized for physical (IR, TGA, XRD, contact angle, microscopic and SEM imaging) and helium gas permeation, confirming their dense, impermeable nature. The FSMs were evaluated for sorption of water and 2 mol L^{-1} salt solution (NaCl/$MgCl_2$). The heat treatment at 350 °C reduced sorption by 1/3rd as that of membranes treated at 80 °C. Although NaCl and $MgCl_2$ solutions exhibited similar sorption, the latter was more sluggish than the earlier one. Although most of the sorption occurred within 1 h, it was equilibrated after 50 h, indicating slow swelling of the polymer matrix.

The FO performance of HFMs was evaluated using aqueous NaCl and $MgCl_2$ at varying concentrations. The water flux (*Jw*) and reverse salt flux (RSF, *Js*) were determined using hollow fiber membrane modules of ~ 250 cm^2 active area. The chemical and heat treatment of HFMs affected the FO favourably, especially the rejection performance. The flux (J_W or J_S)

was lower for ABPBI-MS_{80} than that of $ABPBI_{80}$, attributable to the acid-base interactions. For membranes treated at 350 °C, the J_W and J_S reduced considerably compared to membranes treated at 80 °C due to the tighter chain packing and lower sorption caused by this membrane type. The HFM $ABPBI_{350}$ with a thickness of ~100 µm showed a water flux of 0.16 L m^{-2} h^{-1} and reverse salt flux of 0.003 mol m^{-2} h^{-1} while using 2 mol L^{-1} $MgCl_2$ as a DS and DI water as an FS. The same parameters for ABPBI-MS_{350} were 0.23 L m^{-2} h^{-1} and 0.012 mol m^{-2} h^{-1}, respectively, emphasizing the significance of MSA in the membrane matrix. Although the water flux looks much smaller than those reported in the literature, the importance of membrane heat treatment and the presence of MSA in the ABPBI membrane matrix offers significant insights into membrane material design. The long-term analysis exhibited consistent performance. Given the membrane's reproducible and scalable preparation method, chemically robust nature, and extremely low reverse salt flux, ABPBI can be a promising material for FO application, provided the thickness can be reduced further to elevate fluxes.

2.5 References

[1] K. S. Goh, Y. Chen, D. Y. F. Ng, J. W. Chew, R. Wang, Organic solvent forward osmosis membranes for pharmaceutical concentration, J. Memb. Sci. 642 (2022) 119965-119974. https://doi.org/10.1016/j.memsci.2021.119965.

[2] J. Park and S. Lee, Desalination technology in South Korea: a comprehensive review of technology trends and future outlook, Membranes 12 (2022) 204-213. https://doi.org/10.3390/membranes12020204.

[3] M. Yan, Y. Xi, N. Jiang, Q. Li, S. Zheng, Y. Hu, Y. Liu, W. Bao, M. Huang, High-performance thin film composite forward osmosis membrane for efficient rejection of antimony and phenol from wastewater: Characterization, performance, and MD-DFT simulation, J. Memb. Sci. 703 (2024) 122847-122856. https://doi.org/10.1016/j.memsci.2024.122847.

[4] M. Bassiouny, Y. A. Maksoud, F. Kimera, K. Bahader, H Sewilam, Investigating the potential of growing crops hydroponically utilizing feed and draw solutions from13 fertilizer drawn forward osmosis, Environ. Sci. Eur. 35:68 (2023) 2-17. https://doi.org/10.1186/s12302-023-00770-z.

[5] J. Han, P. Dai, C. Gu, Y. Liao, Y. Zhao, A. G. Razaqpur, G. Sun, S. Chou, Emulsified oily wastewater treatment via fertilizer drawn forward osmosis using a corrugated thin film composite membrane, J. Memb. Sci. 685 (2023) 121926-121935. https://doi.org/10.1016/j.memsci.2023.121926.

[6] M. Gulied, K. Logade, H. Mutahir, S. Shaftah, S. Salauddin, A. Hameed, S. Zavahir, T. Elmakki, H. K. Shon, S. Hong, H. Park, D. S. Han, A review of membrane-based dewatering technology for the concentration of liquid foods, J. Environ. Chem. Eng. 11 (2023) 110583-110598. https://doi.org/10.1016/j.jece.2023.110583.

[7] H. Wang, Y. Zhang, S. Ren, J. Pei, Z. Li, Athermal concentration of apple juice by forward osmosis: Process performance and membrane fouling propensity, Chem. Eng. Res. Des. 177 (2022) 569–577, https://doi.org/10.1016/j.cherd.2021.11.023.

[8] J. Yu, W. Jing, E. Liu, S. Du, H. Cai, H. Du, J. Wang, Sulfonated graphene oxide modified polysulfone-polyamide forward osmosis membrane and its application in fluorine-containing wastewater treatment, Mater. Chem. Phys. 313 (2024) 128757-128765. https://doi.org/10.1016/j.matchemphys.2023.128757.

[9] Y. Chun, D. Mulcahy, L. Zou, I. S. Kim, A short review of membrane fouling in forward osmosis processes, Membranes 7 (2017) 30-52. doi:10.3390/membranes7020030.

[10] B. Van der Bruggen, H. Matsuyama, Y. Lin, J. Zheng, Resource recovery and recycling from water streams: advanced membrane technologies and case studies, ACS EST Water 3 (2023) 1699−1701. https://doi.org/10.1021/acsestwater.3c00315.

[11] A. M. Abou-Elanwar, S. Lee, I. Jang, S. Lee, S. Hong, S. Kim, M.-H. Hwang, J. Kim, Y. Kim, Evaluation of a novel fertilizer-drawn forward osmosis and membrane contactor hybrid system for CO_2 capture using ammonia-rich wastewater, J. Memb. Sci. 700 (2024) 122654-122664. https://doi.org/10.1016/j.memsci.2024.122654.

[12] S. Lee, C. Boo, M. Elimelech, S. Hong, Comparison of fouling behavior in forward osmosis (FO) and reverse osmosis (RO), J. Memb. Sci. 365 (2010) 34–39. https://doi.org/10.1016/j.memsci.2010.08.036.

[13] M. Mohammadifakhr, J. de Grooth, K. Trzaskus, H.D.W. Roesink, A.J.B. Kemperman, Single-step synthesis of a polyelectrolyte complex hollow-fiber membrane for forward osmosis, Sep. Purif. Technol. 264 (2021) 118430-118437. https://doi.org/10.1016/j.seppur.2021.118430.

[14] Z. Zhou, Y. Hu, C. Boo, Z. Liu, J. Li, L. Deng, X. An, High-Performance Thin-Film Composite Membrane with an Ultrathin Spray-Coated Carbon Nanotube Interlayer, Environ. Sci. Technol. Lett. 5 (2018) 243–248. https://doi.org/10.1021/acs.estlett.8b00169.

[15] Q. Long, Y. Jia, J. Li, J. Yang, F. Liu, J. Zheng, B. Yu, Recent advance on draw solutes development in Forward osmosis, Processes 6 (2018) 165-184. https://doi.org/10.3390/pr6090165.

[16] L. Francis, O. Ogunbiyi, J. Saththasivam, J. Lawler, Z. Liu, A comprehensive review of forward osmosis and niche applications, Environ. Sci. (Camb) 6 (2020) 1986–2015. https://doi.org/10.1039/d0ew00181c.

[17] L. A. Handojo, K. Khoiruddin, A. K. Wardani, A. N. Hakim, I. G. Wenten, Advancement in forward osmosis (FO) membrane for concentration of liquid foods, in: IOP Conf. Ser. Mater. Sci. Eng., Institute of Physics Publishing, 547 (2019) 12053-12065. https://doi.org/10.1088/1757-899X/547/1/012053.

[18] H. G. Yuan, Y. Y. Liu, T. Y. Liu, X. L. Wang, Self-standing nanofilms of polysulfone doped with sulfonated polysulfone via solvent evaporation for forward osmosis, J. Memb. Sci. 523 (2017) 567–575. https://doi.org/10.1016/j.memsci.2016.09.034.

[19] M. Li, V. Karanikola, X. Zhang, L. Wang, M. Elimelech, A self-standing, support-free membrane for forward osmosis with no internal concentration polarization, Environ. Sci. Technol. Lett. 5 (2018) 266–271. https://doi.org/10.1021/acs.estlett.8b00117.

[20] G. Li, X. M. Li, T. He, B. Jiang, C. Gao, Cellulose triacetate forward osmosis membranes: Preparation and characterization, Desalin. Water Treat. 51 (2013) 2656–2665. https://doi.org/10.1080/19443994.2012.749246.

[21] Y. H. Cho, J. Han, S. Han, M.D. Guiver, H.B. Park, Polyamide thin-film composite membranes based on carboxylated polysulfone microporous support membranes for forward osmosis, J. Memb. Sci. 445 (2013) 220–227. https://doi.org/10.1016/j.memsci.2013.06.003.

[22] M. Mohammadifakhr, J. de Grooth, H.D.W. Roesink, A.J.B. Kemperman, Forward osmosis: A critical review, Processes 8 (2020) 404-432. https://doi.org/10.3390/PR8040404.

[23] G. T. Gray, J. R. McCutcheon, M. Elimelech, Internal concentration polarization in forward osmosis: role of membrane orientation, Desalination 197 (2006) 1–8. https://doi.org/10.1016/j.desal.2006.02.003.

[24] Y. Chun, D. Mulcahy, L. Zou, I.S. Kim, A short review of membrane fouling in forward osmosis processes, Membranes (Basel) 7 (2017) 30-52. https://doi.org/10.3390/membranes7020030.

[25] T. Majeed, F. Lotfi, S. Phuntsho, J. Khee Yoon, K. Kim, H.K. Shon, Performances of PA hollow fiber membrane with the CTA flat sheet membrane for forward osmosis process, Desalin. Water Treat. 53 (2015) 1744-1754. https://doi.org/10.1080/19443994.2013.859103.

[26] A. Nazif, H. Karkhanechi, E. Saljoughi, S.M. Mousavi, H. Matsuyama, Effective parameters on fabrication and modification of braid hollow fiber membranes: A review, Membranes (Basel) 11 (2021) 884-914. https://doi.org/10.3390/membranes11110884.

[27] C. Z. Liang, M. Askari, L. T. (Simon) Choong, T. S. Chung, Ultra-strong polymeric hollow fiber membranes for saline dewatering and desalination, Nat. Commun. 12 (2021) 2338-2349. https://doi.org/10.1038/s41467-021-22684-1.

[28] L. A. Diaz, G. C. Abuin, H. R. Corti, Water and phosphoric acid uptake of poly [2,5-benzimidazole] (ABPBI) membranes prepared by low and high temperature casting, J. Power Sources 188 (2009) 45–50. https://doi.org/10.1016/j.jpowsour.2008.11.114.

[29] H. R. Lohokare, H. D. Chaudhari, U. K. Kharul, Solvent and pH-stable poly(2,5-benzimidazole) (ABPBI) based UF membranes: Preparation and characterizations, J. Memb. Sci. 563 (2018) 743–751. https://doi.org/10.1016/j.memsci.2018.06.052.

[30] S. C. Kumbharkar, U. K. Kharul, New N-substituted ABPBI: Synthesis and evaluation of gas permeation properties, J. Memb. Sci. 360 (2010) 418–425. https://doi.org/10.1016/j.memsci.2010.05.041.

[31] S. Moorthy, B. Maria Mahimai, D. Kannaiyan, P. Deivanayagam, Synthesis and fabrication of Cu-trimesic acid MOF anchored sulfonated Poly(2,5-benzimidazole)

membranes for PEMFC applications, Int. J. Hydrogen Energy 48 (2023) 36063–36075. https://doi.org/10.1016/j.ijhydene.2023.05.362.

[32] S. Bose, T. Kuila, T.X.H. Nguyen, N.H. Kim, K.T. Lau, J.H. Lee, Polymer membranes for high temperature proton exchange membrane fuel cell: Recent advances and challenges, Prog. Polym. Sci. (Oxford) 36 (2011) 813–843. https://doi.org/10.1016/j.progpolymsci.2011.01.003.

[33] J. A. Asensio, P. Gómez-Romero, Recent developments on proton conducting Poly(2,5-benzimidazole) (ABPBI) membranes for high temperature polymer electrolyte membrane fuel cells, Fuel Cells 5 (2005) 336–343. https://doi.org/10.1002/fuce.200400081.

[34] D. D. W. Rufuss, E. Hosseinipour, S. Arulvel, P.A. Davies, Complete parametric investigation of a forward osmosis process using sodium chloride draw solution, Desalination 547 (2023) 116218-116232. https://doi.org/10.1016/j.desal.2022.116218.

[35] K.H. Gharda, P.D. Trivedi, T.R. Parida, A. Biradar, Method for processing a high temperature resistant thermosetting material, (2015) (U.S. Patent No. US 2015/0183993 A1).

[36] P. Staiti, F. Lufrano, A.S. Aricò, E. Passalacqua, V. Antonucci, Sulfonated polybenzimidazole membranes-preparation and physico-chemical characterization, J. Memb. Sci. 188 (2001) 71-78. https://doi.org/10.1016/S0376-7388(01)00359-3.

[37] J. K. Jang, T. H. Kim, Fabrication of tri-directional poly(2,5-benzimidazole) membrane using direct casting for vanadium redox flow battery, Polymers (Basel) 15 (2023) 3577-3590. https://doi.org/10.3390/polym15173577.

[38] S. Horike, K. Kadota, T. Itakura, M. Inukai, S. Kitagawa, Synthesis of magnesium ZIF-8 from $Mg(BH_4)_2$, Dalton Trans. 44 (2015) 15107–15110. https://doi.org/10.1039/c5dt01183c.

[39] J. A. Asensio, S. Borrós, P. Gómez-Romero, Enhanced conductivity in polyanion-containing polybenzimidazoles. Improved materials for proton-exchange membranes and PEM fuel cells, Electrochem. Commun. 5 (2003) 967–972. https://doi.org/10.1016/j.elecom.2003.09.007.

[40] Y. Wang, T. Shung Chung, M. Gruender, Sulfonated polybenzimidazole membranes for pervaporation dehydration of acetic acid, J. Memb. Sci. 415–416 (2012) 486–495. https://doi.org/10.1016/j.memsci.2012.05.035.

[41] X. Glipa, E. Haddad, D.J. Jones, J. Rozieré", R.R. Rozieré", Synthesis and characterisation of sulfonated polybenzimidazole: a highly conducting proton exchange polymer, Solid State Ion. 97 (1997) 323-331. https://doi.org/10.1016/S0167-2738(97)00032-5.

[42] L.F. Fourie, L. Square, C. Arendse, M. Msimanga, ABPBI/MWCNT for proton radiation shielding in low earth orbit, APL Mater. 11 (2023) 71103-71120. https://doi.org/10.1063/5.0156686.

[43] A. Selim, K. Knozowska, B. Ośmiałowski, J. Kujawa, P. Mizsey, W. Kujawski, The fabrication, characterization, and pervaporation performance of poly(ether-block-amide) membranes blended with 4-(trifluoromethyl)-N(pyridine-2-yl)benzamide and 4-(dimethylamino)-N(pyridine-2-yl)benzamide fillers, Sep. Purif. Technol. 268 (2021) 118707-118721. https://doi.org/10.1016/j.seppur.2021.118707.

[44] Y. Wang, T.S. Chung, B.W. Neo, M. Gruender, Processing and engineering of pervaporation dehydration of ethylene glycol via dual-layer polybenzimidazole (PBI)/polyetherimide (PEI) membranes, J. Memb. Sci. 378 (2011) 339–350. https://doi.org/10.1016/j.memsci.2011.05.020.

[45] K.Y. Wang, T.S. Chung, J.J. Qin, Polybenzimidazole (PBI) nanofiltration hollow fiber membranes applied in forward osmosis process, J. Memb. Sci. 300 (2007) 6–12. https://doi.org/10.1016/j.memsci.2007.05.035.

[46] Q. Yang, K.Y. Wang, T.S. Chung, Dual-layer hollow fibers with enhanced flux as novel forward osmosis membranes for water production, Environ. Sci. Technol. 43 (2009) 2800–2805. https://doi.org/10.1021/es803360t.

[47] F.J. Fu, S. Zhang, S.P. Sun, K.Y. Wang, T.S. Chung, POSS-containing delamination-free dual-layer hollow fiber membranes for forward osmosis and osmotic power generation, J. Memb. Sci. 443 (2013) 144–155. https://doi.org/10.1016/j.memsci.2013.04.050.

[48] Y. Yabuno, K. Mihara, N. Miyagawa, K. Komatsu, K. Nakagawa, T. Shintani, H. Matsuyama, T. Yoshioka, Preparation of polyamide–PVDF composite hollow fiber membranes with well-developed interconnected bicontinuous structure using high-temperature rapid NIPS for forward osmosis, J. Memb. Sci. 612 (2020) 118468-118476. https://doi.org/10.1016/j.memsci.2020.118468.

CHAPTER 3

ABPBI-based Flat Sheet Membrane Preparation, Characterizations, their FO Performance, and Acid Enrichment by FO

Abstract

The ABPBI-based thin, scalable flat sheet membranes (FSMs) were prepared and evaluated for the FO. The membranes treated at 60 and 350 ℃ were analyzed for FO using NaCl, $MgCl_2$, or Na_2SO_4 as a draw solute. A study on the effects of membrane treatment temperature on water flux, reverse salt flux (RSF), and long-duration analysis led to an understanding of the applicability of present thin, scalable ABPBI membranes for FO. Although the membrane treated at 350 ºC possessed a lower water flux than those treated at 60 ºC, the lowering in its RSF was highly attractive. $MgCl_2$, having a larger molecular size than NaCl, led to a higher water flux and a considerable reduction in RSF. With Na_2SO_4, extremely low RSF was observed with this membrane. The long-duration study using 2 mol L^{-1} $MgCl_2$ was also investigated. Given the membrane's reproducible and scalable preparation method, chemically robust nature, and extremely low reverse salt flux, ABPBI can be a promising material for FO application. Towards this, the enrichment of carboxylic acid (acetic acid and methacrylic acid) was investigated. The AA and MAA concentrations are increased by approximately 2-fold and 2.26-fold, respectively, than their initial concentration in the feed.

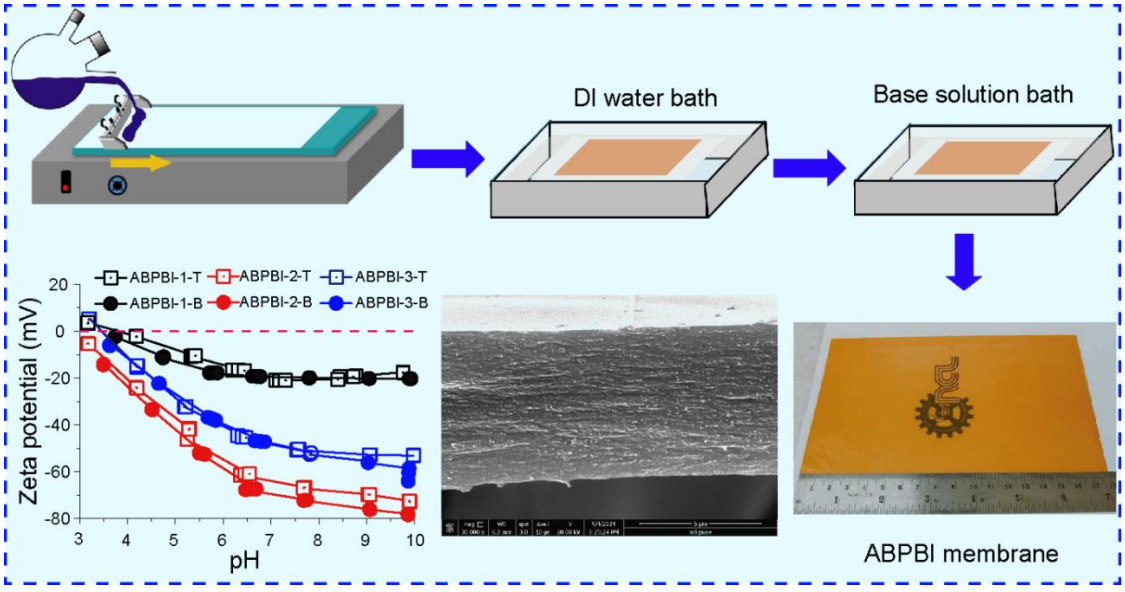

3.1 Introduction

Most demonstrated FO membranes are asymmetric or thin-film composite (TFC) [1-3]. The TFC polyamide (PA) membranes are widely studied and used in FO processes [4-6,3]. It is said that the TFC membranes commonly used in FO technology consist of an ultrathin polyamide (PA) active separation layer and a porous support layer [6]. The porous support layer of such membranes acts as an unstirred diffusive boundary, thus reducing the driving force for water permeation significantly [4,7-9]. Internal concentration polarization (ICP) occurs within the support layer of the membrane and is characterized by differing solute concentrations at the transverse boundaries of that layer [10]. In recent years, researchers have proposed strategies to mitigate ICP by adjusting the membrane structure parameters as well as the hydrophilicity of the support layer (thickness, tortuosity, pore size distribution, and porosity of the membrane support layer) [11-15]. However, significantly reducing the structural parameter of FO membranes is challenging because membranes with thin and highly porous support layers lack the necessary mechanical strength for FO applications [16].

To address this issue, the proposal of using support layer-free, thin films with a symmetric and homogeneous structure merits attention. Freely suspended ultrathin membranes have been a theoretical and experimental curiosity for several decades. Their macroscopic size and infinitesimally small thickness combine the properties of macroscopic materials and individual molecules simultaneously [17,18]. Moreover, as there is no interference (support layer), such a free-standing structure could make the thin membrane versatile in practical applications [19,18]. By removing the support layer, the self-standing nanofilms are especially attractive in FO, anticipating lower energy consumption and much less membrane fouling than pressure-driven membrane processes [20]. The concept of an FO membrane without ICP was proposed in a modeling study of monolayer graphene [21]. The preparation and analysis of support-free FO membranes are well-reported [18,22,20,16,23,24]. However, unlike conventional membranes (that are fabricated on thick porous substrates), mechanical strength is one of the most crucial requirements for a support-free membrane. The freestanding membranes require a certain thickness, commonly a few micrometers or more, to sustain their integrity during operation, which inevitably compromises their water permeability [16,23]. In search of this, the exploration of mechanically robust polymeric materials for scalable fabrication of symmetric FO membranes has yet to be systematically studied [18,23].

Carboxylic acids represent a vital class of organic compounds extensively utilized across the chemical and food industries [25,26]. Their applications include critical

intermediates in organic synthesis, flavoring agents, preservatives, etc. [27]. Among the various carboxylic acids, acetic acid (AA) and methacrylic acid (MAA) are particularly important due to their wide-ranging industrial applications [25,28]. Moreover, releasing acetic acid into industrial effluent due to its widespread use poses significant environmental challenges [29,30]. Recovering carboxylic acids from aqueous solutions is a common challenge in the chemical industry, such as during acid production and wastewater treatment [28]. It is also said that although distillation remains the conventional approach for recovering carboxylic acids from aqueous solutions when their concentration exceeds 50 wt.%, at lower concentrations (<50 wt%), the process becomes highly energy-intensive. Moreover, the propensity of MAA to undergo polymerization at temperatures above the boiling point of water presents an additional challenge, making distillation less effective [31,26]. Solvent extraction offers a viable alternative, but conventional solvents like toluene and heptane have low capacity and selectivity [26]. Therefore, finding a more efficient process for carboxylic acid recovery is essential. The FO was demonstrated using the TFC membrane, whereas FS used various types of carboxylic acids (acetic, butyric, valeric, and lactic acid) [32]. The concentrations obtained by FO after 30 h operation for acetic, butyric, valeric, and lactic acid were 1.65-, 2.2-, 2.3-, and 2.5-fold, respectively. Law et al. [33] employed FO prior to the crystallization process in the downstream recovery of bio-based succinic acid. FO exhibited a remarkable enhancement of concentration factor by 3.9-fold. To our knowledge, the enrichment of MAA and AA to higher concentrations using the FO process has not been previously reported.

For the first time, this work investigates the formation and applicability of a mechanically strong, free-standing, thin, symmetric membrane based on ABPBI for FO. The membranes were fabricated using the phase inversion method. The physicochemical and mechanical properties of the membrane were thoroughly characterized. The water flux and reverse draw solute flux of membranes were determined as a function of membrane heat treatment, different draw solutions, and varying draw solution concentrations. The applicability of this thin, symmetric membrane was demonstrated for the enrichment of AA and MAA. This study provides a new platform for fabricating ABPBI-based scalable membranes with promising FO performance.

3.2 Experimental

3.2.1 Materials

Methanesulfonic acid (MSA) was supplied by Thomas Baker, and sodium bicarbonate ($NaHCO_3$) was procured from Merck. The NaCl, $MgCl_2$, and Na_2SO_4 were procured from

Merck. These chemicals were used without further purification. All draw solutions (DSs) were prepared in deionized water. ABPBI was synthesized as given in Section 2.2.1.

3.2.2 Preparation of FSMs

A 3% (w/w) dope solution was prepared by dissolving ABPBI in MSA at 80 °C while stirring for 24 h, filtered to remove undissolved particles, if any, and degassed for 15 min. Membranes were cast on a flat surface using a tabletop casting machine with a knife gap set at 200 µm, a speed of 5 cm s^{-1}, and water at ambient as a non-solvent (Fig. 3.1). The obtained membranes were washed with DI water to remove free MSA, dipped in 0.1 N $NaHCO_3$ for 8 h to remove bound MSA, and stored at 4 °C until use. These FSMs were heat-treated at 60 and 350 °C for 1 h while sandwiching between porous plates. For ABPBI-3 (Table 3.1), 3 cycles of the heating membrane at 350 °C for 1 h, followed by cooling at ambient for 1 h, was performed. The average membrane thickness was ~17 (±2) µm.

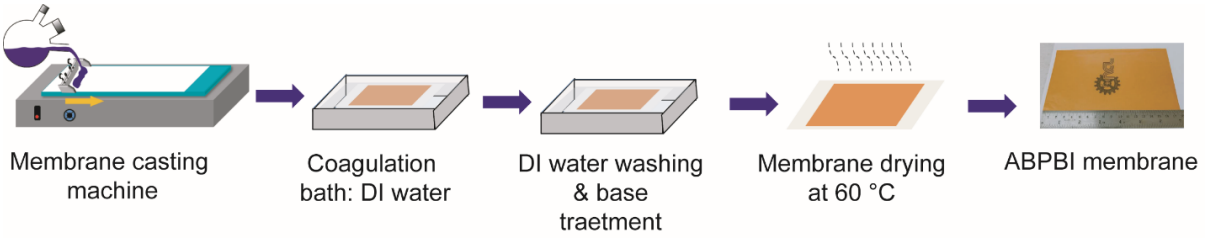

Fig. 3.1 Schematic representation of flat sheet membrane preparation.

Table 3.1 Nomenclature of membranes

Membrane identification	**Treatment temperature for 1 h duration (°C)**	**Number of cycles**
ABPBI-1	60	1
ABPBI-2	350	1
ABPBI-3	350	3

3.2.3 Physical characterization of FSMs

The FTIR spectra were recorded using Bruker Optics ALPHA-E spectrometer with a universal Zn-Se ATR accessory in a 600-4000 cm^{-1} frequency region. The wide-angle X-ray diffraction (WAXD) spectra were recorded with Rigaku SmartLab X-ray diffractometer in reflection mode using CuKα radiation (λ =1.5418 Å). The scan range was 5-40° at a scan rate of 3° min^{-1}. The thermogravimetric analysis (TGA) was performed on TGA-STA6000 (TA Instruments) in an N_2 atmosphere with a heating rate of 10 °C min^{-1}. The water contact angle

of the membrane surface was obtained using Drop Shape Analyzer DSA25- KRÜSS GmbH. A water drop of constant size (20 µL) was placed on the surface, and a digital image was recorded using a built-in drop-shape analysis tool. For each type of membrane, 6 samples were analyzed and data averaged. The streaming potential was measured with a SurPASS3 instrument (Anton-Paar) equipped with an adjustable gap cell. Samples were soaked in 5 mmol L^{-1} KCl as an electrolyte for 12 h, and the streaming potential was measured across the pH range of 3 to 10. The HCl or KOH solutions (0.05 mol L^{-1}) were used to adjust the pH of the electrolyte. Three measurements were made at each pH. The zeta potential was calculated from the measured streaming potential by application of the Helmholtz-Smoluchowski equation using instrument software. The tensile tests were performed at ambient on Linkam TST-350 micro-tensile testing instrument using the dumbbell-shaped film samples (6 samples for each membrane, with a length of 2.8 cm, a width of 1.2 cm and an average thickness of 17 ± 2 µm). The Field Emission Scanning Electron Microscope (FE-SEM) images were analyzed using gold-sputtered cross-section and surface samples of membrane on FEI Nova NanoSEM 650 FE-SEM, with a field emitter as an electron source. Atomic Force Microscopy (AFM, Nanosurf) was used to measure the root mean square roughness (Rq) and arithmetic average roughness (Ra) of the top and bottom membrane surfaces. The Rq and Ra were averaged from 3 different profiles of AFM images of each membrane type.

3.2.3 FO analysis

The FO performance of membranes was evaluated using a plate and frame module (SS-316) with an active area of 120 cm^2 (Fig. 3.2).

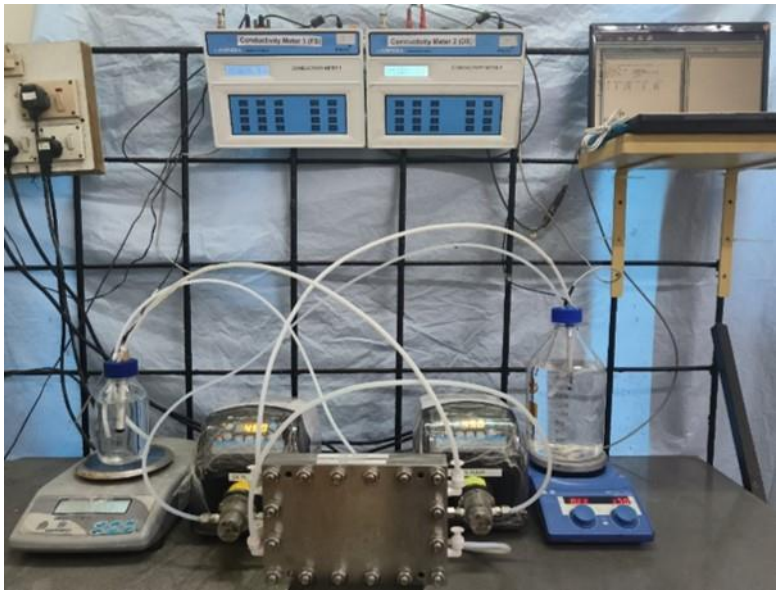

Fig. 3.2 Photographs of the experimental setup of FO with FSM module.

Three membranes were used for each set of experiments, and the results were averaged. The DI water was used as a solvent (feed solution, FS) using varying concentrations (0.5-2 mol L^{-1}) of $MgCl_2$ in DI water as a draw solution (DS). For other experiments, 1.5 mol L^{-1} of NaCl and Na_2SO_4 was used as a DS. Before performing an FO experiment, the membrane was saturated with FS for 2 h. The FS (0.5 L) and DS (2 L) were recycled on the top and bottom side of the membrane, respectively, at ambient using a gear pump (LeadFluid) at the flow rate of 150 ml min^{-1} (cross-flow velocity of 20 cm s^{-1}).

The pressure transmitters were fitted at the outlet of the DS and FS channels to record the pressure exerted on the membrane due to the flow of the solution. It was observed that no pressure was generated until the flow rate of 150 ml min^{-1}. The pressure started increasing beyond this flow rate. An electronic weighing balance (Contech CA-3102, connected to a computer for online data acquisition) was used to monitor weight change in FS. The water flux (J_W) was calculated using Eq. 3.1 [34].

$$J_W = \frac{\Delta M}{A_m \, X \, \Delta t} \tag{3.1}$$

where, ΔM (g) is the change in the weight of FS over the duration, Δt (h) (either 2 or 16 h). The A_m (m^2) is the active membrane area. The concentration of FS was monitored using a conductivity meter (LABINDIA PICO$^+$). The reverse salt flux (RSF) (J_S) was determined using Eq. 3.2 [35].

$$J_s = \frac{C_f V_f - C_i V_i}{A_m \, X \, \Delta t} \tag{3.2}$$

where, C_i and C_f (mol L^{-1}) denote the initial and final concentration of salt in the FS while V_i and V_f represent its initial and final volume, respectively. Thickness normalized total flux (J_N) was calculated using Eq. 3.3.

$$J_N = J_W \, X \, \delta \tag{3.3}$$

where, δ is the membrane thickness in μm. The specific reverse salt flux (SRSF, mol L^{-1}) was calculated using Eq. 3.4 [35].

$$SRSF = \frac{J_S}{J_W} \tag{3.4}$$

3.2.4 Acids enrichment by FO

An initial DS volume was 2 L, and the initial FS (containing AA or MAA) volume was 0.25 L. The temperature of both solutions was maintained at 25 °C. Water permeate volume from FS to DS was detected by measuring the online weight change of the FS with analytical balance as mentioned above (Section 3.2.3), and the acid concentration in the FS/DS was determined periodically by titrating a small sample against standardized 0.5 M NaOH by using

Labindia Automatic Titrator (Titra+). The FO experiment protocols for the AA and MAA enrichments are described in Table 3.4.

To investigate the acid transport, sampling of the DS was taken at varying times, t, till the end of the experiments. Since the DS is getting diluted, the calculated rejection value could be higher than the actual rejection performance. Hence, an adjustment on the concentration of the acid can be performed by taking into account the dilution factor (Eq. 3.5) [36,33]:

$$C_{fs(t)} = C_{fs(DC)} \times \frac{V_{DS(t)}}{V_P} \quad (3.5)$$

where $C_{fs(t)}$ is the corrected concentration of the acid in the DS compartment at time t, $C_{fs(DC)}$ is the measured concentration of acid in the DS compartment at time t, $V_{DS(t)}$ is the volume of the DS at time t, and V_P is the permeate volume of water to the DS at time t.

The acid rejection (R_{FO}) was calculated using Eq. (3.6) [36,33]:

$$R_{FO}(\%) = \left(1 - \frac{C_{fs(t)}}{C_{i(t)}}\right) \times 100\% \quad (3.6)$$

where $C_{i(t)}$ is the concentration of acid in the FS at time *t*.

The acid flux (J_{fs}) was determined using Eq. (3.7) [37,33]:

$$J_{fs} = \frac{m_{fs}}{A_m \times \Delta t} \quad (3.7)$$

where m_{fs} is the mass of the acid in the DS compartment at time t. The mass of the acid (m_{fs}) was measured by analysing acid concentration ($C_{fs(DC)}$) by auto-titrator. The concentration factor (*CF*) of the target solute in the FS at time t was calculated using Eq. 3.8 [32,33]:

$$CF = \frac{C_{i(t)}}{C_{i(0)}} \quad (3.8)$$

3.3 Results and discussion

3.3.1 Characterizations of FSMs

The FTIR spectra of all membranes (Fig. 3.3a) and the TGA curve of ABPBI-3 (Fig. 3.3b) matched well with the respective analyses of polymer (Fig. 2.1 section in 2.3.1), indicating their stability at a treatment temperature of 350 °C. The TGA pattern showed an initial weight loss of 7.5%. This presence of water can be attributed to the ability of ABPBI to pick up moisture from the atmosphere, as reported earlier [38]. It may be noted that the char yield increased from 59% (for the polymer) to 70% for ABPBI-3. Such a high char yield of ABPBI is known in the literature [39-41]. In the WAXD spectra of FSMs (Fig. 3.3c), the peak at ~ 26° (average d-spacing = 3.42 Å) remained the same as that of polymer. After the membranes were treated at 350 °C, the lower 2θ value (10°) pattern was smoothened. It indicates that the heat treatment suppressed domains having larger d-spacing (8.84 Å), which

is beneficial for membrane application in obtaining higher selectivity. Such observation was noted earlier for usual PBI also [42]. The average water contact angle of membranes treated at 60 °C was 63.5° (Fig. 3.3d). It increased to 79.7° (ABPBI-2) after the membrane was treated at 350 °C, probably due to the removal of the water. This data matched with our earlier report [43].

The zeta potential of all three types of membranes (Fig. 3.3e) exhibited a negative charge in a wide range of pH (3 to 10) and thus are capable of repelling anionic [44,45] species present in the DS. The zeta potential values of the top and bottom surfaces of membranes are similar. It indicates that both sides of membranes are symmetric in nature. The stress-strain curves (Fig. 3.3f) show that the ABPBI-1 exhibited the highest elongation at break (26.3%) due to the moisture present in it. After heat treatment at 350 ºC, the modulus and tensile stress increased for ABPBI-2 and ABPBI-3. Similar variations in mechanical properties of ABPBI by annealing are reported by Chaudhari et al. [46].

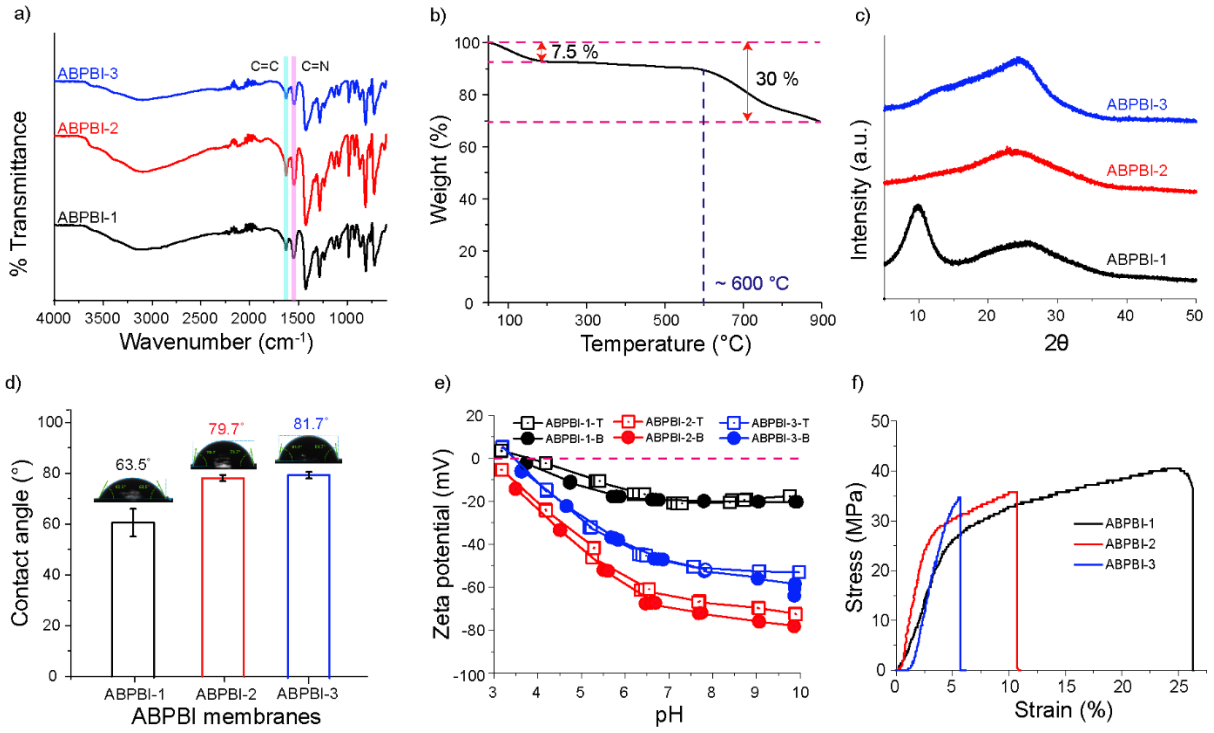

Fig. 3.3 Characterizations of FSMs: a) FT-IR spectra, b) TGA of ABPBI-3, c) WARD pattern, d) contact angle of membrane surfaces, e) zeta potential curves, and f) stress-strain curves.

The present membranes were transparent, thin, and flexible (Fig. 3.4). The FE-SEM images of the surface (top and bottom) and cross-section are shown in Fig. 3.4. The surface morphology on both sides of all three membranes was similar. The cross-section images of

both membranes did not exhibit any porosity. It was demonstrated that the porosity of ABPBI-based membranes is eliminated by heat treatment [46,43].

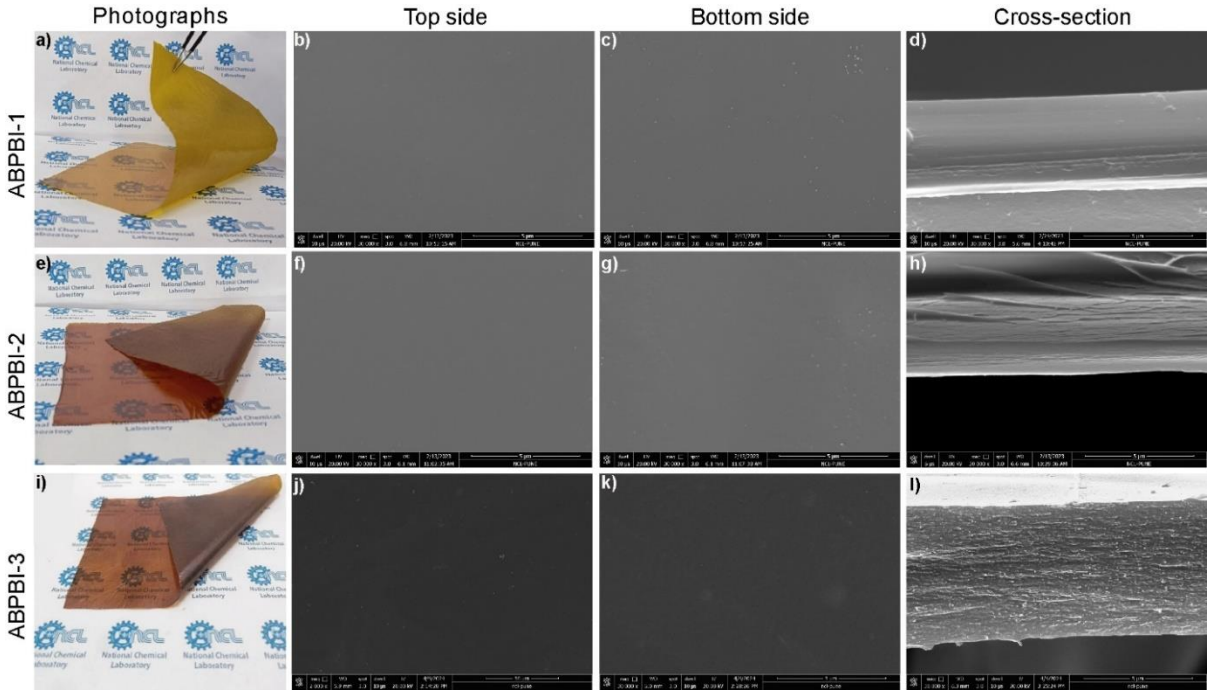

Fig. 3.4 Digital and FESEM images of present membranes.

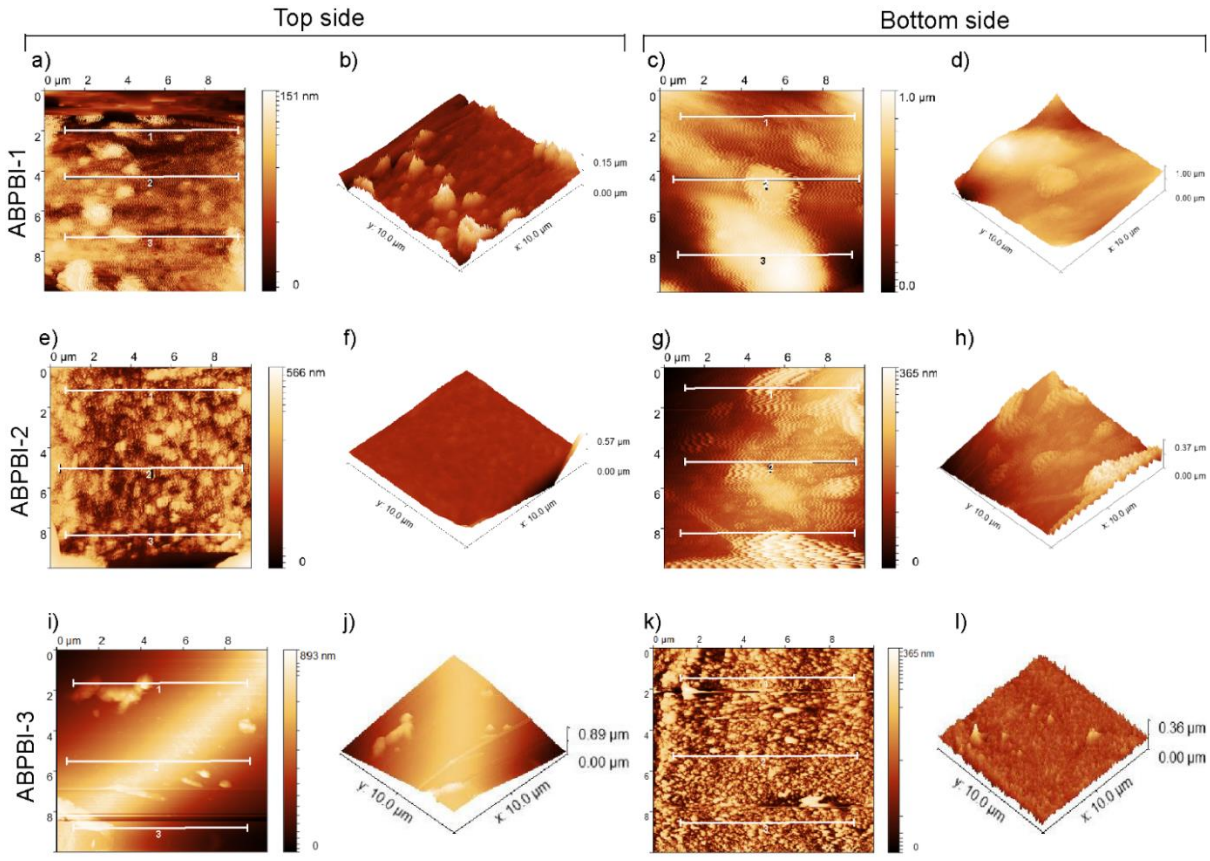

Fig. 3.5 Top and bottom surface topography and 3D AFM images of present membranes.

Table 3.2 The roughness of the membrane surface

Temperature of membrane treatment (°C)	**The surface of the membrane analyzed**	**Roughness (nm)**	
		R_q*	**R_a#**
ABPBI-1	Top	1.64 ± 0.4	1.63 ± 0.4
	Bottom	6.4 ± 1.4	5.1 ± 1.1
ABPBI-2	Top	1.44 ± 0.1	1.15 ± 0.1
	Bottom	2.5 ± 0.13	1.92 ± 0.14
ABPBI-3	Top	0.2 ± 0.05	0.14 ± 0.03
	Bottom	0.6 ± 0.17	0.5 ± 0.14

Rq*: Root mean square average of height deviation taken from the mean image data plane
Ra#: Arithmetic average of the absolute values of the surface height deviations measured from the mean plane

The surface roughness of each membrane was analyzed by AFM on three different profiles, as shown in Fig. 3.5. The Rq and Ra values are summarized in Table 3.2. Although there is a slight difference in the roughness of the top and bottom sides of ABPBI-1 (dried at 60 ºC), it was reduced by heat treatment for ABPBI-2 and ABPBI-3. It is reported that the heat treatment leads to compactness and is characterized by AFM (surface roughness) [45,47]. It may be thus asserted that the top and bottom sides of present membranes are similar.

3.3.2 Effects of membrane heat treatment and different DS

Initially, both membranes, ABPBI-1 and ABPBI-2, were evaluated using DI water as the FS and Na_2SO_4 as a draw solute (Fig. 3.6a). The average J_W for ABPBI-1 and ABPBI-2 was 2.26 and 0.87 L m^{-2} h^{-1}, while the RSF (J_{Na2SO4}) was 0.66 and 0.0044 mol m^{-2} h^{-1}, respectively. The presence of water and domains with larger d-spacing (average d-spacing of 8.84 Å as discussed in Section 3.2.1) in ABPBI-1 could be responsible for its higher RSF and water flux than ABPBI-2. After the heat treatment at 350 °C for the ABPBI-2 membrane, the flux was reduced to ~ 1/3rd, while the J_{Na2SO4} was reduced considerably to 0.7% compared to ABPBI-1. This observation endorses the importance of water removal by heat treatment at 350 ºC. With the removal of water molecules, the H-bonding between water and ABPBI repeat unit is replaced by the intermolecular H-bonding within ABPBI chains. As a result, domains of larger d-spacing are eliminated, and both J_W and J_{Na2SO4} are reduced. It shows that by heat-treating the membrane at 350 ºC, a slight compromise on J_W offered a better advantage of lowering the J_S.

To evaluate the performance of NaCl, $MgCl_2$, and Na_2SO_4 as a draw solute, ABPBI-2 was used, as it performed better than ABPBI-1. Its water and reverse salt fluxes are plotted for various draw solutions with the same concentration of 1.5 mol L^{-1} (Fig. 3.6b). Focusing first on the J_S, it is observed that the J_S was in the order of NaCl>$MgCl_2$>Na_2SO_4. Comparing NaCl and $MgCl_2$, the divalent cation, Mg^{2+}, can be better rejected by the ABPBI-2 membrane. It possessed the lowest reverse salt fluxes for Na_2SO_4 (0.0044 mol m^{-2} h^{-1}). On the other hand, the reverse salt flux of NaCl (the most commonly used DS in the literature) is 0.26 mol m^{-2} h^{-1}, which is much higher. However, it should be noted that although the concentrations of the DSs are equal, the osmotic pressure differs, impacting the water flux. At the same concentration of DS, the osmotic pressure is in the order of $MgCl_2$>NaCl>Na_2SO_4. Therefore, J_W is higher for $MgCl_2$ than the other two.

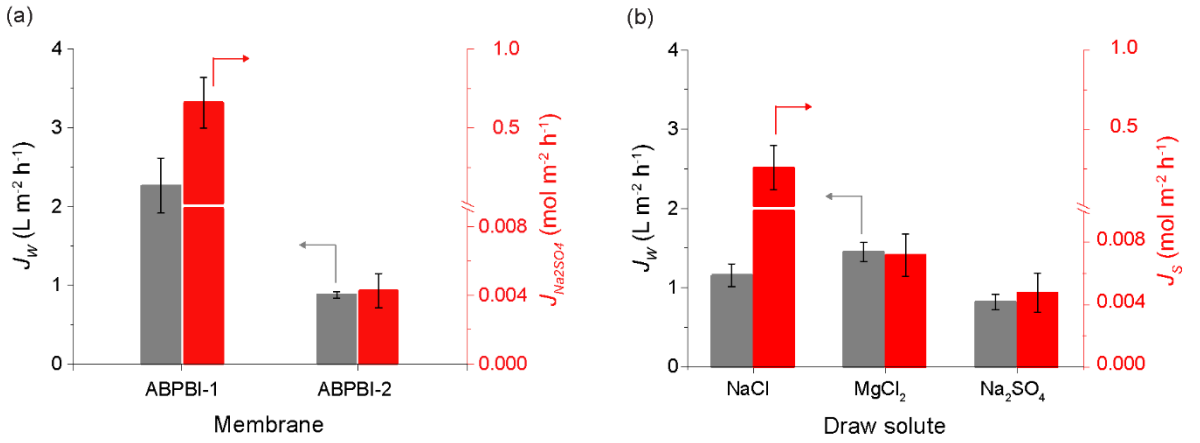

Fig. 3.6 Variation in J_W and RSF (a) with membrane treatment condition (FS: DI water, DS: 1.5 mol L^{-1} aq. Na_2SO_4) and (b) for ABPBI-2 using different DS (conc. 1.5 mol L^{-1}).

3.3.3 Effect of DS concentration and duration analysis

Fig. 3.7a shows that with an increase in the concentration of DS, flux increased linearly for ABPBI-2.

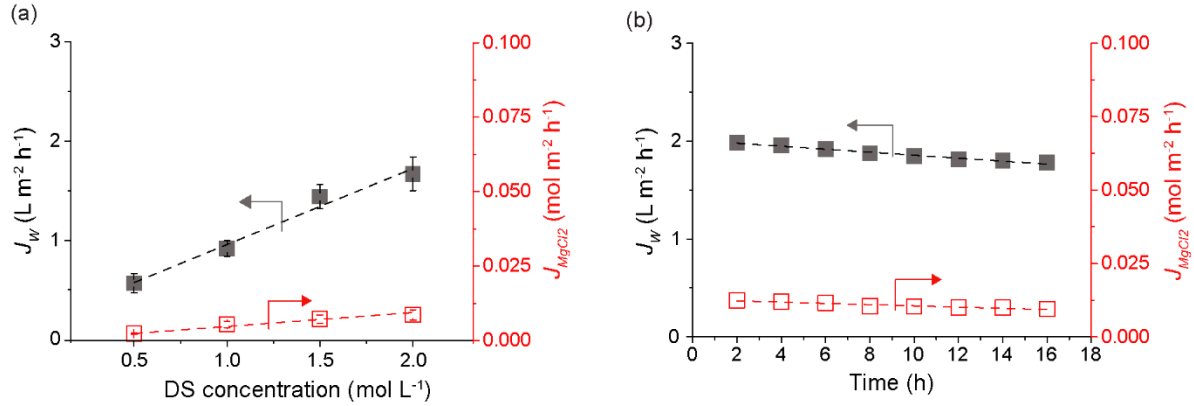

Fig. 3.7 FO performance of ABPBI-2 using $MgCl_2$ as a DS and DI water as FS; (a) variation in DS concentration and (b) long duration stability (DS: 2 mol L^{-1}).

By increasing the DS concentration from 0.5 to 2 mol L^{-1}, J_{MgCl2} increased by ~ 4 times, but the J_W increased by ~ 3. The RSF of 0.0085 mol m^{-2} h^{-1} at a DS concentration of 2 mol L^{-1} is appreciably low. The long-term analysis using ABPBI-2 (Fig. 3.7b) showed an almost linear water and salt flux, with a slight decrease in J_W, attributable to a slight reduction in DS concentration with time. The initial concentration of 2 mol L^{-1} was lowered to 1.85 mol L^{-1} at the end of the experiment (16 h). Although the membrane thickness is low (~17 μm), its stability over a longer duration of operation is evident.

3.3.4 Comparison with the literature

The FO performances of the present membrane (ABPBI-2) and some literature data are given in Table 3.3.

Table 3.3 Comparison of present FO data with the relevant literature

Membrane (thickness, μm)	**DS**	J_W (L m^{-2} h^{-1})	J_N (L μm m^{-2} h^{-1})	J_S (mol m^{-2} h^{-1})	**SRSF** (mol L^{-1})	**Ref.**
ABPBI-2 (17)	2 mol L^{-1} NaCl	1.5	25.5	0.35	0.23	This work
	2 mol L^{-1} $MgCl_2$	1.8	30.6	0.009	0.005	
	1.5 mol L^{-1} Na_2SO_4	0.82	13.94	0.005	0.006	
	4 mol L^{-1} $MgCl_2$	4.3	73.1	0.034	0.008	
SPBI-60 (0.25-0.47)	1.5 mol L^{-1} Na_2SO_4	28.1	7	0.016	0.08	[23]
	1.5 mol L^{-1} $MgCl_2$	19	8.9	0.124	0.68	
	2 mol L^{-1} NaCl	20	9.4	6.4	0.32	
rGO (0.1)	2 mol L^{-1} NaCl	57	5.7	0.022	0.0004	[18]
PA (0.1)	1 mol L^{-1} NaCl	6	0.6	0.005	0.0008	[22]
PA (0.25)	1mol L^{-1} NaCl	80	20	0.6	0.008	[48]
PSf/sPSf (M-1SPSf-35u) (0.046)	1.25 mol L^{-1} Na_2SO_4	46.4	2.1	1.01	0.022	[20]
PTAODH-1.0 (5)	1.5 mol L^{-1} Na_2SO_4	18	90	0.07	0.003	[16]
SPEK-40 (0.6)	2 mol L^{-1} NaCl	35	21	0.68	0.02	[24]

The first column gives the name of the membrane and its thickness. To have uniformity in the performance comparison, we used two terms, viz., normalized flux, J_N (Eq. 3.3), and SRSF (Eq. 3.4). In most of the reported cases, the membrane thickness is at least an order of magnitude lower than the thickness of the present membrane. Thus, when normalized flux is

compared for any of the reported membranes, it is generally higher, and RSF is lower for the present membrane, except for PA-based membranes reported by Cui et al. [22]. If SRSF is compared, the value for $MgCl_2$ in the present case (0.005 mol L^{-1}) is an order of magnitude lower than the data from the literature [23].

3.4 Acid enrichment by FO

The acid enrichment experiments were conducted using the ABPBI-2 membrane, and AA and MAA were chosen as model feed solutes. Before conducting FO-acid experiments, the FO performance of the ABPBI-2 was evaluated using DI water as an FS and 4 mol L^{-1} $MgCl_2$ as a DS. The average J_W and RSF (J_{MgCl2}) was 4.3 L m^{-2} h^{-1} and 0.034 mol m^{-2} h^{-1}, respectively (Table 3.4). By increasing the concentration of $MgCl_2$ from 2 to 4 mol L^{-1}, the J_W increased by ~ 2.5 times. The RSF of 0.034 mol m^{-2} h^{-1} at a DS concentration of 4 mol L^{-1} is undoubtedly low and appreciable from the application perspective.

Table 3.4. FO performance of membrane prior to acid concentration

Membrane	**FS**	**DS**	J_W **(L m^{-2} h^{-1})**	J_{MgCl2} **(mol m^{-2} h^{-1})**
ABPBI-2	DI water	4 mol L^{-1} $MgCl_2$	4.3 ± 0.4	0.034 ± 0.018

The molecular weight, acid dissociation constant (pKa), and concentration of AA and MAA in the FS are given in Table 3.5. The AA or MAA feed solution concentrations were 4.84 and 2.95 mol L^{-1}, while 4 mol L^{-1} $MgCl_2$ solutions were used as DS.

Table 3.5. Acid and their concentration used for acid enrichment using $MgCl_2$ (4 mol L^{-1}) as DS and ABPBI-2 as a membrane

Acid in FS	**Molecular weight (g mol^{-1})**	**Acid dissociation constant (pKa)**	**Concentration of FS**	
			(mol L^{-1})	**(wt. %)**
AA	60.05	4.70	4.84	27.71
MAA	86.06	4.76	2.95	24.90

The variation of acid concentration in FS during the FO experiment is shown in Fig. 3.8. The AA and MAA enrichment by FO was conducted for 12 h and 23 h, respectively. In this case, acid enrichment occurs as water moves from the FS to the DS, causing an increase in the concentration of acids in the FS. Fig. 3.8 shows that AA is concentrated rapidly than MAA, possibly due to differences in their molecular characteristics.

The concentration factor (*CF*) is an important parameter used in FO. As seen in Table 3.6, AA and MAA were concentrated by 2-fold and 2.26-fold, respectively. The AA was

concentrated to 9.7 mol L^{-1} from an initial feed value of 4.84 mol L^{-1}. The MAA was concentrated to 6.7 mol L^{-1} from an initial feed value of 2.95 mol L^{-1}. The observed higher value of MAA could be due to its higher experimental time. The rejection of acid by the FO membrane is presented in Table 3.6. The rejection was >98% for AA and MAA, indicating insignificant acid leakage to the DS. Such observation also explained the high *CF* obtained in this work. The rejection of AA was slightly lower than that of MAA. This can be ascribed to its lower molecular weight and monovalent nature. The reverse chloride fluxes of 4 $MgCl_2$ as DS were between 1.61 and 3.45 mol L^{-1} h^{-1} for MAA and AA as FS, respectively.

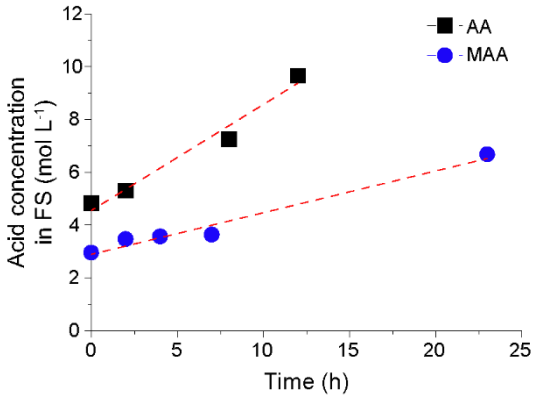

Fig. 3.8 Variation of acid concentration in FS with time.

Table 3.6. Acid concentration factor (*CF*), concentration in FS, acid rejection (R_{FO}), and acid flux (J_{fs}) of AA and MAA

Membrane used	**Acid**	***CF***	$C_{i(0)}$ **(mol L^{-1})**	$C_{i(t)}$ **(mol L^{-1})**	R_{FO} **(%)**	J_{fs} **(mol m^{-2} h^{-1})**	J_W **(L m^{-2} h^{-1})**	J_S **(mol m^{-2} h^{-1})**
ABPBI-2	AA	2.00	4.84	9.7 (12 h)	98.3	2.50	0.92	3.45
	MAA	2.26	2.95	6.7 (23 h)	99.6	0.23	0.50	1.61

Along with the acid rejection, the acid flux indicating the forward transport of acid is also provided in Table 3.6. These findings could be helpful for process design and optimization in FO. Overall, the results implied that FO is feasible in treating actual acidic feed, as water permeates while maintaining almost complete rejection of feed solutes.

3.4.1 Comparison of FO-based acid enrichment with the literature

The comparison of FO-based acid enrichment performances of the present membrane (ABPBI-2) and literature data is given in Table 3.7. Only AA data from the literature is provided to be uniform in the performance comparison. Although the initial feed concentration

of AA was much higher than for reported cases, the present *CF* value is generally higher, except for the TFC membranes reported by Bladin et al. [49]. To the best of our knowledge, no literature report on the MAA enrichment by FO exists. If acid rejection (R_{FO}) is compared, the value for AA in the present case (98.3%) is an order of magnitude higher than the data from the literature [32,49,50], except for CTA membranes reported by Law et al. [33]. This comparison endorses better results for the present membranes than that of reported.

Table 3.7. Comparison of present FO-based acid enrichment with the literature reports

Membrane	**Acid in FS**	**Initial FS concentration (mol L^{-1})**	***CF***	R_{FO} **(%)**	**Ref.**
PS-ABPBI-2	AA	4.84	2	98.3	This work
	MAA	2.95	2.26	99.6	
CTA	AA	0.06	1.9	98.05	[33]
OsMem^{TM} TFC-ES FO	AA	0.01	1.65	71	[32]
PA TFC	AA	0.01	1.0	20	[50]
TFC from Porifera Inc. (Hayward, CA, USA)	AA	0.001	3.75	90	[49]

3.5 Conclusions

Thin, solvent-stable, symmetric ABPBI membranes were successfully prepared for the FO process. The physical characterizations, viz., zeta potential, FE-SEM, and AFM, showed their symmetric, dense nature. The membrane heat treatment, using different DS solutes with varying concentrations, showed its impact on the FO performance. The membrane treated at 350 ºC showed enhanced salt rejection capability. Initial evaluations show that the ABPBI-2 has a higher rejection of draw solute than ABPBI-1. The $MgCl_2$ as a DS shows higher water flux than NaCl and Na_2SO_4 at the same concentration. The ABPBI-2 membrane with 2 mol L^{-1} $MgCl_2$ as a draw solute offered attractive results of water flux (J_W: 1.8 L m^{-2} h^{-1}) and low reverse salt flux (J_{MgCl2}: 0.009 mol m^{-2} h^{-1}). Osmotically driven FO is an exciting method of concentrating AA and MAA at ambient conditions. With acid solution as the FO feed, AA and MAA concentration was increased by approximately 2-fold to 9.7 mol L^{-1} and 2.26-fold to 6.7 mol L^{-1}, from an initial feed value of 4.84 and 2.95 mol L^{-1}, respectively. The ABPBI-2 membrane satisfied the high AA and MAA rejection (> 98%), a crucial requirement in FO operation. The overall findings showcased the applicability of present membranes for FO to increase the concentration of acids.

Although the water flux looks much smaller than those reported in the literature, the importance of membrane heat treatment of the ABPBI membrane matrix enhancing solute rejection offers significant insights into membrane material design. The long-term analysis exhibited consistent performance. Given the scalable preparation method of present membranes, the chemically robust nature of ABPBI, and reproducible results (esp. extremely low reverse salt flux), their practical applicability looks highly promising. To conclude, ABPBI can be a promising membrane material for FO application, provided the thickness can be reduced further to elevate fluxes.

3.6 References

[1] T.P.N. Nguyen, B.-M. Jun, Y.-N. Kwon, The chlorination mechanism of integrally asymmetric cellulose triacetate (CTA)-based and thin film composite polyamide-based forward osmosis membrane, J. Memb. Sci. 523 (2017) 111–121. https://doi.org/10.1016/j.memsci.2016.09.020.

[2] T. Götz, B. Achenbach, T. Schiestel, Cellulose acetate hollow fiber membranes for forward osmosis using the Green solvent agnique AMD 3 L, ACS Appl. Polym. Mater. 5 (2023) 4411–4418. https://doi.org/10.1021/acsapm.3c00522.

[3] W. Suwaileh, S. Attar, F. Abu-Rub, A. El-Ghenym, K. ElSaid, A. Badreldin, M. Al-Hashimi, A. Abdel-Wahab, A. Abdala, Thin-film composite forward osmosis membrane with superior alkaline stability, J. Environ. Chem. Eng. 13 (2025) 114909-114920. https://doi.org/10.1016/j.jece.2024.114909.

[4] A. Tiraferri, N.Y. Yip, W.A. Phillip, J.D. Schiffman, M. Elimelech, Relating performance of thin-film composite forward osmosis membranes to support layer formation and structure, J. Memb. Sci. 367 (2011) 340–352. https://doi.org/10.1016/j.memsci.2010.11.014.

[5] N. Akther, S. Phuntsho, Y. Chen, N. Ghaffour, H.K. Shon, Recent advances in nanomaterial-modified polyamide thin-film composite membranes for forward osmosis processes, J. Memb. Sci. 584 (2019) 20–45. https://doi.org/10.1016/j.memsci.2019.04.064.

[6] N. Abounahia, A.A. Shahab, M.M. Khan, H. Qiblawey, S.J. Zaidi, A comprehensive review of performance of polyacrylonitrile-based membranes for forward osmosis water separation and purification process, Membranes (Basel) 13 (2023) 872-909. https://doi.org/10.3390/membranes13110872.

[7] Q. She, R. Wang, A.G. Fane, C.Y. Tang, Membrane fouling in osmotically driven membrane processes: A review, J. Memb. Sci. 499 (2016) 201–233. https://doi.org/10.1016/j.memsci.2015.10.040.

[8] S.S. Manickam, J.R. McCutcheon, Understanding mass transfer through asymmetric membranes during forward osmosis: A historical perspective and critical review on measuring structural parameter with semi-empirical models and characterization

approaches, Desalination 421 (2017) 110–126. https://doi.org/10.1016/j.desal.2016.12.016.

[9] K.S. Piash, O. Sanyal, Design strategies for forward osmosis membrane substrates with low structural parameters-A review, Membranes (Basel) 13 (2023) 73-102. https://doi.org/10.3390/membranes13010073.

[10] G.T. Gray, J.R. McCutcheon, M. Elimelech, Internal concentration polarization in forward osmosis: role of membrane orientation, Desalination 197 (2006) 1–8. https://doi.org/10.1016/j.desal.2006.02.003.

[11] A.K. Ghosh, E.M.V. Hoek, Impacts of support membrane structure and chemistry on polyamide–polysulfone interfacial composite membranes, J. Memb. Sci. 336 (2009) 140–148. https://doi.org/10.1016/j.memsci.2009.03.024.

[12] X. Li, Q. Li, W. Fang, R. Wang, W.B. Krantz, Effects of the support on the characteristics and permselectivity of thin film composite membranes, J. Memb. Sci. 580 (2019) 12–23. https://doi.org/10.1016/j.memsci.2019.03.003.

[13] L.E. Peng, Z. Yao, Z. Yang, H. Guo, C.Y. Tang, Dissecting the role of substrate on the morphology and separation properties of thin film composite polyamide membranes: Seeing is believing, Environ. Sci. Technol. 54 (2020) 6978–6986. https://doi.org/10.1021/acs.est.0c01427.

[14] F. Xiao, H. Ge, Y. Wang, S. Bian, Y. Tong, C. Gao, G. Zhu, Novel thin-film composite membrane with polydopamine-modified polyethylene support and tannic acid-Fe3+ interlayer for forward osmosis applications, J. Memb. Sci. 642 (2022) 119976-119991. https://doi.org/10.1016/j.memsci.2021.119976.

[15] J. Farahbakhsh, M. Golgoli, M. Khiadani, M. Najafi, W. Suwaileh, A. Razmjou, M. Zargar, Recent advances in surface tailoring of thin film forward osmosis membranes: A review, Chemosphere 346 (2024) 140493-140519. https://doi.org/10.1016/j.chemosphere.2023.140493.

[16] M. Li, V. Karanikola, X. Zhang, L. Wang, M. Elimelech, A self-standing, support-free membrane for forward osmosis with no internal concentration polarization, Environ. Sci. Technol. Lett. 5 (2018) 266–271. https://doi.org/10.1021/acs.estlett.8b00117.

[17] R. Vendamme, S.-Y. Onoue, A. Nakao, T. Kunitake, Robust free-standing nanomembranes of organic/inorganic interpenetrating networks, Nat. Mater. 5 (2006) 494–501. https://doi.org/10.1038/nmat1655.

[18] H. Liu, H. Wang, X. Zhang, Facile fabrication of freestanding ultrathin reduced graphene oxide membranes for water purification, Adv. Mater. 27 (2015) 249–254. https://doi.org/10.1002/adma.201404054.

[19] E. Stratakis, G. Eda, H. Yamaguchi, E. Kymakis, C. Fotakis, M. Chhowalla, Free-standing graphene on microstructured silicon vertices for enhanced field emission properties, Nanoscale 4 (2012) 3069–3074. https://doi.org/10.1039/c2nr30622k.

[20] H.-G. Yuan, Y.-Y. Liu, T.-Y. Liu, X.-L. Wang, Self-standing nanofilms of polysulfone doped with sulfonated polysulfone via solvent evaporation for forward osmosis, J. Memb. Sci. 523 (2017) 567–575. https://doi.org/10.1016/j.memsci.2016.09.034.

[21] J.-G. Gai, X.-L. Gong, Zero internal concentration polarization FO membrane: functionalized graphene, J. Mater. Chem. A 2 (2014) 425-429. https://doi.org/10.1039/c3ta13562d.

[22] Y. Cui, X.-Y. Liu, T.-S. Chung, Ultrathin polyamide membranes fabricated from free-standing interfacial polymerization: Synthesis, modifications, and post-treatment, Ind. Eng. Chem. Res. 56 (2017) 513–523. https://doi.org/10.1021/acs.iecr.6b04283.

[23] W. Cheng, J. Ma, X. Zhang, M. Elimelech, Sub-1 μm free-standing symmetric membrane for osmotic separations, Environ. Sci. Technol. Lett. 6 (2019) 492–498. https://doi.org/10.1021/acs.estlett.9b00364.

[24] S. Phuntsho, J.E. Kim, V.H. Tran, S. Tahara, N. Uehara, N. Maruko, H. Matsuno, S. Lim, H.K. Shon, Free-standing, thin-film, symmetric membranes: Next-generation membranes for engineered osmosis, J. Memb. Sci. 607 (2020) 118145-118154. https://doi.org/10.1016/j.memsci.2020.118145.

[25] N. Murali, K. Srinivas, B.K. Ahring, Biochemical production and separation of carboxylic acids for biorefinery applications, Fermentation 3 (2017) 22-46. https://doi.org/10.3390/fermentation3020022.

[26] Y. Bai, R. Yan, W. Tu, J. Qian, H. Gao, X. Zhang, S. Zhang, Selective separation of methacrylic acid and acetic acid from aqueous solution using carboxyl-functionalized ionic liquids, ACS Sustain. Chem. Eng. 6 (2018) 1215–1224. https://doi.org/10.1021/acssuschemeng.7b03516.

[27] G. Lidén, Carboxylic acid production, Fermentation 3 (2017) 46-48. https://doi.org/10.3390/fermentation3030046.

[28] J. Li, Z. Peng, C. Li, P. Li, R. Gani, Process design and economic analysis of methacrylic acid extraction for three organic solvents, Chin. J. Chem. Eng. 27 (2019) 2909–2916. https://doi.org/10.1016/j.cjche.2019.02.014.

[29] C. Agarwal, A.K. Pandey, Remediation and recycling of inorganic acids and their green alternatives for sustainable industrial chemical processes, Env. Sci. Adv. 2 (2023) 1306–1339. https://doi.org/10.1039/d3va00112a.

[30] E. Gao, R. Meng, Q. Jin, S. Yao, Z. Wu, J. Li, E. Du, Highly effective mineralization of acetic acid wastewater via catalytic ozonation over the promising MnO2/γ-Al2O3 catalyst, Chemical Physics Impact 6 (2023) 100149-100160. https://doi.org/10.1016/j.chphi.2022.100149.

[31] W. Raza, J. Wang, J. Yang, T. Tsuru, Progress in pervaporation membranes for dehydration of acetic acid, Sep. Purif. Technol. 262 (2021) 118338-118358. https://doi.org/10.1016/j.seppur.2021.118338.

[32] T. Ruprakobkit, L. Ruprakobkit, C. Ratanatamskul, Carboxylic acid concentration by forward osmosis processes: Dynamic modeling, experimental validation and

simulation, Chem. Eng. J. 306 (2016) 538–549. https://doi.org/10.1016/j.cej.2016.07.091.

[33] J.Y. Law, A.W. Mohammad, Z.K. Tee, N.K. Zaman, J.M. Jahim, J. Santanaraj, M.S. Sajab, Recovery of succinic acid from fermentation broth by forward osmosis-assisted crystallization process, J. Memb. Sci. 583 (2019) 139–151. https://doi.org/10.1016/j.memsci.2019.04.036.

[34] Y. Cui, T.-S. Chung, Pharmaceutical concentration using organic solvent forward osmosis for solvent recovery, Nat. Commun. 9 (2018) 1426-1434. https://doi.org/10.1038/s41467-018-03612-2.

[35] K.S. Goh, Y. Chen, D.Y.F. Ng, J.W. Chew, R. Wang, Organic solvent forward osmosis membranes for pharmaceutical concentration, J. Memb. Sci. 642 (2022) 119965-119974. https://doi.org/10.1016/j.memsci.2021.119965.

[36] M. Xie, W.E. Price, L.D. Nghiem, M. Elimelech, Effects of feed and draw solution temperature and transmembrane temperature difference on the rejection of trace organic contaminants by forward osmosis, J. Memb. Sci. 438 (2013) 57–64. https://doi.org/10.1016/j.memsci.2013.03.031.

[37] C. Kim, S. Lee, H.K. Shon, M. Elimelech, S. Hong, Boron transport in forward osmosis: Measurements, mechanisms, and comparison with reverse osmosis, J. Memb. Sci. 419–420 (2012) 42–48. https://doi.org/10.1016/j.memsci.2012.06.042.

[38] S. C. Kumbharkar, U. K. Kharul, New N-substituted ABPBI: Synthesis and evaluation of gas permeation properties, J. Memb. Sci. 360 (2010) 418–425. https://doi.org/10.1016/j.memsci.2010.05.041.

[39] S.-K. Kim, T.-H. Kim, T. Ko, J.-C. Lee, Cross-linked poly(2,5-benzimidazole) consisting of wholly aromatic groups for high-temperature PEM fuel cell applications, J. Memb. Sci. 373 (2011) 80–88. https://doi.org/10.1016/j.memsci.2011.02.039.

[40] A. K. Mishra, N. H. Kim, J. H. Lee, Effects of ionic liquid-functionalized mesoporous silica on the proton conductivity of acid-doped poly(2,5-benzimidazole) composite membranes for high-temperature fuel cells, J. Membr. Sci. 449 (2014) 136-145. http://dx.doi.org/10.1016/j.memsci.2013.08.023.

[41] A. Das, P Ghosh, S. Ganguly, D. Banerjee, K. Kargupta, Salt-leaching technique for the synthesis of porous poly(2,5-benzimidazole) (ABPBI) membranes for fuel cell application, J. Appl. Polym. Sci. 135 (2017) 45773-45783. https://doi.org/10.1002/APP.45773.

[42] G. M. Shi, Y. Wang, T. S. Chung, Dual-layer Pbi/p84 hollow fibers for pervaporation dehydration of acetone, AICHE J. 58 (2012) 1133-1145. https://doi.org/10.1002/aic.12625.

[43] S. Gawas, L. Alladi, U. K. Kharul, Chemodialysis of organic acids using ABPBI-based hollow fiber membranes, J. Membr. Sci. 689 (2024) 122153-122162. https://doi.org/10.1016/j.memsci.2023.122153.

[44] D. Breite, M. Went, A. Prager, A. Schulze, The critical zeta potential of polymer membranes: how electrolytes impact membrane fouling, RSC Adv. 6 (2016) 98180-98189. https://doi.org/10.1039/C6RA19239D.

[45] Y. Mansourpanah, S.S. Madaeni, A. Rahimpour, A. Farhadian, The effect of non-contact heating (microwave irradiation) and contact heating (annealing process) on properties and performance of polyethersulfone nanofiltration membranes, Appl. Surf. Sci. 255 (2009) 8395–8402. https://doi.org/10.1016/j.apsusc.2009.05.100.

[46] H. D. Chaudhari, R. Illathvalappil, S. Kurungot, U. K. Kharul, Preparation and investigations of ABPBI membrane for HT-PEMFC by immersion precipitation method, J. Membr. Sci. 564 (2018) 211-217. https://doi.org/10.1016/j.memsci.2018.07.026.

[47] P. Karami, S. A. Aktij, K. Moradi, M. Rastgar, B. Khorshidi, F. Mohammadtabar, J. Peichel, M. McGregor, A. Rahimpour, J. B. P. Soares, M. Sadrzadeh, Comprehensive characterization of commercial reverse osmosis membranes through high-temperature cross-flow filtration, ACS Omega 9 (2024) 1990−1999. https://doi.org/10.1021/acsomega.3c09331.

[48] M. Zheng, X. Zhao, S. Xu, D. Lu, Ultrathin support-free membrane with high water flux for forward osmosis desalination, Water Air Soil Pollut. 230 (2019) 138-145. https://doi.org/10.1007/s11270-019-4192-z.

[49] G. Blandin, B. Rosselló, V.M. Monsalvo, P. Batlle-Vilanova, J.M. Viñas, F. Rogalla, J. Comas, Volatile fatty acids concentration in real wastewater by forward osmosis, J. Memb. Sci. 575 (2019) 60–70. https://doi.org/10.1016/j.memsci.2019.01.006.

[50] N. Asghar, H. Lee, D. Jang, A. Jang, Recovery of volatile fatty acids using forward osmosis: Influence of solution chemistry, temperature, and membrane orientation, Chemosphere 303 (2022) 134814-134823. https://doi.org/10.1016/j.chemosphere.2022.134814.

CHAPTER 4

Thin, Flat Sheet, Solvent-Stable ABPBI-based Membranes for Organic Solvent Forward Osmosis (OSFO)

Abstract

The work demonstrates ABPBI-based thin, solvent-stable, scalable flat sheet membranes for organic solvent forward osmosis (OSFO). The membranes treated at 60 and 350 ℃ were analyzed for OSFO using solvents of industrial significance (methanol, ethanol, acetonitrile, N,N-dimethylformamide, and dimethyl sulphoxide). Although LiCl could be employed as a draw solute with methanol as a solvent, its insolubility in other organic solvents led to the use of a new, simple-to-synthesize acid-base salt, viz., triethylammonium benzoate (TB) as a draw solute. A study on the effects of membrane treatment temperature on solvent flux, reverse salt flux (RSF), ability to use TB as a draw solute with other solvents, long-duration analysis, and use of model organic compounds in the feed side led to an understanding of the applicability of present thin, scalable ABPBI membranes for OSFO. Although membranes treated at 350 ℃ possessed a lower methanol flux than those treated at 60 ºC, the lowering in its RSF was highly attractive. TB, having a larger molecular size than LiCl, led to a slight reduction in methanol flux and a considerable reduction in RSF. The use of TB, which possessed extremely low RSF with the chosen solvents, was a remarkable finding. The long-duration study using MeOH and acetonitrile was also investigated. A complete rejection of all model organic compounds of varying molecular weights and chemical functionality indicated the merits of the present thin, scalable ABPBI membranes for practical applications of OSFO.

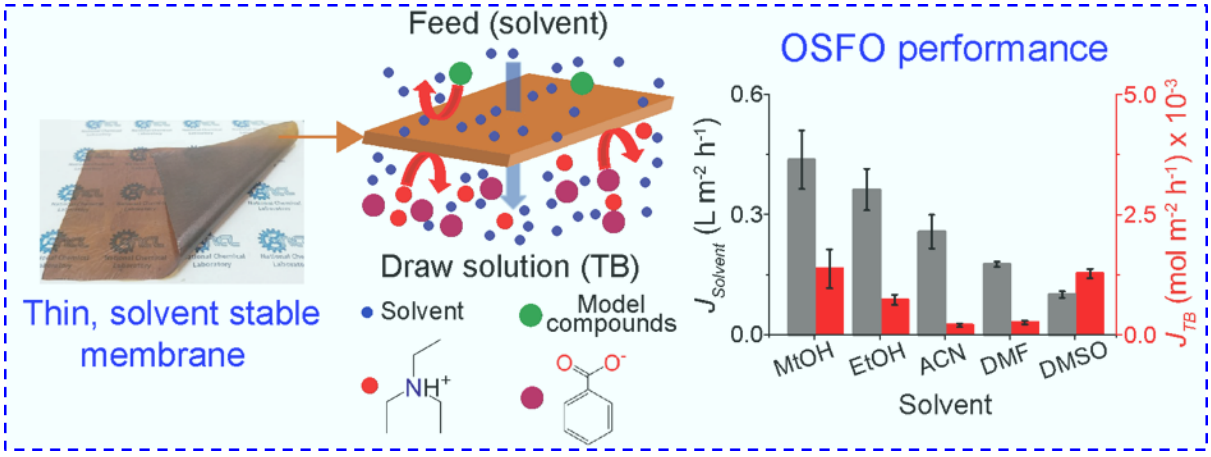

4.1 Introduction

Over the past decade, Organic Solvent Forward Osmosis (OSFO) has attracted attention as an emerging technology for solvent-related separation applications [1-8]. Organic solvents are commonly used in the pharmaceutical industry to synthesize active pharmaceutical ingredients (APIs), cleaning agents, chemicals [9,10], etc. Multiple-stage purification of pharmaceuticals and their intermediates makes solvent removal an essential step [8]. The costs of processing these organic solvents for separation, recovery, or disposal are substantial and comprise a significant fraction of operating expenses [11]. The solvent separation in industries is usually done by distillation, which has high energy consumption due to the latent heat of vaporization [12]. Moreover, manufacturing processes may be heat-sensitive in nature [4]. The membrane-based separations of organic solvents are pervaporation (PV) [13], organic solvent reverse osmosis (OSRO) [14], and organic solvent nanofiltration (OSN) [15]. Energy-efficiency calculations confirmed that OSN uses 25 times less energy per liter of recovered solvent than distillation [11]. However, the high pressure used in OSN remains a concern as it may add extra operating and maintenance costs [8]. OSFO would be economical and potentially enable bulk chemical separations that are not accessible by OSRO [16]. Another benefit of OSFO is that a suitable draw solute can generate sufficiently high osmotic pressure to concentrate APIs [4]. This is difficult to meet by pressure-driven OSN due to the high operating pressure required to overcome the osmotic pressure.

An ideal OSFO membrane should be thin, have a narrow pore size distribution, offer enhanced solvent flux with high solute rejection, and have organic solvent tolerance in long-duration operations [7]. Various efforts of membrane preparation for OSFO are demonstrated in the literature. Cui et al. prepared a TFC membrane consisting of a polyamide (PA) selective layer and a porous polyimide substrate [8]. The authors discussed alternate draw solutes to lithium chloride (LiCl), which is said to be harmful. An MXene-interlayered PA membrane for OSFO exhibited high ethanol flux and low specific salt flux [6]. Tong et al. demonstrated graphene oxide (GO) based membranes for OSFO of methanol, using citric acid as a draw solute [7]. Wei et al. developed a modified simultaneous phase-inversion and crosslinking method for fabricating solvent-resistant polyimide and demonstrated OSFO performance using LiCl-ethanol (1 mol L^{-1}) as a draw solution [17]. A hollow fiber TFC module for OSFO was evaluated using PEG-400 as a DS in acetone and isopropanol as solvents [4]. A polyketone-based TFC hollow fiber membrane with a polyamide selective layer was demonstrated for OSFO using methanol as solvent, sucrose octaacetate as a model API, and polyethylene glycol 400 (PEG-400)/methanol solution as a draw solution [1].

Self-standing support-free films have raised considerable attention because of their ease of fabrication, structural control, and ability to minimize ICP effects [18-23]. Although OSFO is demonstrated for methanol, ethanol, isopropanol, acetone, *N*,*N*-dimethylformamide, and hexane [1-4,6-8,17], other common solvents of industrial significance need a membrane material that is solvent stable. The pharmaceutical/chemical industries use acetonitrile, dichloromethane, dimethyl sulfoxide, 1,4-dioxane, *N*-methyl-*2*-pyrrolidone, tetrahydrofuran, ethyl acetate, toluene, etc. routinely [9,14,24,25], for which need of a stable OSFO membrane material is still awaited. It is said that exploring other membrane materials is of great value for the practical application of OSFO processes in broader fields [7].

In this study, we report, for the first time, the fabrication of free-standing flat sheet membranes for OSFO based on poly(2,5-benzimidazole), commonly known as ABPBI. It is not only known for excellent thermochemical stability [26,27], it is insoluble in common organic solvents (chlorinated solvents, tetrahydrofuran, dioxane, toluene, *N*,*N*-dimethylformamide, *N*,*N*-dimethylacetamide and *N*-methyl-*2*-pyrrolidone) [27,28], which are being used in pharmaceuticals and chemical industries, as stated above. ABPBI has a high N-H group density [29], possesses closed chain packing, and can form H-bonding with water/polar solvents. Moreover, its excellent pH stability is known [27]. It could be a good membrane material for OSFO and open up new avenues owing to its niche characteristics (especially solvent and pH stability). Free-standing, thin, flat sheet membranes (FSMs) were made to investigate their OSFO performance. Initial evaluations used methanol as a solvent and LiCl as a draw solute. Looking at the insolubility of LiCl in many organic solvents, an easy-to-synthesize salt of triethylamine and benzoic acid was used as a draw solute with different solvents. This work investigates scalable OSFO membranes based on ABPBI for various solvents.

4.2 Experimental

4.2.1 Materials

A LiCl was procured from Avra Synthesis. Methanol (MeOH), ethanol (EtOH), *N*,*N*-dimethylformamide (DMF), dimethyl sulfoxide (DMSO), acetonitrile (ACN), triethylamine, and benzoic acid were procured from Merck. The *p*-nitrophenol (NP), *o*-nitroaniline (NA), methyl red (MR), malachite green (MG), rhodamine B (RB), direct red 81 (DR), aniline blue (AB) were procured from Himedia Laboratories Pvt. Ltd.

4.2.2 Preparation of triethylammonium benzoate (TB) and its draw solution (DS)

A salt, TB, was prepared by adding 202.37 g (1 mol) of triethylamine in 2 L of a solvent (MeOH, EtOH, ACN, DMF, or DMSO), followed by dissolving an equimolar amount of benzoic acid (244.24 g) in it while stirring (Scheme 4.1). The formed solution was used as a DS during OSFO experiments.

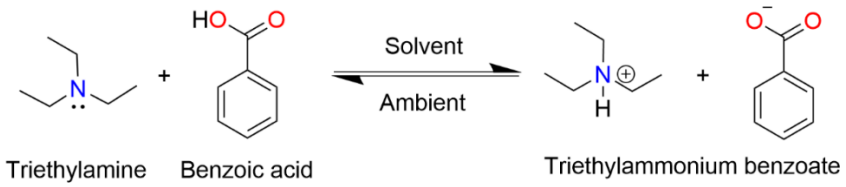

Scheme 4.1. Preparation of triethylammonium benzoate (TB).

4.2.3 OSFO analysis

The OSFO performance of membranes was evaluated with the FO setup and experimental procedure described in Section 3.2.3. Three membranes were used for each set of experiments, and the results were averaged. Initially, MeOH was used as a solvent (FS) using varying concentrations (0.5-2 mol L^{-1}) of LiCl in MeOH (DS). While using another solvent (EtOH, ACN, DMF, or DMSO) as FS, its DS using TB as a draw solute was prepared as given in Section 4.2.2. The maximum concentration of LiCl was taken as 2 mol L^{-1} to compare our results with those reported in the literature at similar concentrations [3,4,6-8]. The TB concentration was based on solubility in the solvent (viz., MeOH, EtOH, ACN, DMF, and DMSO). The solvent flux ($J_{Solvent}$) was calculated using Eq. 4.1 [8].

$$J_{Solvent} = \frac{\Delta M}{A_m \, X \, \Delta t \, X \, \rho} \tag{4.1}$$

where, ΔM (g) is the change in the weight of FS over the 10/16 h, Δt (h), A_m (m^2) is the active membrane area, and ρ (g L^{-1}) is the density of the solvent. The concentration of FS was monitored using a conductivity meter (LABINDIA PICO$^+$). The reverse salt flux (J_S) was determined using Eq. 4.2 [4].

$$J_s = \frac{C_f V_f - C_i V_i}{A_m \, X \, \Delta t} \tag{4.2}$$

where, C_i and C_f (mol L^{-1}) denote the initial and final concentration of salt in the FS; while V_i and V_f represent its initial and final volume, respectively. Thickness normalized total flux (J_N) was calculated using Eq. 4.3.

$$J_N = J_{Solvent} \, X \, \delta \tag{4.3}$$

where, δ is the membrane thickness in μm. The specific reverse salt flux (SRSF, mol L^{-1}) was calculated using Eq. 4.4 [4].

$$SRSF = \frac{Js}{J_{solvent}} \quad (4.4)$$

4.2.4 Analysis using model organic compounds (MOCs)

A 10 mg of each of the following model organic compounds: *p*-nitrophenol (NP, molecular weight = 138), *o*-nitroaniline (NA, 138), methyl red (MR, 269), malachite green (MG, 364), rhodamine B (RB, 479.02), direct red 81 (DR, 675), aniline blue (AB, 737) were dissolved in 1 L methanol and used as a feed solution in OSFO experiments with ABPBI-3 as a membrane. The LiCl and TB (1 mol L^{-1} in MeOH) were evaluated individually as a DS. With acetonitrile as a solvent, 10 mg each of NP, NA, MR, RB, and DR dissolved in 1 L was used as a feed solution (MG and AB are insoluble) while using TB (1 mol L^{-1}) as a draw solute. Usually, the concentration of FS reported in the literature was 100-200 ppm [2,4,7]. The selection of present solutes (MOCs of a broader molecular weight range) in FS depended on their solubility in MeOH and acetonitrile. UV-vis spectrophotometer (Shimadzu UV-1800) was used in the wavelength range of 200 to 900 nm for analyzing the concentration of MOCs. All the OSFO experiments were performed for 10 h, using a membrane area of 360 cm^2.

4.3 Results and discussion

4.3.1 Effects of membrane heat treatment, DS concentration, and duration of analysis

All three membranes (ABPBI-1, -2, and -3) were initially evaluated using MeOH as the FS and LiCl as a draw solute (Fig. 4.1a). The average J_{MeOH} for ABPBI-1, -2, and -3 was 4.25, 1.32, and 1.12 L m^{-2} h^{-1}, while the RSF (J_{LiCl}) was 1.979, 0.054 and 0.019 mol m^{-2} h^{-1}, respectively. As per TGA (Fig 3.2c), the ABPBI matrix holds water till ~295 °C, the removal of which is known to be sluggish [28-30]. The presence of water and domains with larger d-spacing (average d-spacing of 8.84 Å as discussed in Section 3.3.1) in ABPBI-1 could be responsible for its higher RSF and solvent flux than that of ABPBI-2 and -3. After the heat treatment at 350 °C for the ABPBI-2 membrane, the flux was reduced to ~ 1/3rd, while the RSF was reduced considerably to 2.7% as compared to its value for ABPBI-1. This observation endorses the importance of water removal by heat treatment at 350 ºC. With the removal of water molecules, the H-bonding between water and ABPBI repeat unit is replaced by the intermolecular H-bonding within ABPBI chains. As a result, domains of larger d-spacing are eliminated, and both J_{MeOH} and J_{LiCl} are reduced. When the performance of ABPBI-2 and ABPBI-3 is compared, the J_{MeOH} for the latter was reduced by ~ 14%, while J_{LiCl} was lowered by 65 %, compared to the earlier (ABPBI-2). It shows that by heat-treating the membrane three

times, a slight compromise on J_{MeOH} offered a better advantage of reducing the RSF, which is crucial in the OSFO.

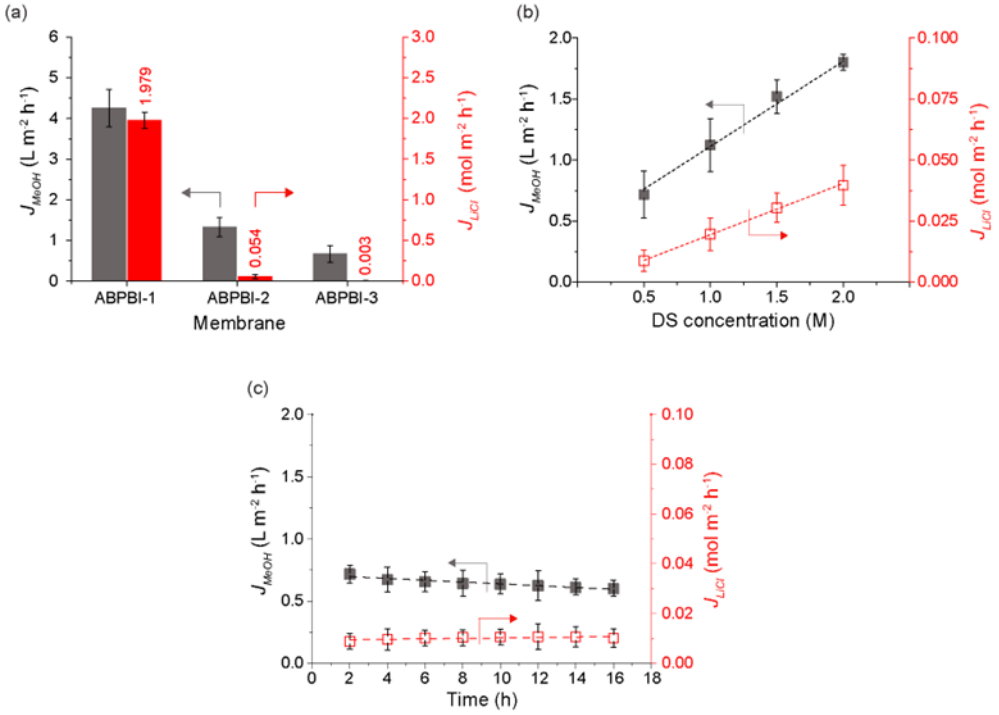

Fig. 4.1. Variation in flux and RSF with (FS: MeOH) (a) membrane treatment condition (DS: 1 mol L^{-1} LiCl in MeOH), (b) DS concentration (DS: 0.5-2 mol L^{-1} LiCl in MeOH) using ABPBI-3, and (c) long duration stability of ABPBI-3 (DS: 0.5 mol L^{-1} LiCl in MeOH).

Fig. 4.1b shows that with an increase in the concentration of DS, flux increased linearly for ABPBI-3. By increasing the DS concentration from 0.5 to 2 mol L^{-1}, J_{LiCl} increased by ~ 4.5 times, but the J_{MeOH} increased by 1.5 times. The RSF of 0.039 mol m^{-2} h^{-1} at a DS concentration of 2 mol L^{-1} is appreciable. The long-term analysis using ABPBI-3 (Fig. 4.1c) showed an almost linear flux of solvent and salt, with a slight decrease in J_{MeOH}. The observed decrease in J_{MeOH} can be attributed to a slight reduction in DS concentration. The initial concentration of 0.5 mol L^{-1} was lowered to 0.45 mol L^{-1} at the end of the experiment (16 h). It is attributable to the lowering of DS concentration with time. Since the membrane thickness is low, its stability over a longer duration of operation is evident.

4.3.2 OSFO using few industrially significant solvents

To evaluate the performance of TB as a draw solute, all three membranes, viz., ABPBI-1, ABPBI-2, and ABPBI-3, were used. Although J_{MeOH} was slightly lowered, the reduction in RSF was more significant than in the case of LiCl as DS (Fig. 4.2a). The lowering in flux could be attributed to the possible lower osmotic pressure created by TB, while the lowering in RSF could be due to its bigger size than LiCl. As could be anticipated from Fig 4.1a, the flux and RSF are higher for ABPBI-1 than for the other two membranes. Between ABPBI-2 and

ABPBI-3, the latter exhibited considerably lower RSF (0.0013 mol L^{-1}). Therefore, it was used to analyze the OSFO performance of EtOH, ACN, DMF, and DMSO. These solvents have a considerable commercial significance [9,24,25]. The concentration of TB was maintained at 1 mol L^{-1} for all solvents. Fig 4.2b shows that the solvent flux varied in an order: MeOH>EtOH>ACN>DMF>DMSO. Although the higher flux of MeOH and EtOH can be correlated to their protic nature, the higher molecular weight/size of other aprotic solvents can also be a reason for their lower flux. There could be another possibility of low osmotic pressure created by TB as the conductivity of respective DS was lower than that of MeOH (Table 4.1). Such an observation of varying conductivity with solvent is reported [8]. The RSF was considerably lower for all the solvents (<0.0013 mol m^{-2} h^{-1}), especially for ACN and DMF. The ACN and DMF exhibited the lowest J_{TB} of 0.0002 and 0.0003 mol m^{-2} h^{-1}, conveying the applicability of ABPBI as a membrane material for these industrially significant solvents.

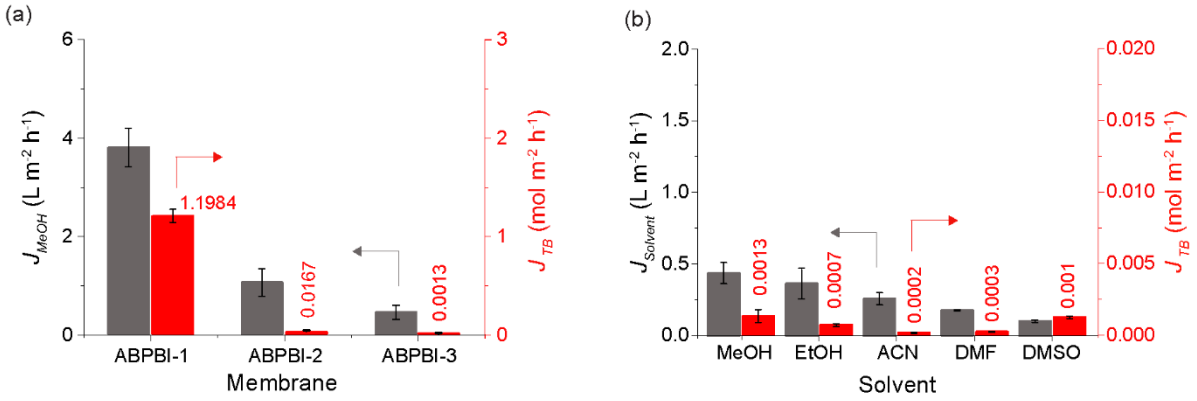

Fig. 4.2. OSFO performance using 1 mol L^{-1} TB as DS: (a) variation in the membrane using MeOH as FS (b) use of different solvents with ABPBI-3 as a membrane.

Table 4.1. DS conductivity

Solvent	**DS (1 mol L^{-1})**	**Conductivity (mS cm^{-1})**
MeOH	LiCl	24.4 ± 0.4
MeOH	TB	15.5 ± 0.2
EtOH		1.91 ± 0.03
ACN		1.86 ± 0.02
DMF		1.24 ± 0.02
DMSO		1.47 ± 0.04

The fluxes can be elevated by lowering the membrane thickness, appropriately choosing DS with high concentration, and tuning the operational parameters (velocity, operational temperature, etc.). The present draw solute (TB) could be made easily by dissolving triethyl amine and benzoic acid in these solvents. Moreover, they are commonly available,

larger-size chemicals (than LiCl), form acid-base salt quickly, and, more importantly, dissolve in various solvents. By further elevating the polarity of benzoic acid by introducing a polar group, the solubility could be increased, and the resulting salt could be more polar.

4.3.3 Long-duration analysis in the presence of MOCs

The long-duration stability of ABPBI-3 was evaluated using 7 MOCs as representatives of APIs/drug molecules. Their chemical structure is shown in Fig. 4.3, and their selection was based on (i) solubility in present solvents, (ii) wide variation in molecular weight (138-737), and (iii) UV-active nature. The experimental setup is shown in Fig.4.4. ABPBI-3 was chosen as a membrane based on its better performance than the other 2 membranes, as covered above. The results obtained at the end of 10 h duration using the membrane area of 360 cm^2 are given in Table 4.2.

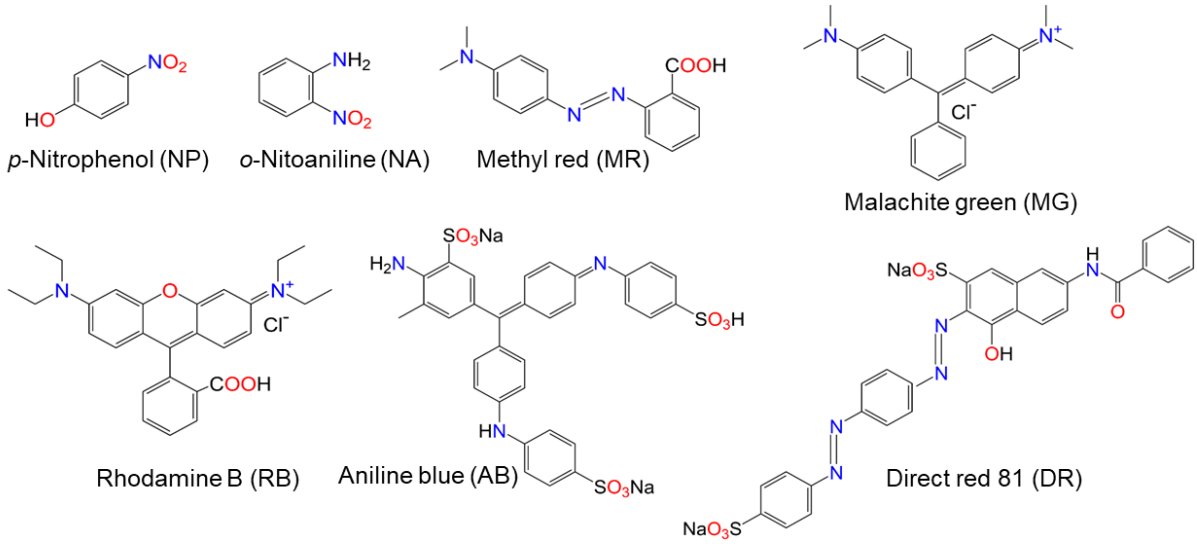

Fig. 4.3 Chemical structure of MOCs.

With either LiCl or TB as a DS, the solvent flux (MeOH/ACN) and RSF given in Table 4.2 are in general agreement with the data seen in Fig 4.1a and Fig. 4.2a. Although some of the MOCs are ionic in nature, their osmotic pressure can be negligible since their overall concentration is low (70 mg L^{-1}). After the experiments, their concentration was increased (~ 11% when LiCl was DS and ~ 4 % when TB was DS). This increase could be attributed to the solvent flow to the DS side. As elaborated below, no MOC was permeated through the membrane.

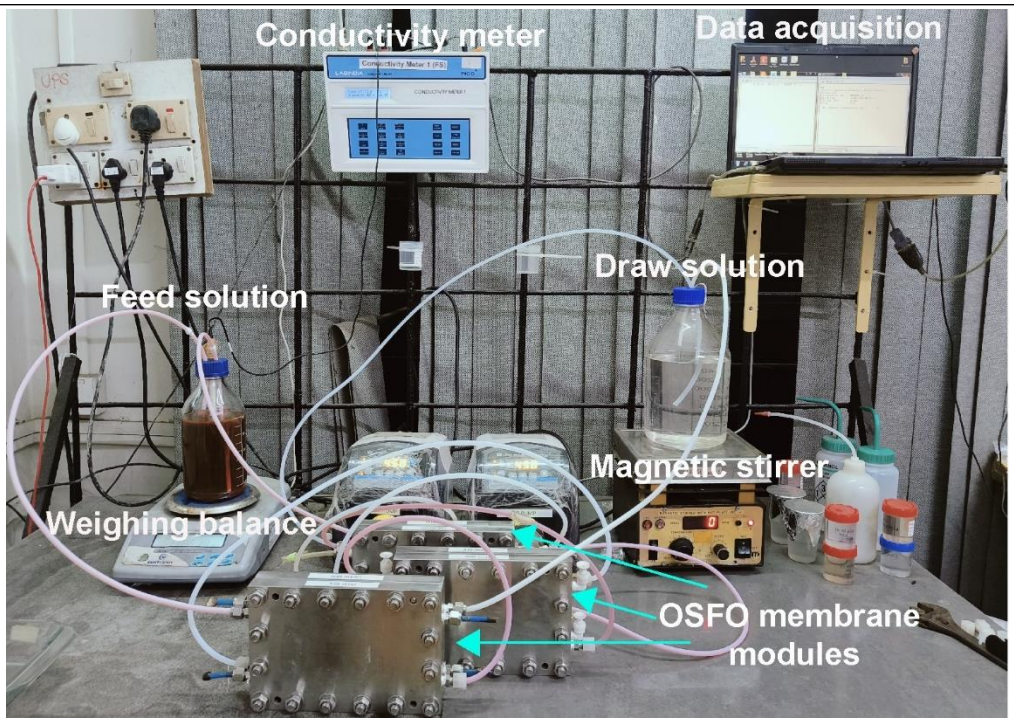

Fig. 4.4 OSFO experimental setup using MOCs in FS.

The UV-spectrum and λ_{max} of individual MOCs dissolved in MeOH are given in Fig. 4.5a. At the end of the experiment, UV spectra of FS (black curve) and DS (red line) are shown in Fig. 4.5b and Fig. 4.5c while using LiCl or TB as the draw solute in MeOH. The MOCs could not be detected in either of the DS cases, indicating their impermeability through the membrane. Fig. 4.5d shows the color of FS and DS supporting this result. With acetonitrile as a solvent, the UV spectra of individual MOCs are demonstrated in Fig. 4.6a. A slight shift in the λ_{max} of RB was observed, while for other MOCs, it remained the same as that of MeOH (Fig. 4.5a). Fig. 4.6b shows results using TB as the DS for the same experimental time of 10 h as that of methanol. There was no MOC permeation to the DS side of the membrane. Given the high UV sensitivity of some of the MOCs [31], it can be easily concluded that there is no permeation of MOC through the membrane, irrespective of the solvent used. These results using MeOH and ACN as solvents show that ABPBI-3 is impermeable to various MOCs with a broad molecular weight range (138 to 737) and chemical nature. These results are highly encouraging, especially for the enrichment of small organic APIs/chemical products and simultaneous recovery of solvents with extremely low permeability of draw solute.

Table 4.2. OSFO performances of ABPBI-3 in the presence of MOCs

Solvent	MOCs in FS	DS	$J_{Solvent}$ (L m^{-2} h^{-1})	J_S / RSF (mol m^{-2}h^{-1})	Feed concentration (mg L^{-1})	
					At start	After experiment
MeOH	NP, NA, MR, MG, RB, DR and AB	1mol L^{-1} LiCl	0.9	0.003	70	104
MeOH	NP, NA, MR, MG, RB, DR and AB	1mol L^{-1} TB	0.40	0.0015	70	82
ACN	NP, NA, MR, RB and DR	1mol L^{-1} TB	0.20	0.0004	50	54

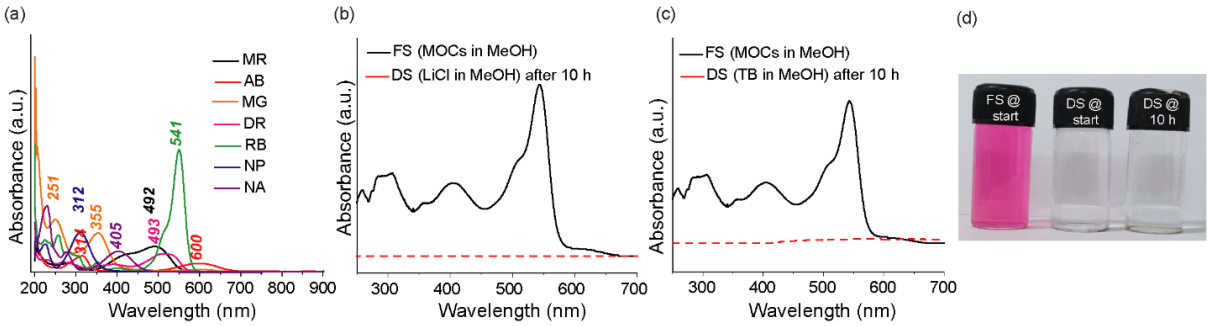

Fig. 4.5. UV-Vis spectra of (a) individual MOCs in MeOH, (b) FS and DS (1 mol L^{-1} LiCl) in MeOH after 10 h, (c) FS and DS (1 mol L^{-1} TB) in MeOH after 10 h.

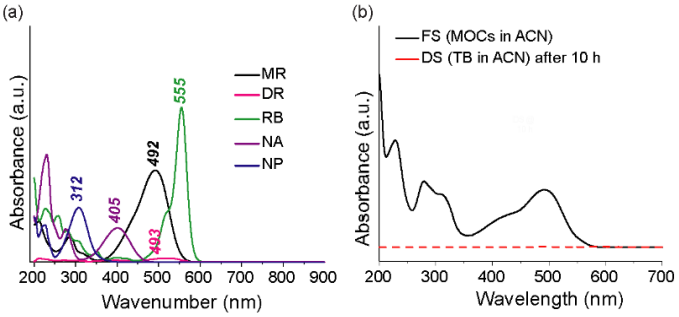

Fig. 4.6. UV-Vis spectra of (a) individual MOCs in ACN, (b) FS and DS in ACN after 10 h.

4.3.4 Comparison with the literature

The OSFO performances of the present membrane (ABPBI-3) and some literature data are given in Table 4.3. The first column gives the name of the membrane, its type, and its thickness. To have uniformity in the performance comparison, we used two terms, viz., normalized flux, J_N (Eq. 4.3), and SRSF (Eq. 4.4). In most of the reported cases, the membrane thickness is at least an order of magnitude lower than the thickness of the present membrane. Thus, if normalized flux is compared for any of the reported solvents (MeOH/EtOH/DMF), it

is generally higher, and RSF is lower for the present membrane, except MOF-based membranes reported by Ma et al. [3].

Table 4.3 Comparison of present data with those reported in the literature

Membrane (type, thickness (μm))	**Solvent**	**DS**	$J_{Solvent}$ ($L\,m^{-2}\,h^{-1}$)	J_N ($L\,\mu m\,m^{-2}\,h^{-1}$)	J_S/**RSF** ($mol\,m^{-2}\,h^{-1}$)	**SRSF** ($mol\,L^{-1}$)	**Ref.**
ABPBI-3 (symmetric, 17)	MeOH	1 mol L^{-1} LiCl	1.1	18.7	0.019	0.02	This work
	MeOH	2 mol L^{-1} LiCl	1.80	30.6	0.04	0.022	
	MeOH	1 mol L^{-1} TB	0.44	7.5	0.001	0.002	
	EtOH	1 mol L^{-1} TB	0.36	6.1	0.0007	0.002	
	ACN	1 mol L^{-1} TB	0.30	5.1	0.0002	0.001	
	DMF	1 mol L^{-1} TB	0.18	3.1	0.0002	0.0001	
	DMSO	1 mol L^{-1} TB	0.10	1.7	0.0012	0.013	
PA (TFC, 0.168)	EtOH	2 mol L^{-1} LiCl	2.52	0.42	0.013	0.005	[8]
MXene-PA (TFC, 0.0012-0.0014)	EtOH	2 mol L^{-1} LiCl	9.5	0.013	~ 0.09	0.01	[6]
HLGO (TFC, 0.24)	MeOH	1 mol L^{-1} CA	~ 3	0.72	0.1	0.03	[7]
	EtOH	2 mol L^{-1} LiCl	3.94	0.95	0.08	0.02	
	DMF	1 mol L^{-1} CA	3.4	0.82	0.065	0.02	
SA-NH-UiO-66/M-E-30 (TFC, 2)	MeOH	2 mol L^{-1} LiCl	34.1	68.2	0.04	0.0012	[3]
	EtOH	2 mol L^{-1} LiCl	9.3	18.6	0.016	0.002	

When SRSF is compared, the value for EtOH in the present case (0.002 mol L^{-1}) is an order of magnitude lower than the data from the literature. Although it looks similar to the MOF-based membrane value [3], it may be noted that the draw solute concentration is half in the present case. Similar superior behavior is seen in the case of MeOH as well. In the case of DMF, the normalized flux, RSF, and SRSF seem superior to the same data reported for the HLGO membrane [7]. The present RSF data for ACN (0.0002 mol $m^{-2}\,h^{-1}$) and DMSO (0.0012 mol $m^{-2}\,h^{-1}$) with reasonably good flux are highly encouraging. It may be noted that the present

membranes are thin, symmetric films, so the ICP effect can be ignored, thus providing an attractive membrane material for OSFO.

4.4 Conclusions

Thin, solvent-stable, symmetric ABPBI membranes were successfully prepared for the OSFO process. The physical characterizations, viz., zeta potential, FE-SEM, and AFM, showed their symmetric, dense nature. The membrane heat treatment, using different DS solutes and organic solvents, showed their impact on the OSFO performance. The membrane treated at 350 ºC was evaluated using organic solvents: methanol, ethanol, acetonitrile DMF, and DMSO. Initial evaluations of methanol as a solvent and 1 mol L^{-1} LiCl as a draw solute offered attractive results of solvent flux (J_{MeOH}: 1.1 L m^{-2} h^{-1}) and low reverse salt flux (J_{LiCl}: 0.019 mol m^{-2} h^{-1}). Since LiCl was freely soluble only in methanol, a salt of commonly available triethyl amine and benzoic acid (TB) soluble in present solvents was successfully employed. An attractive solvent flux (J_{MeOH}: 0.44 L m^{-2} h^{-1}) and better rejection of draw solute (a very low J_{TB} of 0.0013 mol m^{-2} h^{-1}) than LiCl were obtained. The OSFO was dependent on the type of solvent and the osmotic pressure created by a draw solute present in it. While using 1 mol L^{-1} triethylammonium benzoate as a draw solute, the flux of acetonitrile and DMSO were 0.30 and 0.10 L m^{-2} h^{-1}, respectively. The reverse salt flux in the respective solvent was 0.0002 and 0.0012 mol m^{-2} h^{-1}, which is extremely low, conveying the usefulness of employing this draw solute.

OSFO performance in the presence of model organic compounds (MOCs) of varying molecular weight and functional groups using MeOH and acetonitrile as a solvent was highly encouraging, as all MOCs exhibited no transport through the membrane. These results convey the applicability of present membranes for the concentration of APIs/organic compounds of varying size and chemical functionality. Present thin, symmetric, solvent-stable ABPBI membrane can not only overcome the critical challenges of the ICP effect (that limits the performance of current OSFO membranes) but opens up applicability of various solvents possessing high rejection of small solutes organic and draw solutes (LiCl and TB).

4.5 References

[1] R. Takada, R. Takagi, H. Matsuyama, High-degree concentration organic solvent forward osmosis for pharmaceutical pre-concentration, Membranes 14 (2024) 14-26. https://doi.org/10.3390/membranes14010014.

[2] L. Chen, C. Zhou, T. Yang, W. Zhou, Y. Chen, L. Wang, C. Lu, L. Dong, Imparting outstanding dispersibility to nanoscaled 2d COFs for constructing organic solvent

forward osmosis membranes, Small 19 (2023) 2300456-2300463. https://doi.org/10.1002/smll.202300456.

[3] L. Ma, X. Han, S. Zhang, L. Wang, Sulfonated metal−organic framework nanostructure-based membranes with precise sieving for organic solvent forward osmosis, ACS Appl. Nano Mater. 5 (2022) 11324−11333. https://doi.org/10.1021/acsanm.2c02435.

[4] K. S. Goh, Y. Chen, D. Y. F. Ng, J. W. Chew, R. Wang, Organic solvent forward osmosis membranes for pharmaceutical concentration, J. Membr. Sci. 642 (2022) 119965-119974. https://doi.org/10.1016/j.memsci.2021.119965.

[5] Y. Wang, X. Zhang, Y. Liu, L. Wang, H. Yang, P. Lu, Commercial polyethylene supported thin-film composite membranes within 10 μm thickness for organic solvent forward osmosis, Sep. Purif. Technol. 336 (2024) 126250-126260. https://doi.org/10.1016/j.seppur.2023.126250.

[6] X. Wu, M. Ding, H. Xu, W. Yang, K. Zhang, H. Tian, H. Wang, Z. Xie, Scalable ti3c2tx Mxene interlayered forward osmosis membranes for enhanced water purification and organic solvent recovery, ACS Nano 14 (2020) 9125−9135. https://dx.doi.org/10.1021/acsnano.0c04471.

[7] Z. Tong, H. Guo, X. Liu, B. Zhang, Organic solvent forward osmosis of graphene oxide-based membranes for enrichment of target products, Ind. Eng. Chem. Res. 59 (2020) 19012−19019. https://dx.doi.org/10.1021/acs.iecr.0c03780.

[8] Y. Cui, T. S. Chung, Pharmaceutical concentration using organic solvent forward osmosis for solvent recovery, Nat. Commun. 9 (2018) 1426-1442. https://doi.org/10.1038/s41467-018-03612-2.

[9] K. Grodowska, A. Parczewski, Organic solvents in the pharmaceutical industry, Acta Pol. Pharm. 67 (2010) 3-12.

[10] B. H. Lipshutz, F. Gallou, S. Handa, Evolution of solvents in organic chemistry, ACS Sustainable Chem. Eng. 4 (2016) 5838-5849. https://doi.org/10.1021/acssuschemeng.6b01810.

[11] P. Marchetti, M. F. J. Solomon, G. Szekely, A. G. Livingston, Molecular Separation with Organic Solvent Nanofiltration: A Critical Review, Chem. Rev. 114 (2014) 10735−10806. https://doi.org/10.1021/cr500006j.

[12] S. Karan, Z. Jiang, A. G. Livingston, Sub–10 nm polyamide nanofilms with ultrafast solvent transport for molecular separation, Science 348 (2015) 1347-1351. https://doi.org/10.1126/science.aaa5058.

[13] M. L. Hir, A. Magne, T. Clair, E. Carretier, P. Moulin, Solvent regeneration in complex mixture using pervaporation, Org. Process Res. Dev. 25 (2021) 469−485. https://dx.doi.org/10.1021/acs.oprd.0c00442.

[14] C. Liu, R. Takagi, T. Shintani, L. Cheng, K. L. Tung, H. Matsuyama, Organic liquid mixture separation using an aliphatic polyketone supported polyamide organic solvent

reverse osmosis (OSRO) membrane, ACS Appl. Mater. Interfaces 12 (2020) 7586−7594. https://dx.doi.org/10.1021/acsami.9b21519.

[15] L. Jin, L. Hu, S. Liang, Z. Wang, G. Xu, X. Yang, A novel organic solvent nanofiltration (OSN) membrane fabricated by Poly (m-phenylene isophthalamide) (PMIA) under large-scale and continuous process, J. Membr. Sci. 647 (2022) 120259-120269. https://doi.org/10.1016/j.memsci.2022.120259.

[16] R. P. Lively, D. S. Sholl, From water to organics in membrane separations, Nat. Mater. 16 (2017) 276-279. https://doi.org/10.1038/nmat4860.

[17] Y. Wei, Y. Wang, L. Wang, H. Yang, H. Jin, P. Lu, Y. Li, Simultaneous phase-inversion and crosslinking in organic coagulation bath to prepare organic solvent forward osmosis membranes, J. Membr. Sci. 620 (2021) 118829-118839. https://doi.org/10.1016/j.memsci.2020.118829.

[18] S. Phuntsho, J. E. Kim, V. H. Tran, S. Tahara, N. Uehara, N. Maruko, H. Matsuno, S. Lim, H. K. Shon, Free-standing, thin-film, symmetric membranes: Next-generation membranes for engineered osmosis, J. Membr. Sci. 607 (2020) 118145-118154. https://doi.org/10.1016/j.memsci.2020.118145.

[19] W. Cheng, J. Ma, X. Zhang, M. Elimelech, Sub-1 μm free-standing symmetric membrane for osmotic separations, Environ. Sci. Technol. Lett. 6 (2019) 492−498. https://doi.org/10.1021/acs.estlett.9b00364.

[20] M. Li, V. Karanikola, X. Zhang, L. Wang, M. Elimelech, A self-standing, support-free membrane for forward osmosis with no internal concentration polarization, Environ. Sci. Technol. Lett. 5 (2018) 266−271. https://doi.org/10.1021/acs.estlett.8b00117.

[21] T. Y. Liu, H. G. Yuan, Y. Y. Liu, D. Ren, Y. C. Su, X Wang, Metal−organic framework nanocomposite thin films with interfacial bindings and self-standing robustness for high water flux and enhanced ion selectivity, ACS Nano 12 (2018) 9253−9265. https://doi.org/10.1021/acsnano.8b03994.

[22] H. G. Yuan, Y. Y. Liu, T. Y. Liu, X. L. Wang, Self-standing nanofilms of polysulfone doped with sulfonated polysulfone via solvent evaporation for forward osmosis, J. Membr. Sci. 523 (2017) 567-575. http://dx.doi.org/10.1016/j.memsci.2016.09.034.

[23] H. Liu, H. Wang, X. Zhang, Facile fabrication of freestanding ultrathin reduced graphene oxide membranes for water purification, Adv. Mater. 27 (2015) 249–254. https://doi.org/10.1002/adma.201404054.

[24] D. R. Joshi, N. Adhikari, An overview on common organic solvents and their toxicity, J. Pharm. Res. Int. 28(3) (2019) 1-18. https://doi.org/10.9734/jpri/2019/v28i330203.

[25] D. J. C. Constable, C. Jimenez-Gonzalez, R. K. Henderson, Perspective on solvent use in the pharmaceutical industry, Org. Process Res. Dev. 11 (2007) 133-137. https://doi.org/10.1021/op060170h.

[26] J.A. Asensio, P. Gómez-Romero, Recent developments on proton conducting Poly(2,5-benzimidazole) (ABPBI) membranes for high temperature polymer electrolyte

membrane fuel cells, Fuel Cells 5 (2005) 336–343. https://doi.org/10.1002/fuce.200400081.

[27] H.R. Lohokare, H.D. Chaudhari, U.K. Kharul, Solvent and pH-stable poly(2,5-benzimidazole) (ABPBI) based UF membranes: Preparation and characterizations, J. Memb. Sci. 563 (2018) 743–751. https://doi.org/10.1016/j.memsci.2018.06.052.

[28] H. D. Chaudhari, R. Illathvalappil, S. Kurungot, U. K. Kharul, Preparation and investigations of ABPBI membrane for HT-PEMFC by immersion precipitation method, J. Membr. Sci. 564 (2018) 211-217. https://doi.org/10.1016/j.memsci.2018.07.026.

[29] S.C. Kumbharkar, U.K. Kharul, New N-substituted ABPBI: Synthesis and evaluation of gas permeation properties, J. Memb. Sci. 360 (2010) 418–425. https://doi.org/10.1016/j.memsci.2010.05.041.

[30] L.F. Fourie, L. Square, C. Arendse, M. Msimanga, ABPBI/MWCNT for proton radiation shielding in low earth orbit, APL Mater. 11 (2023) 71103-17120. https://doi.org/10.1063/5.0156686.

[31] S. Mukherjee, A. Ghati, G. Paul, An ultraviolet−visible spectrophotometric approach to establish a method for determining the presence of rhodamine b in food articles, ACS Food Sci. Technol. 1 (2021) 1615−1622. https://doi.org/10.1021/acsfoodscitech.1c00172.

CHAPTER 5

Conclusions and Future Directives

5.1 Conclusions

Chapter 1 briefs literature on the recent developments in the FO. Initially, the FO process is briefly introduced, followed by FO applications, hybrid processes incorporating combined benefits from concentration–dilution (e.g., fertilizer-based solutions for agricultural irrigation), advances in the development of FO membrane materials, membrane fabrication techniques, and tailoring and improvements in draw solutions (e.g., thermo-responsive polymers) for targeted applications with minimized reverse solute flux and draw solution regeneration methods. The limiting factors (such as concentration polarization, membrane stability, etc.) that compromise the application of the FO process to real applications are discussed.

The scope, aims, and objectives of this work are thoroughly discussed to establish its significance and potential impact. The primary aim is to address gaps by developing innovative methodologies or materials.

Chapter 2 presents the preparation and FO investigations of ABPBI-based HFMs. This work highlights the potential of these membranes while achieving low RSF and reasonable water flux. The work demonstrated that heat treatment at 350°C significantly enhanced membrane performance by reducing water sorption and improving chain packing, leading to lower RSF. The presence of MSA in the membrane matrix was beneficial, leading to further lowering in RSF and slightly improved water flux. The overall water flux of these membranes is lower than that of reported FO membranes due to their dense structure. The study suggests that reducing membrane thickness can greatly enhance FO performance. The findings provide valuable insights into designing chemically robust hollow fiber types of FO membranes.

Chapter 3 demonstrated the development of thin, solvent-stable, free-standing ABPBI-based membranes for FO. The physical characterizations, viz., zeta potential, FE-SEM, and AFM, showed their symmetric, dense nature. The membrane heat treatment, using different DS solutes at varying concentrations, impacted the FO performance. The membrane treated at 350 ºC showed enhanced salt rejection capability. Initial evaluations show that the ABPBI-2 membrane has a higher rejection of draw solute than ABPBI-1. The $MgCl_2$ as a DS showed higher water flux than that of NaCl and Na_2SO_4 at the same concentration. With acid as the FO

feed, AA and MAA concentrations were increased by approximately 2-fold and 2.26-fold, respectively. The ABPBI-2 membrane satisfied the FO requirement of high AA and MAA rejection (> 98%). The overall findings showcased the ability of FO to increase the acid concentration successfully, contributing to FO applicability.

Chapter 4 demonstrated the development of thin, solvent-stable, free-standing ABPBI-based membranes for OSFO. The results indicate that membrane heat treatment at 350°C significantly improves performance by reducing RSF while maintaining reasonable solvent flux. A novel acid-base salt, triethylammonium benzoate, was introduced as a compelling draw solute, offering superior rejection and solubility in a wide range of solvents than that of LiCl. Investigations using model organic compounds (MOCs) illustrated reiterated excellent solvent stability in the presence of organic solutes. A complete rejection of model organic compounds across various molecular weights and functionalities was observed. This indicated the applicability of present OSFO membranes in practical applications in the pharma and chemical sectors, wherein efficient solvent recovery and organic compound concentration with minimal RSF is of great significance. Reducing membrane thickness and more investigations towards operational conditions may further enhance flux without compromising selectivity.

5.2 Future directives

ABPBI-based membranes for diverse applications: Future research should focus on exploring the performance of ABPBI-based membranes in diverse membrane applications, particularly in harsh environments involving high solute concentrations, extreme pH conditions, and various organic solvents. Investigating membrane stability, selectivity, and flux under these conditions will provide critical insights for expanding their applicability in industries such as wastewater treatment, pharmaceutical separation, and solvent recovery.

Optimization of membrane preparation parameters: Future research should focus on developing thinner ABPBI-based membranes without compromising mechanical strength. This work will enhance water flux while maintaining low RSF and high selectivity. It would also reduce transport resistance without any ICP.

Optimizing operational parameters: Although the present work investigated the applicability of ABPBI as a membrane material, optimizing operational parameters for FO needs further investigation.

Development of novel draw solutes: Future research should focus on developing novel draw solutes possessing (i) higher osmotic pressure, (ii) solubility in a wide range of solvents, and (iii) ease of regeneration to address sustainable and cost-effective operation, minimizing energy consumption and environmental impact while maintaining high separation efficiency.

Moreover, future research should focus on utilizing low-cost energy sources and waste heat to regenerate draw solutes. This includes integrating industrial waste heat, solar energy, or other renewable sources, which could reduce operational costs while maintaining effective solute recovery.

Developing new applications: Given widening technological demands driven by cost-effectiveness, environmental acceptability, and sustainability, newer application development in various sectors (e.g., use of seawater for electrolysis) has a wide scope.

Applications of hybrid processes: The potential of hybrid processes such as FO-RO, FO-MD, and FO-NF to enhance separation efficiency while minimizing energy consumption needs separate attention. Combining FO with complementary technologies can improve water recovery, reduce fouling, and optimize overall system performance for separation applications.

ABSTRACT

Name of the Student: Mr. Thorat Nitin Madhukarrao **Registration No.:** 20EE17A26041
Faculty of Study: Engineering Sciences **Year of Submission:** 2025
AcSIR academic centre/CSIR Lab: CSIR-NCL

Name of the Supervisor(s): Dr. Ashish K. Lele and Dr. Ulhas K. Kharul

Title of the thesis: Development of ABPBI-based Membranes and their Investigations for Forward Osmosis (FO)

Forward osmosis (FO) is a promising upcoming separation technology that can overcome the challenges of conventional and pressure-driven membrane separation processes. The FO process has several advantages over conventional processes, such as natural processes, low energy requirements, fewer channels of fouling, and ease of implementation in a variety of applications. Despite intense research efforts over the past 15 years, industrial and commercial applications of FO technology face some challenges. These changes include (i) the Availability of a robust FO membrane, (ii) the FO membrane with negligible ICP, and (iii) the Availability of ideal draw solute and their cost-effective regeneration.

To address these issues, we have demonstrated the fabrication of ABPBI-based hollow fiber (HFMs) and flat sheet membranes (FSMs). The ABPBI-based HFM in neutral and in the presence of methane sulfonic acid in the membrane matrix was evaluated as a membrane material to generate an understanding of the effects of the absence/presence of acid in the membrane matrix with membrane heat treatment. Higher membrane thickness in HFM restricts the water flux, hence the FSM. The membrane casting parameters were studied to get a thinner membrane. The effect of membrane heat treatment on FO/OSFO performance in terms of water/solvent and reverse solute flux was determined. A long-term FO/OSFO experiment analyzed the integrity of the membrane. The ABPBI-based FSMs were used to investigate the suitability of FO for the enrichment of carboxylic acid (acetic acid and methacrylic acid) in the feed solution. The acetic and methacrylic acid concentrations are increased by approximately 2-fold and 2.26-fold, respectively. The membranes treated at 60 and 350 °C were analyzed for OSFO using solvents of industrial significance (methanol, ethanol, acetonitrile, *N*,*N*-dimethylformamide, and dimethyl sulphoxide). Although LiCl could be employed as a draw solute with methanol as a solvent, its insolubility in other organic solvents led to the use of a new, simple-to-synthesize acid-base salt, viz., triethylammonium benzoate as a draw solute. The use of model organic compounds in the feed side led to an understanding of the applicability of present thin, scalable ABPBI membranes for OSFO. Given the membrane's reproducible and scalable preparation method, chemically robust nature, and extremely low reverse salt flux, ABPBI can be a promising material for FO application.

Details of the Publications Emanating from the Thesis Work

1) List of publication(s) in SCI Journal(s) (published & accepted) emanating from the thesis work, with complete bibliographic details.

(i) Patent: A Polymer Layered Hollow Fiber Membrane Based on Poly(2,5-Benzimidazole), Copolymers, And Substituted Polybenzimidazole, Kharul Ulhas Kanhaiyalal, Chaudhari Harshal Dilip, Shobhana Nishina Achuthan, **Thorat Nitin Madhukarrao**, Gawas Saroj Shivram, Alladi Lavanya, Kunjattu Shebeeb Hassan, Kumar Vipin, Publication date: 23-04-2020, Internal Publication Number: WO 2020/079713 A1**.**

(ii) **N. M. Thorat**, A. K. Lele, U. K. Kharul, ABPBI-based hollow fiber membranes for forward osmosis (FO) possessing low reverse salt flux, Desalin. Water Treat., 320 (2024) 100641. https://doi.org/10.1016/j.dwt.2024.100641.

(iii) **Thorat N. M.**, Valvi S. V., Lele A. K., Kharul U. K., Thin, flat sheet, solvent-stable ABPBI-based membranes for organic solvent forward osmosis (OSFO), J. Membr. Sci., 708 (2024) 123090. https://doi.org/10.1016/j.memsci.2024.123090.

2) List of Papers with abstract presented (oral/poster) at national/international conferences/seminars with complete details.

(i) Presented an oral talk entitled "Thin, Flat Sheet, Solvent-Stable ABPBI-based Membranes for Organic Solvent Forward Osmosis (OSFO)" at the International Conference on Materials and Membranes for Water and Energy (ICMMWE- 2024) held during July 10-12, 2024, at CSIR-Central Salt and Marine Chemicals Research Institute, Bhavnagar (Gujrat).

Abstract: Organic solvents are commonly used in the pharmaceutical industry to synthesize active pharmaceutical ingredients (APIs), cleaning agents, chemicals, etc. Multiple-stage purification of pharmaceuticals and their intermediates makes solvent removal and recovery essential. The costs of processing these organic solvents for separation, recovery, or disposal are substantial and comprise a significant fraction of operating expenses. The membrane-based separations of organic solvents are pervaporation (PV), organic solvent reverse osmosis (OSRO), and organic solvent nanofiltration (OSN). Energy-efficiency calculations confirmed that OSN uses 25 times less energy per liter of recovered solvent than distillation. However, the high pressure used

in OSN remains a concern as it may add extra operating and maintenance costs. Organic Solvent Forward Osmosis (OSFO) would be economical and potentially enable bulk chemical separations inaccessible by conventional methods. We have demonstrated ABPBI-based thin, solvent-stable, scalable flat sheet membranes for OSFO. The membranes were analyzed for OSFO using solvents of industrial significance (methanol, ethanol, acetonitrile, *N*,*N*-dimethylformamide, and dimethyl sulphoxide). Some significant results will be presented, e.g., high solvent flux, excellent rejection of the draw solutes, and long-term stability.

(ii) Presented an oral talk entitled "Developing Self-Standing Support Free Membrane Based On ABPBI For Forward Osmosis (FO)" at the 4th NCL-RF Annual Student's Conference: 2022 held on November 29-30, 2022, at CSIR-National Chemical Laboratory, Pune (Maharashtra).

Abstract: See the abstract for entry (i).

(iii) Presented a poster entitled "Hollow Fiber Membranes based on ABPBI for the Forward Osmosis (FO) Process" at International Conference on Science and Technology of Polymers and Advanced Materials 2022 (SPSI - MACRO – 2022) held during November 2-4, 2022, at CSIR-National Chemical Laboratory, Pune (Maharashtra).

Abstract: Forward osmosis (FO) has received great attention in the last decade for water reuse, seawater desalination, and some niche applications. In industrial applications, especially in pharmaceutical and fine chemicals, recovery of organic solvents is necessary. FO organic solvent recovery is vital and has become a competitive alternative to conventional thermal processes. Most of the present polymeric membranes do not withstand the organic solvent. The present study focused on preparing and evaluating FO performance using solvent-stable polymer. It was shown that one of the members of the polybenzimidazole family, poly(2,5-benzimidazole) (ABPBI), possesses high solvent and pH stability. It also has a higher water sorption capacity than many high-performance polymers, including common PBI[3]. In the present work, ABPBI-based hollow fiber membranes were successfully prepared using a dry-wet jet spinning process and evaluated in lab-scale FO experiments. The preparation and analysis of hollow fiber membranes based on ABPBI showed a high draw solute rejection and convenient water flux in the FO process. The FO experiments were performed using DI water and NaCl solution in DI water of different concentrations as a feed solution and draw solutions, respectively. The ABPBI-based hollow fiber membranes showed >96 % NaCl (draw solute) rejection. This proves that a hollow fiber membrane based on ABPBI is a promising

candidate for FO experiments. Therefore, considering ABPBI membrane material properties and its FO performance, the same will be demonstrated for organic solvent recovery.

(iv) Presented a poster entitled “Developing Support-Free Solvent-Stable Membrane Based on ABPBI for Forward Osmosis (FO) Application” at DAE-BRNS sponsored Tenth Biennial Symposium on Emerging Trends in Separation Science and Technology (SESTEC-2022)" held at Institute of Chemical Technology (ICT), Mumbai during November 22-26, 2022.

Abstract: See the abstract for entry (i).

(v) Presented an oral talk entitled “Establishing ABPBI as a Promising Membrane Material for Forward Osmosis (FO) process” at the Virtual International Conference on Advances in Chemistry And Chemical Engineering 2021, held on April 16-17, 2021, at Sardar Vallabhbhai National Institute Of Technology (SVNIT), Surat (Gujarat).

Abstract: See the abstract for entry (ii).

(vi) Presented a poster entitled “Establishing ABPBI as a Promising Membrane Material for Forward Osmosis (FO) Process” held at National Science Day Celebrations on February 26-27, 2020, at CSIR-National Chemical Laboratory, Pune.

Abstract: See the abstract for entry (ii).

Journal of Membrane Science 708 (2024) 123090

Contents lists available at ScienceDirect

Journal of Membrane Science

journal homepage: www.elsevier.com/locate/memsci

Thin, flat sheet, solvent-stable ABPBI-based membranes for organic solvent forward osmosis (OSFO)

Thorat Nitin M [a,b], Valvi Suresh V [a], Lele Ashish K [a,b], Kharul Ulhas K [a,b,*]

[a] Polymer Science and Engineering Division, CSIR-National Chemical Laboratory, Pune, 411008, India
[b] Academy of Scientific and Innovative Research (AcSIR), Ghaziabad, 201002, India

ARTICLE INFO

Keywords:
ABPBI
Free-standing thin membrane
OSFO
Triethylammonium benzoate
Model organic compounds

ABSTRACT

The work demonstrates poly(2,5-benzimidazole), commonly known as ABPBI, based thin, solvent-stable, scalable flat sheet membranes for organic solvent forward osmosis (OSFO). The membranes treated at 60 and 350 °C were analyzed for OSFO using solvents of industrial significance (methanol, ethanol, acetonitrile, *N,N*-dimethylformamide, and dimethyl sulphoxide). Although LiCl could be employed as a draw solute with methanol as a solvent, its insolubility in other organic solvents led to the use of a new, simple-to-synthesize acid-base salt, viz., triethylammonium benzoate (TB). A study on the effects of membrane treatment temperature on solvent flux, reverse salt flux (RSF), ability to use TB as draw solute with other solvents, long-duration analysis, and use of model organic compounds in the feed side led to an understanding of the applicability of present thin, scalable ABPBI membranes for OSFO. Although membranes treated at 350 °C possessed a lower methanol flux than those treated at 60 °C, the lowering in its RSF was highly attractive. TB, having a larger molecular size than LiCl, led to a slight reduction in methanol flux and a considerable reduction in RSF. With TB, extremely low RSF was observed with the chosen solvents. The long-duration study using MeOH and acetonitrile was investigated. A complete rejection of all model organic compounds of varying molecular weights and chemical functionality indicated the merits of the present thin, scalable ABPBI membranes for practical applications of OSFO.

1. Introduction

Over the past decade, forward osmosis (FO) and organic solvent forward osmosis (OSFO) have attracted attention as emerging technologies for various separation applications, such as desalination [1–4], wastewater treatment [5,6], fertigation [7–10], food processing [11–13], solvent recovery in pharmaceutical industries [14–21], etc. OSFO has received growing interest in solvent recovery and solute concentration in recent years. Organic solvents are commonly used in the pharmaceutical industry to synthesize active pharmaceutical ingredients (APIs), cleaning agents, chemicals [22,23], etc. Multiple-stage purification of pharmaceuticals and their intermediates makes solvent removal an essential step [21]. The costs of processing these organic solvents for separation, recovery, or disposal are substantial and comprise a significant fraction of operating expenses [24]. The solvent separation in industries is usually done by distillation, which has high energy consumption due to the latent heat of vaporization [25]. Moreover, manufacturing processes may be sensitive in nature [17]. The membrane-based separations of organic solvents are pervaporation (PV) [26], organic solvent reverse osmosis (OSRO) [27], and organic solvent nanofiltration (OSN) [28]. Energy-efficiency calculations confirmed that OSN uses 25 times less energy per liter of recovered solvent than distillation [24]. However, the high pressure used in OSN remains a concern as it may add extra operating and maintenance costs [21]. OSFO would be economical and potentially enable bulk chemical separations that are not accessible by OSRO [29]. Another benefit of OSFO is that a suitable draw solute can generate sufficiently high osmotic pressure to concentrate APIs [17]. This is difficult to meet by pressure-driven OSN due to the high operating pressure required to overcome the osmotic pressure.

An ideal OSFO membrane should be thin, have a narrow pore size distribution, offer enhanced solvent flux with high solute rejection, and have organic solvent tolerance in long-duration operations [20]. Various efforts of membrane preparation for OSFO are demonstrated in the literature. Cui et al. prepared a TFC membrane consisting of a polyamide (PA) selective layer and a porous polyimide substrate [21]. The authors discussed alternate draw solutes to lithium chloride (LiCl), which is said to be harmful. An MXene-interlayered PA membrane for OSFO exhibited

* Corresponding author. Polymer Science and Engineering Division, CSIR-National Chemical Laboratory, Pune, 411008, India.
E-mail address: uk.kharul@ncl.res.in (K. Ulhas K).

https://doi.org/10.1016/j.memsci.2024.123090
Received 24 April 2024; Received in revised form 8 July 2024; Accepted 11 July 2024
Available online 14 July 2024

high ethanol flux and low specific salt flux [19]. Tong et al. demonstrated graphene oxide (GO) based membranes for OSFO of methanol, using citric acid as a draw solute [20]. Wei et al. developed a modified simultaneous phase-inversion and crosslinking method for fabricating solvent-resistant polyimide and demonstrated OSFO performance using LiCl-ethanol (1 mol L^{-1}) as a draw solution [30]. A hollow fiber TFC module for OSFO was evaluated using PEG-400 as a DS in acetone and isopropanol as solvents [17]. A polyketone-based TFC hollow fiber membrane with a polyamide selective layer was demonstrated for OSFO using methanol as solvent, sucrose octaacetate as a model API, and polyethylene glycol 400 (PEG-400)/methanol solution as a draw solution [14].

Self-standing support-free films have raised considerable attention because of their ease of fabrication, structural control, and ability to minimize ICP effects [31–36]. Although OSFO is demonstrated for methanol, ethanol, isopropanol, acetone, *N,N*-dimethylformamide, and hexane [14–17,19–21,30], other common solvents of industrial significance need a membrane material that is solvent stable. The pharmaceutical/chemical industries use acetonitrile, dichloromethane, dimethyl sulfoxide, 1,4-dioxane, *N*-methyl-*2*-pyrrolidone, tetrahydrofuran, ethyl acetate, toluene, etc. Routinely [22,27,37,38], for which need of a stable OSFO membrane material is still awaited. It is said that exploring other membrane materials is of great value for the practical application of OSFO processes in broader fields [20].

In this study, we report, for the first time, the fabrication of free-standing flat sheet membranes for OSFO based on poly(2,5-Benzimidazole), commonly known as ABPBI. It is not only known for excellent thermochemical stability [39,40], it is insoluble in common organic solvents (chlorinated solvents, tetrahydrofuran, dioxane, toluene, *N,N*-dimethylformamide, *N,N*-dimethylacetamide and *N*-methyl-*2*-pyrrolidone) [40,41], which are being used in pharmaceuticals and chemical industries, as stated above. ABPBI has a high N–H group density [42], possesses closed chain packing, and can form H-bonding with water/polar solvents. Moreover, its excellent pH stability is known [40]. It could be a good membrane material for OSFO and open up new avenues owing to its niche characteristics (especially solvent and pH stability). Free-standing, thin, flat sheet membranes (FSMs) were made to investigate their OSFO performance. Initial evaluations used methanol as a solvent and LiCl as a draw solute. Looking at the insolubility of LiCl in many organic solvents, a salt of triethylamine and benzoic acid was used as a draw solute with different solvents. This work investigates scalable OSFO membranes based on ABPBI for various solvents.

2. Experimental

2.1. Materials, ABPBI synthesis and characterizations

A *3,4*-diaminobenzoic acid (DABA) was obtained from Gharada Chemicals. The polyphosphoric acid (PPA, ca. 84 % P_2O_5) and LiCl were procured from Avra Synthesis. The *o*-phosphoric acid (OPA), methanol (MeOH), ethanol (EtOH), *N,N*-dimethylformamide (DMF), dimethyl sulfoxide (DMSO), acetonitrile (ACN), triethylamine, and benzoic acid were procured from Merck. Thomas Baker supplied methanesulfonic acid (MSA) and conc. H_2SO_4 (98 %). The *p*-nitrophenol (NP), *o*-nitroaniline (NA), methyl red (MR), malachite green (MG), rhodamine B (RB), direct red 81 (DR), aniline blue (AB) were procured from Himedia Laboratories Pvt. Ltd.

The ABPBI was synthesized by self-condensation of DABA in PPA, which acts as a solvent and dehydrating agent [39,40,42]. The reactor with an overhead stirrer and heating assembly was charged with 2250 g of PPA, heated to 120 °C, and 75 g of DABA was added while stirring. After dissolution, the temperature was raised to 170 °C and maintained for 1 h. The temperature was increased to 210 °C while stirring. After 1 h, 600 g of OPA was added and stirred for an additional hour. The polymer was precipitated in water, crushed in a blender, and washed with water (to remove excess acid) until it was neutral to pH. The polymer was agitated with 0.1 M aq. $NaHCO_3$ for 8 h to remove bound acid present in the polymer matrix. The polymer collected by filtration was washed with water until it was neutral to pH. After soaking in methanol for 15 h, the polymer was filtered, dried at 60 °C for 8 h, and kept in a vacuum oven at 100 °C for 7 days. The inherent (η_{inh}) and intrinsic ([η]) viscosity of the obtained polymer was determined using a Ubbelohde viscometer and 98 % H_2SO_4 as a solvent at 35 °C. The FTIR spectra were recorded using Bruker Optics ALPHA-E spectrometer with a universal Zn–Se ATR accessory in a 600-4000 cm^{-1} frequency region. The wide-angle X-ray diffraction (WAXD) spectra were recorded with Rigaku SmartLab X-ray diffractometer in reflection mode using CuKα radiation (λ = 1.5418 Å). The 2θ scan range was 5–40° at a scan rate of 3° min^{-1}. The thermogravimetric analysis (TGA) was performed on TGA-STA6000 (TA Instruments) in an N_2 atmosphere with a heating rate of 10 °C min^{-1}. FTIR analysis aimed to compare the characteristic IR bands with those reported earlier for ABPBI. Similarly, WAXD analysis and TGA were performed to compare the X-ray and degradation patterns (typical water loss usually observed for ABPBI, its degradation temperature, and the char yield) with that reported in the literature.

2.2. Preparation of FSMs

A 3 % (w/w) dope solution was prepared by dissolving ABPBI in MSA at 80 °C while stirring for 24 h, filtered to remove undissolved particles, if any, and degassed for 15 min. Membranes were cast on a flat surface using a tabletop casting machine with a knife gap set at 200 μm, a speed of 5 cm s^{-1}, and water at ambient as a non-solvent. The obtained membranes were washed with DI water to remove free MSA, dipped in 0.1 N $NaHCO_3$ for 8 h to remove bound MSA, and stored at 4 °C until use. These FSMs were heat-treated at 60 and 350 °C for 1 h while sandwiching between porous plates. For ABPBI-3 (Table 1), 3 cycles of heating the membrane at 350 °C for 1 h and cooling at ambient for 1 h were performed. The average membrane thickness was ~17 (±2) μm.

2.3. Preparation of triethylammonium benzoate (TB) and its draw solution (DS)

A salt, TB, was prepared by adding 202.37 g (1 mol) of triethylamine in 2 L of a solvent (MeOH, EtOH, ACN, DMF, or DMSO), followed by dissolving an equimolar amount of benzoic acid (244.24 g) in it while stirring (Scheme 1). The formed solution was used as a DS during OSFO experiments.

2.4. Physical characterizations of FSMs

The FTIR, WAXD, and TGA spectra of films were recorded using equipment as detailed in Section 2.1. The water contact angle of the membrane surface was obtained using Drop Shape Analyzer DSA25-KRÜSS GmbH. A water drop of constant size (20 μL) was placed on the surface, and a digital image was analyzed using a built-in drop-shape analysis tool. For each type of membrane, 6 samples were analyzed and data averaged. The streaming potential was measured with a SurPASS3 instrument (Anton-Paar) equipped with an adjustable gap cell. Samples were soaked in 5 mmol L^{-1} KCl as an electrolyte for 12 h, and the streaming potential was measured across the pH range of 3–10. The HCl or KOH solutions (0.05 mol L^{-1}) were used to adjust the pH of the

Table 1
Nomenclature of membranes.

Membrane identification	Treatment temperature for 1 h duration (°C)	Number of cycles
ABPBI-1	60	1
ABPBI-2	350	1
ABPBI-3	350	3

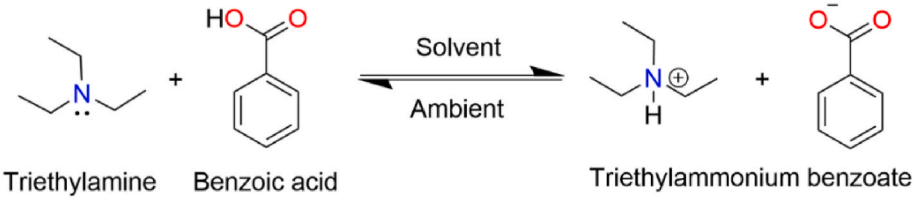

Scheme 1. Preparation of triethylammonium benzoate (TB).

electrolyte. Three measurements were made at each pH. The zeta potential was calculated from the measured streaming potential by application of the Helmholtz-Smoluchowski equation using instrument software. The tensile tests were performed at ambient on Linkam TST-350 microtensile testing instrument using the dumbbell-shaped film samples (6 samples for each membrane, with a length of 2.8 cm, a width of 1.2 cm and an average thickness of 17 ± 2 μm). The Field Emission Scanning Electron Microscope (FE-SEM) images were analyzed using gold-sputtered cross-section and surface samples of membrane on FEI Nova NanoSEM 650 Field Emission Scanning Electron Microscope (FE-SEM), with a field emitter as an electron source. Atomic Force Microscopy (AFM, Nanosurf) was used to measure the root mean square roughness (Rq) and arithmetic average (Ra) roughness of the top and bottom membrane surfaces. The Rq and Ra were averaged from 3 different profiles of AFM images of each membrane type.

2.5. OSFO analysis

The OSFO performance of membranes was evaluated using a plate and frame module (SS-316) with an active area of 120 cm^2. Three membranes were used for each set of experiments, and the results were averaged. Initially, MeOH was used as a solvent (feed solution, FS) using varying concentrations (0.5–2 mol L^{-1}) of LiCl in MeOH as a draw solution (DS). While using another solvent (EtOH, ACN, DMF, or DMSO) as FS, its DS using TB as a draw solute was prepared as given in Section 2.3. The maximum concentration of LiCl was taken as 2 mol L^{-1}, to compare our results with those reported in the literature at similar concentrations [16,17,19–21]. The TB concentration was based on solubility in the solvent (viz., MeOH, EtOH, ACN, DMF, and DMSO). Before performing an experiment, the membrane was saturated with FS for 2 h. The FS (0.5 L) and DS (2 L) were recycled on the top and bottom side of the membrane, respectively, at ambient using a gear pump (LeadFluid) at the flow rate of 150 ml min^{-1} (cross-flow velocity of 20 cm s^{-1}). The pressure transmitters were fitted at the outlet of the DS and FS channels to record the pressure exerted on the membrane due to the flow of the solution. It was observed that until the flow rate of 150 ml min-1, no pressure was generated. The pressure started increasing beyond this flow rate. An electronic weighing balance (Contech CA-3102, connected to a computer for online data acquisition) was used to monitor the change in weight of FS. The solvent flux ($J_{Solvent}$) was calculated using Eq. (1) [21].

$$J_{Solvent} = \frac{\Delta M}{A_m X \Delta t X \rho} \quad (1)$$

where, ΔM (g) is the change in the weight of FS over the 10/16 h of experimental duration, Δt (h), A_m (m^2) is the active membrane area, and ρ (g L^{-1}) is the density of the solvent. The concentration of FS was monitored using a conductivity meter (LABINDIA PICO$^+$). The reverse salt flux (J_S) was determined using Eq. (2) [17].

$$J_s = \frac{C_f V_f - C_i V_i}{A_m X \Delta t} \quad (2)$$

where, C_i and C_f (mol L^{-1}) denote the initial and final concentration of salt in the FS, while V_i and V_f represent its initial and final volume, respectively. Thickness normalized total flux (J_N) was calculated using Eq. (3).

$$J_N = J_{Solvent} X \delta \quad (3)$$

where, δ is the membrane thickness in μm. The specific reverse salt flux (SRSF, mol L^{-1}) was calculated using Eq. (4) [17].

$$SRSF = \frac{J_S}{J_{solvent}} \quad (4)$$

2.6. Analysis using model organic compounds (MOCs)

A 10 mg of each of the following model organic compounds: *p*-nitrophenol (NP, molecular weight = 138), *o*-nitroaniline (NA, 138), methyl red (MR, 269), malachite green (MG, 364), rhodamine B (RB, 479.02), direct red 81 (DR, 675), aniline blue (AB, 737) were dissolved in 1 L methanol and used as a feed solution in OSFO experiments with ABPBI-3 as a membrane. The LiCl and TB (1 mol L^{-1} in MeOH) were evaluated individually as a DS. With acetonitrile as a solvent, 10 mg each of NP, NA, MR, RB, and DR dissolved in 1 L was used as a feed solution (MG and AB are insoluble) while using TB (1 mol L^{-1}) as a draw solute. Usually, the concentration of FS reported in the literature was 100–200 ppm [15,17,20]. The selection of present solutes (MOCs of a broader range of molecular weight) in FS depended on their solubility in MeOH and acetonitrile. UV–vis spectrophotometer (Shimadzu UV-1800) was used in the wavelength range of 200–900 nm for analyzing the concentration of MOCs. The experiments were performed for 10 h, using a membrane area of 360 cm^2.

3. Results and discussion

3.1. ABPBI synthesis and characterizations

The synthesized ABPBI (Fig. 1a) possessed an inherent viscosity of 3.83 dL g^{-1} at 0.2 g dL^{-1} concentration. The intrinsic viscosity of synthesized ABPBI was 2.28 dL g^{-1}, leading to the viscosity averaged molecular weight of 106,888 g mol^{-1}. The Mark-Houwink constants were used as reported for PBI with H_2SO_4 as a solvent [43]. The FT-IR spectra (Fig. 1b) showed characteristic bands at 1630, 1552, and 1419 cm^{-1}, attributable to the C═C and C═N stretching of the benzimidazole groups of ABPBI. The broad band at ~3165 cm^{-1} is attributable to the N–H stretching vibrations. The TGA thermogram (Fig. 1c) showed an initial weight at ~295 °C, amounting to ~16 % water loss from the membrane matrix. The polymer decomposition started at ~624 °C, conveying excellent thermal stability. The char yield at 900 °C was 59.0 %. High char yield is a peculiar ABPBI property, as observed earlier [40–44]. The degradation is facilitated in the air atmosphere. The polymer degradation in air starts at 548 °C, while under N_2, it starts at 624 °C. At 900 °C, the air atmosphere completely burns the polymer, yielding zero char. The FTIR bands, sluggish water loss, degradation temperature, nature of the TGA curve, and WAXD pattern (Fig. 1b, c, and d) of ABPBI matched well with literature reports [39–42,44–46].

3.2. Characterizations of FSMs

3.2.1. Physical properties

The FTIR spectra of all membranes (Fig. 2a) and the TGA curve of

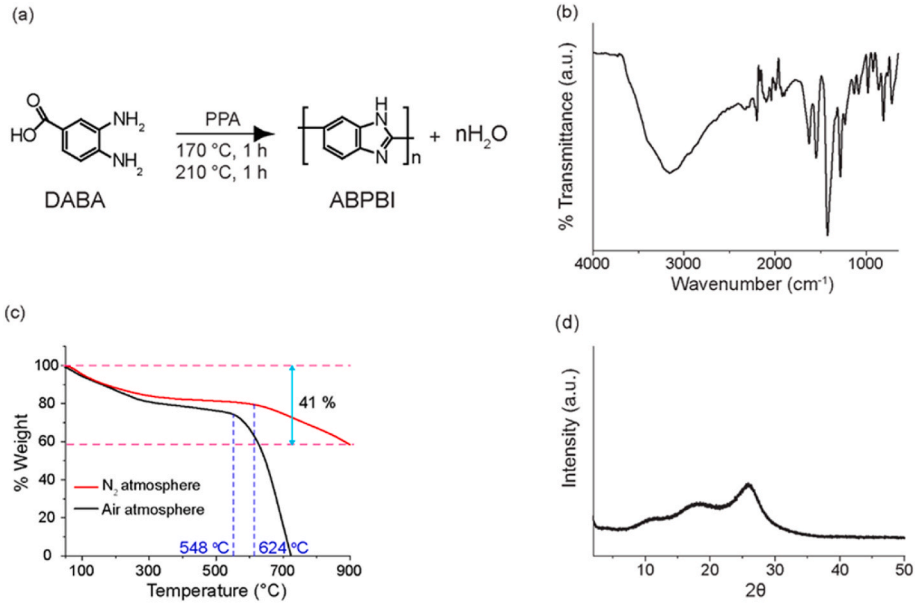

Fig. 1. a) Synthesis of ABPBI, its b) FT-IR, c) TGA, and d) WAXD pattern.

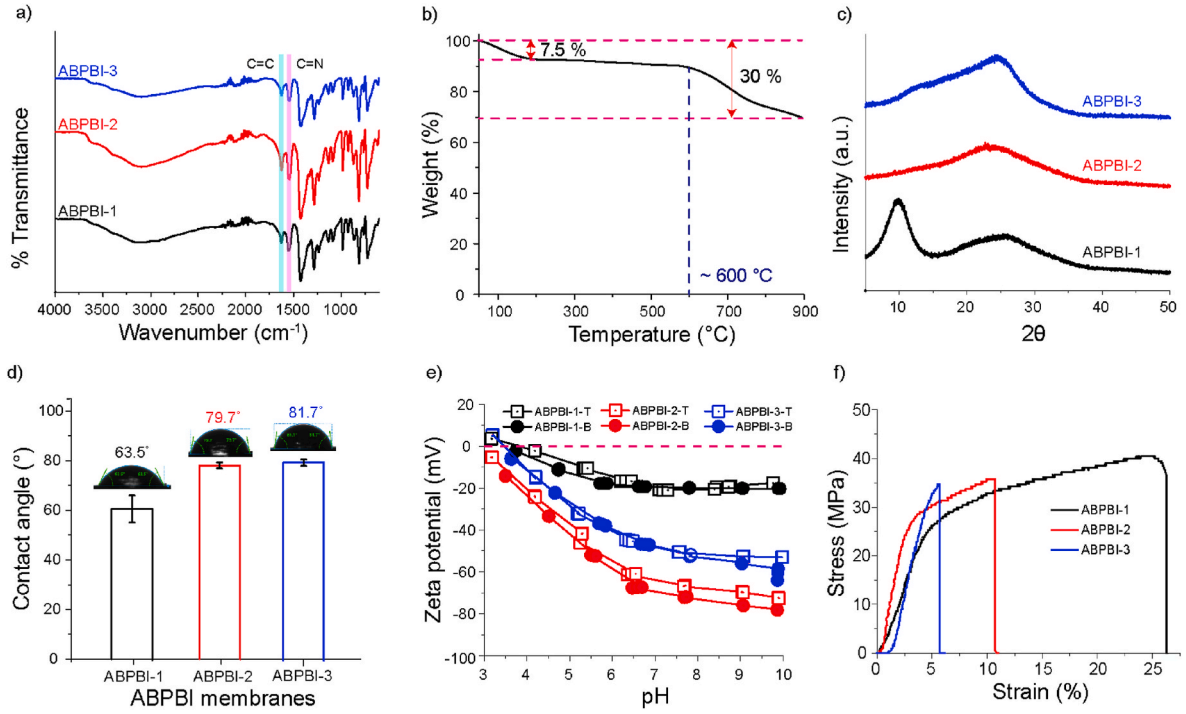

Fig. 2. Characterizations of FSMs: a) FT-IR spectra, b) TGA of ABPBI-3, c) WAXD pattern, d) contact angle of membrane surfaces, e) zeta potential curves, and f) stress-strain curves.

ABPBI-3 (Fig. 2b) matched well with the respective analyses of polymer (Fig. 1), indicating their stability at a treatment temperature of 350 °C. The TGA pattern showed an initial weight loss of 7.5 %. This presence of water can be attributed to the ability of ABPBI to pick up moisture from the atmosphere, as it has the N–H group in its repeat unit. It may be noted that the char yield increased from 59 % (for the polymer) to 70 % for ABPBI-3. Such a high char yield of ABPBI is known in the literature [47–49]. In the WAXD spectra of FSMs (Fig. 2c), the peak at ~26° (average d-spacing = 3.42 Å) remained the same as that of polymer. After the membranes were treated at 350 °C, the lower 2 value (~10) pattern was smoothened. It indicates that the heat treatment suppressed domains having larger d-spacing (8.84 Å), which is beneficial for membrane application. Such observation was noted earlier for PBI [50]. The average water contact angle of membranes treated at °C was 63.5° (Fig. 2d). It increased to 79.7° (ABPBI-2) after the membrane was treated at 350 °C, probably due to the removal of the water. This data matched with our earlier report [46].

The zeta potential of all three types of membranes (Fig. 2e) exhibited a negative charge in a wide range of pH (3–10) and thus is capable of repelling anionic [51] present in the DS. The zeta potential values of the top and bottom surfaces of membranes are similar. It indicates that both sides of membranes are symmetric in nature. The stress-strain curves

(Fig. 2f) show that the ABPBI-1 exhibited the highest elongation at break (26.3 %) due to the moisture present in it. After heat treatment at 350 °C, the modulus and tensile stress increased for ABPBI-2 and ABPBI-3. Similar variations in mechanical properties of ABPBI by annealing are reported by Chaudhari et al. [41].

The present membranes were transparent, thin, and flexible (Fig. 3). The FE-SEM images of the surface (top and bottom) and cross-section are shown in Fig. 3. The surface morphology on both sides of all three membranes was similar. The cross-section images of both membranes did not exhibit any porosity. It was demonstrated that the porosity of ABPBI-based membranes is eliminated by heat treatment [41,46].

The surface roughness of each membrane was analyzed by AFM on three different profiles, as shown in Fig. 4. The Rq and Ra values are summarized in Table 2. Although there is a slight difference in the roughness of the top and bottom sides of ABPBI-1 (dried at 60 °C), it was reduced by heat treatment for ABPBI-2 and ABPBI-3. It is reported that the heat treatment leads to compactness and is characterized by AFM (surface roughness). This phenomenon is well-known in the literature [52,53]. It may be thus asserted that the top and bottom sides of present membranes are similar.

3.2.2. *Effects of membrane heat treatment, DS concentration, and duration of analysis*

Initially, all three membranes were evaluated using MeOH as the FS and LiCl as a draw solute (Fig. 5a). The average J_{MeOH} for ABPBI-1, -2, and -3 was 4.25, 1.32, and 1.12 L m^{-2} h^{-1}, while the RSF (J_{LiCl}) was 1.979, 0.054 and 0.019 mol m^{-2} h^{-1}, respectively. As per TGA (Fig. 1c), the ABPBI matrix holds water till ~295 °C, the removal of which is known to be sluggish [41,42,44]. The presence of water and domains with larger d-spacing (average d-spacing of 8.84 Å as discussed in Section 3.2.1) in ABPBI-1 could be responsible for its higher RSF and solvent flux than that of ABPBI-2 and -3. After the heat treatment at 350 °C for the ABPBI-2 membrane, the flux was reduced to ~1/3rd, while the RSF was reduced considerably to 2.7 % compared to ABPBI-1. This observation endorses the importance of water removal by heat treatment at 350 °C. With the removal of water molecules, the H-bonding between water and ABPBI repeat unit is replaced by the intermolecular H-bonding within ABPBI chains. As a result, domains of larger d-spacing are eliminated, and both J_{MeOH} and J_{LiCl} are reduced. When the performance of ABPBI-2 and ABPBI-3 is compared, the J_{MeOH} for the latter was reduced by ~14 %, while J_{LiCl} was lowered by 65 % compared to the earlier. It shows that by heat-treating the membrane three times, a slight compromise on J_{MeOH} offered a better advantage of reducing the RSF.

Fig. 5b shows that with an increase in the concentration of DS, flux increased linearly for ABPBI-3. By increasing the DS concentration from 0.5 to 2 mol L^{-1}, J_{LiCl} increased by ~4.5 times, but the J_{MeOH} increased by 1.5 times. The RSF of 0.039 mol m^{-2} h^{-1} at a DS concentration of 2 mol L^{-1} is appreciable. The analysis for long duration using ABPBI-3 (Fig. 5c) showed an almost linear flux of solvent and salt, with a slight decrease in J_{MeOH}. The observed decrease in J_{MeOH} can be attributed to a slight reduction in DS concentration. The initial concentration of 0.5 mol L^{-1} was lowered to 0.45 mol L^{-1} at the end of the experiment (16 h). It is attributable to the lowering of DS concentration with time. Since the membrane thickness is low, its stability over a longer duration of operation is evident.

3.2.3. *OSFO using few industrially significant solvents*

To evaluate the performance of TB as a draw solute, all three membranes, viz., ABPBI-1, ABPBI-2, and ABPBI-3, were used. Although J_{MeOH} was slightly lowered, the reduction in RSF was more significant than in the case of LiCl as DS (Fig. 6a). The lowering in flux could be attributed to the possible lower osmotic pressure created by TB, while the lowering in RSF could be due to its bigger size than LiCl. As could be anticipated from Fig. 5a, the flux and RSF are higher for ABPBI-1 than for the other two membranes. Between ABPBI-2 and ABPBI-3, the latter exhibited considerably lower RSF (0.0013 mol L^{-1}). Therefore, it was used to analyze the OSFO performance of EtOH, ACN, DMF, and DMSO. These solvents were chosen since they have commercial significance [22,37,38]. The concentration of TB was maintained at 1 mol L^{-1} for all solvents. Fig. 6b shows that the solvent flux varied in an order: MeOH > EtOH > ACN > DMF > DMSO. Although the higher flux of MeOH and EtOH can be correlated to their protic nature, the higher molecular weight/size of other aprotic solvents can also be a reason for their lower flux. There could be another possibility of low osmotic pressure created by TB as the conductivity of respective DS was lower than that of MeOH (Table 3). Such an observation of varying conductivity with solvent is

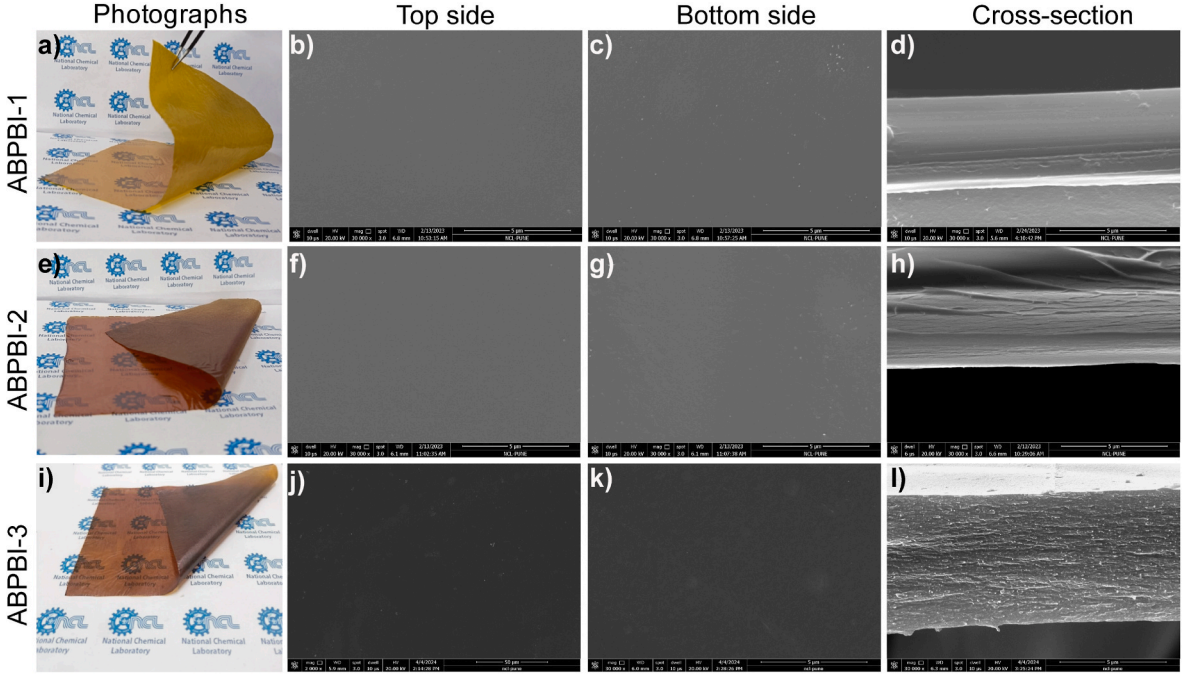

Fig. 3. Digital and FESEM images of present membranes.

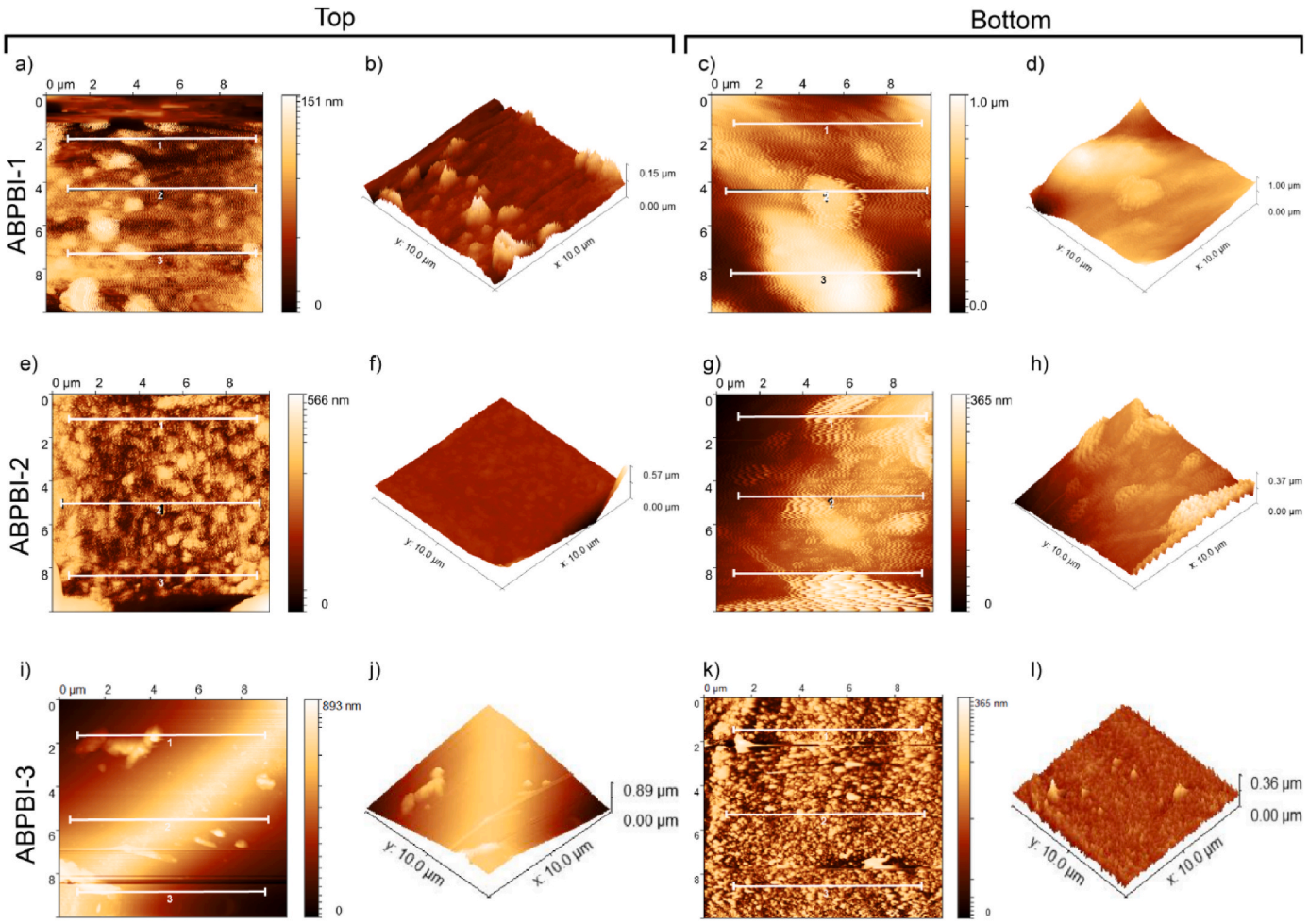

Fig. 4. Top and bottom surface topography and 3D AFM images of present membranes.

Table 2
The roughness of the membrane surface.

Temperature of membrane treatment (°C)	The surface of the membrane analyzed	Roughness (nm)	
		R_q*	$R_a^{\#}$
ABPBI-1	Top	1.64 ± 0.4	1.63 ± 0.4
	Bottom	6.4 ± 1.4	5.1 ± 1.1
ABPBI-2	Top	1.44 ± 0.1	1.15 ± 0.1
	Bottom	2.5 ± 0.13	1.92 ± 0.14
ABPBI-3	Top	0.2 ± 0.05	0.14 ± 0.03
	Bottom	0.6 ± 0.17	0.5 ± 0.14

Rq*: Root mean square average of height deviation taken from the mean image data plane.
Ra#: Arithmetic average of the absolute values of the surface height deviations measured from the mean plane.

reported [21]. The RSF was considerably lower for all the solvents (<0.0013 mol m^{-2} h^{-1}), especially for ACN and DMF. The ACN and DMF exhibited the lowest J_{TB} of 0.0002 and 0.0003 mol m^{-2} h^{-1}, conveying the applicability of ABPBI as a membrane material for these industrially used solvents.

The fluxes can be elevated by lowering the membrane thickness, appropriately choosing DS with high concentration, and tuning the operational parameters (velocity, operational temperature, etc.). The present draw solute (TB) could be made easily by dissolving triethyl amine and benzoic acid in these solvents. Moreover, they are commonly available, larger-size chemicals (than LiCl), form acid-base salt quickly, and, more importantly, dissolve in various solvents. By further elevating the polarity of benzoic acid by introducing a polar group, the solubility could be increased, and the resulting salt could be more polar.

3.2.4. *Long-duration analysis in the presence of MOCs*

The long-duration stability of ABPBI-3 was evaluated for 10 h in the presence of 7 MOCs as representatives of APIs/drug molecules. Their chemical structure is shown in Fig. 7, and their selection was based on (i) solubility in present solvents, (ii) wide variation in molecular weight (138–737), and (iii) UV-active nature. ABPBI-3 was chosen as a membrane based on its better performance than the other two membranes covered above. The results obtained at the end of 10 h duration (membrane area: 360 cm^2) are given in Table 4.

With either LiCl or TB as a DS, the solvent flux (MeOH/ACN) and RSF are in general agreement with the data seen in Fig.s. 5a and 6a. Although some of the MOCs are ionic in nature, osmotic pressure created by them can be negligible since their overall concentration was low (70 mg L^{-1}). After the experiments, their concentration was increased to 50 % when LiCl was DS and the solvent was MeOH. In the case of TB as a DS, the increase in MOC concentration was lower, owing to lower solvent (MeOH/ACN) flux. This increase could be attributed to the solvent flow to the DS side. As elaborated below, no MOC was permeated through the membrane.

The UV-spectrum and λ_{max} of individual MOCs dissolved in MeOH

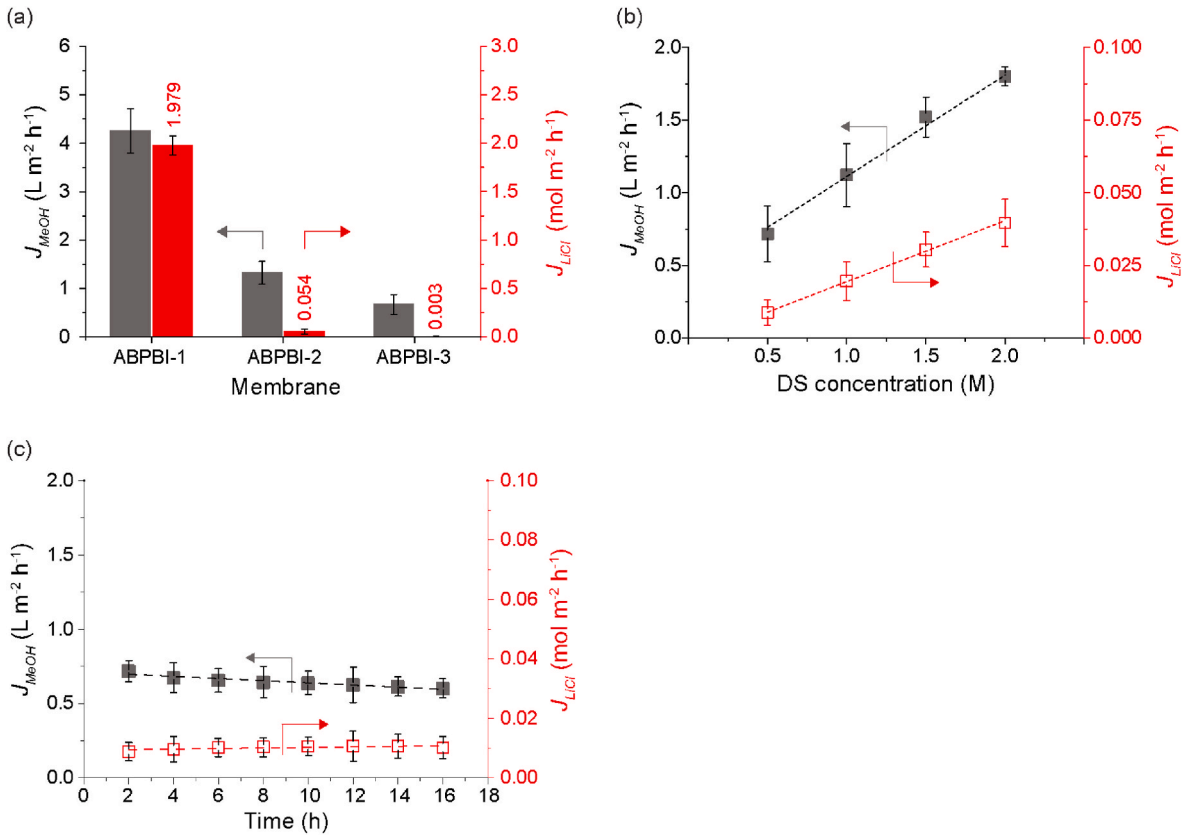

Fig. 5. Variation in flux and RSF with (a) membrane treatment condition (FS: MeOH, DS: 1 mol L^{-1} LiCl in MeOH), (b) DS concentration (FS: MeOH, DS: 0.5–2 mol L^{-1} LiCl in MeOH) using ABPBI-3, and (c) long duration stability of ABPBI-3 (DS: 0.5 mol L^{-1} LiCl in MeOH).

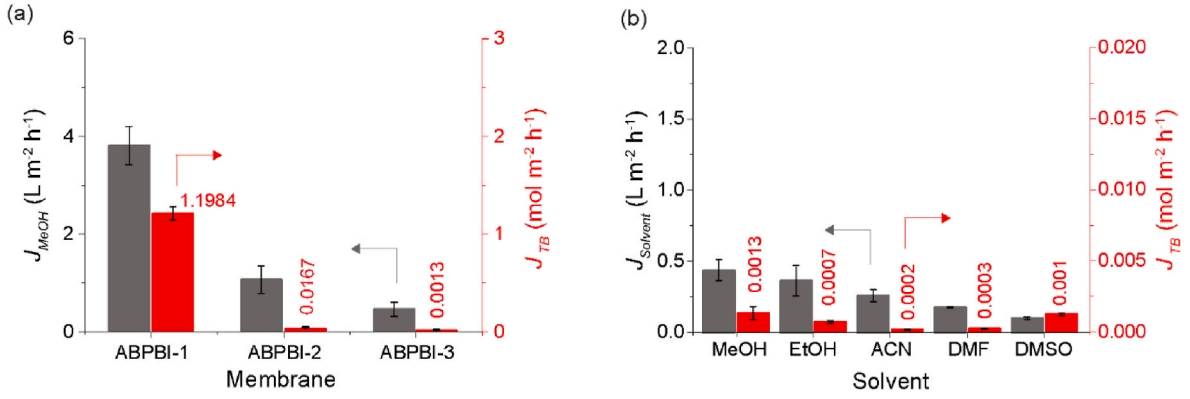

Fig. 6. OSFO performance using 1 mol L^{-1} TB as DS: (a) variation in the membrane using MeOH as FS (b) use of different solvents with ABPBI-3 as a membrane.

Table 3
DS conductivity.

Solvent	DS (1 mol L^{-1})	Conductivity (mS cm^{-1})
MeOH	LiCl	24.4 ± 0.4
MeOH	TB	15.5 ± 0.2
EtOH		1.91 ± 0.03
ACN		1.86 ± 0.02
DMF		1.24 ± 0.02
DMSO		1.47 ± 0.04

are given in Fig. 8a. At the end of the experiment, UV spectra of FS (black curve) and DS (red line) are shown in Fig. 8b and c while using LiCl or TB as the draw solute in MeOH. The MOCs could not be detected in either of the DS cases, indicating their impermeability through the membrane. Fig. 8d shows the color of FS and DS supporting this result. With acetonitrile as a solvent, UV spectra of individual MOCs are demonstrated in Fig. 9a. A slight shift in the λ_{max} of RB was observed, while for other MOCs, it remained the same as that of MeOH (Fig. 8a). Fig. 9b shows results using TB as the DS for the same experimental time of 10 h as that of methanol. There was no MOC permeation to the DS side of the membrane. Given the high UV sensitivity of some of the MOCs [54], it can be easily concluded that there is no permeation of MOC through the membrane, irrespective of the solvent used. These results using MeOH and ACN as solvents show that ABPBI-3 is impermeable to various MOCs with a wide range of molecular weight (138–737) and chemical nature. These results are highly encouraging, especially for the enrichment of small organic APIs/chemical products and simultaneous recovery of solvents with extremely low permeability of draw solute.

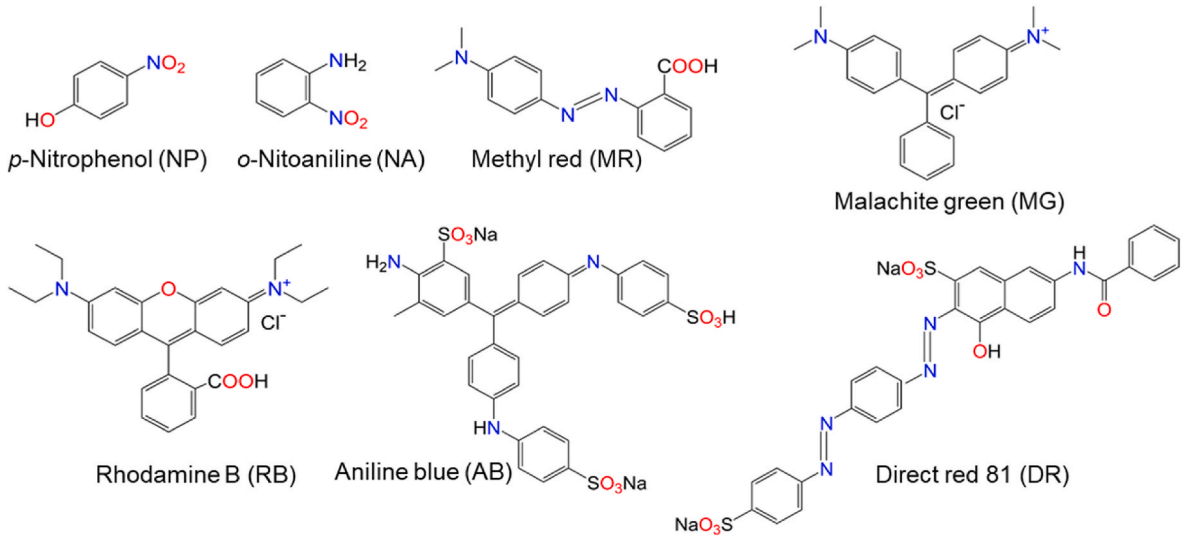

Fig. 7. Chemical structure of MOCs.

Table 4
OSFO performances of ABPBI-3 in the preence of MOCs.

Solvent	MOCs in FS	DS	$J_{Solvent}$ (L m^{-2} h^{-1})	J_S/RSF (mol $m^{-2}h^{-1}$)	Feed concentration (mg L^{-1})	
					At start	After experiment
MeOH	NP, NA, MR, MG, RB, DR and AB	1 mol L^{-1} LiCl	0.9	0.003	70	104
MeOH	NP, NA, MR, MG, RB, DR and AB	1 mol L^{-1} TB	0.40	0.0015	70	82
ACN	NP, NA, MR, RB and DR	1 mol L^{-1} TB	0.20	0.0004	50	54

3.2.5. *Comparison with the literature*

The OSFO performances of the present membrane (ABPBI-3) and some literature data are given in Table 5. The first column gives the name of the membrane, its type, and its thickness. To have uniformity in the performance comparison, we used two terms, viz., normalized flux, J_N (Eq. (3)), and SRSF (Eq. (4)). In most of the reported cases, the membrane thickness is at least an order of magnitude lower than the thickness of the present membrane. Thus, if normalized flux is compared for any of the reported solvents (MeOH/EtOH/DMF), it is generally higher, and RSF is lower for the present membrane, except MOF-based membranes reported by Ma et al. [16]. If SRSF is compared, the value for EtOH in the present case (0.002 mol L^{-1}) is an order of magnitude lower than the data from the literature. Although it looks similar to the MOF-based membrane value [16], it may be noted that the draw solute concentration is half in the present case. Similar superior behavior is seen in the case of MeOH as well. In the case of DMF, the normalized flux, RSF, and SRSF seem superior to the same data reported for the HLGO membrane [20]. The present RSF data for ACN (0.0002 mol m^{-2} h^{-1}) and DMSO (0.0012 mol m^{-2} h^{-1}) with reasonably good flux are highly encouraging. It may be noted that the present membranes are thin, symmetric films, so the ICP effect can be ignored, thus providing an attractive membrane material for OSFO.

4. Conclusions

Thin, solvent-stable, symmetric ABPBI membranes were successfully prepared for the OSFO process. The physical characterizations, viz., zeta potential, FE-SEM, and AFM, showed their symmetric, dense nature. The membrane heat treatment, using different DS solutes and organic solvents, showed their own impact on the OSFO performance. The membrane treated at 350 °C was evaluated using organic solvents: methanol, ethanol, acetonitrile DMF, and DMSO. Initial evaluations of methanol as a solvent and 1 mol L^{-1} LiCl as a draw solute offered attractive results of solvent flux (J_{MeOH}: 1.1 L m^{-2} h^{-1}) and low reverse salt flux (J_{LiCl}: 0.019 mol m^{-2} h^{-1}). Since LiCl was freely soluble only in methanol, a salt of commonly available triethyl amine and benzoic acid (TB) soluble in

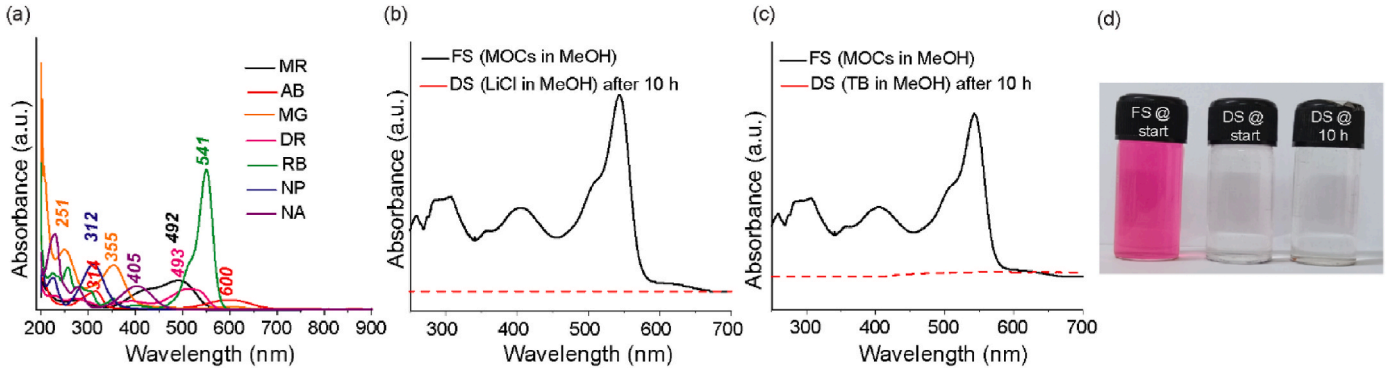

Fig. 8. UV–Vis spectra of (a) individual MOCs in MeOH, (b) FS and DS (1 mol L^{-1} LiCl) in MeOH after 10 h, (c) FS and DS (1 mol L^{-1} TB) in MeOH after 10 h.

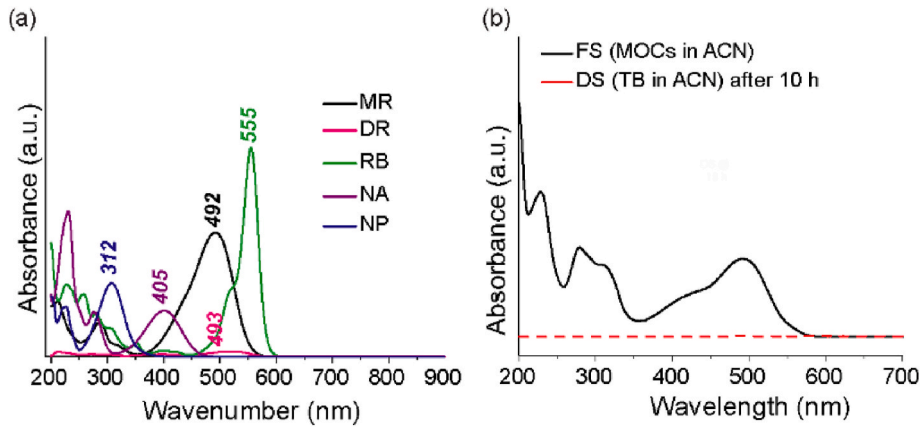

Fig. 9. UV–Vis spectra of (a) individual MOCs in ACN, (b) FS and DS in ACN after 10 h.

Table 5
Comparison of present data with those reported in the literature.

Membrane (type, thickness (μm))	Solvent	DS	$J_{Solvent}$ (L m^{-2} h^{-1})	J_N (L μm m^{-2} h^{-1})	J_S/RSF (mol m^{-2} h^{-1})	SRSF (mol L^{-1})	Ref.
ABPBI-3 (symmetric, 17)	MeOH	1 mol L^{-1} LiCl	1.1	18.7	0.019	0.02	This work
	MeOH	2 mol L^{-1} LiCl	1.80	30.6	0.04	0.022	
	MeOH	1 mol L^{-1} TB	0.44	7.5	0.001	0.002	
	EtOH	1 mol L^{-1} TB	0.36	6.1	0.0007	0.002	
	ACN	1 mol L^{-1} TB	0.30	5.1	0.0002	0.001	
	DMF	1 mol L^{-1} TB	0.18	3.1	0.0002	0.0001	
	DMSO	1 mol L^{-1} TB	0.10	1.7	0.0012	0.013	
PA (TFC, 0.168)	EtOH	2 mol L^{-1} LiCl	2.52	0.42	0.013	0.005	[21]
MXene-PA (TFC, 0.0012–0.0014)	EtOH	2 mol L^{-1} LiCl	9.5	0.013	~0.09	0.01	[19]
HLGO (TFC, 0.24)	MeOH	1 mol L^{-1} CA	~3	0.72	0.1	0.03	[20]
	EtOH	2 mol L^{-1} LiCl	3.94	0.95	0.08	0.02	
	DMF	1 mol L^{-1} CA	3.4	0.82	0.065	0.02	
SA–NH–UiO-66/M-E−30 (TFC, 2)	MeOH	2 mol L^{-1} LiCl	34.1	68.2	0.04	0.0012	[16]
	EtOH	2 mol L^{-1} LiCl	9.3	18.6	0.016	0.002	

present solvents was successfully employed. An attractive solvent flux (J_{MeOH}: 0.44 L m^{-2} h^{-1}) and better rejection of draw solute (a very low J_{TB} of 0.0013 mol m^{-2} h^{-1}) than LiCl were obtained. The OSFO was dependent on the type of solvent and the osmotic pressure created by a draw solute present in it. While using 1 mol L^{-1} triethylammonium benzoate as a draw solute, the flux of acetonitrile and DMSO were 0.30 and 0.10 L m^{-2} h^{-1}, respectively. The reverse salt flux in the respective solvent was 0.0002 and 0.0012 mol m^{-2} h^{-1}, which is extremely low, conveying the usefulness of employing this draw solute.

OSFO performance in the presence of model organic compounds (MOCs) of varying molecular weight and functional groups using MeOH and acetonitrile as a solvent was highly encouraging, as all MOCs exhibited no transport through the membrane. These results convey the applicability of present membranes for the concentration of APIs/organic compounds of varying size and chemical functionality. Present thin, symmetric, solvent-stable ABPBI membrane can not only overcome the critical challenges of the ICP effect (that limits the performance of current OSFO membranes) but opens up applicability of various solvents possessing high rejection of small solutes organic and draw solutes (LiCl and TB).

CRediT authorship contribution statement

Thorat Nitin M: Writing – original draft, Visualization, Validation, Methodology, Investigation, Funding acquisition, Formal analysis, Data curation, Conceptualization. **Valvi Suresh V:** Formal analysis. **Lele Ashish K:** Writing – review & editing, Visualization. **Kharul Ulhas K:** Writing – review & editing, Supervision, Resources, Project administration, Funding acquisition, Conceptualization.

Declaration of competing interest

The authors declare the following financial interests/personal relationships which may be considered as potential competing interests: Ulhas K Kharul reports financial support was provided by Department of Science and Technology, Govt. of India. If there are other authors, they declare that they have no known competing financial interests or personal relationships that could have appeared to influence the work reported in this paper.

Data availability

Data will be made available on request.

Acknowledgments

The funding received from the Department of Science and Technology (Grant No. DST/TM/WTI/WIC/2K17/100(G)) and SRF-fellowship to Nitin M. Thorat received from Council of Scientific and Industrial Research, Govt. of India (Award letter No. 31/11(1088)/2019-EMR-I) are highly acknowledged. The authors thank Prof. Devin Shaffer (Civil & Environmental Engineering, University of Houston) and Dr. Rahul Shevate (PSE Division, CSIR-National Chemical Laboratory) for the zeta potential analyses.

References

[1] F. Yu, H. Shi, J. Shi, K. Teng, Z. Xu, X. Qian, High performance forward osmosis membrane with ultra-fast water transport channel and ultra-thin polyamide layer, J. Membr. Sci. 616 (2020) 118611, https://doi.org/10.1016/j.memsci.2020.11861.

[2] P. Lu, Y. Wang, L. Wang, Y. Wei, W. Li, Y. Li, C.Y. Tang, Immobilization of sulfonated polysulfone via 2D LDH nanosheets during phase-inversion: a novel strategy towards greener membrane synthesis and enhanced desalination performance, J. Membr. Sci. 614 (2020) 118508, https://doi.org/10.1016/j.memsci.2020.118508.

[3] L. Xu, T. Yang, M. Li, J. Chang, J. Xu, Thin-film nanocomposite membrane doped with carboxylated covalent organic frameworks for efficient forward osmosis desalination, J. Membr. Sci. 610 (2020) 118111, https://doi.org/10.1016/j.memsci.2020.118111.

[4] X. Wang, X. Baa, N. Cui, Z. Mac, L. Wang, Z. Wang, X. Gao, Preparation, characterisation, and desalination performance study of cellulose acetate membranes with MIL-53(Fe) additive, J. Membr. Sci. 590 (2019) 117057, https://doi.org/10.1016/j.memsci.2019.04.061.

[5] N.K. Khanzada, M.U. Farid, J.A. Kharraz, J. Choi, C.Y. Tang, L.D. Nghiem, A. Jang, A.K. An, Removal of organic micropollutants using advanced membrane-based water and wastewater treatment: a review, J. Membr. Sci. 598 (2020) 117672, https://doi.org/10.1016/j.memsci.2019.117672.

[6] A.J. Ansari, F.I. Hai, W.E. Price, J.E. Drewes, L.D. Nghiem, Forward osmosis as a platform for resource recovery from municipal wastewater - a critical assessment of the literature, J. Membr. Sci. 529 (2017) 195–206, https://doi.org/10.1016/j.memsci.2017.01.054.

[7] G.A. Bazedi, N. Soliman, H. Sewilam, Novel organic draw solution in forward osmosis process for fertigation: performance evaluation and flux prediction, Environ. Sci. Pollut. R. 29 (2022) 68881–68891, https://doi.org/10.1007/s11356-022-20674-4.

[8] R.A. Wahid, W.L. Ang, A.W. Mohammad, D.J. Johnson, N. Hilal, Evaluating fertilizer-drawn forward osmosis performance in treating anaerobic palm oil mill effluent, Membranes 11 (2021) 566, https://doi.org/10.3390/membranes11080.

[9] L. Francis, O. Ogunbiyi, J. Saththasivam, J. Lawler, Z. Liu, A comprehensive review of forward osmosis and niche applications, Environ. Sci.: Water Res. Technol. 6 (2020) 1986, https://doi.org/10.1039/D0EW00181C.

[10] Y. Kim, Y.C. Woo, S. Phuntsho, L.D. Nghiem, H.K. Shon, S. Hong, Evaluation of fertilizer-drawn forward osmosis for coal seam gas reverse osmosis brine treatment and sustainable agricultural reuse, J. Membr. Sci. 537 (2017) 22–31, https://doi.org/10.1016/j.memsci.2017.05.032.

[11] M. Gulied, K. Logade, H. Mutahir, S. Shaftah, S. Salauddin, A. Hameed, S. Zavahir, T. Elmakki, H.K. Shon, S. Hong, H. Park, D.S. Han, A review of membrane-based dewatering technology for the concentration of liquid foods, J. Environ. Chem. Eng. 11 (2023) 110583, https://doi.org/10.1016/j.jece.2023.110583.

[12] H. Wang, Y. Zhang, S. Ren, J. Pei, Z. Li, Athermal concentration of apple juice by forward osmosis: process performance and membrane fouling propensity, Chem. Eng. Res. Des. 177 (2022) 569–577, https://doi.org/10.1016/j.cherd.2021.11.023.

[13] K. Zhang, X. An, Y. Bai, C. Shen, Y. Jiang, Y. Hu, Exploration of food preservatives as draw solutes in the forward osmosis process for juice concentration, J. Membr. Sci. 635 (2021) 119495, https://doi.org/10.1016/j.memsci.2021.119495.

[14] R. Takada, R. Takagi, H. Matsuyama, High-degree concentration organic solvent forward osmosis for pharmaceutical pre-concentration, Membranes 14 (2024) 14, https://doi.org/10.3390/membranes14010014.

[15] L. Chen, C. Zhou, T. Yang, W. Zhou, Y. Chen, L. Wang, C. Lu, L. Dong, Imparting outstanding dispersibility to nanoscaled 2d cofs for constructing organic solvent forward osmosis membranes, Small 19 (2023) 2300456, https://doi.org/10.1002/smll.202300456.

[16] L. Ma, X. Han, S. Zhang, L. Wang, Sulfonated metal−organic framework nanostructure-based membranes with precise sieving for organic solvent forward osmosis, ACS Appl. Nano Mater. 5 (2022) 11324–11333, https://doi.org/10.1021/acsanm.2c02435.

[17] K.S. Goh, Y. Chen, D.Y.F. Ng, J.W. Chew, R. Wang, Organic solvent forward osmosis membranes for pharmaceutical concentration, J. Membr. Sci. 642 (2022) 119965, https://doi.org/10.1016/j.memsci.2021.119965.

[18] Y. Wang, X. Zhang, Y. Liu, L. Wang, H. Yang, P. Lu, Commercial polyethylene supported thin-film composite membranes within 10 μm thickness for organic solvent forward osmosis, Sep. Purif. Technol. 336 (2024) 126250, https://doi.org/10.1016/j.seppur.2023.126250.

[19] X. Wu, M. Ding, H. Xu, W. Yang, K. Zhang, H. Tian, H. Wang, Z. Xie, Scalable ti3c2tx mxene interlayered forward osmosis membranes for enhanced water purification and organic solvent recovery, ACS Nano 14 (2020) 9125–9135, https://doi.org/10.1021/acsnano.0c04471.

[20] Z. Tong, H. Guo, X. Liu, B. Zhang, Organic solvent forward osmosis of graphene oxide-based membranes for enrichment of target products, Ind. Eng. Chem. Res. 59 (2020) 19012–19019, https://doi.org/10.1021/acs.iecr.0c03780.

[21] Y. Cui, T.S. Chung, Pharmaceutical concentration using organic solvent forward osmosis for solvent recovery, Nat. Commun. 9 (2018) 1426, https://doi.org/10.1038/s41467-018-03612-2.

[22] K. Grodowska, A. Parczewski, Organic solvents in the pharmaceutical industry, Acta Pol, Pharm. Times 67 (2010) 3–12.

[23] B.H. Lipshutz, F. Gallou, S. Handa, Evolution of solvents in organic chemistry, ACS Sustainable Chem. Eng. 4 (2016) 5838–5849, https://doi.org/10.1021/acssuschemeng.6b01810.

[24] P. Marchetti, M.F.J. Solomon, G. Szekely, A.G. Livingston, Molecular separation with organic solvent nanofiltration: a critical review, Chem. Rev. 114 (2014) 10735–10806, https://doi.org/10.1021/cr500006j.

[25] S. Karan, Z. Jiang, A.G. Livingston, Sub–10 nm polyamide nanofilms with ultrafast solvent transport for molecular separation, Science 348 (2015) 1347–1351, https://doi.org/10.1126/science.aaa5058.

[26] M.L. Hir, A. Magne, T. Clair, E. Carretier, P. Moulin, Solvent regeneration in complex mixture using pervaporation, Org. Process Res. Dev. 25 (2021) 469–485, https://doi.org/10.1021/acs.oprd.0c00442.

[27] C. Liu, R. Takagi, T. Shintani, L. Cheng, K.L. Tung, H. Matsuyama, Organic liquid mixture separation using an aliphatic polyketonesupported polyamide organic solvent reverse osmosis (OSRO) membrane, ACS Appl. Mater. Interfaces 12 (2020) 7586–7594, https://doi.org/10.1021/acsami.9b21519.

[28] L. Jin, L. Hu, S. Liang, Z. Wang, G. Xu, X. Yang, A novel organic solvent nanofiltration (OSN) membrane fabricated by Poly (m-phenylene isophthalamide) (PMIA) under large-scale and continuous process, J. Membr. Sci. 647 (2022) 120259, https://doi.org/10.1016/j.memsci.2022.120259.

[29] R.P. Lively, D.S. Sholl, From water to organics in membrane separations, Nat. Mater. 16 (2017) 276–279, https://doi.org/10.1038/nmat4860.

[30] Y. Wei, Y. Wang, L. Wang, H. Yang, H. Jin, P. Lu, Y. Li, Simultaneous phase-inversion and crosslinking in organic coagulation bath to prepare organic solvent forward osmosis membranes, J. Membr. Sci. 620 (2021) 118829, https://doi.org/10.1016/j.memsci.2020.118829.

[31] S. Phuntsho, J.E. Kim, V.H. Tran, S. Tahara, N. Uehara, N. Maruko, H. Matsuno, S. Lim, H.K. Shon, Free-standing, thin-film, symmetric membranes: next-generation membranes for engineered osmosis, J. Membr. Sci. 607 (2020) 118145, https://doi.org/10.1016/j.memsci.2020.118145.

[32] W. Cheng, J. Ma, X. Zhang, M. Elimelech, Sub-1 μm free-standing symmetric membrane for osmotic separations, Environ. Sci. Technol. Lett. 6 (2019) 492–498, https://doi.org/10.1021/acs.estlett.9b00364.

[33] M. Li, V. Karanikola, X. Zhang, L. Wang, M. Elimelech, A self-standing, support-free membrane for forward osmosis with no internal concentration polarization, Environ. Sci. Technol. Lett. 5 (2018) 266–271, https://doi.org/10.1021/acs.estlett.8b00117.

[34] T.Y. Liu, H.G. Yuan, Y.Y. Liu, D. Ren, Y.C. Su, X. Wang, Metal−organic framework nanocomposite thin films with interfacial bindings and self-standing robustness for high water flux and enhanced ion selectivity, ACS Nano 12 (2018) 9253–9265, https://doi.org/10.1021/acsnano.8b03994.

[35] H.G. Yuan, Y.Y. Liu, T.Y. Liu, X.L. Wang, Self-standing nanofilms of polysulfone doped with sulfonated polysulfone via solvent evaporation for forward osmosis, J. Membr. Sci. 523 (2017) 567–575, https://doi.org/10.1016/j.memsci.2016.09.034.

[36] H. Liu, H. Wang, X. Zhang, Facile fabrication of freestanding ultrathin reduced graphene oxide membranes for water purification, Adv. Mater. 27 (2015) 249–254, https://doi.org/10.1002/adma.201404054.

[37] D.R. Joshi, N. Adhikari, An overview on common organic solvents and their toxicity, J. Pharm. Res. Int. 28 (3) (2019) 1–18, https://doi.org/10.9734/jpri/2019/v28i330203.

[38] D.J.C. Constable, C. Jimenez-Gonzalez, R.K. Henderson, Perspective on solvent use in the pharmaceutical industry, Org. Process Res. Dev. 11 (2007) 133–137, https://doi.org/10.1021/op060170h.

[39] J.A. Asensio, P. Gómez-Romero, Recent developments on proton conducting Poly (2,5-benzimidazole) (ABPBI) membranes for high temperature polymer electrolyte membrane fuel cells, Fuel Cell. 5 (2005) 336–343, https://doi.org/10.1002/fuce.200400081.

[40] H.R. Lohokare, H.D. Chaudhari, U.K. Kharul, Solvent and pH-stable poly(2,5-benzimidazole) (ABPBI) based UF membranes: preparation and characterizations, J. Memb. Sci. 563 (2018) 743–751, https://doi.org/10.1016/j.memsci.2018.06.052.

[41] H.D. Chaudhari, R. Illathvalappil, S. Kurungot, U.K. Kharul, Preparation and investigations of ABPBI membrane for HT-PEMFC by immersion precipitation method, J. Membr. Sci. 564 (2018) 211–217, https://doi.org/10.1016/j.memsci.2018.07.026.

[42] S.C. Kumbharkar, U.K. Kharul, New N-substituted ABPBI: synthesis and evaluation of gas permeation properties, J. Memb. Sci. 360 (2010) 418–425, https://doi.org/10.1016/j.memsci.2010.05.041.

[43] Y. Yuan, F. Johnson, I. Cabasso, Polybenzimidazole (PBI) molecular weight and Mark-Houwink equation, J. Appl. Polym. Sci. 112 (2009) 3436–3441, https://doi.org/10.1002/app.29817.

[44] L.F. Fourie, L. Square, C. Arendse, M. Msimanga, ABPBI/MWCNT for proton radiation shielding in low earth orbit, Apl. Mater. 11 (2023) 071103, https://doi.org/10.1063/5.0156686.

[45] P. Gomez-Romero, J.A. Asensio, S. Borros, Hybrid proton-conducting membranes for polymer electrolyte fuel cells Phosphomolybdic acid doped poly(2,5-benzimidazole)—(ABPBI-$H_3PMo_{12}O_{40}$), Electrochim. Acta 50 (2005) 4715–4720, https://doi.org/10.1016/j.electacta.2005.02.029.

[46] S. Gawas, L. Alladi, U.K. Kharul, Chemodialysis of organic acids using ABPBI-based hollow fiber membranes, J. Membr. Sci. 689 (2024) 122153, https://doi.org/10.1016/j.memsci.2023.122153.

[47] S.K. Kim, T.H. Kim, T. Ko, J.C. Lee, Cross-linked poly(2,5-benzimidazole) consisting of wholly aromatic groups for high-temperature PEM fuel cell applications, J. Membr. Sci. 373 (2011) 80–88, https://doi.org/10.1016/j.memsci.2011.02.039.

[48] A.K. Mishra, N.H. Kim, J.H. Lee, Effects of ionic liquid-functionalized mesoporous silica on the proton conductivity of acid-doped poly(2,5-benzimidazole) composite membranes for high-temperature fuel cells, J. Membr. Sci. 449 (2014) 136–145, https://doi.org/10.1016/j.memsci.2013.08.023.

[49] A. Das, P. Ghosh, S. Ganguly, D. Banerjee, K. Kargupta, Salt-leaching technique for the synthesis of porous poly(2,5-benzimidazole) (ABPBI) membranes for fuel cell application, J. Appl. Polym. Sci. 135 (1–11) (2017) 45773, https://doi.org/10.1002/APP.45773.

[50] G.M. Shi, Y. Wang, T.S. Chung, Dual-layer Pbi/p84 hollow fibers for pervaporation dehydration of acetone, AIChE J. 58 (2012) 1133–1145, https://doi.org/10.1002/aic.12625.
[51] D. Breite, M. Went, A. Prager, A. Schulze, The critical zeta potential of polymer membranes: how electrolytes impact membrane fouling, RSC Adv. 6 (2016) 98180, https://doi.org/10.1039/C6RA19239D.
[52] Y. Mansourpanah, S.S. Madaeni, A. Rahimpour, A. Farhadian, The effect of non-contact heating (microwave irradiation) and contact heating (annealing process) on properties and performance of polyethersulfone nanofiltration membranes, Appl. Surf. Sci. 255 (2009) 8395–8402, https://doi.org/10.1016/j.apsusc.2009.05.100.
[53] P. Karami, S.A. Aktij, K. Moradi, M. Rastgar, B. Khorshidi, F. Mohammadtabar, J. Peichel, M. McGregor, A. Rahimpour, J.B.P. Soares, M. Sadrzadeh, Comprehensive characterization of commercial reverse osmosis membranes through high-temperature cross-flow filtration, ACS Omega 9 (2024) 1990–1999, https://doi.org/10.1021/acsomega.3c09331.
[54] S. Mukherjee, A. Ghati, G. Paul, An ultraviolet−visible spectrophotometric approach to establish a method for determining the presence of rhodamine b in food articles, ACS Food Sci. Technol. 1 (2021) 1615–1622, https://doi.org/10.1021/acsfoodscitech.1c00172.

Desalination and Water Treatment 320 (2024) 100641

Contents lists available at ScienceDirect

Desalination and Water Treatment

journal homepage: www.sciencedirect.com/journal/desalination-and-water-treatment/

ABPBI-based hollow fiber membranes for forward osmosis (FO) possessing low reverse salt flux

Nitin M. Thorat[a,b], Ashish K. Lele[a,b], Ulhas K. Kharul[a,b,*]

[a] Polymer Science and Engineering Division, CSIR-National Chemical Laboratory, Pune 411008, India
[b] Academy of Scientific and Innovative Research (AcSIR), Ghaziabad 201002, India

ARTICLE INFO

Keywords:
Forward osmosis
ABPBI
Hollow fiber membrane
Low reverse salt flux

ABSTRACT

The poly(2,5-Benzimidazole), known for its excellent thermochemical stability, was evaluated as a membrane material for forward osmosis. The dope in methane sulfonic acid was used to make hollow fiber membranes. The availability of bound MSA in HFMs was compared with its neutral form. Aqueous solutions of two common salts reported for FO (NaCl and $MgCl_2$) were used as a draw solution at varying concentrations. The performance was determined in terms of water flux and reverse salt flux. The long-term performance of the membrane was assessed. The heat pretreatment of membranes was beneficial in offering low reverse salt flux, a crucial parameter in FO. The heat treatment at 350 °C exhibited excellent performance of low-RSF, irrespective of the draw solute used. The presence of MSA in the membrane matrix was found to be beneficial. Present HFMs exhibited reverse salt flux as low as 0.003 mol m^{-2} h^{-1} using 2 mol L^{-1} $MgCl_2$ as a draw solution. The water flux of present membranes was lower than that of reported FO-membranes, which is attributable to the larger thickness of the present membranes. The findings will be used to make ABPBI-based membranes in thin form to elevate the fluxes and their practical applicability.

1. Introduction

FO is emerging as a crucial membrane separation technology for organic solvent recovery in pharmaceutical industries [1], seawater desalination [2], wastewater treatment [3], fertigation [4,5], fruit juice concentration [6,7], and emergency drinking water [8]. Its advantages over conventional methods include energy efficiency, lower Fouling, resource recovery, and better operational flexibility and scalability [1,2,9,10]. Unlike pressure-driven processes, FO is a concentration-driven membrane process for transporting water or organic solvent, utilizing osmotic pressure difference across a selectively permeable membrane as the driving force [11]. The main advantages of FO are that it operates at low or no hydraulic pressure, it can achieve high rejection of a wide range of contaminants, and it may have lower irreversible fouling than pressure-driven membrane processes [12]. Energy efficiency is brought by the usage of waste or low-quality energy (e.g., high saline brine or residual heat) instead of clean energy (electricity) [13]. The semipermeable membranes are a barrier between DS (possessing high osmotic pressure) and feed solution (FS, containing solute of interest). The FO membrane allows water or organic solvents to be transported while FS concentrates. The highly selective membranes enabling rapid water transport and maintaining low salt permeation are at the core of this emerging process [14].

The FO process still faces challenges in achieving techno-economic feasibility in various industrial applications. The need for a draw solute includes its high solubility in water, high osmotic pressure, and ease of regeneration [15]. The membranes with high water/solvent permeability, high mechanical strength combined with low RSF (diffusion of draw solutes into the FS), fouling, and internal concentration polarization (ICP) [13,16,17] still need to be addressed to enlarge the application canvas of FO process. Some efforts are made to fabricate self-standing, thin film membranes with a symmetric homogeneous structure that reduces the ICP effect. A polysulfone (PSf) based self-standing nanofilm was designed for FO by the solvent evaporation method and doping sulfonated polysulfone from 0 to 5 wt% to tune the structure and surface properties of the nanofilm [18]. Li et al. [19] reported the synthesis of COOH-derived polyoxadiazole copolymer and fabricated a self-standing, selective thin film, eliminating ICP.

Several polymers are demonstrated for making FO membranes, including cellulose acetate (CA), cellulose triacetate (CTA), polysulfone (PS)/polyethersulfone (PES), polyamide TFC, and polybenzimidazole (PBI) [16]. These membranes are either asymmetric or thin film composite (TFC), consisting of an active thin layer on the top of a porous substrate [20,21].

* Corresponding author at: Polymer Science and Engineering Division, CSIR-National Chemical Laboratory, Pune 411008, India.
E-mail address: uk.kharul@ncl.res.in (U.K. Kharul).

https://doi.org/10.1016/j.dwt.2024.100641
Received 13 April 2024; Received in revised form 16 July 2024; Accepted 24 July 2024

Table 1
Spinning parameters used for making HFMs.

Parameters	Specifications
Dope pressure (psi)	40
Bore fluid	DI water
Bore fluid flow rate (ml min^{-1})	0.5
Air gap (cm)	1
Take-up speed (m min^{-1})	9.8
External Coagulant	Water at ambient temperature
Dimensions of spinneret (mm)	ID/OD = 0.7/2

Table 2
Nomenclature of membranes.

FSM/HFM	Form of ABPBI	Treatment temperature for 9 h duration
$ABPBI_{80}$	Neutral	80 °C
$ABPBI_{350}$		350 °C
$ABPBI\text{-}MS_{80}$	As spun, MSA-bound	80 °C
$ABPBI\text{-}MS_{350}$		350 °C

Since most membranes are asymmetric, ICP reduces effective driving force and thus lowers fluxes [19,21,22]. The ICP occurs within the support layer of a membrane and is characterized by differing solute concentrations at the transverse boundaries of that layer. The result is a reduction in the osmotic pressure gradient across the active layer of the membrane and a corresponding decrease in water flux [23]. FO also faces external concentration polarization (ECP) at the active surface of the membrane, leading to the lowering of the osmotic driving force [24]. Such results indicate the need for a support-free membrane to further the FO technology.

Membranes used for FO are either in flat sheet or hollow fiber form. Compared to flat sheets, most of the developed hollow fiber FO membranes demonstrated proven performance in terms of high water flux and lower RSF [25]. The HFMs possess desired properties such as high surface area and packing density relative to flat sheets [26]. Moreover, the HFM is easier to scale up and simpler in module fabrication than the flat sheet membranes [27].

One of the PBI family of polymers, poly(2,5-Benzimidazole), usually referred to as ABPBI, possesses higher water uptake than conventional PBI [28] and has high solvent and pH stability [29]. It has a high N-H group density [30], which can take part in H-bonding with water/polar solvent and could possess high flux if it could be evaluated for FO. Although it is well investigated as a membrane material for proton exchange membrane fuel cells (PEMFCs) [31,32], the applicability of its niche characteristics (especially solvent and pH stability) as a membrane material for separation are feebly addressed in the literature. Its investigation as a FO membrane material could open up new avenues.

The present work examines the intrinsic FO performance of ABPBI-based hollow fiber membranes (especially rejection, since higher membrane thickness in hollow fiber form could restrict the flux). ABPBI in neutral and in the presence of methane sulfonic acid in the membrane matrix was evaluated as a membrane material to generate an understanding of the effects of the absence/presence of acid in the membrane matrix. Aqueous solutions of two different draw solutes at varying concentrations were evaluated to determine water flux and RSF, the niche characteristics of an FO membrane. It is demonstrated that ABPBI could be a potential membrane material for FO, possessing low RSF.

2. Experimental

2.1. Materials, ABPBI synthesis and characterizations

A *3,4*-diaminobenzoic acid (DABA) was obtained from Gharada Chemicals. The polyphosphoric acid (PPA, ca. 84 % P_2O_5) was procured from Avra Synthesis (India). The *ortho*-phosphoric acid (OPA), NaCl, and $MgCl_2$ were procured from Merck. Methanesulfonic acid (MSA) and sulphuric acid (H_2SO_4) (98 %) were supplied by Thomas Baker. A 2-component epoxy resin (Epocast 130 resin and hardener PX 01) was provided by Rand Polyproducts (India). These chemicals were used without further purification. All draw solutions (DSs) were prepared in deionized water.

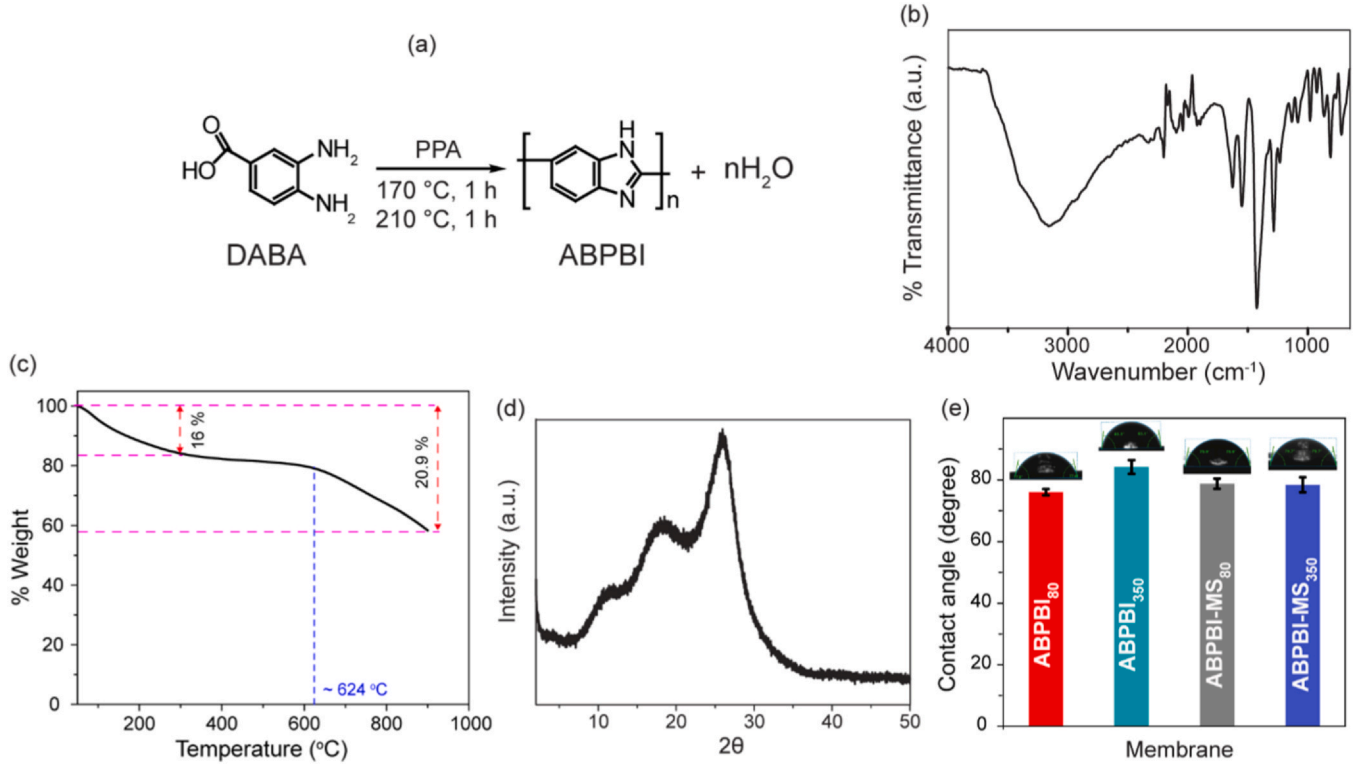

Fig. 1. a) Scheme of ABPBI synthesis, b) FT-IR and c) TGA spectra, d) WAXD pattern, and e) contact angle of an ABPBI FSM.

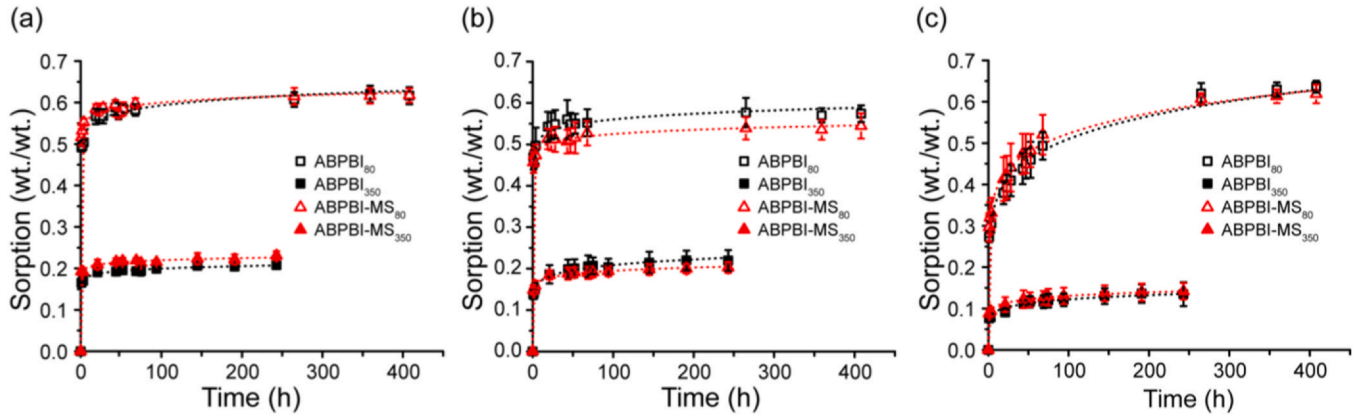

Fig. 2. Sorption of a) water, b) aq. 2 mol L^{-1} NaCl, and c) aq. 2 mol L^{-1} $MgCl_2$ in ABPBI FSMs.

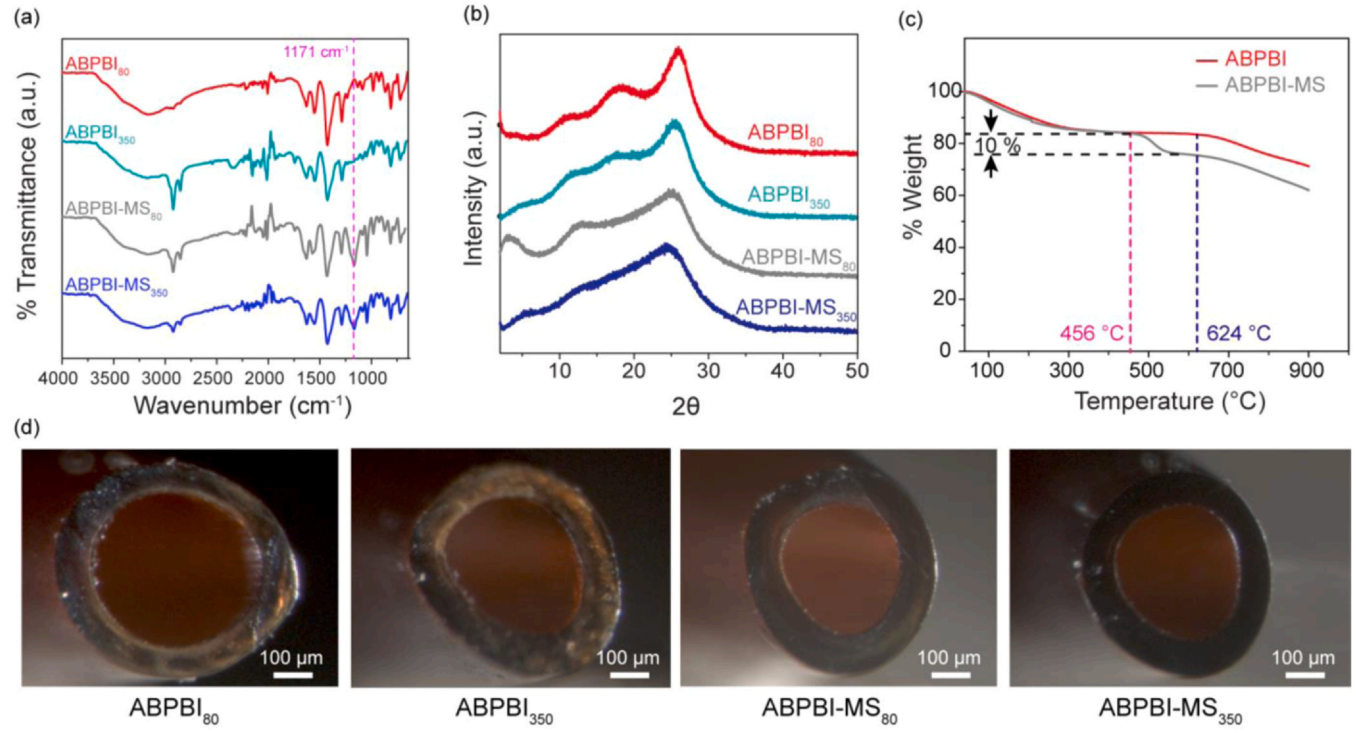

Fig. 3. Characterization of ABPBI HFMs: a) FT-IR spectra, b) WAXD pattern, c) TGA curves, and d) microscopic images.

As reported earlier, the ABPBI was obtained by self-condensation of DABA in PPA as a solvent [30,33]. The reactor with an overhead stirrer and heating assembly was charged with 2250 g of PPA. It was heated to 120 °C, and 75 g DABA was added while stirring. After complete dissolution, the temperature was raised to 170 °C and maintained for an hour. The temperature was increased further to 210 °C while stirring. After 1.5 h, 600 g of OPA was added to the reaction mixture and stirred for 1 h. The polymer was precipitated in water, crushed in the blender, and washed with water to remove excess acid until neutral to pH. The polymer was treated with 0.1 N aq. $NaHCO_3$ for 8 h to remove bound acid present in the polymer matrix. The polymer was filtered and washed with water until it was neutral to pH. After soaking in methanol for 15 h, the polymer was dried at 60 °C for 8 h, then in a vacuum oven at 100 °C for 7 days. The inherent viscosity (η_{inh}) was determined using 0.2 g dL^{-1} solution in conc. H_2SO_4 at 35 °C.

2.2. Preparation of flat sheet membranes (FSMs)

A 5 % (wt/wt) dope solution was prepared by dissolving ABPBI in MSA at 80 °C while stirring for 24 h, filtered to remove undissolved particles, if any, and degassed for 30 min. The casting was done at ambient on a PTFE sheet using a continuous casting machine with a speed of 0.75 m min^{-1} and water as a non-solvent. The membrane was peeled off from the PTFE surface while it was in the water. The delaminated membrane was cut into pieces. Some of them were washed with DI water until it was neutral pH. They were heated in a quartz tube furnace under an N_2 atmosphere for 9 h at 80 and 350 °C and were designated as ABPBI-MS_{80FSM} and ABPBI-MS_{350FSM}, respectively. The remaining membranes were dipped in 0.1 N $NaHCO_3$ for 8 h, washed with DI water until neutral to pH, and thermally treated as above. These membranes were designated as $ABPBI_{80FSM}$ and $ABPBI_{350FSM}$. These FSMs were prepared for the sorption analysis.

2.3. Physical characterizations of FSMs

The FTIR spectra were recorded at ambient using Bruker Optics ALPHA-E spectrometer with a universal Zn-Se ATR (attenuated total reflection) accessory in a 600–4000 cm^{-1} region. The wide-angle X-ray diffraction (WAXD) spectra were recorded with Rigaku SmartLab X-ray

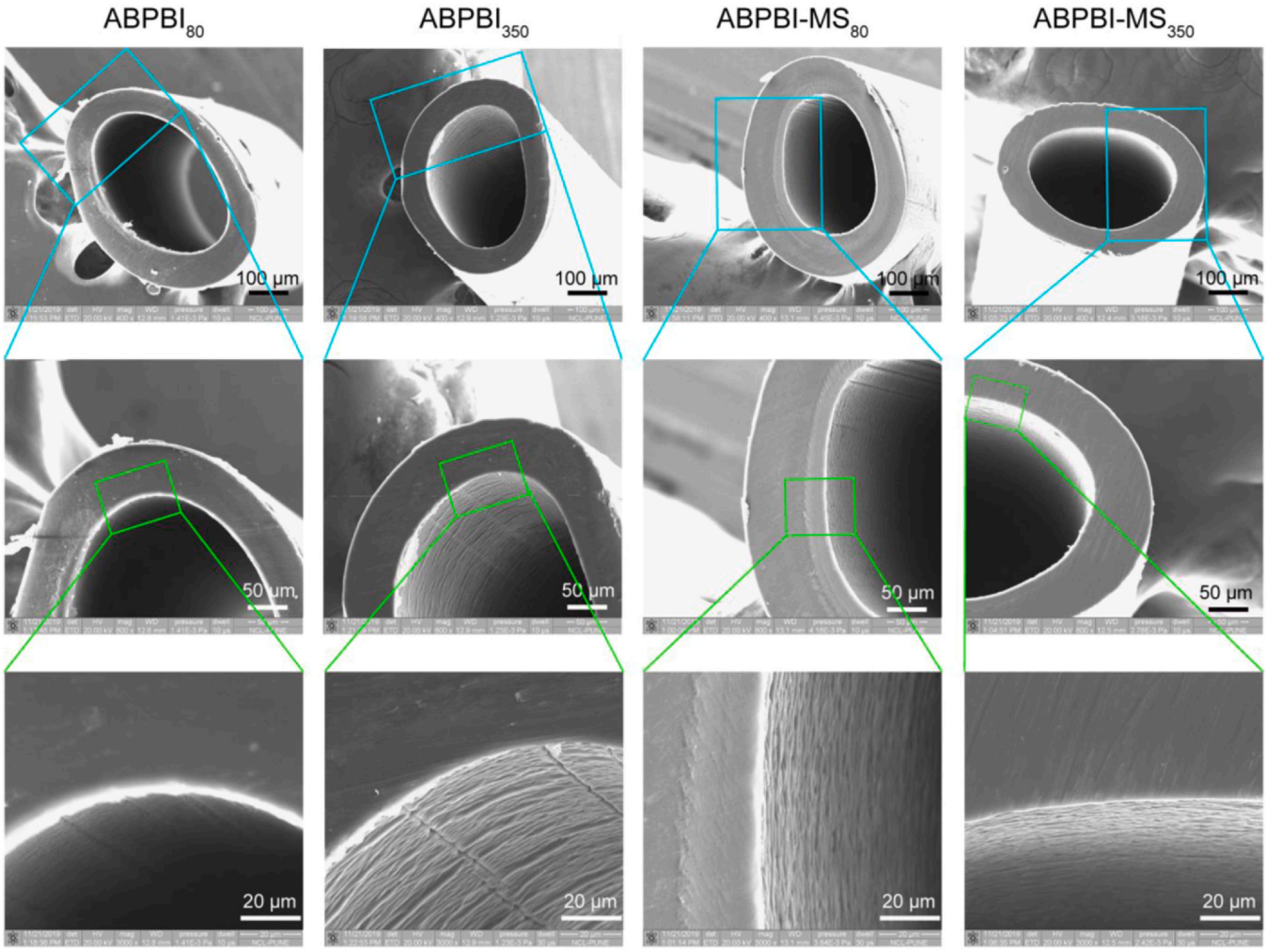

Fig. 4. SEM images of HFMs.

Table 3
Physical size and helium permeation characteristics of HFMs.

Membrane identification	Average membrane dimensions (µm)			Permeance of He (GPU*)	
	Thickness	Outer diameter	Inner diameter	At 50 psi	At 60 psi
$ABPBI_{80}$	98.2 ± 23	587.3 ± 69	388.6 ± 44	0.0065	0.007
$ABPBI_{350}$	99.7 ± 8	514.4 ± 45	315 ± 41	Nil	
$ABPBI\text{-}MS_{80}$	107.7 ± 26	573.1 ± 65	370.5 ± 50	0.087	0.1
$ABPBI\text{-}MS_{350}$	95.6 ± 9	519 ± 29	331.1 ± 35	0.00089	0.00095

* 1 GPU = 10–6 (cm3(STP)/cm2·cmHg·sec)

diffractometer in reflection mode using CuKα radiation (λ = 1.5418 Å). The 2θ scan range was 5–40° at a scan rate of 3° min^{-1}. The thermogravimetric analysis (TGA) was performed on TGA-STA6000 (TA Instruments, USA) in an N_2 atmosphere with a heating rate of 10 °C min^{-1}. The water contact angle of the membranes was obtained using Drop Shape Analyzer DSA25- KRÜSS GmbH. Water drops of constant size were placed on the membrane surface. The digital image from the camera was analyzed using a built-in drop-shape analysis tool. The reported contact angle for each membrane is an average of 6 samples.

2.4. Sorption analysis using FSMs

The sorption of water, 2 mol L^{-1} NaCl, and 2 mol L^{-1} $MgCl_2$ in FSMs was evaluated at 40 °C. The 2 mol L^{-1} solutions were chosen for sorption since they were the maximum concentration used in the FO experiments. The samples were taken out at regular time intervals, wiped out, and weighed. The sorption experiments were continued till the equilibrium was reached. Five samples were analyzed for each FSM type, and data was averaged (deviation ± 1.53 %). The sorption was calculated using Eq. (1).

$$Sorption\left(\frac{wt}{wt}\right) = \frac{W_t - W_0}{W_0} \quad (1)$$

where, W_0 and W_t represent the weight of the membrane in the dry state and after sorption at the time, t, respectively.

2.5. Spinning of hollow fiber membranes (HFMs) and characterizations

The dope solution of 2.5 % (wt/wt) ABPBI was prepared in MSA while heating at 80 °C for 24 h. The spinning was done using the dry-jet/wet phase inversion method using a tube-in-orifice spinneret. The

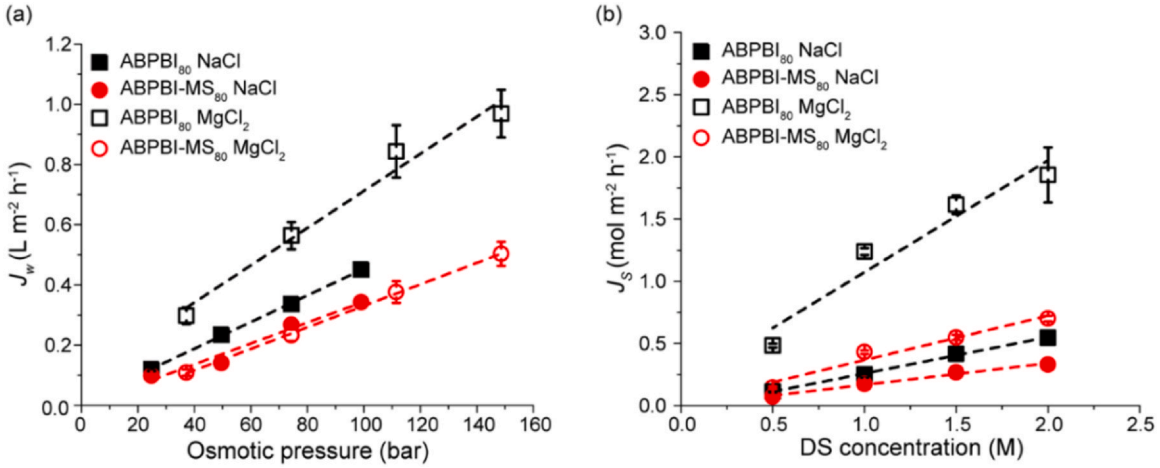

Fig. 5. The performance of ABPBI and ABPBI-MS treated at 80 °C: Variation in (a) J_W with an osmotic pressure of DS and (b) J_S with the concentration of DS.

Table 4
FO performance at 2 mol L^{-1} concentration of DS.

Membrane identification	J_W (L m^{-2} h^{-1})		J_S (mol m^{-2} h^{-1})	
	DS: NaCl	DS: $MgCl_2$	DS: NaCl	DS: $MgCl_2$
$ABPBI_{80}$	0.45	0.97	0.55	1.85
$ABPBI\text{-}MS_{80}$	0.34	0.50	0.32	0.70
$ABPBI_{350}$	0.11	0.16	0.07	0.003
$ABPBI\text{-}MS_{350}$	0.19	0.23	0.09	0.012

spinning parameters are given in Table 1. The spun HFMs were post-treated as that of FSMs, as given in Section 2.2. They were designated based on the treatment conditions, as shown in Table 2.

2.6. Characterizations of HFMs and module making

The HFM cross-sectional images were recorded using gold-sputtered samples on an FEI Nova NanoSEM 650 Scanning Electron Microscope (SEM) with a field emitter as an electron source. The FTIR, WAXD spectra, and TGA were recorded using the same equipment as for FSMs. The membrane modules were prepared using 50 HFMs (active membrane area: 253 cm^2) in PVC shells. The potting was done using 2-component epoxy resin. The membrane integrity was assessed by analyzing helium permeation at 50 and 60 psi upstream pressure.

2.7. FO experiments using HFM modules

The performance of HFM modules was evaluated at 25 °C using the FO setup. All membranes shown in Table 2 were initially saturated with DI water for 1 h. Each FO experiment was performed for an 8 h duration. The DS and FS used were aq. 0.5–2 mol L^{-1} NaCl/$MgCl_2$ and DI water, respectively. The FS and DS were passed through the shell and lumen side at the flow rate of 10 ml min^{-1}, respectively. For each membrane type, 3 modules were evaluated, and results were averaged. The water flux, J_W (L m^{-2} h^{-1}), was calculated using Eq. (2).

$$J_W = \frac{\Delta V}{A_m \Delta t} \tag{2}$$

where, ΔV (L) is the change in the volume of FS over the defined experimental time Δt (h) and A_m (m^2) is the active membrane area. The conductivity meter, Metler Toledo MC226, was used to determine the salt concentration in a solution. The reverse salt flux (J_S, mol m^{-2} h^{-1}) from the DS to the FS side was determined from the increased conductivity of the FS (DI water) and was calculated using Eq. (3).

$$J_S = \frac{\Delta(CV)}{A_m \quad \Delta t} \tag{3}$$

where, ΔC (mol L^{-1}) is the change in the salt concentration in FS, and ΔV (L) is the change in the volume of FS. The osmotic pressure, π of a DS, was calculated using Eq. (4) [34].

$$\pi = \text{nMRT} \tag{4}$$

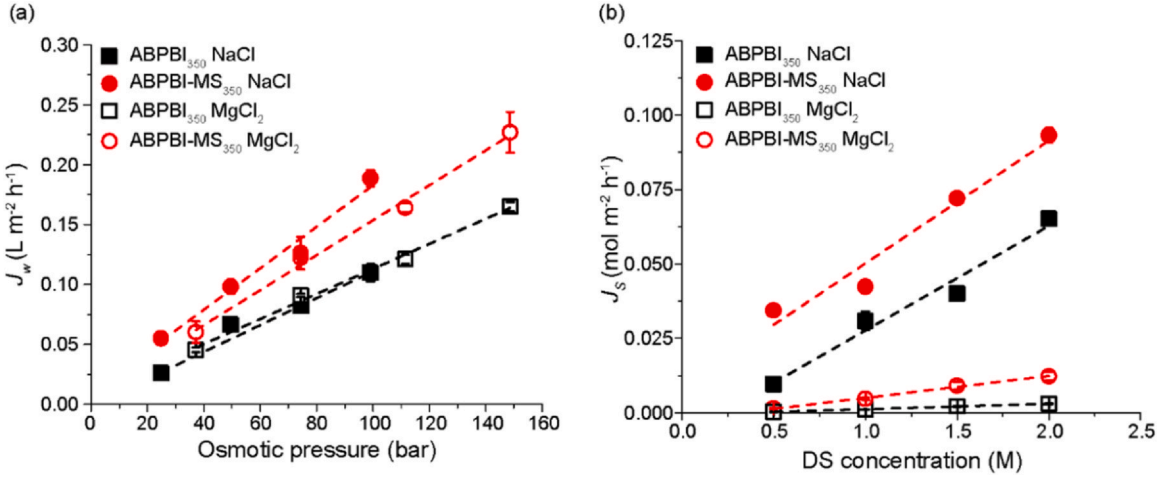

Fig. 6. The performance of ABPBI and ABPBI-MS treated at 350 °C: Variation in (a) J_W with the osmotic pressure of DS and (b) J_S with the concentration of DS.

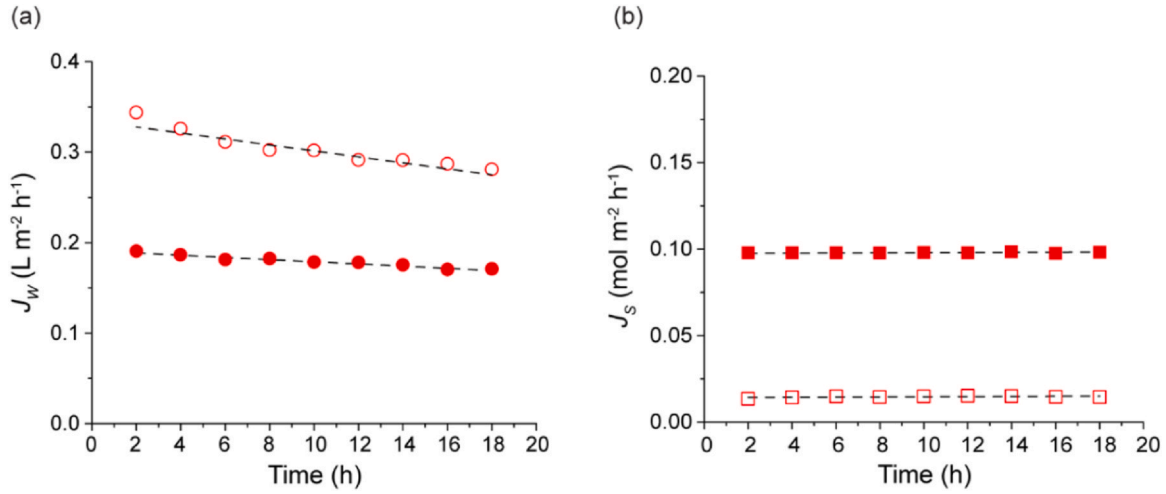

Fig. 7. The long-term analysis of ABPBI-MS_{350} using 2 mol L^{-1} NaCl (filled symbols) and $MgCl_2$ (unfilled symbols) as a DS: Variation of (a) *JW* and (b) *JS* with time.

Table 5
Comparison of FO performances of fabricated ABPBI-based HFM with those of HFMs reported in the literature.

Membrane/ thickness (μm)	DS	J_S (mol m^{-2} h^{-1}) /Rejection (%)[b]	J_W (L m^{-2} h^{-1})	J_N[a] (L μm m^{-2} h^{-1})	Reference
ABPBI-MS_{350}/95	2 M NaCl	0.09/99.1	0.19	18	This work
	2 M $MgCl_2$	0.012/99.9	0.23	21.7	This work
$ABPBI_{350}$/100	2 M NaCl	0.07/98.4	0.11	11.2	This work
	2 M $MgCl_2$	0.003/99.9	0.16	16.4	This work
PBI/-	2 M NaCl	97.31[c]	3.84	-	[45]
	2 M $MgCl_2$	99.79[c]	9.02	-	
PBI-PES DL/1.5	2 M $MgCl_2$	0.003	15	22.5	[46]
PBI-POSS/1.2	2 M NaCl	0.8	25.4	30.38	[47]
PA-PVDF TFC/-	1 M NaCl	0.14	18.9	-	[48]

[a] Normalized water flux (J_N, L μm m^{-2} h^{-1}) = J_W x Membrane thickness (active layer);
[b] Rejection of draw solute (%) = [1-(Salt concentration in FS/Salt concentration in DS)]x100; [c]Salt selectivity.

where, *n* is a Van't Hoff factor (2 for NaCl and 3 for $MgCl_2$), *M* is the molar concentration of the solute, *R* (0.0831 L bar K^{-1} mol^{-1}) is a universal gas constant, and *T* is the temperature of the solution (298 K).

3. Results and discussion

3.1. ABPBI synthesis and characterizations

The ABPBI synthesized by polycondensation (Fig. 1a) exhibited an inherent viscosity of 4.4 dL g^{-1}. The FT-IR spectra (Fig. 1b) showed the characteristic bands at 1630, 1552, and 1419 cm^{-1}, attributable to the C=C and C=N stretching of the benzimidazole groups of ABPBI. The broad band at ~3165 cm^{-1} is attributable to the N-H stretching vibrations. The TGA thermogram (Fig. 1c) showed an initial decomposition temperature of 295 °C, amounting to 16 % water loss in the membrane matrix. The polymer decomposition started at 624 °C, conveying its excellent thermal stability. The char yield at 900 °C was 69.7 %. The FTIR bands, sluggish loss of water, and degradation temperature seen from the TGA and WAXD pattern of ABPBI (Fig. 1b, c, and d) matched well with those reported earlier [29]. The $ABPBI_{350}$ membrane showed the highest contact angle of 84.2°. All remaining types of membrane showed a contact angle of 76 to 78°.

3.2. Sorption analysis of FSMs

The sorption was studied with a 2 mol L^{-1} concentration of salt (NaCl/$MgCl_2$). As seen from Fig. 2, FSMs, after dipping in DI water or salt solutions, the sorption increased rapidly within half an hour and equilibrated after ~ 50 h. After this time, sorption still seems to rise until the time of evaluation (400 h), but at a sluggish rate. This slow increase in sorption can be attributed to the sluggish swelling of the polymer matrix by a sorbent (water, salt molecules). ABPBI is well known to be a rigid polymer with a high glass transition temperature of 485 °C [35]. The imidazole group in the ABPBI backbone is known to facilitate the sorption of water molecules by hydrogen bonding [36,37]. ABPBI, being wholly aromatic and rigid in nature, might take a long time to achieve a 'thermodynamically stable configuration' of polymer chains.

The amount of sorption of either water or salt solutions mainly depended on the treatment temperature of FSM. The effect of chemical nature (ABPBI in neutral form or MS-based) is not quantitatively distinctive. Fig. 2a shows that after ~ 50 h, the amount of water sorbed by $ABPBI_{80}$ or ABPBI-MS_{80} is ~ 3 times higher than that of $ABPBI_{350}$ or ABPBI-MS_{350}. Similar holds for the sorption of salt solutions (Fig. 2b, c). FSMs treated at 350 °C are associated with water removal, as indicated by TGA (Fig. 1c). Removing water from the polymer matrix increases H-bonding between polymer chains, leading to their better packing. When such membranes undergo sorption, diffusion of sorbent (water/salt solution) through the membrane matrix could be sluggish as polymer chains are densely packed.

When the sorption of salt solutions for FSM heated at 80 °C is compared (Fig. 2b, c), it was seen that the sorption of the $MgCl_2$ solution is almost half of that of NaCl. For membranes treated at 350 °C, the sorption of the $MgCl_2$ solution is sluggish as compared to NaCl. This behavior is prominently seen up to ~ 50 h duration. Beyond 200 h, sorption of aq. $MgCl_2$ is slightly higher than that of water or aq. NaCl. This could be due to the further swelling of the polymer matrix, which was assisted by the coordination of divalent $MgCl_2$ with the imidazole group of the PBI matrix, as it is a known phenomenon [38].

3.3. Preparation of HFMs and their characterizations

The dope ABPBI solution concentration of ABPBI was 2.5 % (wt./wt.). At such a low concentration, the dope pressure needed was 40 psi,

and the take-up was 9.8 m min^{-1} (Table 1), owing to the higher molecular weight of the polymer indicated by its high inherent viscosity of 4.4 dL g^{-1}. The obtained wet HFMs were rubbery in nature. The FTIR spectra (Fig. 3a) of ABPBI$_{80}$, especially in the fingerprint region, matched well with that of the ABPBI polymer (Fig. 1d). The MSA-bound membranes (ABPBI-MS$_{80}$ and ABPBI-MS$_{350}$) showed a new band at 1171 cm^{-1} due to O═S═O stretching, as also reported earlier [39,40]. Although the primary peak position in WAXD spectra of all HFMs (Fig. 3b) remains similar at 26°, irrespective of their treatment temperature (80 or 350 °C), the pattern at lower 2θ values is different. Their smoothened pattern indicated that thermal treatment suppresses domains with larger d-spacing. It may be recalled from Section 3.2 that the sorption of FSMs treated at 350 °C is much lower than that of FSMs treated at 80 °C due to denser chain packing in the earlier cases. It could be due to the elimination of domains with larger d-spacing. The TGA curves (Fig. 3c) of ABPBI and ABPBI-MS HFMs show initial decomposition till ~ 300 °C, attributable to water loss, as observed for FSM (Fig. 1c). The degradation for ABPBI-based HFM started at 624 °C, while for ABPBI-MS, the degradation started at 456 °C attributable to sulfonate groups [40,41]. At 900 °C, the char yield was high, viz., 71.3 % and 62.4 % for ABPBI and ABPBI-MS HFMs, respectively. Higher char yield is a peculiar property of ABPBI, as observed earlier [42].

The cross-sectional microscopic (Fig. 3d) and SEM images (Fig. 4) of HFMs based on ABPBI and ABPBI-MS treated at 80/350 °C did not reveal any porosity. The structure seems to be uniform throughout the membrane thickness. The HFM modules were prepared using all four types of HFMs. The integrity of membranes and modules was evaluated by pressurizing helium from the shell side at different pressures. The obtained permeance is given in Table 3. For the ABPBI$_{350}$ module, no permeance was observed at either applied pressure. Other modules exhibited extremely low helium permeance, owing to the gas diffusion through the membrane matrix. It confirms the SEM observation that the membranes do not have any porosity and are dense in nature.

3.4. FO performance

Initially, the membranes heated at 80 °C were analyzed with varying concentrations of NaCl and $MgCl_2$ (Fig. 5). The water flux (J_W) and reverse salt flux (J_S) increased linearly with increasing osmotic pressure/concentration of DS. The J_W in the case of ABPBI$_{80}$ with $MgCl_2$ as DS was higher than that of the other 3 cases (Fig. 5a). A similar observation is noted for salt flux in this case (Fig. 5b). For membranes treated at 350 °C, the J_W and J_S reduced considerably more than those treated at 80 °C. As elaborated above, it could be related to the tighter chain packing and lower sorption caused by this membrane type.

The effect of membrane treatment temperature (80/350 °C), type (ABPBI/ABPBI-MS), and draw solute used (NaCl/$MgCl_2$) can be better visualized from Table 4, wherein results obtained using 2 mol L^{-1} DS are tabulated. When the performance of membranes treated at 80 °C is compared, the flux (J_W or J_S) is lower for ABPBI-MS$_{80}$ than for ABPBI$_{80}$ for a particular DS. It could be due to multiple H-bonding possible by an MSA molecule with different imidazole groups, that might bring chains closer. When membranes are treated at 350 °C, the chain compactness caused by heating offers an appreciable reduction in the salt flux compared to the decrease in water flux of membranes treated at 80 °C. For a particular DS, the J_W in the case of ABPBI-MS$_{350}$ was higher than that exhibited by ABPBI$_{350}$ (Fig. 6). The difference in J_S (either for NaCl or $MgCl_2$) is insignificant. Here, the peculiarity of the presence of MSA in the membrane matrix is visualized. From Fig. 3b, it can be deduced that the d-spacing of ABPBI-MS$_{350}$ in dry form is ~3.6 Å, while for ABPBI$_{350}$, it is 3.54 Å. Although the difference is small, it may be responsible for increased water flux. It may be noted that the present membranes are dense in nature, having a thickness of ~ 100 µm (Table 3). Although the water flux values appear much smaller, the significance of membrane drying and the presence of MSA in the membrane matrix leading to considerably lower J_S offers highly significant inputs in membrane material design.

Based on the above study (especially Fig. 6b), ABPBI-MS$_{350}$ was chosen as a membrane for the long-term study, and the obtained results are plotted in Fig. 7. In a continuous experiment for 18 h, a small decrease in J_W and a linear nature of J_S were observed. The observed decrease in J_W can be attributed to a slight reduction in DS concentration due to the passage of water from the DS side to the FS side, leading to a lowering of the DS concentration. This effect is more pronounced for $MgCl_2$, owing to its high osmotic pressure (Fig. 7a). The consistency in J_S (Fig. 7b) indicated excellent membrane stability over time.

3.5. Comparison with the literature

It would be worth comparing the FO performance of present ABPBI-based membranes with those reported in the literature. Table 5 lists the reverse salt flux (J_S)/rejection, water flux (J_W), and normalized flux (J_N) as FO performance of hollow fiber membranes. Normalized flux (J_N) is a common way of representing the performance of pervaporation membranes [43,44]. Present membranes are dense, with 95–100 µm thicknesses, while most reported membranes are asymmetric. The skin layer thickness (wherever available) was used to calculate J_N for reported membranes.

It could be seen that the rejection of present membranes is similar to/better than that of reported PBI membranes [45]. The water flux, J_W, of present membranes is much lower than that of reported membranes. This is attributable to the dense nature and, thus, the large thickness of present membranes (66–83 times higher than reported membranes [46,47]). Thus, J_N could be a better term for comparing fluxes. The estimated values of J_N for present membranes are lower by 3.6 to 63 % than those for reported data [46,47]. It indicates that the thickness reduction in present membranes could bring remarkable improvements in the water flux, assuming rejection performance remains the same. It may be recalled that ABPBI is stable in harsh environments of pH and solvents (DMF, DMAc, chloroform, toluene, and hexane), as reported earlier [29]. The present work thus offers a new avenue for broader applications, especially in harsher environments of solvent and temperature, provided membrane thickness is reduced. It becomes the path of our future work.

4. Conclusions

This work presents the preparation of symmetric, dense, flat sheet (FSM) and hollow fiber (HFM) membranes based on ABPBI using methane sulfonic acid as a solvent for the dope. The prepared membranes were categorized based on chemical (neutral and containing MSA in the membrane matrix) and thermal treatment (80 and 350 °C). The membranes were characterized for physical (IR, TGA, XRD, contact angle, microscopic and SEM imaging) and helium permeation, confirming their dense, impermeable nature. The FSMs were evaluated for sorption of water and 2 mol L^{-1} salt solution (NaCl/$MgCl_2$). The heat treatment at 350 °C reduced sorption by 1/3rd as that of membranes treated at 80 °C. Although NaCl and $MgCl_2$ solutions exhibited similar sorption, the latter was more sluggish than the earlier one. Although most of the sorption occurred within 1 h, it was equilibrated after 50 h, indicating slow swelling of the polymer matrix.

The FO performance of HFMs was evaluated using aqueous NaCl and $MgCl_2$ at varying concentrations. The water flux (*Jw*) and reverse salt flux (RSF, *Js*) were determined using hollow fiber membrane modules of ~ 250 cm^2 active area. The chemical and heat treatment of HFMs affected the FO favorably, especially the rejection performance. The flux (J_W or J_S) was lower for ABPBI-MS$_{80}$ than that of ABPBI$_{80}$, attributable to the acid-base interactions. For membranes treated at 350 °C, the J_W and J_S reduced considerably compared to membranes treated at 80 °C due to the tighter chain packing and lower sorption caused by this membrane type. The HFM ABPBI$_{350}$ with a thickness of

~100 µm showed a water flux of 0.16 L m^{-2} h^{-1} and reverse salt flux of 0.003 mol m^{-2} h^{-1} while using 2 mol L^{-1} $MgCl_2$ as a DS and DI water as an FS. The same parameters for ABPBI-MS_{350} were 0.23 L m^{-2} h^{-1} and 0.012 mol m^{-2} h^{-1}, respectively, emphasizing the significance of MSA in the membrane matrix. Although the water flux looks much smaller than those reported in the literature, the importance of membrane heat treatment and the presence of MSA in the ABPBI membrane matrix offers significant insights into membrane material design. The long-term analysis exhibited consistent performance. Given the membrane's reproducible and scalable preparation method, chemically robust nature, and extremely low reverse salt flux, ABPBI can be a promising material for FO application, provided the thickness can be reduced further to elevate fluxes.

CRediT authorship contribution statement

Ashish K Lele: Writing – review & editing. **Nitin M Thorat**: Writing – original draft, Investigation, Formal analysis, Data curation. **Ulhas Kharul**: Writing – review & editing, Supervision, Project administration, Investigation, Funding acquisition, Conceptualization.

Data Availability

Data will be made available on request.

Declaration of Competing Interest

None.

Acknowledgments

The funding from the Department of Science and Technology (Grant No. DST/TM/WTI/WIC/2K17/100(G)) is highly appreciated. Nitin Thorat acknowledges the funding from the Council of Scientific and Industrial Research, Govt. of India (CSIR-SRF fellowship Award letter No. 31/11(1088)/2019-EMR-I).

References

[1] Goh KS, Chen Y, Ng DYF, Chew JW, Wang R. Organic solvent forward osmosis membranes for pharmaceutical concentration. J Memb Sci 2022;642:119965. https://doi.org/10.1016/j.memsci.2021.119965.
[2] Park J, Lee S. Desalination technology in south korea: a comprehensive review of technology trends and future outlook. Membranes 2022;12:204. https://doi.org/10.3390/membranes12020204.
[3] Yan M, Xi Y, Jiang N, Li Q, Zheng S, Hu Y, et al. High-performance thin film composite forward osmosis membrane for efficient rejection of antimony and phenol from wastewater: Characterization, performance, and MD-DFT simulation. J Memb Sci 2024;703:122847. https://doi.org/10.1016/j.memsci.2024.122847.
[4] Bassiouny M, Maksoud YA, Kimera F, Bahader K, Sewilam H. Investigating the potential of growing crops hydroponically utilizing feed and draw solutions from13 fertilizer drawn forward osmosis. Environ Sci Eur 2023;35(68):2–17. https://doi.org/10.1186/s12302-023-00770-z.
[5] Han J, Dai P, Gu C, Liao Y, Zhao Y, Razaqpur AG, et al. Emulsified oily wastewater treatment via fertilizer drawn forward osmosis using a corrugated thin film composite membrane. J Memb Sci 2023;685:121926. https://doi.org/10.1016/j.memsci.2023.121926.
[6] Gulied M, Logade K, Mutahir H, Shaftah S, Salauddin S, Hameed A, et al. A review of membrane-based dewatering technology for the concentration of liquid foods. J Environ Chem Eng 2023;11:110583. https://doi.org/10.1016/j.jece.2023.110583.
[7] Wang H, Zhang Y, Ren S, Pei J, Li Z. Athermal concentration of apple juice by forward osmosis: process performance and membrane fouling propensity. Chem Eng Res Des 2022;177:569–77. https://doi.org/10.1016/j.cherd.2021.11.023.
[8] Yu J, Jing W, Liu E, Du S, Cai H, Du H, et al. Sulfonated graphene oxide modified polysulfone-polyamide forward osmosis membrane and its application in fluorine-containing wastewater treatment. Mater Chem Phys 2024;313:128757. https://doi.org/10.1016/j.matchemphys.2023.128757.
[9] Chun Y, Mulcahy D, Zou L, Kim IS. A short review of membrane fouling in forward osmosis processes. Membranes 2017;7:30. https://doi.org/10.3390/membranes7020030.
[10] Van der Bruggen Bart, Matsuyama Hideto, Lin Yuqing, Zheng Junfeng. Resource recovery and recycling from water streams: advanced membrane technologies and case studies. ACS EST Water 2023;3:1699–701. https://doi.org/10.1021/acsestwater.3c00315.
[11] Abou-Elanwar AM, Lee S, Jang I, Lee S, Hong S, Kim S, et al. Evaluation of a novel fertilizer-drawn forward osmosis and membrane contactor hybrid system for CO_2 capture using ammonia-rich wastewater. J Memb Sci 2024;700:122654. https://doi.org/10.1016/j.memsci.2024.122654.
[12] Lee S, Boo C, Elimelech M, Hong S. Comparison of fouling behavior in forward osmosis (FO) and reverse osmosis (RO). J Memb Sci 2010;365:34–9. https://doi.org/10.1016/j.memsci.2010.08.036.
[13] Mohammadifakhr M, de Grooth J, Trzaskus K, Roesink HDW, Kemperman AJB. Single-step synthesis of a polyelectrolyte complex hollow-fiber membrane for forward osmosis. Sep Purif Technol 2021;264:118430. https://doi.org/10.1016/j.seppur.2021.118430.
[14] Zhou Z, Hu Y, Boo C, Liu Z, Li J, Deng L, et al. High-performance thin-film composite membrane with an ultrathin spray-coated carbon nanotube interlayer. Environ Sci Technol Lett 2018;5:243–8. https://doi.org/10.1021/acs.estlett.8b00169.
[15] Long Q, Jia Y, Li J, Yang J, Liu F, Zheng J, et al. Recent advance on draw solutes development in Forward osmosis. Processes 2018;6:165. https://doi.org/10.3390/pr6090165.
[16] Francis L, Ogunbiyi O, Saththasivam J, Lawler J, Liu Z. A comprehensive review of forward osmosis and niche applications. Environ Sci (Camb 2020;6:1986–2015. https://doi.org/10.1039/d0ew00181c.
[17] Handojo LA, Khoiruddin K, Wardani AK, Hakim AN, Wenten IG. Advancement in Forward Osmosis (FO) Membrane for Concentration of Liquid Foods. IOP Conf. Ser. Mater. Sci. Eng. 547. Institute of Physics Publishing; 2019:012053. https://doi.org/10.1088/1757-899X/547/1/012053.
[18] Yuan HG, Liu YY, Liu TY, Wang XL. Self-standing nanofilms of polysulfone doped with sulfonated polysulfone via solvent evaporation for forward osmosis. J Memb Sci 2017;523:567–75. https://doi.org/10.1016/j.memsci.2016.09.034.
[19] Li M, Karanikola V, Zhang X, Wang L, Elimelech M. A self-standing, support-free membrane for forward osmosis with no internal concentration polarization. Environ Sci Technol Lett 2018;5:266–71. https://doi.org/10.1021/acs.estlett.8b00117.
[20] Li G, Li XM, He T, Jiang B, Gao C. Cellulose triacetate forward osmosis membranes: preparation and characterization. Desalin Water Treat 2013;51:2656–65. https://doi.org/10.1080/19443994.2012.749246.
[21] Cho YH, Han J, Han S, Guiver MD, Park HB. Polyamide thin-film composite membranes based on carboxylated polysulfone microporous support membranes for forward osmosis. J Memb Sci 2013;445:220–7. https://doi.org/10.1016/j.memsci.2013.06.003.
[22] Mohammadifakhr M, de Grooth J, Roesink HDW, Kemperman AJB. Forward osmosis: a critical review. Processes 2020;8:404. https://doi.org/10.3390/PR8040404.
[23] Gray GT, McCutcheon JR, Elimelech M. Internal concentration polarization in forward osmosis: role of membrane orientation. Desalination 2006;197:1–8. https://doi.org/10.1016/j.desal.2006.02.003.
[24] Chun Y, Mulcahy D, Zou L, Kim IS. A short review of membrane fouling in forward osmosis processes. Membr (Basel) 2017;7:30. https://doi.org/10.3390/membranes7020030.
[25] Majeed T, Lotfi F, Phuntsho S, Yoon JKhee, Kim K, Shon HK. Performances of PA hollow fiber membrane with the CTA flat sheet membrane for forward osmosis process. Desalin Water Treat 2015;53:1744–54. https://doi.org/10.1080/19443994.2013.859103.
[26] Nazif A, Karkhanechi H, Saljoughi E, Mousavi SM, Matsuyama H. Effective parameters on fabrication and modification of braid hollow fiber membranes: A review. Membr (Basel) 2021;11:884. https://doi.org/10.3390/membranes11110884.
[27] Liang CZ, Askari M, (Simon) Choong LT, Chung TS. Ultra-strong polymeric hollow fiber membranes for saline dewatering and desalination. Nat Commun 2021;12:2338. https://doi.org/10.1038/s41467-021-22684-1.
[28] Diaz LA, Abuin GC, Corti HR. Water and phosphoric acid uptake of poly [2,5-benzimidazole] (ABPBI) membranes prepared by low and high temperature casting. J Power Sources 2009;188:45–50. https://doi.org/10.1016/j.jpowsour.2008.11.114.
[29] Lohokare HR, Chaudhari HD, Kharul UK. Solvent and pH-stable poly(2,5-benzimidazole) (ABPBI) based UF membranes: preparation and characterizations. J Memb Sci 2018;563:743–51. https://doi.org/10.1016/j.memsci.2018.06.052.
[30] Kumbharkar SC, Kharul UK. New N-substituted ABPBI: synthesis and evaluation of gas permeation properties. J Memb Sci 2010;360:418–25. https://doi.org/10.1016/j.memsci.2010.05.041.
[31] Moorthy S, Maria Mahimai B, Kannaiyan D, Deivanayagam P. Synthesis and fabrication of Cu-trimesic acid MOF anchored sulfonated Poly(2,5-benzimidazole) membranes for PEMFC applications. Int J Hydrog Energy 2023;48:36063–75. https://doi.org/10.1016/j.ijhydene.2023.05.362.
[32] Bose S, Kuila T, Nguyen TXH, Kim NH, Lau KT, Lee JH. Polymer membranes for high temperature proton exchange membrane fuel cell: Recent advances and challenges. Prog Polym Sci (Oxf) 2011;36:813–43. https://doi.org/10.1016/j.progpolymsci.2011.01.003.
[33] Asensio JA, Gómez-Romero P. Recent developments on proton conducting Poly(2,5-benzimidazole) (ABPBI) membranes for high temperature polymer electrolyte membrane fuel cells. Fuel Cells 2005;5:336–43. https://doi.org/10.1002/fuce.200400081.
[34] Rufuss DDW, Hosseinipour E, Arulvel S, Davies PA. Complete parametric investigation of a forward osmosis process using sodium chloride draw solution. Desalination 2023;547:116218. https://doi.org/10.1016/j.desal.2022.116218.
[35] K.H. Gharda, P.D. Trivedi, T.R. Parida, A. Biradar, Method for processing a high temperature resistant thermosetting material, (2015) (U.S. Patent No. US 2015/0183993 A1).
[36] Staiti P, Lufrano F, Aricò AS, Passalacqua E, Antonucci V. Sulfonated polybenzimidazole membranes-preparation and physico-chemical characterization. J Memb Sci 2001;188:71–8. https://doi.org/10.1016/S0376-7388(01)00359-3.

[37] Jang JK, Kim TH. Fabrication of Tri-Directional Poly(2,5-benzimidazole) membrane using direct casting for vanadium redox flow battery. Polym (Basel) 2023;15:3577. https://doi.org/10.3390/polym15173577.
[38] Horike S, Kadota K, Itakura T, Inukai M, Kitagawa S. Synthesis of magnesium ZIF-8 from Mg(BH4)2. Dalton Trans 2015;44:15107–10. https://doi.org/10.1039/c5dt01183c.
[39] Asensio JA, Borrós S, Gómez-Romero P. Enhanced conductivity in polyanion-containing polybenzimidazoles. Improved materials for proton-exchange membranes and PEM fuel cells. Electrochem Commun 2003;5:967–72. https://doi.org/10.1016/j.elecom.2003.09.007.
[40] Wang Y, Shung Chung T, Gruender M. Sulfonated polybenzimidazole membranes for pervaporation dehydration of acetic acid. J Memb Sci 2012;415–416:486–95. https://doi.org/10.1016/j.memsci.2012.05.035.
[41] Glipa X, Haddad E, Jones DJ, Rozieré J, Rozieré RR. Synthesis and characterisation of sulfonated polybenzimidazole: a highly conducting proton exchange polymer. Solid State Ion- 1997;97:323–31. https://doi.org/10.1016/S0167-2738(97)00032-5.
[42] Fourie LF, Square L, Arendse C, Msimanga M. ABPBI/MWCNT for proton radiation shielding in low earth orbit. APL Mater 2023;11:071103. https://doi.org/10.1063/5.0156686.
[43] Selim A, Knozowska K, Ośmiałowski B, Kujawa J, Mizsey P, Kujawski W. The fabrication, characterization, and pervaporation performance of poly(ether-block-amide) membranes blended with 4-(trifluoromethyl)-N(pyridine-2-yl)benzamide and 4-(dimethylamino)-N(pyridine-2-yl)benzamide fillers. Sep Purif Technol 2021;268:118707. https://doi.org/10.1016/j.seppur.2021.118707.
[44] Wang Y, Chung TS, Neo BW, Gruender M. Processing and engineering of pervaporation dehydration of ethylene glycol via dual-layer polybenzimidazole (PBI)/polyetherimide (PEI) membranes. J Memb Sci 2011;378:339–50. https://doi.org/10.1016/j.memsci.2011.05.020.
[45] Wang KY, Chung TS, Qin JJ. Polybenzimidazole (PBI) nanofiltration hollow fiber membranes applied in forward osmosis process. J Memb Sci 2007;300:6–12. https://doi.org/10.1016/j.memsci.2007.05.035.
[46] Yang Q, Wang KY, Chung TS. Dual-layer hollow fibers with enhanced flux as novel forward osmosis membranes for water production. Environ Sci Technol 2009;43:2800–5. https://doi.org/10.1021/es803360t.
[47] Fu FJ, Zhang S, Sun SP, Wang KY, Chung TS. POSS-containing delamination-free dual-layer hollow fiber membranes for forward osmosis and osmotic power generation. J Memb Sci 2013;443:144–55. https://doi.org/10.1016/j.memsci.2013.04.050.
[48] Yabuno Y, Mihara K, Miyagawa N, Komatsu K, Nakagawa K, Shintani T, et al. Preparation of polyamide–PVDF composite hollow fiber membranes with well-developed interconnected bicontinuous structure using high-temperature rapid NIPS for forward osmosis. J Memb Sci 2020;612:118468. https://doi.org/10.1016/j.memsci.2020.118468.

(12) INTERNATIONAL APPLICATION PUBLISHED UNDER THE PATENT COOPERATION TREATY (PCT)

(19) World Intellectual Property Organization
International Bureau

(43) International Publication Date
23 April 2020 (23.04.2020)

WIPO | PCT

(10) International Publication Number
WO 2020/079713 A1

(51) International Patent Classification:
C08L 79/00 (2006.01) *C08G 73/00* (2006.01)
C07D 235/00 (2006.01) *B01D 69/00* (2006.01)

(21) International Application Number:
PCT/IN2019/050776

(22) International Filing Date:
21 October 2019 (21.10.2019)

(25) Filing Language: English

(26) Publication Language: English

(30) Priority Data:
201811014986 20 October 2018 (20.10.2018) IN

(71) Applicant: **COUNCIL OF SCIENTIFIC & INDUSTRIAL RESEARCH** [IN/IN]; Anusandhan Bhawan, 2 Rafi Marg, New Delhi 110 001 (IN).

(72) Inventors: **KHARUL, Ulhas Kanhaiyalal**; National Chemical Laboratory, Dr Homi Bhabha Road, Pune 411008 (IN). **CHAUDHARI, Harshal Dilip**; National Chemical Laboratory, Dr Homi Bhabha Road, Pune 411008 (IN). **SHOBHANA, Nishina Achuthan**; National Chemical Laboratory, Dr Homi Bhabha Road, Pune 411008 (IN). **THORAT, Nitin Madhukarrao**; National Chemical Laboratory, Dr Homi Bhabha Road, Pune 411008 (IN).

(74) Agent: **SINGH, Manisha**; LexOrbis, 709-710 Tolstoy House, 15-17 Tolstoy Marg, New Delhi 110001 (IN).

(81) Designated States *(unless otherwise indicated, for every kind of national protection available)*: AE, AG, AL, AM, AO, AT, AU, AZ, BA, BB, BG, BH, BN, BR, BW, BY, BZ, CA, CH, CL, CN, CO, CR, CU, CZ, DE, DJ, DK, DM, DO, DZ, EC, EE, EG, ES, FI, GB, GD, GE, GH, GM, GT, HN, HR, HU, ID, IL, IN, IR, IS, JO, JP, KE, KG, KH, KN, KP, KR, KW, KZ, LA, LC, LK, LR, LS, LU, LY, MA, MD, ME, MG, MK, MN, MW, MX, MY, MZ, NA, NG, NI, NO, NZ, OM, PA, PE, PG, PH, PL, PT, QA, RO, RS, RU, RW, SA, SC, SD, SE, SG, SK, SL, SM, ST, SV, SY, TH, TJ, TM, TN, TR, TT, TZ, UA, UG, US, UZ, VC, VN, ZA, ZM, ZW.

(84) Designated States *(unless otherwise indicated, for every kind of regional protection available)*: ARIPO (BW, GH, GM, KE, LR, LS, MW, MZ, NA, RW, SD, SL, ST, SZ, TZ, UG, ZM, ZW), Eurasian (AM, AZ, BY, KG, KZ, RU, TJ, TM), European (AL, AT, BE, BG, CH, CY, CZ, DE, DK, EE, ES, FI, FR, GB, GR, HR, HU, IE, IS, IT, LT, LU, LV, MC, MK, MT, NL, NO, PL, PT, RO, RS, SE, SI, SK, SM, TR), OAPI (BF, BJ, CF, CG, CI, CM, GA, GN, GQ, GW, KM, ML, MR, NE, SN, TD, TG).

Declarations under Rule 4.17:
— *as to applicant's entitlement to apply for and be granted a patent (Rule 4.17(ii))*
— *as to the applicant's entitlement to claim the priority of the earlier application (Rule 4.17(iii))*

Published:
— *with international search report (Art. 21(3))*
— *in black and white; the international application as filed contained color or greyscale and is available for download from PATENTSCOPE*

(54) Title: A POYMER LAYERED HOLLOW FIBER MEMBRANE BASED ON POLY(2,5-BENZIMIDAZOLE), COPOLYMERS AND SUBSTITUTED POLYBENZIMIDAZOLE

(57) Abstract: The present invention relates to a polymer layered hollow fiber membrane based on poly(2,5-benzimidazole) (ABPBI), ABPBI copolymers and substituted polybenzimidazole (PBI) and a process for preparation thereof.

WO 2020/079713 A1

A POYMER LAYERED HOLLOW FIBER MEMBRANE BASED ON POLY(2,5-BENZIMIDAZOLE), COPOLYMERS AND SUBSTITUTED POLYBENZIMIDAZOLE

FIELD OF THE INVENTION

The present invention relates to a polymer layered hollow fiber membrane based on poly(2,5-benzimidazole) (ABPBI), poly(2,5-benzimidazole) (ABPBI) copolymers and substituted polybenzimidazole (PBI). Particularly, the present invention relates to a process for the preparation of polymer layered hollow fiber membrane based on poly(2,5-benzimidazole) (ABPBI), poly(2,5-benzimidazole) (ABPBI) copolymers and substituted polybenzimidazole (PBI).

BACKGROUND AND PRIOR ART OF THE INVENTION

Inorganic acids are commonly used in many industries such as steel, metal surface treatment and refining (Cr, Ni, Zn, Cu, etc.), electronics, chemical manufacture, etc. Their processing at various stages generates a large amount of acid solution streams. The membrane technology is the most feasible approach; due to its operational simplicity, acceptable permeation properties, low energy requirement, environmental compatibility, easy control, and scale-up and large operational flexibility. However, application of polymeric membranes is limited mainly due to the poor membrane stability towards high acid concentration, co-transport of other solutes leading to poor selectivity and membrane fouling. Further, microporous flat sheet and hollow fiber membranes are well known in the art. Such membranes are typically made by a solution-casting process (flat sheets) or by a solution extrusion-precipitation process (hollow fibers). Membranes made from conventional polymers cannot be used to treat feed streams containing solvents, acids or other harsh chemicals. To overcome these shortcomings, an efficient membrane is needed.

Polybenzimidazole (PBIs) are a family of polymer widely used in different applications due to its high thermal chemical and mechanical stability. The polymer backbone consists of heteroaromatic moiety with N-H group which furnish excellent rigidity to the polymer. This outstanding rigidity of PBIs imparts the capability to sustain at a high and cryogenic temperature which makes it a suitable candidate for gas separation application. The poor permeability and solubility of PBIs lead to the necessity of structural modification. The first effort was a structural modification of acid and amine moiety with the bulky group, still, the performance was not competing with the other polymers. Structural modification by N-substitution was the other approach to enhance the permeability, tertiarybutylbenzyl

substituted polymer was successfully synthesized having 4 and 17 times enhanced the permeability than the parental polymer PBI-BuI and PBI-I respectively. These properties were demonstrated on the flat sheet form (film of ~ 40-50 µm thickness). For practical applications of gas separations, the membrane needs to be asymmetric with a thin skin of ~ 10 µm thickness supported on the porous substructure. This way, high flux while retaining intrinsic selectivity of the skin layer can be obtained. Making hollow fiber membranes based on solely PBI does not make practical sense due to the high cost of the monomer and to extract the better membrane performance. The dual-layer hollow fiber membranes can address the discussed issues.

The energy requirement of the forward osmosis process is ~ 10 % in comparison to the reverse osmosis and is less prone to the fouling than the pressure-driven membrane processes. In industrial applications, especially in pharmaceutical and fine chemicals, the use of an organic solvent is necessary. Most of the present polymeric membranes do not withstand the organic solvent. It thus becomes necessary to improve the solvent stability of the membranes, which becomes the aim of the present work.

Pervaporation is established for the dehydration of organic solvents. One of the major drawbacks of polymeric membranes is their limited solvent stability. The uses of polymeric membranes are also restricted by temperature limitation.

WO-2011104602 discloses a porous ABPBI [phosphoric acid doped poly (2,5-benzimidazole] membrane and process of preparing the same, wherein the ABPBI porous membranes have excellent stability towards strong acids, bases, common organic solvents, and harsh environmental conditions.

Although conventional PBI is demonstrated for making its hollow fiber membranes in US-6986844B2 as well as dual-layer membranes in US-20110266222, ABPBI based hollow fibers are not demonstrated in the literature for separation applications. They can be used for several applications such as pervaporation, forward osmosis, gas separation, etc. Although the excellent solvent and temperature stability of ABPBI is demonstrated in the literature, it is not demonstrated for hollow fiber membrane preparation for separation applications.

So there is need to develop a hollow fiber membrane based on poly(2,5-benzimidazole) (ABPBI), ABPBI copolymers and substituted polybenzimidazole (PBI).

OBJECTIVES OF THE INVENTION

The main objective of the present invention is to provide a substantially non-porous polymer layered hollow fiber membrane based on poly(2,5-benzimidazole) (ABPBI), poly(2,5-benzimidazole) (ABPBI) copolymers and substituted polybenzimidazole (PBI).

Another objective of the present invention is to provide a process for the preparation of the substantially non-porous polymer layered hollow fiber membrane based on poly(2,5-benzimidazole) (ABPBI), poly(2,5-benzimidazole) (ABPBI) copolymers, blends and substituted polybenzimidazole (PBI).

Yet another object of the present invention is to provide use of the polymer layered hollow fiber membrane for separation or transport of solvents, solutes, acids, bases, chemicals and gases in selective manner.

SUMMARY OF THE INVENTION

Accordingly, present invention provides a polymer layered fiber membrane comprising one to three polymers layers wherein

i. the polymer for a first layer is selected from the group consisting of poly(2,5-benzimidazole)(ABPBI), or poly(2,5-benzimidazole) (ABPBI) copolymers, or substituted polybenzimidazole (PBI) or blends thereof;
ii. the polymer for a second layer is selected from the group consisting of polyetherimide, polyamide, polyacrylonitrile, polysulfones, polyether sulfone, polyvinylidene fluoride, polyimide, polyphenylene oxide, cellulose acetates alone or in combinations thereof;
iii. the polymer for a third layer is selected from the group consisting of silicone rubber, ethyl cellulose, poly(phyneleneoxide), poly(tetramethyl bisphenol-A-iso-terephthalate) or poly[1-(trimethylsilyl)-1-propyne;

wherein one layer of said membrane is polymer of first layer;

wherein said membrane is hollow fiber and substantially non-porous.

In an embodiment of the present invention, poly(2,5-benzimidazole) (ABPBI) copolymers is selected from the group consisting of ABPBI-co-PBI, ABPBI-co-substituted PBI or ABPBI-co-naphthalene dicarboxylic acid based PBIs.

In another embodiment of the present invention, said substituted polybenzimidazole is selected from the group consisting of tert-butyl substituted polybenzimidazole, hexafluoroisopropylidene substituted polybenzimidazole, dimethylsubstituted polybenzimidazole or di-tert-butylbenzyl substituted polybenzimidazole.

In yet another embodiment of the present invention, said membrane is useful for separation or transport of solvents, solutes, acids, bases, chemicals and gases in selective manner.

In yet another embodiment, present invention provides a process for the preparation of polymer membrane comprising the steps of:

a) preparing a first dope solution by dissolving the first polymer in a solvent or solvent mixtures followed by stirring the mixture at temperature in the range of 60 to 120 °C for the period in the range of 1 to 72 h;

b) preparing a second dope solution by dissolving second polymer in solvent followed by stirring the reaction mixture at temperature in the range of 60 to 90 °C for the period in the range of 1 to 72 h;

c) subjecting the first dope solution of step (a) and second dope solution of step (b) to dry-jet/wet spinning process to afford polymer layered hollow fiber membrane; and

d) coating the membrane of step (c) with a third polymer to afford three layered membrane.

In yet another embodiment of the present invention, wherein said solvent is selected from group consisting of pyridine, dimethyl sulfoxide, N,N-dimethyl formamide, N,N-dimethyl acetamide, N-Methyl-2-pyrrolidone, methane sulphonic acid, sulphuric acid, phosphoric acid, polyphosphoric acid, formic acid, acetone, tetrahydrofuran or mixture thereof.

In yet another embodiment of the present invention, said first polymer is selected from the group consisting of poly(2,5-benzimidazole), or poly(2,5-benzimidazole) copolymers, or substituted polybenzimidazole; wherein said substituted polybenzimidazole are selected from tert-butyl substituted polybenzimidazole, hexafluoroisopropylidene substituted polybenzimidazole, dimethylsubstituted polybenzimidazole, di-tert-butylbenzyl substituted polybenzimidazole.

In yet another embodiment of the present invention, said second polymer is selected from the group consisting of polyetherimide, polyamide, polyacrylonitrile, polysulfones, polyether sulfone, polyvinylidene fluoride, polyimide, polyphenylene oxide, cellulose acetates either alone or combination thereof.

In yet another embodiment of the present invention, said third polymer is selected from the group consisting of silicone rubber, ethyl cellulose, poly(phyneleneoxide), poly(tetramethyl bisphenol-A-iso-terephthalate) or poly[1-(trimethylsilyl)-1-propyne.

ABBREVIATION:

ABPBI: Poly(2,5-benzimidazole)

PBI: Polybenzimidazole

PAN: Polyacrylonitrile

PSF: Polysulfones

PBI-BuI: Tert-butyl group substituted polybenzimidazole

PEI: Polyetherimide

PA:Polyamide

PAN: Polyacrylonitrile

PES: Polyether sulfone

PVDF: Polyvinylidene fluoride

PI: Polyimide

PPO: Polyphenylene oxide

CA: Cellulose acetates

PTMSP: poly[1-(trimethylsilyl)-1-propyne

BRIEF DESCRIPTION OF THE DRAWINGS

Fig. 1: Optical image of a neat ABPBI based hollow fiber membrane.

Fig. 2: Optical image of dual layer ABPBI-PAN fiber; (a)-ABPBI layer and (b)-PAN layer

Fig. 3: Optical image of dual layer PBI-BuI-PSF fiber; (a)- PBI-BuI layer and (b)-PSF layer.

DETAILED DESCRIPTION OF THE INVENTION

The term "substantially non-porous" states that "a membrane that is substantially non-porous is a membrane capable of being used for chemodialysis, forward osmosis, pervaporation, gas separation, nanofiltration, ultrafiltraion or reverse osmosis."

The present invention provides a polymer layered hollow fiber membrane based on poly(2,5-benzimidazole) (ABPBI), poly(2,5-benzimidazole) (ABPBI) copolymers and substituted polybenzimidazole (PBI) and a process for the preparation thereof.

The present invention provides a substantially non-porous polymer layered hollow fiber membrane comprising one or more polymers layers, wherein

i. the polymer for a first layer is selected from the group consisting of poly(2,5-benzimidazole) (ABPBI), poly(2,5-benzimidazole) (ABPBI) copolymers, or substituted polybenzimidazole (PBI) or blends thereof;
ii. the polymer for a second layer is selected from the group consisting of polyetherimide (PEI), polyamide (PA), polyacrylonitrile (PAN), polysulfones (PS), polyether sulfone (PES), polyvinylidene fluoride (PVDF), polyimide (PI), polyphenylene oxide (PPO), cellulose acetates (CA) alone or in combinations thereof;
iii. the polymer for third layer is selected from the group consisting of silicone rubber, ethyl cellulose, poly(phyneleneoxide), poly(tetramethyl bisphenol-A-iso-terephthalate) or poly[1-(trimethylsilyl)-1-propyne (PTMSP);

with the proviso that one layer of the membrane is polymer of first layer and when the membrane wherein the polymer layered hollow fiber membrane is substantially non-porous.

In an embodiment of the present invention, poly(2,5-benzimidazole) (ABPBI) copolymer is selected from the group consisting of ABPBI-co-PBI, ABPBI-co-substituted PBI or ABPBI-co-naphthalene dicarboxylic acid based PBIs.

The single layered membrane further comprises blends of poly(2,5-benzimidazole) (ABPBI) or its copolymer or their blends with substituted polybenzimidazole (PBI).

The thickness of the layer of single, double or three layer membrane is in the range of 0.05 to 300 μm.

The non-porous polymer layered hollow fiber membrane based on poly(2,5-benzimidazole) (ABPBI), ABPBI copolymers and substituted polybenzimidazole (PBI) further comprising the polymer of third layer.

The polymer for third layer is selected from Silicone rubber, ethyl cellulose, poly(phyneleneoxide), poly(tetramethyl bisphenol-A-iso-terephthalate) or poly[1-(trimethylsilyl)-1-propyne (PTMSP).

The substituted polybenzimidazole is selected from tert-butyl substituted polybenzimidazole, hexafluoroisopropylidene substituted polybenzimidazole, dimethylsubstituted polybenzimidazole, di-tert-butylbenzyl substituted polybenzimidazole

The structure of poly(2,5-benzimidazole) (ABPBI), is disclosed in the reference WO-2011104602.

The structure of tert-butyl substituted polybenzimidazole is disclosed in the reference *J. Membr. Sci.* **286** (2006) 161.

The structure of hexafluoroisopropylidene substituted polybenzimidazole is disclosed in the reference *J. Membr. Sci.* **286** (2006) 161.

The structure of dimethylsubstituted polybenzimidazole is disclosed in the reference *Eur. Polym. J.* **45** (2009) 3363.

The structure of di-tert-butylbenzyl substituted polybenzimidazole is disclosed in the reference *Eur. Polym. J.* **45** (2009) 3363.

The present invention provides a process for the preparation of the substantially non-porous polymer layered hollow fiber membrane comprising the steps of:

a) preparing a first dope solution by dissolving the first polymer in a solvent or solvent mixtures followed by stirring the mixture at temperature in the range of 60 to 120°C for the period in the range of 1 to 72 h;

b) preparing a second dope solution by dissolving second polymer in solvent followed by stirring the reaction mixture at temperature in the range of 60 to 90 °C for the period in the range of 1 to 72 h;

c) subjecting the first dope solution of step (a) and second dope solution of step (b) to dry-jet/wet spinning process to afford one or two layered hollow fiber membrane; and

d) coating the membrane of step (c) with a third polymer to afford three layered membrane.

The solvent is selected from the group consisting of pyridine, dimethyl sulfoxide, N,N-dimethyl formamide, N,N-dimethyl acetamide, N-Methyl-2-pyrrolidone, methane sulphonic acid, sulphuric acid, phosphoric acid, polyphosphoric acid, formic acid, acetone, tetrahydrofuran or mixture thereof.

The first polymer is selected from the group consisting of poly(2,5-benzimidazole) (ABPBI), or poly(2,5-benzimidazole) (ABPBI) copolymers, or substituted polybenzimidazole (PBI) or blends thereof.

The second polymer is selected from the group consisting of polyetherimide, polyamide, polyacrylonitrile, polysulfones, polyether sulfone, polyvinylidene fluoride, polyimide, polyphenylene oxide, cellulose acetates alone or in combinations thereof.

The third polymer is selected from the group consisting of Silicone rubber, ethyl cellulose, poly(phyneleneoxide), poly(tetramethyl bisphenol-A-iso-terephthalate) or poly[1-(trimethylsilyl)-1-propyne (PTMSP).

The present invention further provides use of the polymer layered hollow fiber membrane for separation or transport of solvents, solutes, acids, bases, chemicals and gases in selective manner.

The present invention further provides the hollow fiber membrane modules of having different shapes. In the present invention, shell and tube type and U-shaped membranes modules are used for transport analysis. The transport analysis is carried out by flux studies. Different solvents, solutes, acids, bases, chemicals and gases are used for transport analysis.

The shell and tube type membrane module is prepared by potting the hollow fiber membrane by using two-component epoxy glue. When the shell and tube type membrane module is used for transport analysis, feed solution is passed through shell side and stripping solution is passed through tube side or vice versa.

The U-shaped membrane module is prepared by potting the hollow fiber membrane by using two-component epoxy glue. When the U-shaped membrane module is used for transport analysis, module is dipped in the feed solution container (feed side) and the stripping solution is passed through tube side (strip side) or vice versa.

The U-shaped membrabe module is used for the transport analysis of acid. In the present invention, inventor studies the transport analysis by dipping U-shaped module into the acid container (feed side) and water was circulated from the tube side (strip side). The transport of different acids viz., HNO_3, H_2SO_4 or H_3PO_4 was evaluated at different concentrations: 0.5 M, 1 M, 1.5 M and 2M. The flux of acid (amount transported from feed side to tube side) transported on the tube side is monitored by sampling and titration. The flux data for single layer membrane is given in Table 1.

Table 1: Flux of inorganic acids for single layer membrane

Acid	Flux of acid ($g.m^{-2}.h^{-1}$)			
	At feed concentration = 0.5 M	At feed concentration = 1.0 M	At feed concentration = 1.5 M	At feed concentration = 2.0 M
HNO_3	87.0	178.2	231.5	524.5
H_2SO_4	62.1	64.9	128.9	246.9
H_3PO_4	24.1	43.1	49.5	71.3

The transport of organic acids from the feed side to the tube side (strip side) of the membrane module was evaluated using acetic acid, glycolic acid, and lactic acid. The feed concentration for individual acid was varied from 0.5 M, 1.5M and 2M and the acid transported to the tube side was evaluated by titration. The flux data is given in Table 2.

Table 2: Flux of organic acids for single layer membrane

Acid	Flux of acid ($g.m^{-2}.h^{-1}$)		
	At feed concentration = 0.5 M	At feed concentration = 1.5 M	At feed concentration = 2 M
Acetic acid	36.5	84.5	258.6
Glycolic acid	36.1	77.2	188.7
Lactic acid	21.11	64.9	107.8

The shell and tube type membrane module was used for gas permeation analysis. The individual gas (He, N_2, CO_2 or CH_4) was pressurized to the shell side of the membrane at either 50, 60 or 70 psi. The permeation analysis is as given in Table 3

Table 3: Gas permeation data of PEI and PBI-BuI dual-layer hollow fiber membrane **coated with silicon rubber**

Feed P (psi)	He (GPU)	N_2 (GPU)	CO_2 (GPU)	CH_4 (GPU)	Selectivity (He/N_2)	Selectivity (CO_2/N_2)	Selectivity (CO_2/CH_4)
50	1.04	0.02	0.15	0.02	49.14	7.09	6.89
60	1.15	0.02	0.18	0.02	49.11	7.67	8.25
70	1.21	0.03	0.16	0.03	46.52	6.22	5.78

EXAMPLES

Following examples are given by way of illustration therefore should not be construed to limit the scope of the invention.

Example 1: Preparation of ABPBI and copolymers

Example 1a: Preparation of ABPBI

The ABPBI was synthesized in a reactor equipped with an overhead stirrer. It was charged with polyphosphoric acid (PPA, 2100 g) and heated at 170°C. A 70 g of *3,4*-diaminobenzoic acid (DABA) was added and heated for 1 h. The temperature was raised to 200°C, maintained for 1 h while stirring. The polymer was precipitated in water, cut into pieces, crushed, and agitated in water till the water wash was neutral to pH. It was then agitated in 1 % NaOH solution for 12 hours, then washed with water till the filtrate was neutral to pH. The obtained polymer was filtered, soaked in acetone, again filtered and then dried in a vacuum oven at 100 °C for 5 days.

Example 1b: Preparation of co-ABPBI-1

A 2300g of PPA, 100g of *3,4*-diaminobenzoic acid and 14.1 g of 2,6-naphthalenedicarboxylic acid were added to a three-neck round flask. The temperature was raised to 170 ºC and maintained for 3.5 h. The temperature was then lowered to 140 ºC, 13.9 g of 3,3'-diaminobenzidine was added, stirred for 0.5 h and the temperature was raised to 170ºC for 1 h. The temperature was further elevated to 200ºC and maintained for 5 h. The polymer was precipitated in water and processed as given in Example 1a in order to obtain the dried polymer.

Example 1c: Preparation of co-ABPBI-2

The co-ABPBI-2 was prepared by adding 2300 g of PPA, 60 g of *3,4*-diaminobenzoic acid and 32.8 g of isophthalic acid in a reactor. The temperature was raised to 170ºC and maintained for 3.5 h with stirring. The temperature was lowered down to 140ºC, 42.3 g of 3,3'-diaminobenzidine was added and stirred for 0.5 h. The temperature was then raised to 170 ºC and stirred for 1 h. The temperature was further elevated to 200 ºC and the reaction mixture was stirred for 5 h. The polymer was precipitated in water, cut into pieces and processed as given in Example 1a in order to obtain the polymer.

Example 1d: Preparation of co-ABPBI-3

The co-ABPBI-3 was prepared as given in Example-1c, except, the terephthalic acid was used in place of isophthalic acid.

Example 1e: Preparation of co-ABPBI-4

The co-ABPBI-4 was prepared by adding 3070 g of PPA, 60 g of *3,4*-diaminobenzoic acid and 8.5 g of 2,6-naphthalenedicarboxylic acid into a reactor. The temperature of the reactor was raised to 170 ºC and maintained for 1.5 h. Then 26.2 g of terephthalic acid was added and stirred for 1 h. The temperature was lowered down to 140ºC and 42.3 g of 3,3'-diaminobenzidine was added and stirred for 0.5 h. The temperature was again raised to 170 ºC for 1 h and then to 200ºC and maintained for 3 h while stirring. The polymer was precipitated in water, cut into pieces and processed as given in Example 1a in order to obtain the polymer in dry form.

Example 2: Preparation of substituted polymers

Example 2a: The tert-butyl group substituted polybenzimidazole, PBI-BuI was synthesized as given in prior art (*J. Membr. Sci.* **286** (2006) 161).

Example 2b: The hexafluoroisopropylidene substituted polybenzimidazole, PBI-HFA was prepared as given in the prior art. (*J. Membr. Sci.* **286** (2006) 161).

Example 2c: The dimethylsubstituted polybenzimidazole, DMPBI-BuI was prepared as given in the prior art (*Eur. Polym. J.* **45** (2009) 3363).

Example 2d: The di-tert-butylbenzyl substituted polybenzimidazole was prepared as given in the prior art (*Eur. Polym. J.* **45** (2009) 3363).

Example 2e: The N-sodium salt of PBI-BuI was reacted with methyl iodide to form a polyionic liquid, as given in the prior art (US-20130184412A1, *Polym. Chem.* **5** (2014), 4083). A 3-necked round-bottomed flask was charged with 600 ml of dry DMSO, added 20 g of PBI (PBI-I or PBI-BuI) and 2.1 molar equivalents of NaH (60% mineral oil dispersion form) and stirred under dry N_2 atmosphere at ambient temperature for 24 h. The reaction mixture was then heated at 80 ^{0}C for an h. The reaction mixture was allowed to cool to ambient and 4.2 equivalent of methyl iodide was added. The reaction temperature was elevated to 80 ^{0}C and further stirred for 24 h, the temperature was lowered to ambient and then precipitated in a mixture of toluene–acetone (1:1). The obtained golden yellow precipitate was dried at 80 ^{0}C for 24 h. It was further purified by dissolving in DMSO and re-precipitation in the same non-solvent. The obtained polymer was dried at 80^{0}C for three days.

Example 2f: The iodide anion of polyionic liquid as synthesized in Example 2e was exchanged as given in the prior art (WO-2012035556A1, *Polym. Chem.* **5** (2014), 4083). A two necked flask equipped with calcium chloride guard tube was charged with 5 g of a [TMPBI-BuI][I]and 100 ml of DMF. After the complete dissolution, 2 molar equivalent of $AgBF_4$ was added while stirring. The AgI precipitated and the anion exchanged polymer remained in the solution. The precipitated AgI was removed by centrifugation and the anion exchanged polymer ([TMPBI-BuI][BF_4]) was recovered from the supernatant by solvent evaporation.

Example 3: Preparation of dope solution

Example 3a: A round-bottomed flask equipped with a mechanical stirrer was charged with 975 g of methanesulphonic acid, heated to 80ºC, added a single polymer as prepared in Example 1a-e and stirred for 24 h to obtain a dope solution of a different polymer.

Example 3b: A round-bottomed flask equipped with a mechanical stirrer was charged with 970g of MSA, 15 g of ABPBI, as synthesized in Example 1a and 15 g of co-ABPBI as synthesized in Example 1d and heated to 80 ºC for 24 h.

Example 3c: A round-bottomed flask equipped with a mechanical stirrer was charged with 930 g of N,N-dimethyl acetamide (DMAc), 70 g of DMPBI-BuI, synthesized as given in Example 2c, heated to 80 ºC for 24 h while stirring to make a dope solution.

Example 3d: Preparation of dope solution using polyetherimide

The dope solution was prepared in a round-bottomed flask by charging 292 g of N-methyl-2-pyrrolidone (NMP) and 108 g of polyetherimide (Ultem-1000 grade) and stirring using mechanical stirrer for 48 hours at ambient temperature.

Example 3e: Preparation of dope solution using polyacrlonitrile (PAN)

A round-bottomed flask was charged with 740 g of *N,N*-dimethylformamide (DMF), heated at 60°C, added 140 g of PAN and 40 g of citric acid (CA) and stirred for 48 h.

Example 3f: Preparation of dope solution using PBI-BuI that was synthesized as given in Example 2a

A round-bottomed flask was charged with 770 g of N-methyl-2-pyrrolidone (NMP) and 30 g of lithium chloride (LiCl). After the dissolution of LiCl, 200 g of PBI-BuI was added. The heating at 80 ºC was done for 36 hours.

Example 3g: Preparation of dope solution using PBI-HFA that was synthesized as given in Example 2b

A round-bottomed flask was charged with 810 g of NMP and 40 g LiCl. A 150 g of PBI-HFA was added and stirred at 80 ºC for 30 hours.

Example 4: Preparation of hollow fiber membrane

Example 4a

The hollow fiber membranes using the dope solution as prepared in Example 3a-c were prepared by phase inversion process as known in the art [US-6986844B2]. In a typical procedure, the hollow fiber membranes were prepared by a dry-jet, wet spinning process. A tube-in-orifice type spinneret was used to spin the hollow fiber membrane. The water was used as a bore fluid as well as external coagulation bath. The membranes were spun at ambient temperature.

Example 4b: The reaction mixture as prepared in Example 1a, 1b, 1c, 1d, and 1e was further diluted with methanesulphonic acid and used as a dope solution for the preparation of hollow fiber membrane by the method as given in Example 4b.

Example 5: Preparation of dual-layer hollow fiber membrane

Example 5a: The dope solution as prepared in Example 3a-c was used for forming the outer layer of the dual-layer membrane.The solutions as prepared in Example 3d or 3e was used as an inner layer. The dual-layer hollow fiber membrane was spun with as known in the prior art [US-20110266222]. In a typical procedure, the hollow fiber membranes were prepared by a dry-jet, wet spinning process. The water was used as a bore fluid as well as external coagulation bath. The membranes were spun at ambient temperature.

Example 5b: In another dual-layer type of hollow fiber membranes, the dope solution as prepared in Example 3f and 3g was used for forming the outer layer. The solutions as prepared in Example 3d or 3e was used for forming inner layer of the dual-layer membrane. The method was the same as used in Example 5a.

Example 6: Cross-linking of hollow fiber membranes: The dried hollow fiber membrane as prepared in Example 4a, 4b, 5a or 5b were dipped in 10 % (wt./wt.) *1,4*-dibromobutane in acetonitrile as a solvent. The membranes were further dried at 80 ^{o}C for 24 h. The crosslinked hollow fiber membranes were coated with 1.96 wt. % of silicone rubber in petroleum ether solution.

Example 7: Preparation of membrane module: The hollow fiber membrane modules as prepared in Example 4a, 4b, 5a, or 5b were potted by using two-component epoxy glue.

Example 7A: Preparation of U-Shaped membrane module: The hollow fiber membrane modules as prepared in Example 4a, 4b, 5a, or 5b were potted by using two-component epoxy glue.

Example 8: Transport through hollow fiber membrane modules

Example 8a: Transport study of NaCl: The hollow fiber membrane as spun in Example 4a (using the polymer prepared as given in Example 1a, and the dope solution as prepared in Example 3a) and the module prepared as given in Example 7 was used for this study. The NaCl solution was circulated from the shell side of the membrane, while water was circulated from the bore side of the hollow fiber membrane. In different experiments, NaCl concentration was varied as 0.1 wt.%, 0.5 wt.% and 5 wt. % in water. The concentration of shell and tube side solution was continuously monitored for NaCl concentration by using online conductivity meter for 24 h. The flux of NaCl (amount transported from shell side to

tube side) for 0.1, 0.5 and 5 wt. % feed concentration was found to be $1.17x10^{-3}$, $3.31x10^{-2}$ and $2.13x10^{-1}$ g m^{-2} h^{-1}, respectively.

Example 8b: Transport of inorganic acids: The hollow fiber membrane as spun in Example 4a (using the polymer prepared as given in Example 1a, and the dope solution as prepared in Example 3a) and the U-shaped module prepared as given in Example 7was used for this study. The transport of different acids viz., HNO_3, H_2SO_4 or H_3PO_4 was evaluated at different concentrations: 0.5 M, 1 M, 1.5 M and 2M. The flux of acid (amount transported from feed side to tube side) transported on the tube side is monitored by sampling and titration. The flux data is given in Table 1. (Refer table 1)

Example 8c: Transport of organic acids: The hollow fiber membranes as spun in Example 4b (using the polymer prepared as given in Example 1a, and the dope solution as prepared in Example 3a) and the module prepared as given in Example 7 was used. The transport of organic acids from the feed side to the tube side (strip side) of the membrane module was evaluated using acetic acid, glycolic acid, and lactic acid. The experiments were carried out as given in Example 8b. The feed concentration for individual acid was varied from 0.5 M, 1.5M and 2M and the acid transported to the tube side was evaluated by titration. The flux data is given in Table 2.

Example 8d: Transport using HNO_3+$Fe(NO_3)_3$ solution: The hollow fiber membranes spun as given in Example 4a (using the polymer prepared as given in Example 1a, and the dope solution as prepared in Example 3a) and the module prepared as given in Example 7 was used for this study. The concentration of HNO_3taken in the shell (feed) side was 1M, while the concentration of $Fe(NO_3)_3$ was 0.25M. The flux for HNO_3 was found to be 118.8 $g.m^{-2}.h^{-1}$ and the flux for $Fe(NO_3)_3$ was found to be 1.45 x 10^{-2} $g.m^{-2}.h^{-1}$, offering selectivity of HNO_3 over $Fe(NO_3)_3$ as 8194.

Example 8e: Transport using H_2SO_4+$FeSO_4$ solution: The hollow fiber membranes spun in Example 4a (using the polymer prepared as given in Example 1a, and the dope solution as prepared in Example 3a) and module prepared as given in Example 7 was used for this study. The acid concentration on the shell (feed) side was 1M, while the concentration of $FeSO_4$ was 0.25M. The flux H_2SO_4 was found to be 62.9 $g.m^{-2}.h^{-1}$ and the flux for $FeSO_4$ was 7.62 x 10^{-1} $g.m^{-2}.h^{-1}$. The selectivity of H_2SO_4 over $FeSO_4$ was found to be 83.

Example 8f: Pervaporation using methanol-water: The hollow fiber membranes spun in Example 4b(using the polymer prepared as given in Example 1a, and the dope solution as prepared in Example 3a) and module prepared as given in Example 7 was used for this study. The 90% aqueous methanol was circulated from the shell side. The tube side pressure was

maintained at 700 mbar. The permeate flux was found to be 574 $g.m^{-2}.h^{-1}$ with the selectivity of water over methanol as 55.

Example 8g: Forward osmosis using NaCl as a draw solution: The hollow fiber membrane as spun in Example 4a (using the polymer prepared as given in Example 1a, and the dope solution as prepared in Example 3a) and module prepared as given in Example 7 was used for this study. A 2M aqueous NaCl solution was taken as a draw solution on the tube side, while DI water was used as feed solution on the shell side. The water flux was found to be 193.73 $g.m^{-2}.h^{-1}$.

Example 8h: Pervaporation using IPA-water: The dual-layer hollow fiber membranes spun in Example 5a (outer layer formed using dope solution given in Example 3a and an inner layer formed using dope solution given in Example 3d) were used to make the module as given in Example 7. A solution made with 75 % IPA and 25 % water was circulated from the shell side of the module. The tube side pressure was maintained at 700 mbar. The permeate flux was 33 $g.m^{-2}.h^{-1}$. The composition of the permeate was 94 % water and 6 % IPA.

Example 8i: Forward osmosis study: The module was prepared as given in Example 7 using dual-layer hollow fibers prepared in Example 5a (outer layer formed using dope solution given in Example 3a, based on polymer prepared in Example 1a and inner layer formed using dope solution given in Example 3e). A 2M NaCl was used as the draw solution on the tube side and DI water was circulated on the shell side. The water flux obtained was 593 $g.m^{-2}.h^{-1}$ with NaCl rejection as 99.49 %.

Example 8j: Transport of acids in dual-layer hollow fiber membrane: The hollow fiber membranes spun in Example 5a (outer layer formed using dope solution given in Example 3b based on polymer prepared in Example 1c and inner layer formed using dope solution given in Example 3d) were used to make module as given in Example7. The flux of 0.5M HNO_3 was 176 $g.m^{-2}.h^{-1}$; while the flux of 1M lactic acid was 68 $g.m^{-2}.h^{-1}$.

Example 8k: Gas permeation through dual layer hollow fiber membrane coated with silicon rubber: The hollow fiber membrane prepared as given in Example 5b (outer layer formed using dope solution given in Example 3f and inner layer formed using dope solution given in Example 3d) were used to prepare a module as given in Example 6 and 7. The individual gas (He, N_2, CO_2or CH_4) was pressurized to the shell side of the membrane at either 50, 60 or 70 psi. The permeation analysis is as given in Table 3. Refer Table 3

ADVANTAGES OF THE INVENTION

- The polymeric materials with high Tg and chemical stability, like substituted PBI-BuI and PBI-HFA which offers high permeance and selectivity as a skin layer and, the core of which will be composed of commercial low-cost polymers.
- The advantages of using ABPBI based membrane (over conventional PBI) is their higher NH-group density (molar mass of N–H group per repeat unit of a PBI) that is anticipated to lead to high acid complexation ability.
- The membrane can be prepared solely with one polymer or dual-layer membranes with the inner and outer layer of adequate polymers along with ABPBI or its copolymers.
- The hollow fiber membranes prepared solely with ABPBI or its copolymer can be used under harsh environment.
- These hollow fibers can cater to the need of various separations such as chemodialysis, gas separation, pervaporation, reverse osmosis, forward osmosis, etc.

We claim

1. A polymer layered fiber membrane comprising one to three polymers layers wherein
   i. the polymer for a first layer is selected from the group consisting of poly(2,5-benzimidazole)(ABPBI), or poly(2,5-benzimidazole) (ABPBI) copolymers, or substituted polybenz imidazole (PBI) or blends thereof;
   ii. the polymer for a second layer is selected from the group consisting of polyetherimide, polyamide, polyacrylonitrile, polysulfones, polyether sulfone, polyvinylidene fluoride, polyimide, polyphenylene oxide, cellulose acetates alone or in combinations thereof; and
   iii. the polymer for a third layer is selected from the group consisting of silicone rubber, ethyl cellulose, poly(phyneleneoxide), poly(tetramethyl bisphenol-A-iso-terephthalate) or poly[1-(trimethylsilyl)-1-propyne;

   wherein one layer of said membrane is polymer of first layer;

   wherein said membrane is hollow fiber and substantially non-porous.
2. The polymer membrane as claimed in claim 1, wherein said poly(2,5-benzimidazole) (ABPBI) copolymers is selected from the group consisting of ABPBI-co-PBI, ABPBI-co-substituted PBI or ABPBI-co-naphthalene dicarboxylic acid based PBIs.
3. The polymer membrane as claimed in claim 1, wherein said substituted polybenzimidazole is selected from the group consisting of tert-butyl substituted polybenzimidazole, hexafluoroisopropylidene substituted polybenzimidazole, dimethylsubstituted polybenzimidazole or di-tert-butylbenzyl substituted polybenzimidazole.
4. The polymer membrane as claimed in claim 1, wherein said membrane is useful for separation or transport of solvents, solutes, acids, bases, chemicals and gases in selective manner.
5. A process for the preparation of polymer membrane as claimed in claim 1, comprising the steps of:
   a) preparing a first dope solution by dissolving the first polymer in a solvent or solvent mixtures followed by stirring the mixture at temperature in the range of 60 to 120 °C for the period in the range of 1 to 72 h;

b) preparing a second dope solution by dissolving second polymer in solvent followed by stirring the reaction mixture at temperature in the range of 60 to 90 °C for the period in the range of 1 to 72 h;

c) subjecting the first dope solution of step (a) and second dope solution of step (b) to dry-jet/wet spinning process to afford polymer layered hollow fiber membrane; and

d) coating the membrane of step (c) with a third polymer to afford three layered membrane.

6. The process as claimed in claim 5, wherein said solvent is selected from group consisting of pyridine, dimethyl sulfoxide, N,N-dimethyl formamide, N,N-dimethyl acetamide, N-Methyl-2-pyrrolidone, methane sulphonic acid, sulphuric acid, phosphoric acid, polyphosphoric acid, formic acid, acetone, tetrahydrofuran or mixture thereof.

7. The process as claimed in claim 5, wherein said first polymer is selected from the group consisting of poly(2,5-benzimidazole), or poly(2,5-benzimidazole) copolymers, or substituted polybenzimidazole; wherein said substituted polybenzimidazole are selected from tert-butyl substituted polybenzimidazole, hexafluoroisopropylidene substituted polybenzimidazole, dimethylsubstituted polybenzimidazole, di-tert-butylbenzyl substituted polybenzimidazole.

8. The process as claimed in claim 5, wherein said second polymer is selected from the group consisting of polyetherimide, polyamide, polyacrylonitrile, polysulfones, polyether sulfone, polyvinylidene fluoride, polyimide, polyphenylene oxide, cellulose acetates either alone or combination thereof.

9. The process as claimed in claim 5, wherein said third polymer is selected from the group consisting of silicone rubber, ethyl cellulose, poly(phyneleneoxide), poly(tetramethyl bisphenol-A-iso-terephthalate) or poly[1-(trimethylsilyl)-1-propyne.

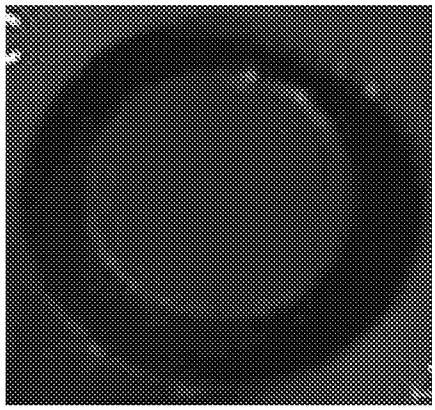

Fig. 1

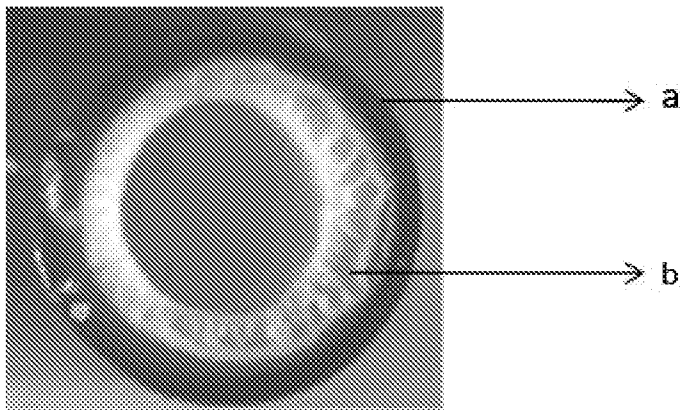

Fig. 2

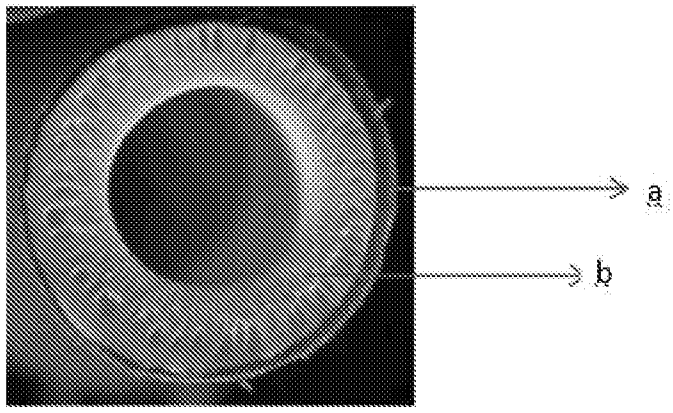

Fig. 3

INTERNATIONAL SEARCH REPORT

International application No.
PCT/IN2019/050776

A. CLASSIFICATION OF SUBJECT MATTER
C08L79/00,C07D235/00,C08G73/00,B01D69/00 Version=2020.01

According to International Patent Classification (IPC) or to both national classification and IPC

B. FIELDS SEARCHED

Minimum documentation searched (classification system followed by classification symbols)

C08L,C07D,C08G,B01D

Documentation searched other than minimum documentation to the extent that such documents are included in the fields searched

Electronic data base consulted during the international search (name of data base and, where practicable, search terms used)

TotalPatent One, IPO Internal Database

C. DOCUMENTS CONSIDERED TO BE RELEVANT

Category*	Citation of document, with indication, where appropriate, of the relevant passages	Relevant to claim No.
Y	US20110192281A1 (NATIONAL UNIVERSITY OF SINGAPORE) 11 AUGUST 2011 (11-08-2011) Claims 3-6,13;Paras 0089-0091	1-9
Y	US20110266223A1 (NATIONAL UNIVERSITY OF SINGAPORE) 03 NOVEMBER 2011 (03-11-2011) Abstract;Claims 1-18	1-9
Y	WO2011104602A1 (cited in the application) (COUNCIL OF SCIENTIFIC AND INDUSTRIAL RESEARCH) 01 SEPTEMBER 2011 (01-09-2011) Whole document	1-9
Y	EP1702942A1 (KOREA ADVANCED INSTITUTE OF SCIENCE AND TECHNOLOGY) 20 SEPTEMBER 2006 (20-09-2006) Paras 0002-0023	1-9

☐ Further documents are listed in the continuation of Box C. ☒ See patent family annex.

* Special categories of cited documents:
"A" document defining the general state of the art which is not considered to be of particular relevance
"D" document cited by the applicant in the international application
"E" earlier application or patent but published on or after the international filing date
"L" document which may throw doubts on priority claim(s) or which is cited to establish the publication date of another citation or other special reason (as specified)
"O" document referring to an oral disclosure, use, exhibition or other means
"P" document published prior to the international filing date but later than the priority date claimed
"T" later document published after the international filing date or priority date and not in conflict with the application but cited to understand the principle or theory underlying the invention
"X" document of particular relevance; the claimed invention cannot be considered novel or cannot be considered to involve an inventive step when the document is taken alone
"Y" document of particular relevance; the claimed invention cannot be considered to involve an inventive step when the document is combined with one or more other such documents, such combination being obvious to a person skilled in the art
"&" document member of the same patent family

Date of the actual completion of the international search	Date of mailing of the international search report
22-01-2020	22-01-2020
Name and mailing address of the ISA/ Indian Patent Office Plot No.32, Sector 14,Dwarka,New Delhi-110075 Facsimile No.	Authorized officer Divyanshu Mishra Telephone No. +91-1125300200

INTERNATIONAL SEARCH REPORT
Information on patent family members

International application No.
PCT/IN2019/050776

Citation	Pub.Date	Family	Pub.Date
US 20110192281 A1	11-08-2011	WO 2010042602 A1	15-04-2010
US 20110266223 A1	03-11-2011	WO 2010045430 A2	22-04-2010
		KR 20110074585 A	30-06-2011
		CN 102186565 A	14-09-2011
WO 2011104602 A1	01-09-2011	KR 20130007584 A	18-01-2013
		AU 2011219494 A1	20-09-2012
		EP 2539057 A1	02-01-2013
		ES 2649892 T3	16-01-2018
		SG 183404 A1	27-09-2012
		CN 102844098 A	26-12-2012
		US 20130053467 A1	28-02-2013
		US 20140284269 A1	25-09-2014
EP 1702942 A1	20-09-2006	KR 20060100689 A	21-09-2006
		US 20060211844 A1	21-09-2006
		JP 2006257390 A	28-09-2006